UNIVERSITY OF CALIFORNIA,

IRVINE

β-Sheet Macrocycles that Mimic Amyloid Oligomers and Inhibit Amyloid Aggregation

DISSERTATION

Submitted in partial satisfaction of the requirements for the degree of

DOCTOR OF PHILOSOPHY

In Chemistry

by

Pin-Nan Cheng

Dissertation Committee:

Professor James S. Nowick, Chair

Professor David Van Vranken

Professor Elizabeth R. Jarvo

2012

TABLE OF CONTENTS

List of Figures

List of Schemes

List of Tables

Acknowledgments

First and foremost, I would like to thank Prof. James S. Nowick for his guidance throughout my Ph.D. career. His philosophy about science tremendously influences how I do research, his philosophy about his graduate students changes how I look at the relationship between professors and students, and his philosophy about teaching models how I value a good teacher. As an international student, I need his extra guidance. He teaches me not only doing scientific research, but also oral and written communication skills in English. He is also my English teacher. Of course, he is not only an outstanding scientist, but also a great mentor. Besides science, he also guides me in all aspects of academic life in US. I appreciate his incredible patience and extra guidance. After five years, I have become a more mature graduate scientist.

Also, I would like to thank Dr. Cong Liu, Dr. Minglei Zhao, and Prof. David Eisenberg for the great and fruitful collaboration. I would like to thank Dr. John Greaves for assistance with the mass spectroscopic studies, Dr. Philip R. Dennison for assistance with the NMR studies, Jaime M. Albano for her fantastic English classes, the students and professors of our department for their helpful scientific discussions, the current and former Nowick group members for being such good teammates, and Prof. David Van Vranken and Prof. Elizabeth R. Jarvo for guidance and being my committee members.

Furthermore, I would like to thank National Institutes of Health, National Science Foundation, Allergan Graduate Fellowship, and UC Regents Dissertation Fellowship for the support of my research.

Lastly, I would like to thank my wife Connie, my family members, and my friends for their unconditional support.

Curriculum Vitae
Pin-Nan Cheng

Contact Information:

Email: pinnanc@uci.edu
Address: Department of Chemistry, 1102 Natural Science II, Irvine, CA 92697-2025

Educational History:

Department of Chemistry, University of California, Irvine; Ph. D., 2007-2012
Department of Chemistry, National Taiwan University; M.S., 2005
Department of Agricultural Chemistry, National Taiwan University; B.S. 2003
Taipei Municipal Cheng Kung Senior High School, 1999

Research Experience:

2007-2012	Doctoral Reasearch Advisor: Dr. James S. Nowick Research topics: 1. β-Sheet Peptides that Inhibit Aggregation of Alzheimer's-Related Peptides 2. Mimicry of Amyloid β-Sheets 3. Giant Macrolactams Based on β-Sheet Peptides
2005-2007	Substitute Civilian Serviceman, Environmental Protection Bureau, Taoyuan County Government, Taiwan. R. O. C. Toxic Substance Management
2003-2005	Master's Research Advisor: Dr. Chiu, Sheng-Hsien Research area: Supramolecular Chemistry and Organic Chemistry Thesis title: Toward a New Molecular Recognition System and Its Related Interlocked Molecules
2002-2003	Undergraduate Research Advisor: Dr. Chiu, Sheng-Hsien Research area: Supramolecular Chemistry and Organic Chemistry

Teaching Experience:

Teaching Assistant for Chem 51LB (organic chemistry lab) in 2008, and Chem H52A (honors organic chemistry), Chem 1LC (general chemistry lab), and Chem 203 (organic spectroscopy) in 2010

Honors and Awards:

- Regent's Dissertation Fellowship, University of California, Irvine, 2011
- American Institute of Chemists Foundation Student Award, 2011
- School of Physical Sciences Faculty Endowed Fellowship, University of California, Irvine, 2011
- Allergan Graduate Fellowship, 2011

- Dean's List, College of Science, National Taiwan University, 2005
- Yen Thesis award, Department of Chemistry, National Taiwan University, 2005
- Poster Award, Department of Chemistry, National Taiwan University, 2005

Publications:

Pin-Nan Cheng, Johnny D. Pham, James S. Nowick*, "The Supramolecular Chemistry of β-Sheets" Manuscript in Preparation.

Cong Liu, Minglei Zhao, Lin Jiang, **Pin-Nan Cheng**, Jiyong Park, Michael R. Sawaya, Anna Pensalfini, Dawei Guo, Arnold Berk, Charles Glabe, James S. Nowick*, David Eisenberg*, "Out-of-Register β-Sheets Suggest a Pathway to Toxic Amyloid Aggregates" Manuscript in Preparation.

Pin-Nan Cheng, R. Jeremy Woods, Charles G. Glabe, and James S. Nowick*, "Heterodivalent Linked Macrocyclic β-Sheet Peptides with Enhanced Activity against Aβ Aggregation: Two Sites are Better than One" Submitted.

Pin-Nan Cheng, Cong Liu, Minglei Zhao, David Eisenberg*, James S. Nowick*, "Amyloid β-Sheet Mimics that Antagonize Amyloid Aggregation and Reduce Amyloid Toxicity" *Nature Chem.* **2012**, in press.

Pin-Nan Cheng, James S. Nowick*, "Mimicry of Amyloid β-Sheets" *Proc. Am. Pept. Symp.* **2011**, 136–137.

Pin-Nan Cheng, James S. Nowick*, "Giant Macrolactams Based on β-Sheet Peptides" *J. Org. Chem*. **2011**, 3166–3173.

Cong Liu, Michael R. Sawaya, **Pin-Nan Cheng**, Jing Zheng, James S. Nowick, David Eisenberg*, "Self-Assembly of Amyloid-Related Tetrameric Oligomers Revealed by Crystal Structures of Designed Macrocyclic β-Sheet Mimics" *J. Am. Chem. Soc*. **2011**, 6736–6744.

Yi-Lin Huang, Chi-Feng Lin, **Pin-Nan Cheng**, Chien-Chen Lai, Yi-Hung Liu, Shie-Ming Peng, Sheng-Hsien Chiu*, "Bis-p-xylyl[26]crown-6/Pyridinium Ion Recognition: One-Pot Synthesis of Molecular Shuttles" *Tetrahedron Lett.* **2008**, 1665–1669.

Pin-Nan Cheng, Chi-Feng Lin, Yi-Huang Liu, Chien-Chen Lai, Shie-Ming Peng, and Sheng-Hsien Chiu*, "[3]Pseudorotaxane-Like Complexes Formed between Bipyridinium Dications and Bis-*p*-xylyl[26]crown-6" *Org. Lett*. **2006**, 435–438.

Pin-Nan Cheng, Po-Yi Huang, Wan-Sheung Li. Shau-Hua Ueng, Wei-Chung Hung, Yi-Hung Liu, Chien-Chen Lai, Yu Wang, Shie-Ming Peng, Ito Chao and Sheng-Hsien Chiu*, "Is [N^+–H···O] Hydrogen Bonding the Most Important Noncovalent Interaction in Macrocycle–Dibenzylammonium Ion Complexes?" *J. Org. Chem.* **2006**, 2373–2383.

Pinn-Tsong Chiang, **Pin-Nan Cheng**, Chi-Feng Lin, Yi-Hung Liu, Chien-Chen Lai, Shie-Ming Peng and Sheng-Hsien Chiu*, "A Macrocycle–Molecular Clip Complex that Functions as a Quadruply Controllable Molecular Switch." *Chem. Eur. J.* **2006**, 865–876.

Pin-Nan Cheng, Wei-Chung Hung and Sheng-Hsien Chiu*, "A New Macrocycle that Forms Pseudorotaxane-Like Complexes with Dibenzylammonium ions." *Tetrahedron Lett.* **2005**, 4239–4242.

Pin-Nan Cheng, Pinn-Tsong Chiang and Sheng-Hsien Chiu* "A Switchable Macrocycle–Clip Complex that Functions as a NOR Logic Gate." *Chem. Comm.* **2005**, 1285–1287.

Talks and Posters:

Cheng, P.-N.; Nowick*, J. S. "β-Sheet Macrocycles that Mimic and Antagonize Amyloid Aggregation and Reduce Amyloid Oligomer Cytotoxicity" Presented at the DOC Graduate Research Symposium, University of California, Santa Barbara, July 14, 2011 (Oral Presentation)

Cheng, P.-N.; Nowick*, J. S. "Mimicry of Amyloid β-Sheets" Presented at the 22nd American Peptide Symposium, San Diego, CA, June 26, 2011. (Poster)

Cheng, P.-N.; Nowick*, J. S. "Giant Macrolactams Based on β-Sheet Peptides" Presented at the 241th National Meeting of the American Chemical Society, Anaheim, CA, March 27, 2011; paper ORGN 193. (Poster)

Cheng, P.-N.; Nowick*, J. S. "Mimicry of Amyloid β-Sheets" Presented at the 240th National Meeting of the American Chemical Society, Boson, MA, August 24, 2010; paper ORGN 577. (Oral Presentation)

Professional Societies:

American Chemical Society
American Peptide Society

References:

Prof. James S. Nowick
jsnowick@uci.edu
949-824-6091
Department of Chemistry, University of California, Irvine, Irvine, CA 92697-2025

Prof. Elizabeth R. Jarvo
erjarvo@uci.edu
(949) 824-7105
Department of Chemistry, University of California, Irvine, 4114 Natural Sciences 1, Irvine, CA. 92697-2025

Prof. David Van Vranken
david.vv@uci.edu
(949) 824-5455
Department of Chemistry, University of California, Irvine, 2046D Reines Hall, Irvine, CA. 92697-2025

Abstract of Dissertation

β-Sheet Macrocycles that Mimic Amyloid Oligomers and Inhibit Amyloid Aggregation

by

Pin-Nan Cheng

Doctor of Philosophy in Chemistry

University of California, Irvine, 2012

Professor James S. Nowick, Chair

The chemical models of protein β-sheets described herein provide tools to address amyloid aggregation through β-sheet interactions. Amyloid aggregation and oligomers are now recognized as central in many devastating human diseases such as AIDS, cancer, Alzheimer's disease, prion diseases, and amyloid-related diseases. This dissertation describes new insights gained through chemical models into the rich supramolecular chemistry of β-sheets, particularly in amyloid aggregation and oligomers.

Chapter 1 provides representative examples of β-sheet structures and interactions that occur ubiquitously in proteins and amyloids. It particularly points out the importance of the β-sheet structures and interactions in amyloid aggregation associated with human diseases. Chapter 1 also describes insights into the edge-to-edge hydrogen-bonding interactions and face-to-face hydrophobic interactions among β-sheets. By understanding and using the common features of protein β-sheets, it may be possible to gain unique insights with which to further control β-sheet interactions in Alzheimer's and other diseases.

Chapter 2 describes the development of amyloid β-sheet mimics (ABSMs), a family of robust β-sheet macrocycles that can display a variety of amyloidogenic sequences from different amyloid proteins. ABSMs contain a 54-membered ring comprising a heptapeptide β-strand (the upper strand), one tripeptide β-strand mimic Hao flanked by two dipeptides (the lower strand), and two δ-linked ornithine turns. This chapter also describes the structures and inhibitory properties of ABSMs that can be tailored to antagonize aggregation of various amyloid proteins such as amyloid β-peptide associated with Alzheimer's disease, thereby reducing toxicity of amyloid aggregates. The crystallographic structures of ABSMs suggest structural models that provide insights into the elusive structures of amyloid fibrils and oligomers.

Chapter 3 reports the development of a series of heterodivalent linked macrocyclic β-sheets that are not only far more active against Aβ aggregation than their monovalent components, but also are dramatically more active than their homodivalent counterparts. This chapter also includes a model to explain the enhanced activity of the heterodivalent compounds against Aβ aggregation. The work described in this chapter suggests a design strategy for inhibitors of amyloid aggregation, that is, polyvalent inhibitors that can target multiple regions of amyloidogenic peptides and proteins are better than those that only target a single region.

Chapter 4 describes a side project derived from chapters 2 and 3. It demonstrates an attempt to use natural amino acids, the tripeptide β-strand mimic Hao, and the β-turn mimic δ-linked ornithine to generate water-soluble 54-, 78-, and 102-membered ring macrolactams. It also demonstrates the powerful macrocyclization that helps these giant

macrocylces fold into β-sheet structures and reports a synthesis route with which these macrocycles were efficiently synthesized.

CHAPTER 1
The Supramolecular Chemistry of β-Sheets

Preamble

Chapter 1 started as a review article about the importance of the supramolecular chemistry of β-sheets, which I wrote at the end of my Ph.D. career. It describes the importance of the supramolecular interactions of β-sheets in protein tertiary and quaternary structure, protein oligomerization, protein-protein interaction, peptide/protein aggregation in Alzheimer's disease and amyloid-related diseases.

Writing this chapter and the review article provided a different research experience in my Ph.D. career—a research project on paper, rather than on bench. Because I needed to select the representative examples that can convey our perspectives about β-sheets, I had a chance to read literature and plan the outline. In doing so, I learned how to choose good examples from the vast literature to communicate with my readers and how to summarize the work from other research groups. This project required high-quality figures; I learned a lot of skills from James in Photoshop, Illustrator, and PyMol. These skills will be helpful in my professional career as a chemist, as both visual and written communication skills are essential.

Doing this project inspired me. It not only broadened my vision, but also deepened my understanding about β-sheet structures and interactions. The insights I gained from this project helped me better understand the chemical models of protein β-sheets described in chapters 2, 3, and 4.

Introduction

The molecular recognition that is central to organization and communication in living cells relies on hydrogen bonding, hydrophobic, and other non-covalent interactions between biomolecules.[1] The edge-to-edge hydrogen bonding of the A-T and C-G bases of DNA helps encode genetic information. Interactions among coiled coils such as the leucine zippers of Fos and Jun help regulate transcription, as do the interactions of transcription factors with DNA. Molecular recognition between antibodies and antigens is not only central to the functioning of the immune system but also serves as the basis for many biochemical assays. Unlike these well-studied interactions, the interaction among β-sheets has not received the attention it deserves. This chapter seeks to shed light on this important, yet under-appreciated mode of biomolecular recognition.

β-Sheet structures and interactions occur ubiquitously in protein tertiary and quaternary structure, protein dimerization and oligomerization, protein-protein interaction, peptide/protein aggregation, and more.[2] Figure 1.1 illustrates some of these structures and interactions. Notably, protein aggregation through β-sheet interactions has increasingly drawn attention because it occurs in many devastating human diseases such as AIDS,[3] cancer,[4] Alzheimer's disease,[5] prion diseases,[6] and amyloid-related diseases.[7] Understanding interactions between β-sheets not only provides insights into biomolecular recognition but also provide a prospective avenue of intervention in human diseases involving β-sheet interactions.[8]

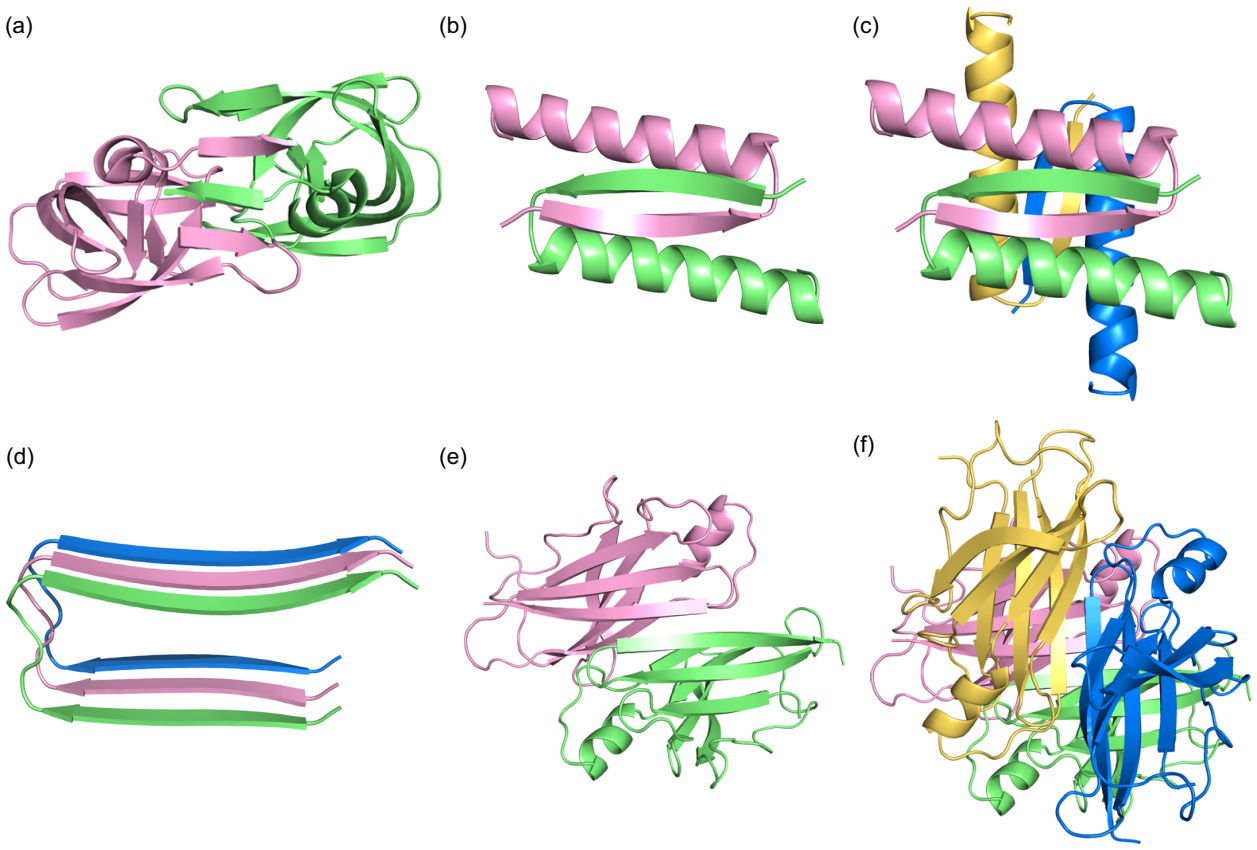

Figure 1.1. Structures and interactions of β-sheets. (a) Homodimer of HIV protease (PDB, 3HVP). (b) Homodimer of the p53 tetramerization domain (PDB, 1C26). (c) Homotetramer of the p53 tetramerization domain. (d) NMR-based model of $A\beta_{1-42}$ fibril (PDB, 2BEG). (e) Homodimer of transthyretin (PDB, 1TTR). (f) Homotetramer of transthyretin.

The understanding gained from protein β-sheets helps develop chemical models which in turn provide insights into β-sheet structures and interactions.[9] (Chapters 2, 3, and 4 describe how I got inspired and how I better understood chemical models of protein β-sheets. I used these synthetic molecules to mimic, control, and understand β-sheet structures and interactions that occur in the folding of β-sheets, dimerization through exposed hydrogen bonding edges, assembly to form protein quaternary structures and oligomers, and aggregation.)

β-Sheet Structures

Anatomy of β-Sheets. β-Sheets comprise extended polypeptide β-strands that are aligned laterally and hydrogen bonded and are often further stabilized by interactions between the side chains. A β-strand is a pleated linear array of amino acids whose side chains alternate above and below the polypeptide backbone (Figure 1.2a). The β-strands can run in either the same or opposite direction, forming either parallel or antiparallel β-sheets. Parallel β-sheets form a network of hydrogen-bonded 12-membered rings (Figure 1.2b), while antiparallel β-sheets form a network of alternating hydrogen-bonded 10- and 14-membered rings (Figure 1.2c). The 10- and 14-membered rings of antiparallel β-sheets are respectively known as the hydrogen-bonded (HB) and non-hydrogen-bonded (NHB) pairs, because the amino acids in the 10-membered rings are hydrogen bonded to each other while those in the 14-membered rings are not. The side chains of the alternate amino acids in the β-strands make up the "top" and "bottom" faces of the β-sheet, which sit above and below the hydrogen-bonded backbones (Figure 1.2d).

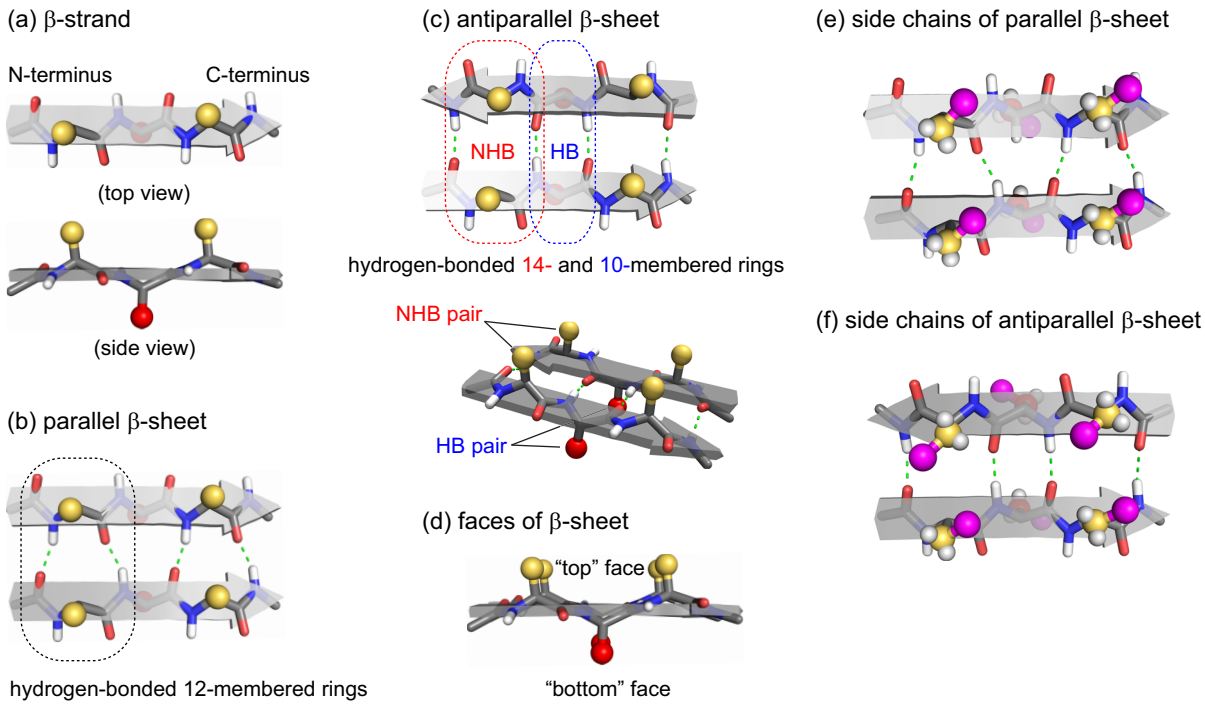

Figure 1.2. Anatomy of β-sheets. (a) A β-strand. (b) A parallel β-sheet. (c) An antiparallel β-sheet. (d) Faces of a β-sheet. (e) Common side chain orientation of a parallel β-sheet. (f) Common side chain orientation of an antiparallel β-sheet.

Interstrand interactions among the amino acid side chains are important in β-sheet structure and stability. Amino acids other than glycine and alanine contain β-substitutents that can interact in antiparallel and parallel β-sheets. In the non-hydrogen-bonded pairs of antiparallel β-sheets, the side chains can gear and clash to a greater extent than those in the hydrogen-bonded pairs (Figure 1.2f) or in parallel β-sheets (Figure 1.2e). The side-chain pairing preferences of amino acids in β-sheets has been studied both experimentally and statistically,[10] and our laboratory has co-authored a database of intermolecular amino acid pairing preferences in β-sheets.[11]

Twist of β-Sheets. β-Sheets are generally not flat in proteins, but are twisted in a right-handed fashion.[12] The β-sheets of the transthyretin monomer illustrate this twist (Figure 1.3a). One may envision this twist by holding a piece of paper horizontally (like horizontal peptide β-strands) and pulling the upper right-hand corner and lower left-hand corner toward each other, above the plane of the page, while simultaneously pushing the upper left-hand corner and lower right-hand corner toward each other below the plane of the page (Figure 1.3b).

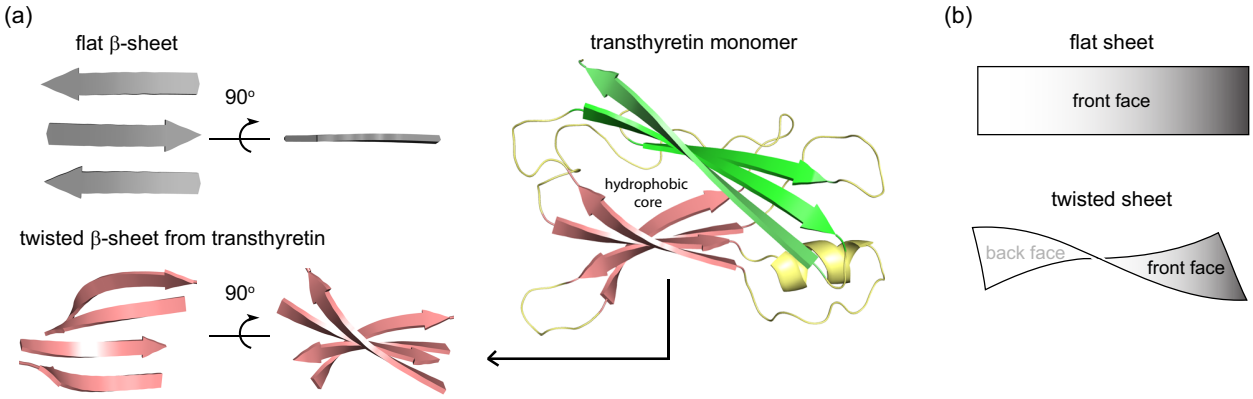

Figure 1.3. Twist of β-sheets. (a) Cartoons of a flat β-sheet and the twisted β-sheets of transthyretin (PDB, 1TTR). (b) Representation of sheets of paper with flat and twisted surfaces.

β-Sandwich. β-Sheets in proteins do not typically occur as isolated structures, but rather pack through hydrophobic interactions with α-helices or other β-sheets to create compact globular tertiary (intramolecular) or quaternary (intermolecular) structures. β-Sandwiches form when two β-sheets pack together through hydrophobic face-to-face interactions.[1] Often the β-sheets comprising this sandwich-like structure present more hydrophilic faces to water. β-Sandwiches are abundant in protein tertiary domains, and

assembly among β-sandwiches often provides unique quaternary protein structures with specific functions. Figure 1.3a illustrates the β-sandwich structure of transthyretin, which forms quaternary structures that transport thyroxine and retinol.[13]

Two β-sandwiches can further assemble through face-to-face interactions to form four-layered structures. The immunoglobulin G (IgG) light and heavy chains assemble to form functional antibodies through face-to-face quaternary interactions between the β-sandwiches of these two components. The resulting four-layered β-sandwich acts as a scaffold to display six loops as a specific binding site for antigens. Figure 1.4 illustrates these structures and interactions in immunoglobulin G2a (IgG2a).[14]

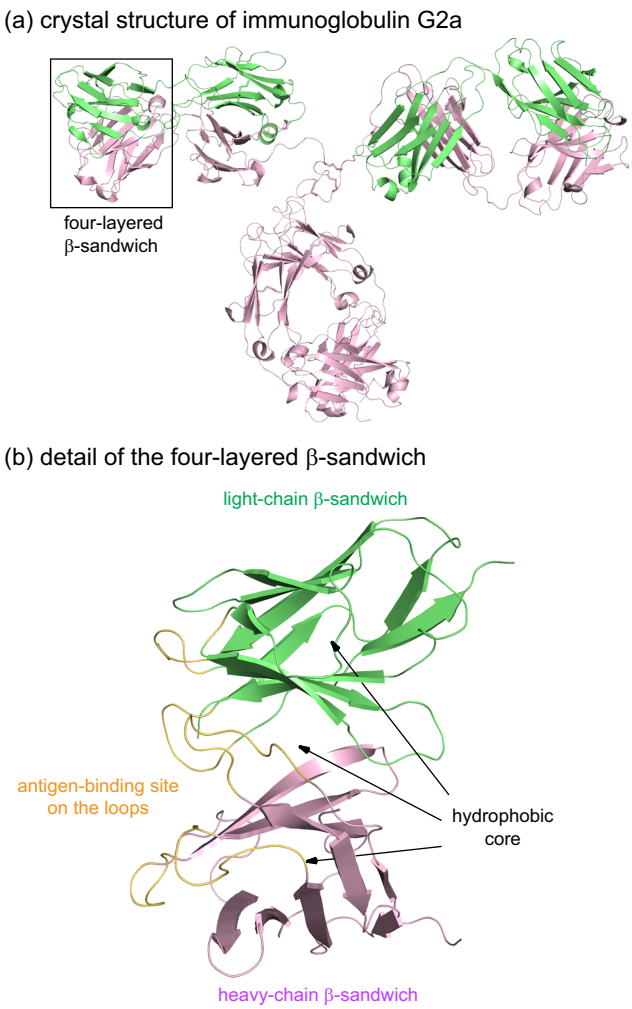

Figure 1.4. β-Sandwich structures. (a) Immunoglobulin G2a (PDB, 1IGT). (b) Detail illustrating the specific antigen-binding site of IgG2a, the hydrophobic cores of the light-chain and heavy-chain β-sandwiches, and the hydrophobic core between two β-sandwiches.

β-Barrel. β-Sheets can also pack to form closed structures without exposed hydrogen-bonding edges, in which the β-strands resemble staves in a barrel. Small β-barrel structures can resemble a β-sandwich in which the edges of the two layers have hydrogen bonded together; larger β-barrels generally form a cavity that can accommodate additional matter within. Figure 1.5 illustrates a variety of β-barrels.

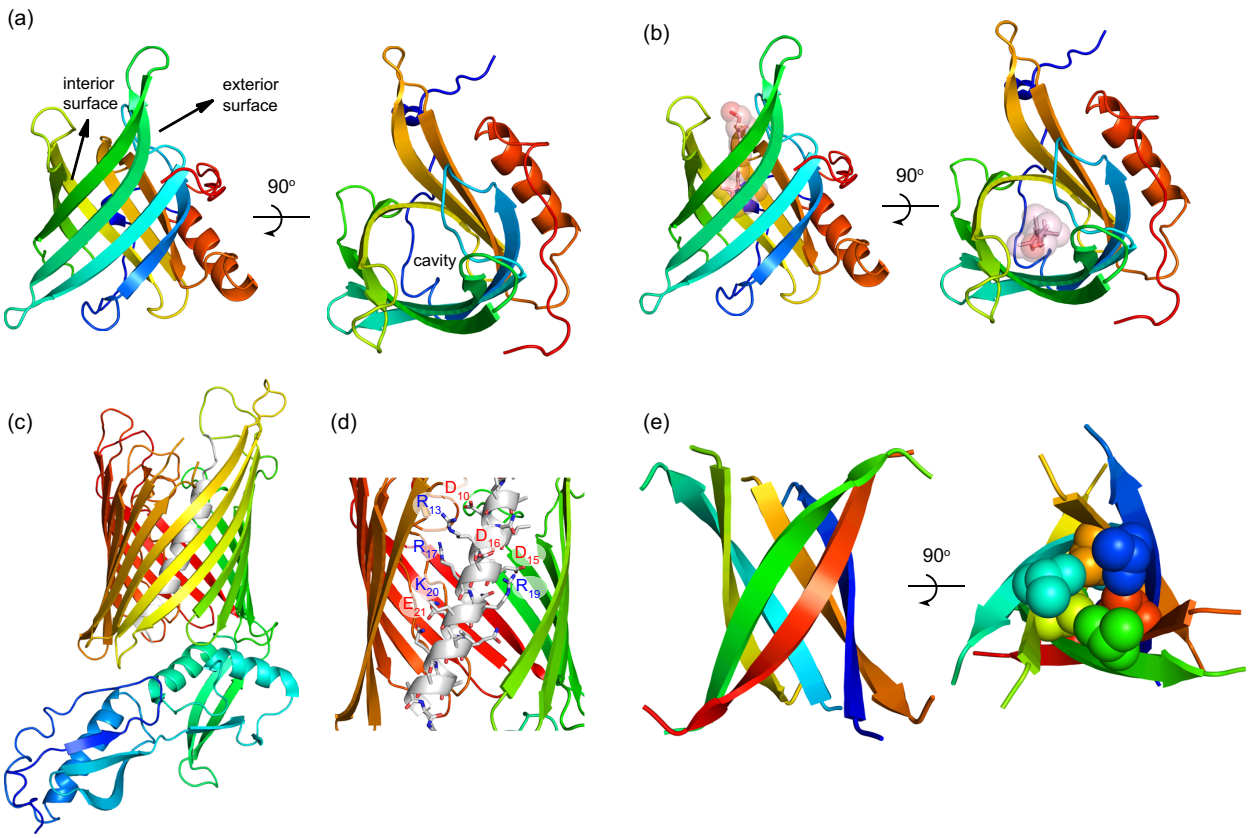

Figure 1.5. β-Barrel structures. (a) The eight-stranded β-barrel of human plasma retinol-binding protein (PDB, 1BRP). (b) The complex of human plasma retinol-binding protein and retinol. (c) The 16-stranded β-barrel of the membrane protein FhaC (PDB, 2QDZ). (d) Cutaway view of the 16-stranded β-barrel of FhaC. (e) The six-stranded β-barrel formed by peptide fragment KVKVLGDVIEV (K11V) derived from protein αB crystallin (PDB, 3SGO).

β-Barrels occur widely in enzymes, protein transporters, membrane pores, and binding proteins.[1] The human plasma retinol-binding protein (RBP), for example, contains an eight-stranded β-barrel with a hydrophobic cavity that binds retinol and facilitates its transport (Figures 1.5a and 1.5b).[15] The membrane protein FhaC is an essential component of the protein transporter machinery for gram-negative bacteria and eukaryotic organelles.[16] It contains a 16-stranded β-barrel with a hydrophilic cavity

containing 17 charged residues. When FhaC is inactive, the cavity of the β-barrel is plugged by an α helix that displays complementary charged residues (Figures 1.5c and 1.5d). When FhaC is active and helps translocate proteins across the membrane, the cavity is unplugged so that proteins can translocate through the cavity.

β-Barrels may also play an important role in the elusive structures of small amyloid oligomers, which are generally thought to be the key neurotoxic species in Alzheimer's and other neurodegenerative diseases.[17] Thus, an oligomer of an amyloidogenic peptide fragment from αB crystallin was recently found to form a six-stranded β-barrel containing three pairs of antiparallel β-sheets and a filled interior (Figure 1.5e).

β-Helix. A β-sheet structure that is less common in globular proteins—the β-helix—sets the stage for the structures of amyloid fibrils, the visible hallmark of Alzheimer's and many other diseases involving protein aggregation. β-Helices are helical structures composed of alternating β-strands and loops that run nearly orthogonal to the helical axis. The β-strands hydrogen bond together to form parallel β-sheets, which are often arranged in a triad about the helical axis. The β-sheets may collapse on each other forming sandwich-like structures or may form a triangular cavity, like a β-barrel. Figure 1.6 illustrates three representative β-helix structures.

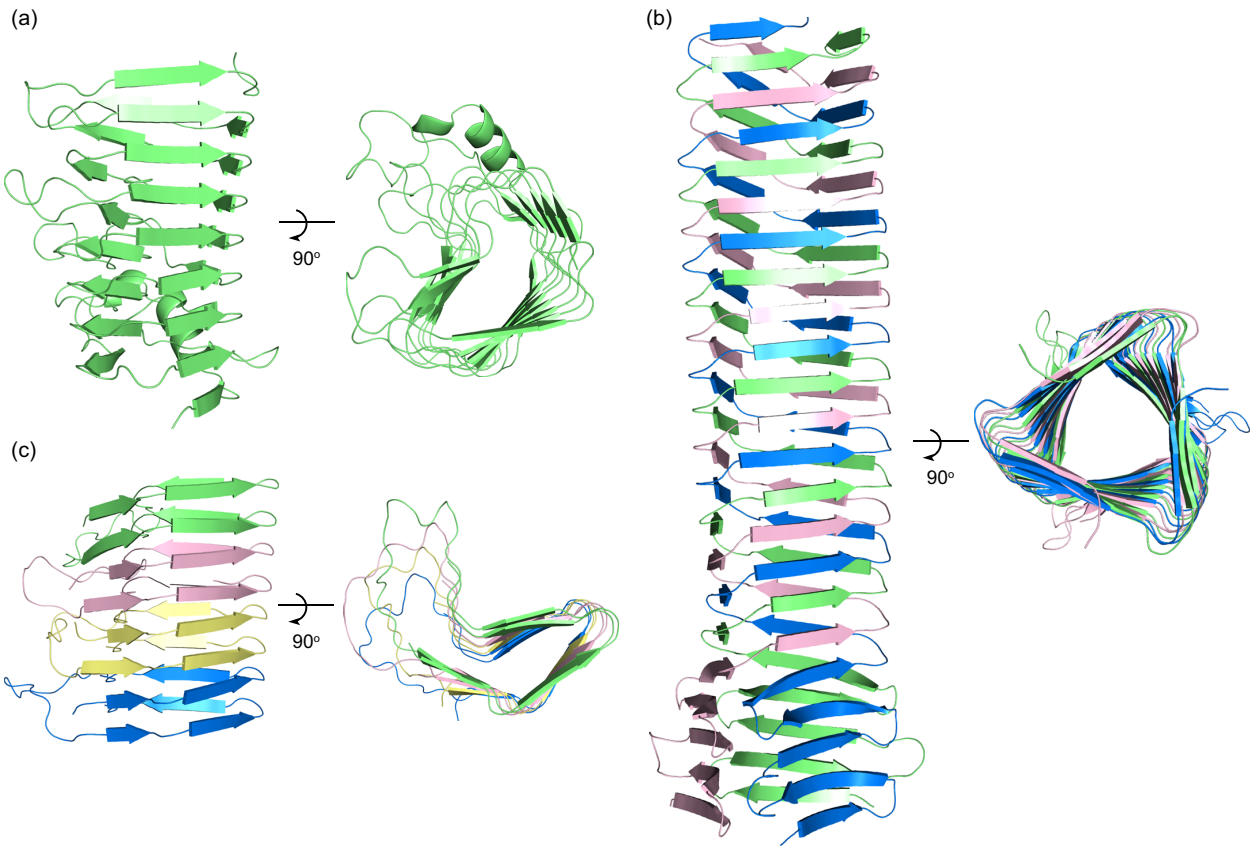

Figure 1.6. β-Helix structures. (a) The β-helix formed by pectate lyase C (PDB, 2PEC). (b) The trimeric β-helix of the (gp27-gp5*-gp5C)$_3$ complex of the cell-puncturing device of bacteriophage T4 (PDB, 1K28). (c) A stack of β-helices formed by residues 218-289 of HET-s (PDB, 2RNM). Colors in these figures represent different polypeptide chains. Extraneous residues are omitted for clarity.

The β-helix was first discovered in the bacterial protein pectate lyase C in 1993.[18] The β-helix of pectate lyase C consists of a single polypeptide chain that coils into three parallel β-sheets separated by loops (Figure 1.6a). The β-sheets form a collapsed structure in which two of the three sheets make a sandwich-like structure and the third, in conjunction with additional loops, spans the layers of the sandwich. β-Helices can also form through the assembly of multiple polypeptide chains. The β-helix of the (gp27-

gp5*-gp5C)$_3$ complex of the cell-puncturing device of bacteriophage T4 is a triple helix comprising three separate polypeptide chains wrapped about the helical axis to give a triangular cavity (Figure 1.6b).[19] β-Helices are integral to the aggregation of the fungal HET-s prion-forming protein that aggregates to form amyloid fibrils.[20] A fragment comprising residues 218-289 of HET-s has been shown to form a stack of β-helices running along the fibril axis (Figure 1.6c).

Higher-Order Supramolecular Structures of β-Sheets. β-Sheets have a propensity to form four-layered sandwich structures.[21] β-Sandwiches and β-helices with hydrophobic exterior surfaces can further self-assemble through hydrophobic interactions into higher-order structures containing four-layered sandwiches. The C_2 symmetric form of amyloid β-peptide ($A\beta_{1\text{-}40}$) fibrils associated with Alzheimer's disease consists of a four-layered β-sandwich similar to that of IgG (above).[22] The fibrils comprise two β-sandwiches formed by two separate networks of $A\beta_{1\text{-}40}$ tightly laminated through hydrophobic interactions to form a C_2 symmetric four-layered β-sandwich structure (Figure 1.7a, green and pink structures). $A\beta_{1\text{-}40}$ fibrils also form as a C_3 symmetric polymorph, which shares structural features with the C_2 form but lacks the tight lamination.[23] In this polymorph, two β-sandwiches tilt to form a more loosely laminated four-layered structure that can accommodate the third β-sandwich (Figure 1.7b). A similar sort of C_3 symmetric structure occurs in the P22 tail-spike protein, which consists of a supramolecular assembly of three β-helices (Figure 1.7c).[24]

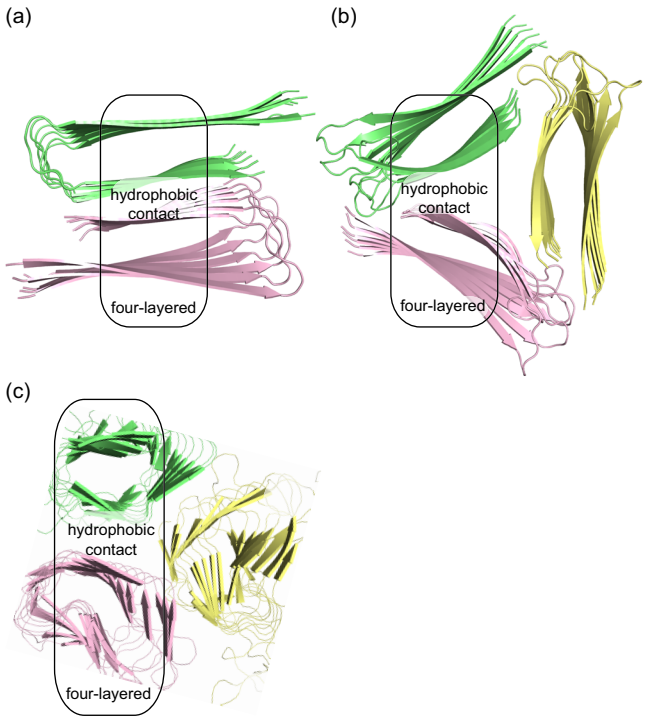

Figure 1.7. Four-layered β-sandwich structures. (a) The C_2 symmetric form of $A\beta_{1\text{-}40}$ fibrils. (b) The C_3 symmetric form of $A\beta_{1\text{-}40}$ fibrils. (c) The triangular superstructure with C_3 symmetry formed by the P22 tail-spike protein (PDB, 1TSP). Extraneous residues are omitted for clarity.

β-Sheet Interactions through Edge-To-Edge Hydrogen Bonding

Dimerization of folded proteins through the exposed hydrogen-bonding edges of β-sheets is a fundamental type of protein-protein interaction that occurs broadly in protein structure.[2a] The topology of a folded protein with an exposed β-sheet hydrogen-bonding edge favors intermolecular hydrogen bonding to form a C_2 symmetric antiparallel β-sheet dimerization interface. Hydrophobic interactions between the hydrophobic residues of the interface and the hydrophobic interior of the protein typically stabilize the dimerization interface. The resulting quaternary structures can involve multiply stranded β-sheets, individual β-strands, or the interdigitation of β-strands and are often necessary for the biological function of the protein.

β-Sheet Dimerization of Multiply-Stranded β-Sheets. The protein ParB forms a homodimer that helps partition DNA at cell division.[25] ParB dimerizes by forming an antiparallel β-sheet dimerization interface in which the exposed edges of two three-stranded β-sheets hydrogen bond to form six hydrogen bonds (Figure 1.8a). The interface is further stabilized through hydrophobic contact between residues F_{300}, Y_{302}, and F_{304} of the interface and the hydrophobic surface created by the α-helices of the protein (Figure 1.8b).

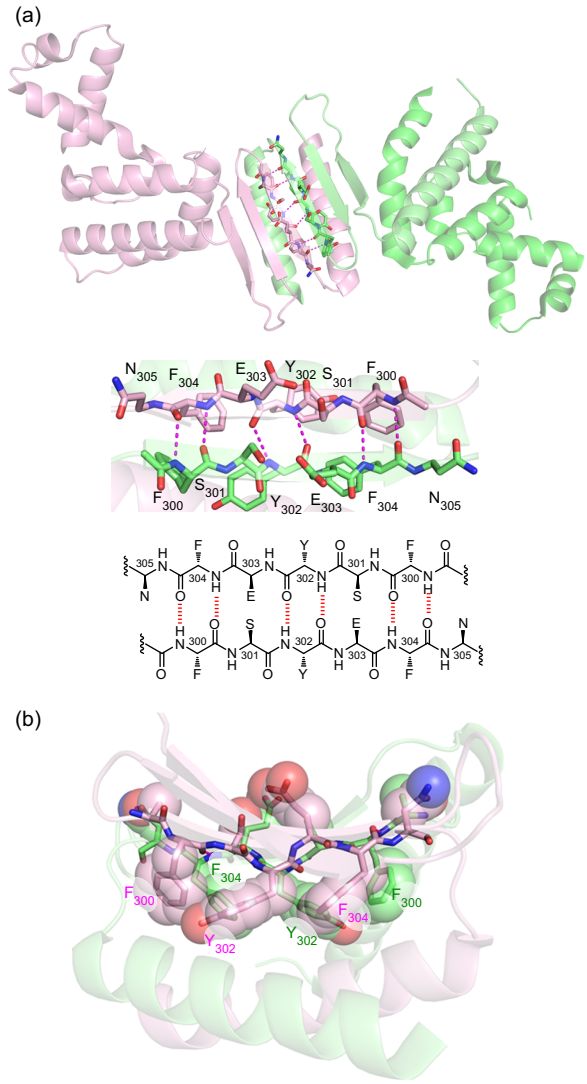

Figure 1.8. β-Sheet dimerization interface between two multiply-stranded β-sheets of protein ParB. (a) Homodimer of ParB and detail of the antiparallel β-sheet dimerization interface of ParB homodimer (PDB, 1ZX4). (b). Hydrophobic contact between residues F_{300}, Y_{302}, and F_{304} of the dimerization interface and the hydrophobic surface created by the α-helices of the protein.

Transthyretin helps transport thyroid hormones and retinol and functions as a homotetramer comprising a dimer and β-sheet dimers (Figure 1.1f).[26] Transthyretin dimerizes by forming an antiparallel β-sheet dimerization interface between two

three-stranded β-sheets (Figure 1.1e). Two of the dimers further self-assemble into a homotetramer through hydrophobic contact (Figure 1.1f).

β-Sheet Dimerization of Single β-Strands. The *met* repressor protein helps regulate the biosynthesis of methionine and functions as a homodimer. The *met* repressor protein dimerizes by forming an antiparallel β-sheet dimerization interface in which the two single β-strands hydrogen bond to form eight hydrogen bonds (Figure 1.9a).[27] The interface is further stabilized through hydrophobic contact between residues I_{24}, V_{26}, and I_{28} of the interface and the hydrophobic surface created by the α-helices of the protein (Figure 1.9b).

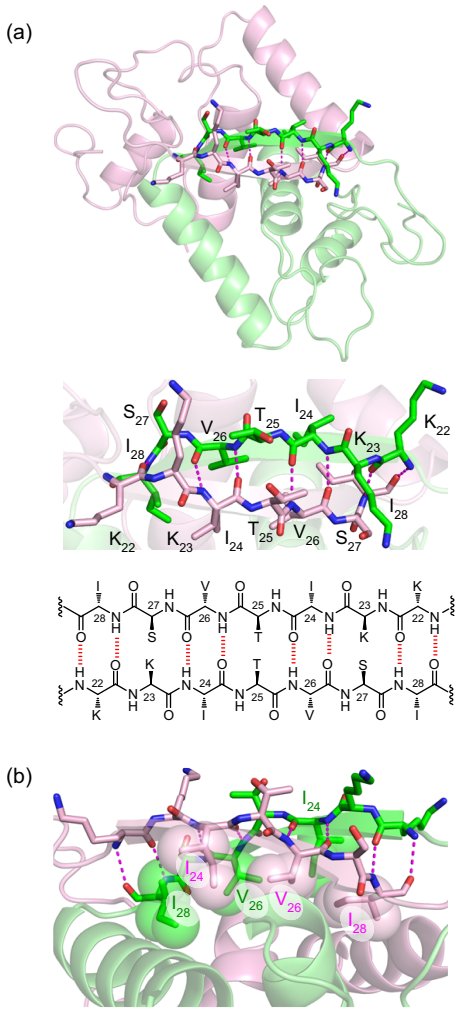

Figure 1.9. β-Sheet dimerization of single β-strands of the *met* repressor protein. (a) Homodimer of the *met* repressor and detail of the antiparallel β-sheet dimerization interface of the *met* homodimer (PDB, 1CMB). (b) Hydrophobic contact between residues I_{24}, V_{26}, and I_{28} of the antiparallel β-sheet dimerization interface and the hydrophobic surface created by the α-helices of the protein.

The tumor suppressor protein p53, which contains 393 residues, is a transcription factor that helps inhibit cancer development and functions as a homotetramer.[28] The p53 tetramerization domain (residues 325-356) controls the tetramerization. The p53 tetramerization domain dimerizes by packing two α-helices in an antiparallel fashion and by forming an antiparallel β-sheet dimerization interface (Figure 1.1b).[29] In this interface, two single β-strands hydrogen bond to form eight hydrogen bonds (Figure 1.10a). The interface is further stabilized through hydrophobic contact between residues F_{328}, L_{330}, and I_{332} of the interface and the hydrophobic surface created by the α-helices (Figure 1.10b). The homotetramer assembles through hydrophobic contact between the four pairs of residues L_{344} and L_{348} of the α-helices (Figure 1.10b).

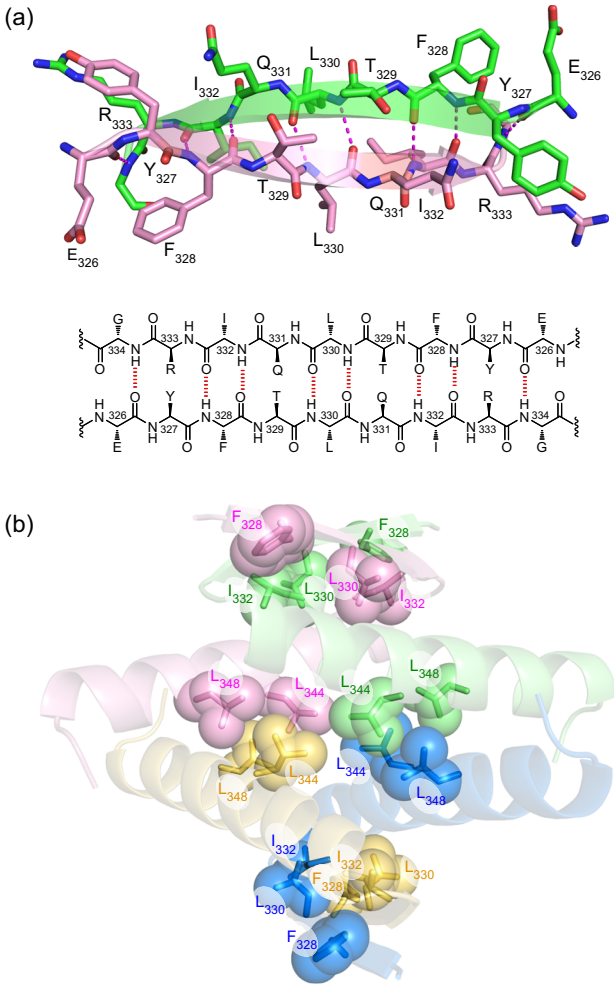

Figure 1.10. β-Sheet dimerization of single β-strands of the p53 tetramerization domain. (a) The antiparallel β-sheet dimerization interface of the p53 tetramerization domain homodimer (PDB, 1C26). (b) Hydrophobic contact between residues F_{328}, L_{330}, and I_{332} and the hydrophobic surface created by the α-helices; hydrophobic contact between the four pairs of residues L_{344} and L_{348} of the α-helices.

β-Sheet Dimerization through Interdigitation of β-Strands. HIV-1 protease is an important drug target that is essential for reproduction of AIDS virus and functions as a homodimer (Figure 1.1a).[30] It dimerizes by forming an antiparallel β-sheet dimerization interface in which two β-strands of each protein interdigitate to form a four-stranded antiparallel β-sheet (Figure 1.11a). The four-stranded-β-sheet interface is further stabilized not only by hydrophobic contact between residues I_3, L_{97}, and F_{99} of the interface and the hydrophobic surface created by the protein (Figure 1.11b) but also by additional hydrogen bonding between side chains of Q_2 and N_{99} and between the *N*- and *C*-termini (Figure 1.11a).

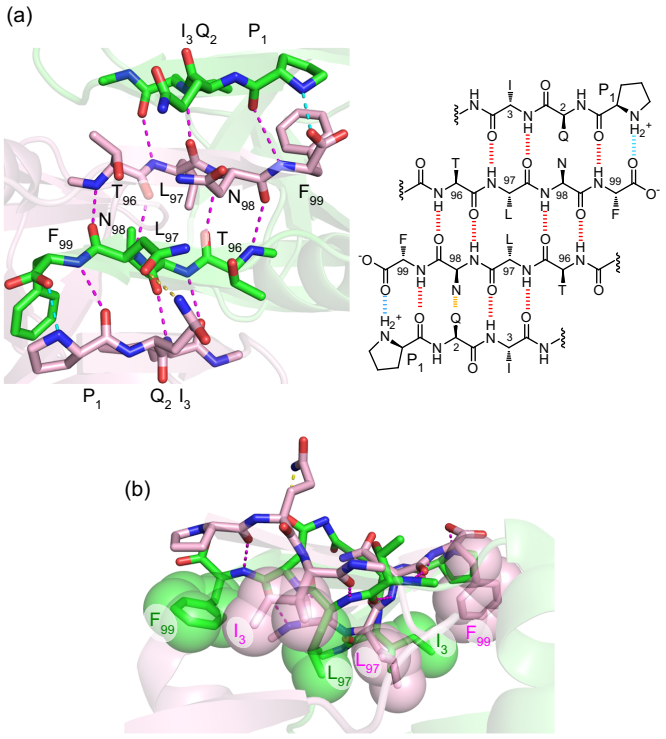

Figure 1.11. β-Sheet dimerization interface through interdigitation of β-strands of HIV-1 protease. (a) Four-stranded antiparallel β-sheet dimerization interface of the HIV protease homodimer (PDB, 3HVP). The side-chain hydrogen bond between Q_2 and N_{99} is shown in yellow and the salt bridges between the *N*- and *C*-termini are shown in cyan. (b) Hydrophobic contact between residues I_3, L_{97}, and F_{99} of the dimerization interface and the hydrophobic surface created by the protein.

β-Sheet Interactions through Face-To-Face Interactions

Assembly through face-to-face interactions between β-sheets is another fundamental type of protein-protein interaction that occurs broadly in protein and amyloid structure. Face-to-face interactions among β-sheets occur not only in protein tertiary and quaternary structures, such as β-sandwiches and β-helices, but also in higher-order superstructures, such as the four-layered sandwich structures of $A\beta_{1-40}$ amyloid fibrils and IgG as described above. These face-to-face interactions typically involve hydrophobic surfaces with good shape complementarity that are held together through van der Waals interactions and the hydrophobic effect.

Face-to-Face Interactions of Layered β-Sheets. Face-to-face interactions between layered β-sheets typically involve hydrophobic contact, interdigitation, or knob-hole interactions between opposing residues (Figure 1.12). Hydrophobic contact occurs in aligned or offset structures and typically features a large contact area created by large non-polar side chains (Figure 1.12a). Contact can occur either in an aligned fashion, in which residue j primarily contacts its intersheet neighbor i, or in an offset fashion, in which residue j primarily contacts its intersheet neighbors i and i+2. This specific face-to-face interaction generally favors the large, branched, non-polar side chains of valine, leucine, isoleucine, and phenylalanine, because they can provide large hydrophobic areas for intimate contact and thus maximize van der Waals interaction and the hydrophobic effect. Although large non-polar residues are favored, some polar residues such as tyrosine, tryptophan, serine, and threonine, can also participate.

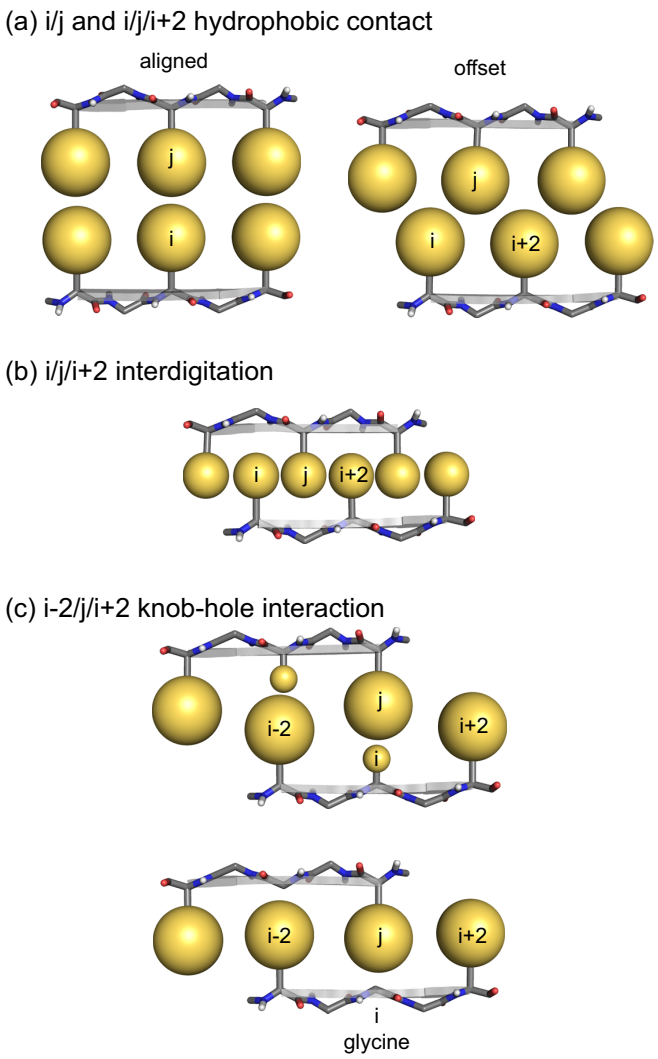

Figure 1.12. Face-to-face interactions of β-sheets. (a) The i/j and i/j/i+2 hydrophobic contact. (b) The i/j/i+2 interdigitation. (c) The i-2/j/i+2 knob-hole interaction.

Interdigitation occurs in offset structures and features a zipper-like packing in which side chains of the two sheets interdigitate tightly. Figure 1.12b illustrates this interaction in which residue j is embedded between intersheet neighbors i and i+2. Interdigitation often involves uncharged unbranched residues, such as alanine, asparagine, and glutamine. These tight interresidue contacts involve hydrophobic interactions and may involve hydrogen bonding with the exclusion of water.

Knob-hole interaction occurs in aligned structures and features a knob-into-hole-like packing in which a large residue serving as a *knob* is tightly buried in a *hole* created by a small residue such as glycine or alanine. Figure 1.12c illustrates this specific interaction in which residue j is aligned with intersheet neighbor i and primarily contacts intersheet neighbors i-2 and i+2. Unlike interdigitation, residue j is not embedded between residues i and i+2. Knob-hole interaction in β-sheets is reminiscent of the knob-into-hole packing in α-helix coiled-coils.[31] Although both van der Waals interaction and the hydrophobic effect are important in knob-hole interaction, the steric complementarity of knobs and holes between layered β-sheet structures is critical to this interaction.

Orientations of Layered β-Sheets. Layered β-sheets can adopt different orientations to achieve optimal face-to-face packing. The β-sheets in the adjacent layers can be aligned, offset, or rotated, as illustrated in Figure 1.13. In an aligned orientation, the β-strands of the two layers overlap, so that the side chains of one β-strand interact primarily with those of one β-strand in the adjacent layer (Figure 1.13a). In an offset orientation, the side chains of one β-strand interact primarily with those of two β-strands in the adjacent layer. The exposed edge of this orientation can present both a hydrogen-bonding edge and a hydrophobic ledge, with the potential for interaction with additional β-strands (Figure 1.13b). This structure and its potential for further interaction are reminiscent of the sticky ends in DNA.

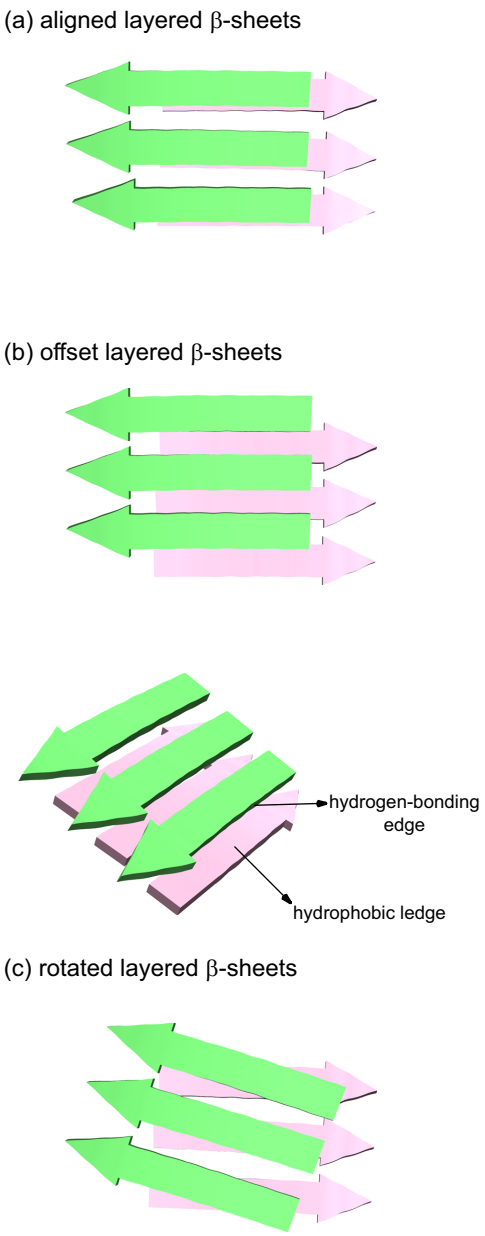

Figure 1.13. Orientation of layered β-sheets. (a) Aligned layered β-sheets. (b) Offset layered β-sheets. (c) Rotated layered β-sheets.

Layered β-Sheets in Protein, Amyloid Fibril, and Amyloid-like Fibril Structures. β-Sandwiches are common layered β-sheet structures in proteins. Transthyretin (TTR), for example, features a β-sandwich structure as described above (Figure 1.3a). The two

layers of β-sheets of TTR pack together to form a rotated layered β-sheet structure in which face-to-face interactions involve offset hydrophobic contact (Figure 1.14).

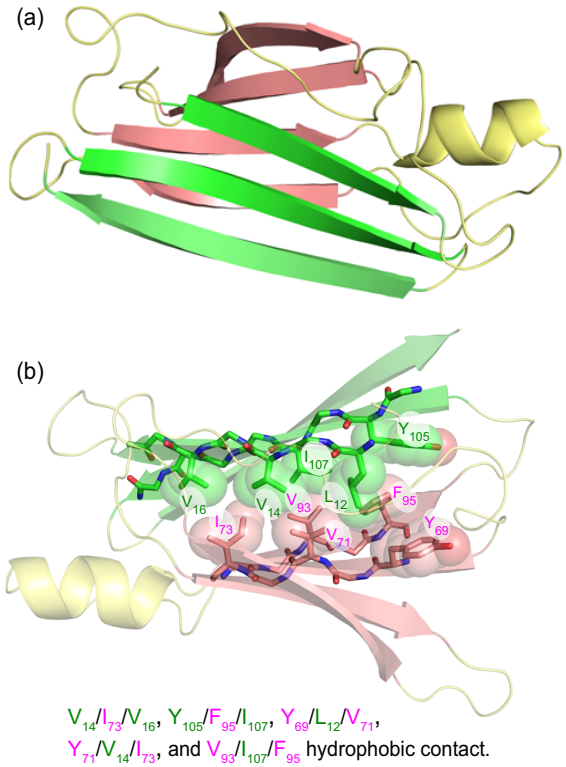

Figure 1.14. Orientation and face-to-face interactions in the layered β-sheets of the TTR β-sandwich (PDB, 1TTR). (a) The rotated layered β-sheets of the TTR β-sandwich. (b) The i/j/i+2 hydrophobic contacts in the TTR β-sandwich.

The HET-s protein aggregates to form amyloid fibrils, like those in prion diseases. Residues 218-289 of HET-s aggregate into fibrils that feature a β-helix structure, as described above (Figure 1.6c). Figure 1.15 illustrates that the HET-s β-helix contains offset layered β-sheets and two side-chain packing interfaces in which face-to-face interactions involve hydrophobic contact, interdigitation, and knob-hole interaction.

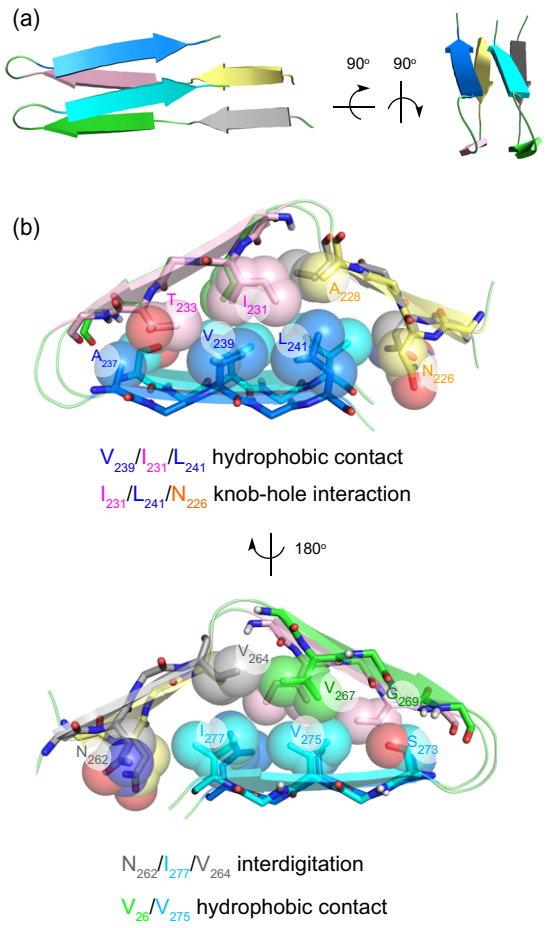

Figure 1.15. Orientation and face-to-face interactions in the layered β-sheets of the HET-s β-helix (PDB, 2RNM). (a) The offset layered β-sheets of residues 218-289 of HET-s. (b) The i/j and i/j/i+2 hydrophobic contacts, i/j/i+2 interdigitation, and i-2/j/i+2 knob-hole interaction in residues 218-289 of HET-s.

The $A\beta_{1\text{-}40}$ fibrils associated with Alzheimer's disease feature a four-layered β-sandwich in which two layers of β-sheets in a two-layered β-sandwich are layered in an offset fashion (Figure 1.16a) and face-to-face interactions involve hydrophobic contact and knob-hole interaction (Figures 1.16b and 1.16c). Of particular interest is that glycine, which is not typically thought of as favoring β-sheet formation, plays a special role in the assembly, with residues G_{33}, G_{37}, and G_{38} creating holes for the knob-hole interactions within and between the two-layered β-sandwiches.

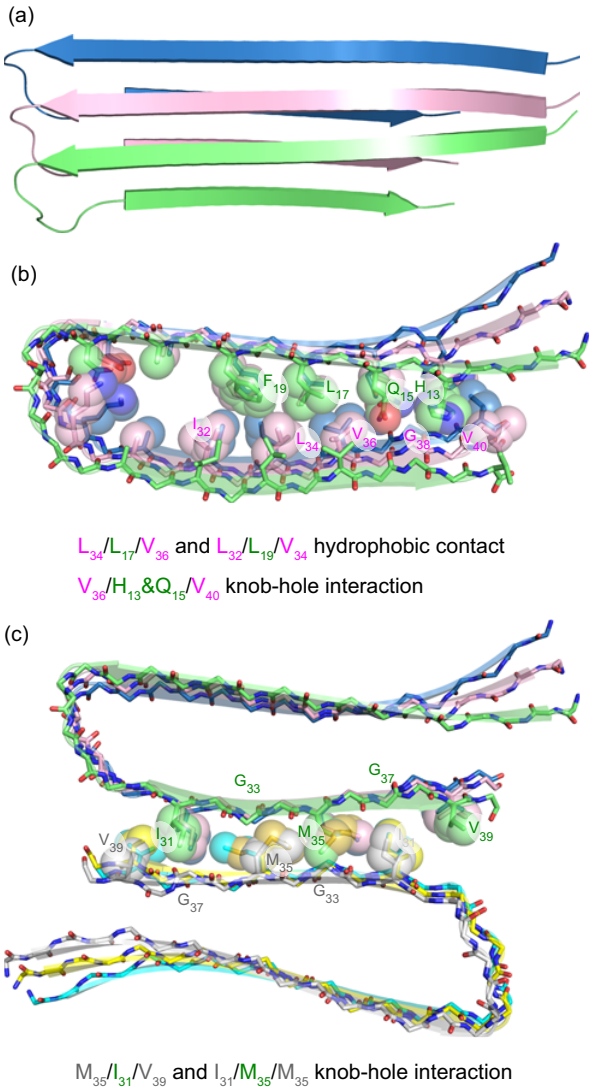

Figure 1.16. Orientation and face-to-face interactions in the layered β-sheets in $A\beta_{1\text{-}40}$ fibrils. (a) The offset layered β-sheets of the $A\beta_{1\text{-}40}$ fibrils. (b) The i/j/i+2 hydrophobic contacts and i-2/j/i+2 knob-hole interaction in the $A\beta_{1\text{-}40}$ fibrils. (c) The i-2/j/i+2 knob-hole interaction in $A\beta_{1\text{-}40}$ fibrils.

The structures of amyloid-like fibrils from amyloidogenic peptide fragments often shed light on amyloid fibril structures and provide useful insights into how amyloid self-assembles into fibrils.[32] The crystallographic structure of GNNQQNY from prion protein Sup35 shows that it self-assembles into an offset layered β-sheet structure in which face-to-face interactions involve interdigitation (Figure 1.17a).[32a] NMR-based structural models show that the central residues AAAAGAVV of peptide fragment $PrP_{106-126}$ from the human prion protein self-assemble into an rotated layered β-sheet structure in which face-to-face interactions involve interdigitation (Figure 1.17b).[33] The crystallographic structure of KLVFFA from Aβ shows that it self-assembles into an aligned layered β-sheet structure in which face-to-face interactions involve aligned and offset hydrophobic contact (Figure 1.17c).[32g]

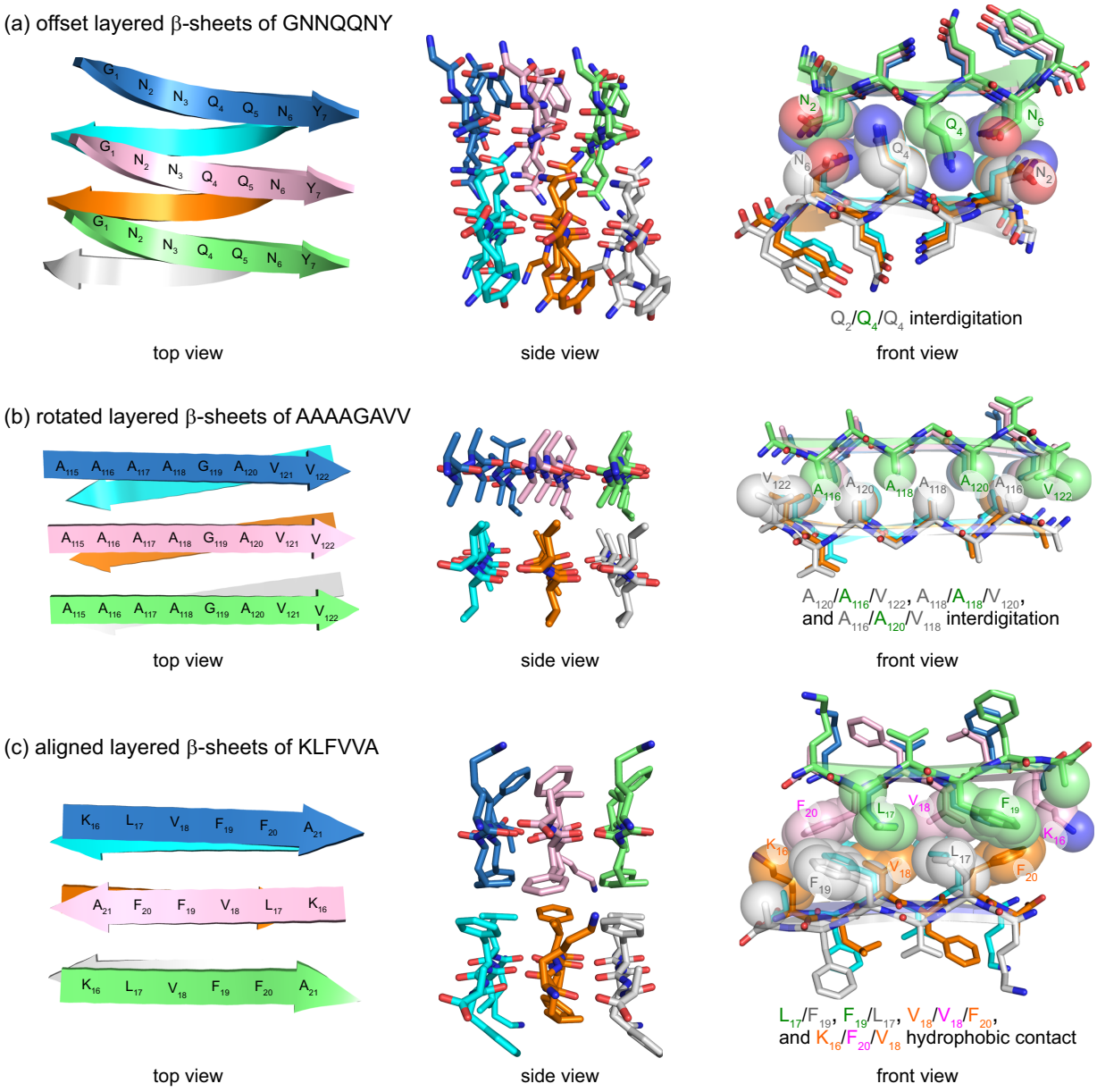

Figure 1.17. Orientations and face-to-face interactions in the layered β-sheets from amyloidogenic peptide fragments. (a) Crystal structure of GNNQQNY (PDB, 1YJP). (b) NMR-based structural model of AAAAGAVV. (c) Crystal structure of KLVFFA (PDB, 1YJP).

Conclusion

The β-sheet structures and interactions described herein have given us deeper insights into the rich supramolecular chemistry of β-sheets and have helped us better understand the types of supramolecular interactions in protein quaternary structure and in amyloids. A unifying theme that has emerged in natural proteins and amyloids is the confluence of edge-to-edge hydrogen-bonding interactions and face-to-face hydrophobic interactions among β-sheets that result in layered sandwich-like structures. Complementarity among the faces of the β-sheets is particularly important, through features such as aligned and offset hydrophobic contacts, interdigitation, and knob-hole interactions. Offset layered β-sheets that provide hydrogen-bonding edges over hydrophobic ledges provide unique potential for further interactions and may be especially important in β-sheet aggregation. By understanding and using these features, it may be possible to gain unique insights with which to further control β-sheet interactions in Alzheimer's and other diseases.

References and Notes

1. (a) Alberts, B.; Johnson, A.; Lewis, J.; Raff, M.; Roberts, K; Walter, P. *Molecular Biology of the Cell,* 5th ed. Garland Press: New York, 2007. (b) Branden C.; Tooze J. Introduction to Protein Structure. 2nd ed. Garland Press: New York, 1999.

2. (a) Maitra, S.; Nowick, J. S. In *The Amide Linkage: Structural Significance in Chemistry, Biochemistry, and Materials Science*; Greenberg, A., Breneman, C. M., Liebman, J. F., Eds.; Wiley: New York, 2000; pp 495–518. (b) Remaut, H.; Waksman, G., *Trends Biochem. Sci.* **2006**, *31*, 436–444.

3. Münch, J.; Rücker, E.; Ständker, L.; Adermann, K.; Goffinet, C.; Schindler, M.; Wildum, S.; Chinnadurai, R.; Rajan, D.; Specht, A.; Giménez-Gallego, G.; Sánchez, P. C.; Fowler, D. M.; Koulov, A.; Kelly, J. W.; Mothes, W.; Grivel, J.-C.; Margolis, L.; Keppler, O. T.; Forssmann, W.-G.; Kirchhoff, F., *Cell* **2007**, *131*, 1059–1071.

4. (a) Joerger, A. C.; Fersht, A. R., *Annu. Rev. Biochem.* **2008**, *77*, 557–582. (b) Xu, J.; Reumers, J.; Couceiro, J. R.; De Smet, F.; Gallardo, R.; Rudyak, S.; Cornelis, A.; Rozenski, J.; Zwolinska, A.; Marine, J.-C.; Lambrechts, D.; Suh, Y.-A.; Rousseau, F.; Schymkowitz, J., *Nat. Chem. Biol.* **2011**, *7*, 285–295.

5. (a) Haass, C.; Selkoe, D. J., *Nat. Rev. Mol. Cell Biol.* **2007**, *8*, 101–112. (b) Jakob-Roetne, R.; Jacobsen, H., *Angew. Chem., Int. Ed.* **2009**, *48*, 3030–3059. (c) Jaworski, T.; Dewachter, I.; Seymour, C. M.; Borghgraef, P.; Devijver, H.; Kügler, S.; Van Leuven, F., *BBA Mol. Basis Dis.* **2010**, *1802*, 808–818. (d) Karran, E.; Mercken, M.; Strooper, B. D., *Nat. Rev. Drug. Discov.* **2011**, *10*, 698–712.

6. (a) Prusiner, S., *Science* **1991**, *252*, 1515–1522. (b) Prusiner, S., *Science* **1982**, *216*, 136–144. (c)Prusiner, S. B.; Scott, M. R.; DeArmond, S. J.; Cohen, F. E., *Cell* **1998**, *93*, 337–348.

7. (a) May, B. C. H.; Govaerts, C.; Prusiner, S. B.; Cohen, F. E., *Trends Biochem. Sci.* **2004**, *29*, 162–165. (b) Chiti, F.; Dobson, C. M., *Annu. Rev. Biochem.* **2006**, *75*, 333–366. (c) Luheshi, L. M.; Crowther, D. C.; Dobson, C. M., *Curr. Opin. Chem. Biol.* **2008**, *12*, 25–31. (d) Eisenberg, D.; Jucker, M., *Cell* **2012**, *148*, 1188–1203.

8. (a) Sievers, S. A.; Karanicolas, J.; Chang, H. W.; Zhao, A.; Jiang, L.; Zirafi, O.; Stevens, J. T.; Munch, J.; Baker, D.; Eisenberg, D., *Nature* **2011**, *475*, 96–100. (b) Härd, T.; Lendel, C., *J. Mol. Biol.* DOI:10.1016/j.jmb.2011.12.062.

9. (a) Nowick, J. S.; Smith, E. M.; Pairish, M., *Chem. Soc. Rev.* **1996**, *25*, 401–415. (b) Nowick, J. S., *Acc. Chem. Res.* **1999**, *32*, 287–296. (c) Nowick, J. S., *Org. Biomol. Chem.* **2006**, *4*, 3869-3885. (d) Khakshoor, O.; Nowick, J. S., *Curr. Opin. Chem. Biol.* **2008**, *12*, 722–729. (e) Nowick, J. S., *Acc. Chem. Res.* **2008**, *41*, 1319-1330.

10. (a) Smith, C. K.; Regan, L., *Science* **1995**, *270*, 980–982. (b) Wouters, M. A.; Curmi, P. M. G., *Proteins: Struct., Funct., Bioinf.* **1995**, *22*, 119–131. (c) Smith, C. K.; Regan, L., *Acc. Chem. Res.* **1997**, *30*, 153-161. (d) Adrian, P. C.; Paul, M. G. C.; Ross, C.; Christine, D.; Andrew, E. T., *Proteins: Struct., Funct., Genet.* **1998**, *32*, 175–189. (e) Fooks, H. M.; Martin, A. C. R.; Woolfson, D. N.; Sessions, R. B.; Hutchinson, E. G., *J. Mol. Biol.* **2006**, *356*, 32–44.

11. Dou, Y.; Baisnee, P.-F.; Pollastri, G.; Pecout, Y.; Nowick, J.; Baldi, P., *Bioinformatics* **2004**, *20*, 2767–2777.

12. (a) Chothia, C., *J. Mol. Biol.* **1973**, *75*, 295–302. (b) Wang, L.; O'Connell, T.; Tropsha, A.; Hermans, J., *J. Mol. Biol.* **1996**, *262*, 283–293. (c) Ho, B. K.; Curmi, P. M. G., *J. Mol. Biol.* **2002**, *317*, 291–308.

13. (a) Blake, C.C.F., Geisow, M.J., Swan, I.D.A., Rerat, C., Rerat, B., *J. Mol. Biol*., **1974**, *88*, 1–12. (b) Blake, C.C.F., Oatley, S.J., *Nature*, **1977**, *268*, 115–120. (c) Damas, A. M.; Ribeiro, S.; Lamzin, V. S.; Palha, J. A.; Saraiva, M. J., *Acta Crystallogr. Sect. D* **1996**, *52*, 966–972.

14. Harris, L. J.; Larson, S. B.; Hasel, K. W.; McPherson, A., *Biochemistry* **1997**, *36*, 1581–1597.

15. Zanotti, G.; Ottonello, S.; Berni, R.; Monaco, H. L., *J. Mol. Biol.* **1993**, *230*, 613–624.

16. Clantin, B.; Delattre, A.-S.; Rucktooa, P.; Saint, N.; Méli, A. C.; Locht, C.; Jacob-Dubuisson, F.; Villeret, V., *Science* **2007**, *317*, 957–961.

17. Laganowsky, A.; Liu, C.; Sawaya, M. R.; Whitelegge, J. P.; Park, J.; Zhao, M.; Pensalfini, A.; Soriaga, A. B.; Landau, M.; Teng, P. K.; Cascio, D.; Glabe, C.; Eisenberg, D., *Science* **2012**, *335*, 1228–1231.

18. (a) Yoder, M.; Keen, N.; Jurnak, F., *Science* **1993**, *260*, 1503–1507. (b) Yoder, M.; Jurnak, F., *FASEB* **1995**, *9*, 335–342. (c) Scavetta R. D.; Herron S. R.; Hotchkiss A. T.; Kita N.; Keen N. T.; Benen J. A.; Kester H. C.; Visser J.; Jurnak F., *Plant Cell*, **1999**, *11*, 1081–1092.

19. Kanamaru, S.; Leiman, P. G.; Kostyuchenko, V. A.; Chipman, P. R.; Mesyanzhinov, V. V.; Arisaka, F.; Rossmann, M. G., *Nature* **2002**, *415*, 553–557.

20. Wasmer, C.; Lange, A.; Van Melckebeke, H.; Siemer, A. B.; Riek, R.; Meier, B. H., *Science* **2008**, *319*, 1523–1526.

21. Blake, C.; Serpell, L., *Structure* **1996**, *4*, 989–998

22. (a) Petkova, A. T.; Yau, W.-M.; Tycko, R., Biochemistry 2006, 45, 498–512. (b) Finder, V. H.; Glockshuber, R., *Neurodegener. Dis.* **2007**, *4*, 13–27. (c) Fändrich, M.; Schmidt, M.; Grigorieff, N., *Trends Biochem. Sci.* **2011**, *36*, 338–345.

23. Paravastu, A. K.; Leapman, R. D.; Yau, W.-M.; Tycko, R., Proc. *Natl. Acad. Sci. USA* **2008**, *105*, 18349–18354. (b) Meinhardt, J.; Sachse, C.; Hortschansky, P.; Grigorieff, N.; Fändrich, M., *J. Mol. Biol.* **2009**, *386*, 869–877. (c) Miller, Y.; Ma, B.; Nussinov, R., *Chem. Rev.* **2010**, *110*, 4820–4838.

24. Steinbacher, S.; Seckler, R.; Miller, S.; Steipe, B.; Huber, R.; Reinemer, P., *Science* **1994**, *265*, 383–386.

25. Schumacher, M. A.; Funnell, B. E., *Nature* **2005**, *438*, 516–519.

26. (a) Monaco, H.; Rizzi, M.; Coda, A., *Science* **1995**, *268*, 1039–1041. (b) Prapunpoj, P.; Leelawatwattana, L., *FEBS J.* **2009**, *276*, 5330–5341.

27. (a) Rafferty, J. B.; Somers, W. S.; Saint-Girons, I.; Phillips, S. E. V., *Nature* **1989**, *341*, 705–710. (b) Somers, W. S.; Phillips, S. E. V., *Nature* **1992**, *359*, 387–393.

28. (a) Okorokov, A. L.; Orlova, E. V., *Curr. Opin. Struct. Biol.* **2009**, *19*, 197–202. (b) Brosh, R.; Rotter, V., *Nat. Rev. Cancer* **2009**, *9*, 701–713.

29. Jeffrey, P.; Gorina, S.; Pavletich, N., *Science* **1995**, *267*, 1498–1502.

30. Wlodawer, A.; Miller, M.; Jaskolski, M.; Sathyanarayana, B.; Baldwin, E.; Weber, I.; Selk, L.; Clawson, L.; Schneider, J.; Kent, S., *Science* **1989**, *245*, 616–621.

31. (a) Crick, F. H. S., *Acta Crystallogr* **1953**, *6*, 689–697. (b) Hadley, E. B.; Testa, O. D.; Woolfson, D. N.; Gellman, S. H., *Proc. Natl. Acad. Sci. USA* **2008**, *105*, 530–535.

32. (a) Nelson, R.; Sawaya, M. R.; Balbirnie, M.; Madsen, A. O.; Riekel, C.; Grothe, R.; Eisenberg, D., *Nature* **2005**, *435*, 773–778. (b) Sambashivan, S.; Liu, Y.; Sawaya, M. R.; Gingery, M.; Eisenberg, D., *Nature* **2005**, *437*, 266–269. (c) Nelson, R.; Eisenberg, D., *Curr. Opin. Struct. Biol.* **2006**, *16*, 260–265. (d) Sawaya, M. R.; Sambashivan, S.; Nelson, R.; Ivanova, M. I.; Sievers, S. A.; Apostol, M. I.; Thompson, M. J.; Balbirnie, M.; Wiltzius, J. J.; McFarlane, H. T.; Madsen, A. O.; Riekel, C.; Eisenberg, D., *Nature* **2007**, *447*, 453–457. (e) Wiltzius, J. J. W.; Sievers, S. A.; Sawaya, M. R.; Cascio, D.; Popov, D.; Riekel, C.; Eisenberg, D., *Protein Sci.* **2008**, *17*, 1467–1474. (f) Ivanova, M. I.; Sievers, S. A.; Sawaya, M. R.; Wall, J. S.; Eisenberg, D., *Proc. Natl. Acad. Sci. U. S. A.* **2009**, *106*, 18990–18995. (g) Colletier, J.-P.; Laganowsky, A.; Landau, M.; Zhao, M.; Soriaga, A. B.; Goldschmidt, L.; Flot, D.; Cascio, D.; Sawaya, M. R.; Eisenberg, D., *Proc. Natl. Acad. Sci. U. S. A.* **2011**, *108*, 16938–16943.

33. Walsh, P.; Simonetti, K.; Sharpe, S. *Structure* **2009**, 17, 417–426.

CHAPTER 2

Amyloid β-Sheet Mimics that Antagonize Amyloid Aggregation and Reduce Amyloid Toxicity

Preamble

Chapter 2 describes a new class of β-sheet macrocycles that can tolerate a wide range of amyloidogenic sequences and their applications in inhibition of amyloid aggregation and detoxification of amyloid β-peptide aggregates associated with Alzheimer's disease. The project of amyloid β-sheet mimics started with the dream of developing a chemical model of protein β-sheets that could accommodate any amino acid sequence and still fold into β-sheet structures. With this goal in mind, I set out to modify the chemical models which had been developed by our group. (For structures of the introduced chemical models, see **2.4** in chapter 2 and **4.1** in chapter 4.)

My new macrocycles **2.1**, although similar to the others that the Nowick group had introduced, proved especially valuable, because the small changes I had introduced made a big difference in its tolerance for a variety of amino acid sequesnces. James and I decided to further investigate the new macrocycle with amyloidogenic sequences (amyloid β-sheet mimics, ABSMs) from amyloids because of their diversity in the amino acid sequence and their importance in many human diseases. We also envisioned that ABSMs are potential inhibitors of amyloid aggregation and can provide insights into amyloid oligomers and aggregation.

In my studies, I had the opportunities to collaborate with Drs. C. Liu and M. Zhao of the Eisenberg group. They provided X-ray crystallographic and biological tools to study ABSMs. Drs. Liu and Zhao grew the crystal and solved the structure of ABSM **2.1r**.

Dr. Liu especially helped study the effect of ABSMs on amyloid-β peptide (1-42) and β_2 microglobulin aggregation and Dr. Zhao helped study the effect of ABSMs on α-synnulein aggregation. Dr. Liu helped study the toxicity of ABSMs **2.1a**, **2.1m**, and **2.1o** towards cells. With a close collaboration, we further gained more understanding about ABSMs. This chapter reports the structural studies of ABSMs, their effect upon amyloid aggregation and toxicity, and the insights into the amyloid oligomers.

Introduction

Amyloid aggregation is associated with many intractable protein aggregation diseases, notably including Alzheimer's disease, Huntington's disease, Parkinson's disease, type II diabetes, and prion diseases.[1] Amyloid fibrils with characteristic highly ordered cross-β structures are the ultimate products of amyloid aggregation. More than 30 proteins have been linked to amyloidogenesis and they exhibit enormous variations in sequences and polymorphic fibril structures.[1,2] Fibril formation of a given polypeptide, however, greatly depends on its specific residue order.[3] Crystallographic structures of amyloidlike fibrils formed by amyloidogenic peptide fragments suggest that the formation of highly-ordered parallel or antiparallel β-sheets and a steric-zipper interface between β-sheets are two essential elements for amyloid fibril formation.[4]

While amyloid fibrils are the most visible evidence of pathology, soluble oligomers are proving to be more important in amyloid toxicity.[5] Although increasing evidence shows that these transient, unstable structures are rich in β-sheets, their dynamic and polymorphic properties make amyloid oligomers difficult to study at the atomic level.[6] Additional tools are needed to study amyloid oligomers and aggregation and to shed light on controlling these processes.

β-Sheet mimics that can display amyloid β-strands provide a means to study amyloid oligomers and aggregation. We previously introduced 42-membered ring macrocyclic β-sheets containing pentapeptide fragments from amyloid-β peptide (Aβ) and tau protein (Tau) to mimic amyloidlike β-sheets and shed a light on the structures of transient amyloid oligomers.[7] We have also used these macrocyclic β-sheets to inhibit

aggregation of the peptide Ac-VQIVYK-NH_2 (AcPHF6) derived from Tau to provide insights into the aggregation process.[8]

The development of a robust chemical model of β-sheets that can tolerate a variety of amino acid sequences has been challenging because amyloidogenic sequences vary enormously and because folding of β-sheet mimics largely depends on the amino acid sequence.[1,9] In this chapter, we introduce a new class of β-sheet macrocycles that can tolerate a wide range of amino acid sequences from amyloid proteins and still fold into β-sheet structures. We call these macrocycles amyloid β-sheet mimics (ABSMs).

ABSM **2.1** is a 54-membered ring and comprises a heptapeptide β-strand (the upper strand), one Hao unit flanked by two dipeptides (the lower strand), and two δ-linked ornithine ($^{\delta}$Orn) turns (Figure 2.1a). The "upper" β-strand of ABSM **2.1** incorporates different heptapeptide fragments from Aβ, Tau, yeast Sup35 prion protein (Sup35), human prion protein (hPrP), human β_2-microglobulin (hβ_2M), human α-synuclein (hαSyn), and human islet amyloid polypeptide (hIAPP). Hao is a tripeptide β-strand mimic that not only serves as a template for *intra*molecular hydrogen bonding but also minimizes the exposed hydrogen-bonding functionality of the "lower" strand.[10] This structural design of Hao helps prevent ABSMs **2.1** from aggregating in solution to form an infinite network of β-sheets; instead, ABSMs **2.1** dimerize and then further self-assemble into oligomers. The "upper" and "lower" strands of ABSM **2.1** are connected by two $^{\delta}$Orn β-turn mimics.[11]

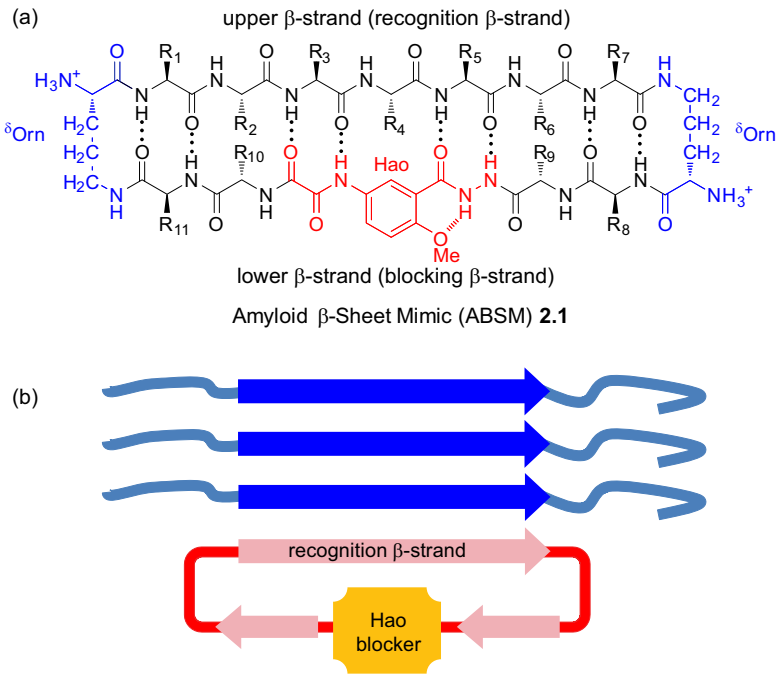

Figure 2.1. Design of amyloid β-sheet mimic **2.1**. (a) Representation of ABSM **2.1** illustrating the upper β-strand (recognition β-strand), the δ-linked ornithine ($^{\delta}$Orn) turn unit, and the Hao amino acid blocker unit. (b) Representation of ABSM **2.1** recognizing and blocking amyloid aggregation through β-sheet interactions.

We envisioned that ABSM **2.1** would fold well because it is conformationally constrained by cyclicity and has a Hao template to promote *intra*molecular hydrogen bonding and two $^{\delta}$Orn β-turn mimics to promote turn formation. We also envisioned that four pairs of side chains (R_1-R_{11}, R_2-R_{10}, R_6-R_9, and R_7-R_8) would provide stabilizing transannular interactions. We anticipated that the flexibility of the dipeptides flanking Hao in the "lower" strand would better accommodate the flatness of the Hao template and thus minimize the kinks in the β-strands that we had previously observed in the 42-membered ring macrocycles.[7]

We designed ABSMs **2.1** to display exposed heptapeptide β-strands so that these β-strands can recognize and bind their parent amyloid proteins (Figure 2.1b). We

envisioned recognition between ABSMs **1** and their parent amyloid proteins to take place through the β-sheet interactions observed in amyloid aggregation.

Here, we present structural studies of these ABSMs **2.1** and describe their effect upon amyloid aggregation and toxicity.

Results

1. Design of Amyloid β-Sheet Mimics 2.1. To test the folding of ABSMs **2.1**, we selected 16 amyloidogenic heptapeptide β-strands from seven β-sheet-rich amyloid proteins for positions 1–7 in the "upper" strands (Table 2.1). ABSMs **2.1a-g** contain heptapeptide sequences from two important hydrophobic and fibril-forming regions of Aβ associated with Alzheimer's disease, residues 16–23 and 29–40.[2,12] ABSMs **2.1a-d** and **2.1f** contain native heptapeptide sequences, while ABSMs **2.1e** and **2.1g** are G33F and G37F mutants, in which the aromatic residue across from Hao promotes better folding.[7] ABSM **2.1h** contains residues 7–13 from Sup35, which has been widely used as a model to study amyloid formation.[4] ABSM **2.1i** contains residues 116–122 from hPrP, which is the infectious agent of prion diseases.[13] ABSM **2.1j** contains residues 305–311 from Tau, which forms neurofibrillary tangles.[14] ABSMs **2.1k-m** contain residues 62–68 and 63–69 from hβ_2M associated with dialysis-related amyloidosis.[15] ABSMs **2.1n** and **2.1o** contain residues 69–75 and 75–81 from hαSyn associated with Parkinson's disease.[16] ABSMs **2.1p** and **2.1q** contain residues 11–17 and 26–32 from hIAPP associated with type II diabetes.[17] We chose polar and hydrophobic residues at positions 8–11 in the "lower" strands of ABSMs **2.1** to promote solubility in water and to increase hydrophobic residues that favor β-sheet formation.

Table 2.1. Amino Acid Sequences of ABSMs **2.1**

	Sequence	R_1–R_7	R_8–R_{11}
2.1a	$A\beta_{16\text{-}22}$	KLVFFAE	KLIE
2.1b	$A\beta_{17\text{-}23}$	LVFFAED	KLIE
2.1c	$A\beta_{29\text{-}35}$	GAIIGLM	KFYK
2.1d	$A\beta_{30\text{-}36}$	AIIGLMV	KFYK
2.1e	$A\beta_{30\text{-}36}$ G33F	AIIFLMV	KFYK
2.1f	$A\beta_{34\text{-}40}$	LMVGGVV	KFYK
2.1g	$A\beta_{34\text{-}40}$ G37F	LMVFGVV	KFYK
2.1h	$Sup35_{7\text{-}13}$	GQQNNQY	KFYK
2.1i	$hPrP_{116\text{-}122}$	AAAGAVV	KFYK
2.1j	$Tau_{305\text{-}311}$	SVQIVYK	EFYK
2.1k	$h\beta_2M_{62\text{-}68}$	FYLLYYT	KNSA
2.1l	$h\beta_2M_{63\text{-}69}$	YLLYYTE	FKVS
2.1m	$h\beta_2M_{63\text{-}69}$	YLLYYTE	KVVK
2.1n	$h\alpha Syn_{69\text{-}75}$	AVVTGVT	KFYV
2.1o	$h\alpha Syn_{75\text{-}81}$	TAVANKT	VFYK
2.1p	$hIAPP_{11\text{-}17}$	RLANFLV	KFYK
2.1q	$hIAPP_{26\text{-}32}$	ILSSTNV	KFYK
2.1r	$A\beta_{30\text{-}36}$	AIIGLMV	$KFF^{Br}K$

2. Synthesis of Amyloid β-Sheet Mimics 2.1. ABSMs **2.1** were prepared by synthesizing the corresponding protected linear peptides **2.2**, followed by solution-phase cyclization and deprotection.[18] The protected linear peptide precursors were synthesized on 2-chlorotrityl chloride resin by conventional Fmoc-based solid-phase peptide synthesis. Macrocyclization was typically performed using HCTU and *N*,*N*-diisopropylethylamine in DMF at ca. 0.5 mM concentration to produce protected cyclized peptides **2.3**. The cyclization condition used here efficiently avoids problematic epimerization because the C-terminus of the protected linear peptide comprises an α-amino acid carbamate (Boc-NH-CHR-COOH). Final deprotection was carried out with TFA solution. The ABSMs **2.1** were isolated in ca. 20–30% overall yield after HPLC purification and lyophilization. Each synthesis produces tens of milligrams of ABSMs **2.1** as fluffy white solids.

Scheme 2.1 Synthesis of ABSMs **2.1**

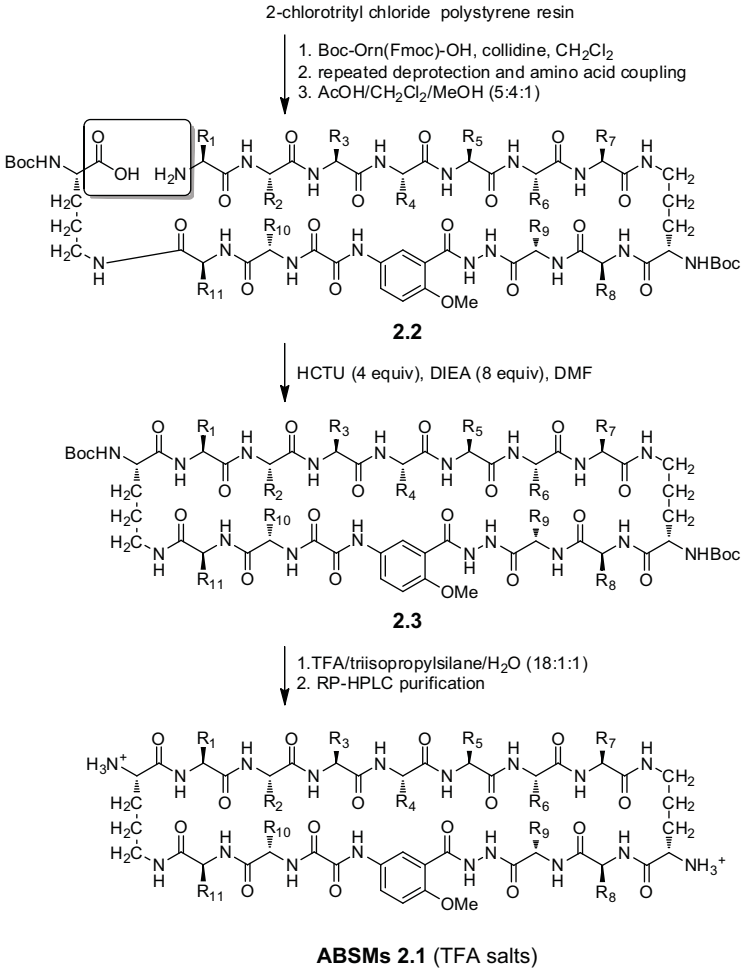

ABSMs 2.1 (TFA salts)

3. X-Ray Crystallographic Studies of Amyloid β-Sheet Mimic 2.1r. X-ray crystallography of ABSM **2.1r** validates the design of ABSMs **1** (Figure 2.2). ABSM **2.1r** is a homologue of ABSM **2.1d** in which the Tyr residue in the "lower" strand is replaced with 4-bromophenylalanine for crystallographic phase determination. ABSM **2.1r** adopts a β-sheet structure in which the "upper" and "lower" strands are *intra*molecularly hydrogen-bonded to form eight hydrogen bonds (Figure 2.2a). The two $^{\delta}$Orn residues of ABSM **2.1r** fold into β-turnlike conformations, Hao mimics a tripeptide β-strand, and the "upper" strand displays an exposed heptapeptide β-sheet edge.

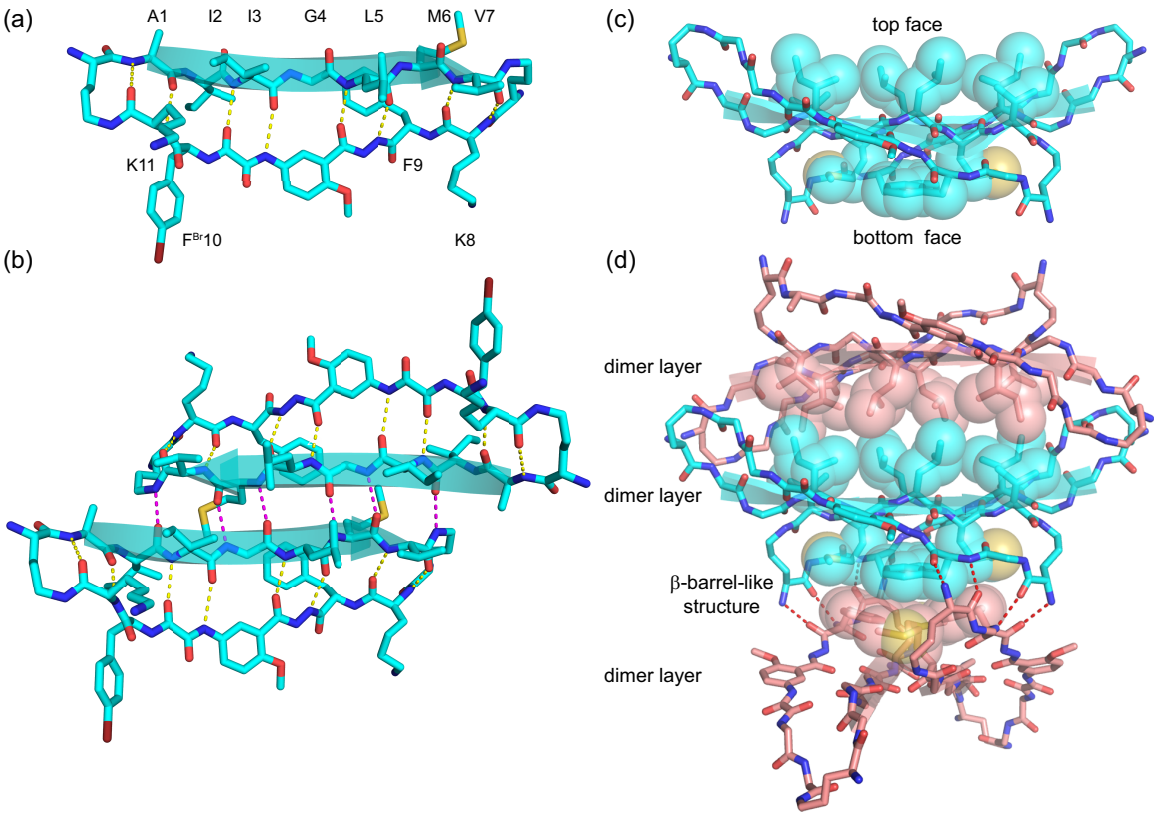

Figure 2.2. X-ray crystallographic structure of ABSM **2.1r**, which contains the heptapeptide sequence AIIGLMV ($A\beta_{30\text{-}36}$). (a) The monomer. (b) The dimer: top view. Intermolecular hydrogen bonds are shown in magenta; intramolecular hydrogen bonds are shown in yellow. (c) The dimer: side view. (d) Stacked layers of dimer in the crystal lattice. Intermolecular hydrogen bonds are shown in red. Note that the view in b is perpendicular to the β-sheet (top view), whereas the view in c and d is 90° away, parallel to the β-sheet (side view) and shows the hydrophobic contacts. Some side chains in c and d have been omitted for clarity.

ABSM **2.1r** forms a dimer in the crystal lattice in which the two recognition β-strands come together in an antiparallel β-sheet fashion (Figure 2.2b). The β-strands of the dimerization interface are shifted out of register, forming only six hydrogen bonds instead of the eight that would form through in-register contact.

The dimers stack in the crystal lattice, with hydrophobic contacts and hydrogen bonds between the layers of the stack. The Ile, Leu, and Val, at positions 3, 5, and 7 on the "top" face of the dimer pack together in one set of hydrophobic contacts "above" the

dimer (Figures 2.2c and 2.2d). The Met and Phe at positions 6 and 9 on the "bottom" face of the dimer pack together in another set of hydrophobic contacts "below" the dimer and make up the hydrophobic core of a β-barrel-like structure, whose “staves” are held together by four hydrogen bonds between the Lys and Phe at positions 8 and 9 on the front and symmetrical hydrogen bonds on the back(Figure 2.2d).The hydrophobic contacts and hydrogen bonds between the dimer layers appear to be important in the crystallization and supramolecular assembly of ABSM **2.1r** and may explain the formation of the out-of-register interface within the dimer.

4. ^{1}H NMR Studies of Amyloid β-Sheet Mimics 2.1. ^{1}H NMR studies of ABSMs **2.1a-q** in D_2O solution further validate the design of ABSMs **2.1** and establish that ABSMs **2.1** generally adopt folded β-sheet structures in solution. The ^{1}H NMR spectra of ABSMs **2.1** show sharp, disperse resonances at submillimolar and low millimolar concentrations in D_2O solution, suggesting ABSMs **2.1** to be non-aggregating in water. Antiparallel β-sheets have close contacts between the α-protons of the non-hydrogen-bonded pairs of amino acids, which generally give strong *inter*strand NOE cross-peaks (NOEs). In ABSMs **2.1**, these close contacts should involve the α-protons of residues 2 and 10 (2-10) and residues 6 and 9 (6-9). There should also be homologous contacts involving the α-proton of residue 4 and H_6 of Hao (4-Hao$_6$) and the α- and *pro-S* δ-protons of the $^{\delta}$Orn turns (Orn$_{\alpha\text{-}\delta S}$). Table 2.2 illustrates these contacts.

Table 2.2. Key NOEs of ABSMs **2.1a-q** in D_2O.

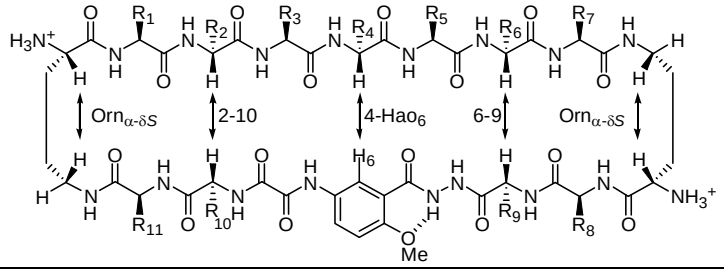

	Orn$_{\alpha\text{-}\delta S}$	2-10	4-Hao$_6$	6-9	Orn$_{\alpha\text{-}\delta S}$	Folding
2.1a	S[a]	—[b]	S	S	S	good
2.1b	S	S	S	S	S	good
2.1c	S	S	S	S	S	good
2.1d	S	S	S	S	S	good
2.1e	S	S	S	S	S	good
2.1f	S	S	W[a]	—[c]	S	moderate
2.1g	S	S	S	S	S	good
2.1h	W	—[c]	—[c]	—[c]	W	poor
2.1i	W	W	—[c]	—[c]	W	poor
2.1j	S	S	S	S	S	good
2.1k	S	S	S	—[b]	S	good
2.1l	W	—[c]	—[c]	—[c]	W	poor
2.1m	S	—[d]	S	—[d]	S	good
2.1n	S	S	S	—[d]	S	good
2.1o	S	S	S	—[d]	S	good
2.1p	S	S	S	S	S	good
2.1q	S	S	S	S	S	good

a. S: strong NOE; W: weak NOE.
b. NOE not observed due to overlap of proton resonances.
c. NOE not observed.
d. NOE not able to be observed due to overlap with HOD.

All ABSMs, except **2.1h**, **2.1i**, and **2.1l**, exhibit most of these key NOEs (Table 2.2). ABSMs **2.1a-e**, **2.1g**, **2.1j**, **2.1k**, and **2.1m-q** show strong 2-10, 6-9, 4-Hao$_6$, and Orn$_{\alpha\text{-}\delta S}$ NOEs and thus exhibit good folding. ABSM **2.1f** shows strong Orn$_{\alpha\text{-}\delta S}$ and 2-10 NOEs and a weak 4-Hao$_6$ NOE and thus exhibits moderate folding. ABSMs **2.1h**, **2.1i**, and **2.1l** show only Orn$_{\alpha\text{-}\delta S}$ NOEs and thus exhibit weak folding. Although the lack of the *inter*strand NOEs indicates poor folding of ABSMs **2.1h**, **2.1i**, and **2.1l**, the Orn$_{\alpha\text{-}\delta S}$ NOEs

suggest that their $^{\delta}$Orn residues fold at least partially into a β-turnlike conformation. Table 2.2 summarizes the observed key NOEs and the folding of ABSMs **2.1**.

The magnetic anisotropy of the $^{\delta}$Orn turns of **2.1** provides an additional indicator of β-sheet folding. When ABSMs **2.1** fold into well-defined β-sheets, their $^{\delta}$Orn turns fold into β-turn-like structures and exhibit a value of ca. 0.6 ppm magnetic anisotropy in water. The $\Delta\delta^{\delta}$Orn values of **2.1a**, **2.1b**, **2.1e**, **2.1g**, **2.1j**, **2.1m**, and **2.1p** are greater than 0.5 ppm, suggesting they fold well. ABSMs **2.1h** and **2.1i** exhibit $\Delta\delta^{\delta}$Orn values of 0.23 and 0.13 ppm, suggesting they fold poorly, and **2.1f** exhibits a $\Delta\delta^{\delta}$Orn value of 0.3, suggesting its moderate folding. The folding of ABSMs through the $\Delta\delta^{\delta}$Orn values is consistent with that through the NOE studies. Although the $\Delta\delta^{\delta}$Orn values of **2.1c**, **2.1d**, **2.1k**, **2.1l**, **2.1n**, **2.1o**, and **2.1q** suggest moderate or poor folding, their strong *inter*strand NOEs indicate that they do indeed fold into β-sheet structures. Table 2.3 summarizes these average $\Delta\delta^{\delta}$Orn values of ABSMs **2.1a-q**.

Table 2.3. Average $\Delta\delta^{\delta}$Orn Values of ABSMs **2.1a-q** in D_2O at 298 K.

	$\Delta\delta^{\delta}$Orn	$\Delta\delta^{\delta}$Orn	Average
2.1a	0.65	0.51	0.58
2.1b	0.61	0.41	0.51
2.1c	0.40	0.28	0.34
2.1d	0.39	0.4	0.40
2.1e	0.64	0.53	0.59
2.1f	0.40	0.19	0.30
2.1g	0.59	0.62	0.61
2.1h	0.25	0.21	0.23
2.1i	0.15	0.11	0.13
2.1j	0.56	0.58	0.57
2.1k	0.15	0.32	0.24
2.1l	0.32	0.46	0.39
2.1m	0.59	0.44	0.52
2.1n	0.44	0.18	0.31
2.1o	0.30	0.11	0.21
2.1p	0.47	0.53	0.50
2.1q	0.34	0.15	0.25

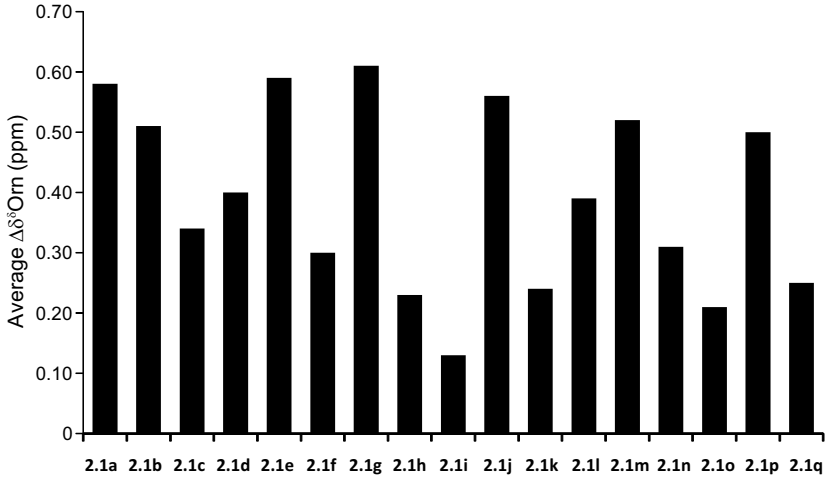

5. Inhibition of Amyloid Aggregation by Amyloid β-Sheet Mimics 2.1.

Thioflavin T (ThT) fluorescence assays and transmission electron microscopy (TEM) studies show that the ABSMs containing amyloidogenic sequences can inhibit aggregation of amyloid proteins. We studied inhibition of $A\beta_{40}$ and $A\beta_{42}$ aggregation by ABSM **2.1a**, inhibition of $h\beta_2M$ aggregation by ABSM **2.1m**, and inhibition of truncated human α-synuclein ($h\alpha Syn_{1\text{-}100}$) aggregation by ABSM **2.1o**.

ThT fluorescence assays show that ABSMs **2.1a**, **2.1m**, and **2.1o** effectively delay aggregation of their parent proteins at sub-stoichiometric concentrations in a dose-dependent manner (Figures 2.3-2.8). ABSM **2.1a** delays $A\beta_{40}$ and $A\beta_{42}$ aggregation by 280% and 350% respectively at 0.2 equivalents and by 430% and 600% at 0.5 equivalents (Figures 2.3a and 2.3b). Although ThT fluorescence assays show that Aβ aggregation exhibits comparable lag times at 0.5 and 1.0 equivalents of ABSM **2.1a**, the growth phases of the aggregation are much slower at 1.0 equivalent than at 0.5 equivalents. TEM studies of samples taken directly from the ThT assays show that Aβ forms fibrils without ABSMs and do not form fibrils with ABSMs (1.0 equivalent) during the delayed lag time (Figures 2.3c and 2.3d).

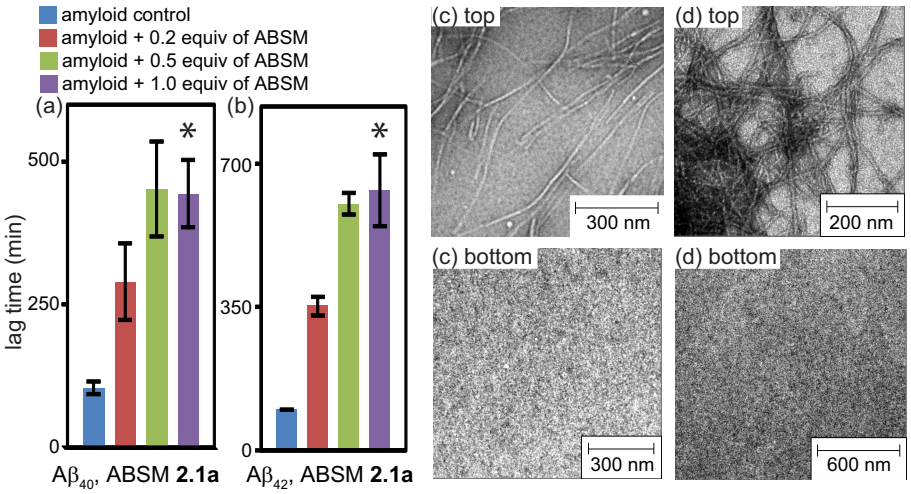

Figure 2.3. Effect of ABSMs on inhibition of $A\beta_{40}$ and $A\beta_{42}$ aggregation monitored by thioflavin T fluorescence assays and transmission electron microscopy. (a) Lag time of $A\beta_{40}$ (20 μM) aggregation in the absence and presence of ABSM **2.1a**. (b) Lag time of $A\beta_{42}$ (20 μM) aggregation in the absence and presence of ABSM **2.1a**. (c) TEM of $A\beta_{40}$ (20 μM) after incubation for 6 h without ABSM **2.1a** (top) and incubation for 6 h with 1.0 equivalent of ABSM **2.1a** (bottom). (d) TEM of $A\beta_{42}$ (20 μM) after incubation for 7 h without ABSM **1a** (top) and incubation for 7 h with 1.0 equivalent of ABSM **2.1a** (bottom). * For explanation, see the text and Figures 2.4 and 2.5. For experimental details, see the experimental section.

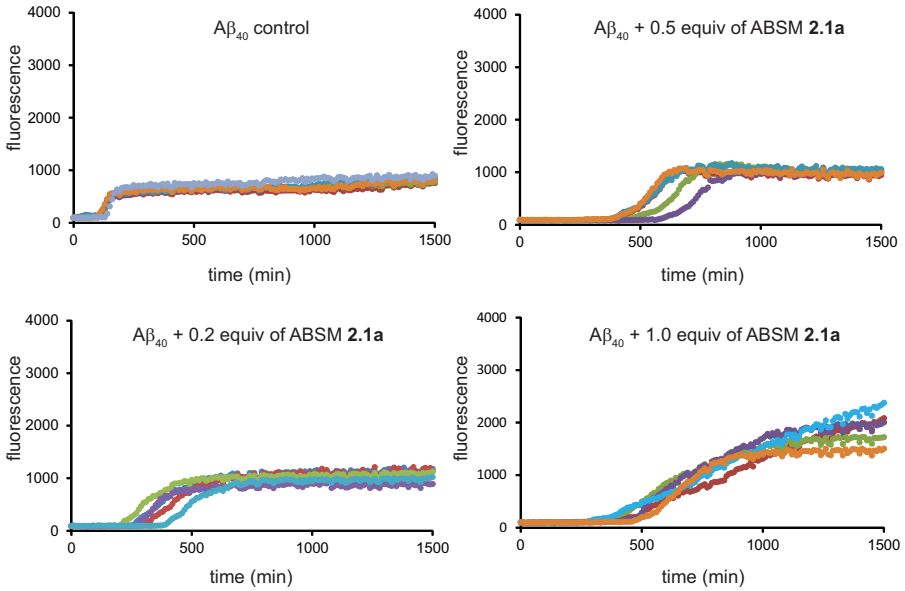

Figure 2.4. Effect of ABSM **2.1a** on inhibition of $A\beta_{40}$ aggregation monitored by ThT fluorescence assay. Different color data points correspond to data from multiple experiments run under identical conditions in the same plate.

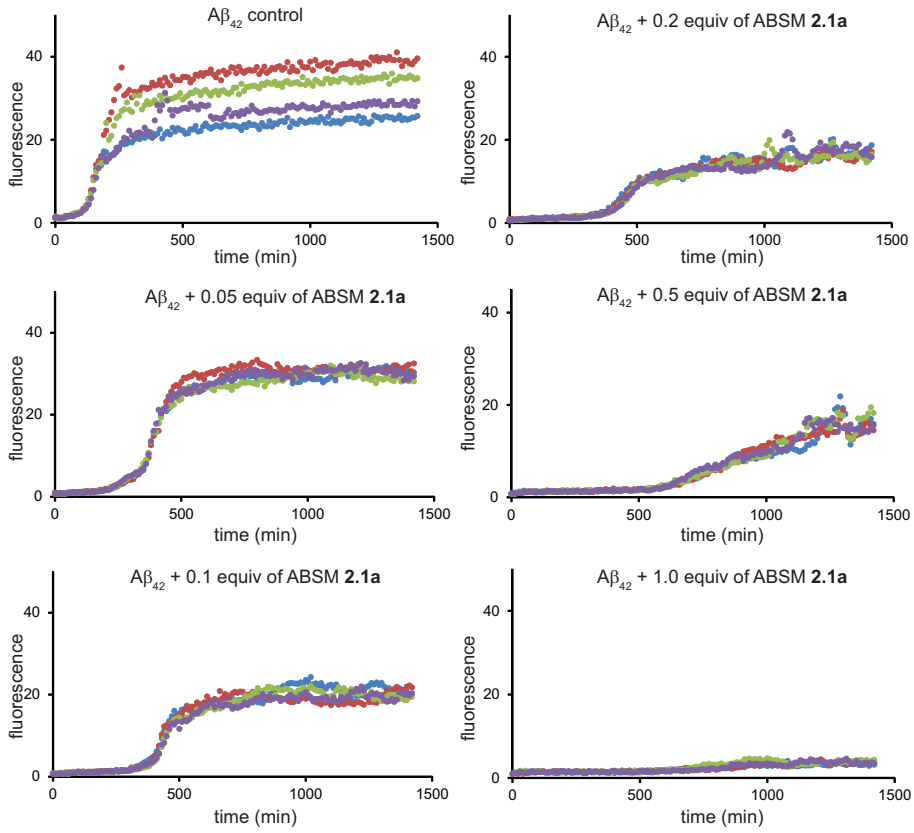

Figure 2.5. Effect of ABSM **2.1a** on inhibition of $A\beta_{42}$ aggregation monitored by ThT fluorescence assay. Different color data points correspond to data from multiple experiments run under identical conditions in the same plate.

ABSM **2.1m** delays $h\beta_2M$ aggregation by 160% at 0.2 and 0.5 equivalents and by 340% at 1.0 equivalent (Figure 2.6a). ABSM **2.1o** delays $h\alpha Syn_{1\text{-}100}$ aggregation by 150% at 0.2 equivalents (Figure 2.6b). Although $h\alpha Syn_{1\text{-}100}$ aggregation exhibits longer lag times with 0.5 and 1.0 equivalents of ABSM **2.1o** than with 0.2 equivalents, some runs showed complete suppression of aggregation, while other runs showed typical sigmoidal curves. Because of this scatter in the data, the precise lag times are not reported. (* in Figure 2.6b. For details, see Figure 2.8.) TEM studies of samples taken directly from the ThT assays show that $h\beta_2M$ and $h\alpha Syn_{1\text{-}100}$ form fibrils without ABSMs and do not form fibrils with ABSMs (1.0 equivalent) during the delayed lag time (Figures 2.6c and 2.6d).

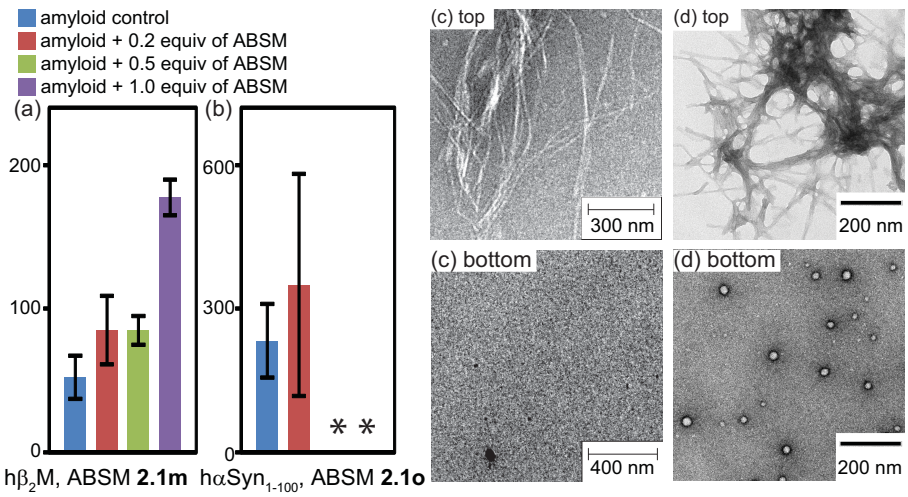

Figure 2.6. Effect of ABSMs on inhibition of hβ$_2$M and hαSyn$_{1\text{-}100}$ aggregation monitored by thioflavin T fluorescence assays and transmission electron microscopy. (a) Lag time of hβ$_2$M (30 μM) aggregation in the absence and presence of ABSM **2.1m**. (b) Lag time of hαSyn$_{1\text{-}100}$ (50 μM) aggregation in the absence and presence of ABSM **2.1o**. (c) TEM of hβ$_2$M (30 μM) after incubation for 2 h without ABSM **2.1m** (top) and incubation for 2 h with 1.0 equivalent of ABSM **2.1m** (bottom). (d) TEM of hαSyn$_{1\text{-}100}$ (50 μM) after incubation for 72 h without ABSM **2.1o** (top) and incubation for 72 h with 1.0 equivalent of ABSM **2.1o** (bottom). * For explanation, see the text and Figures 2.8. For experimental details, see the experimental section.

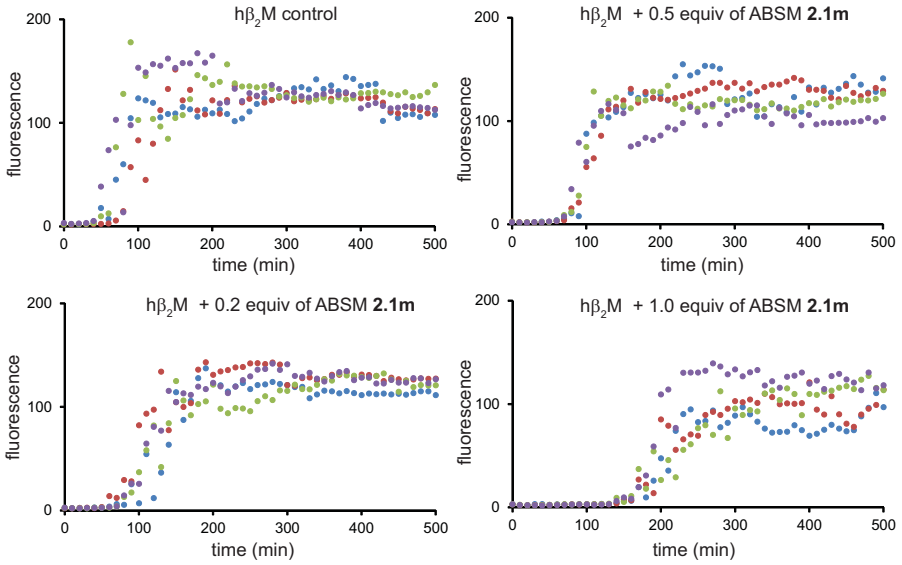

Figure 2.7. Effect of ABSM **2.1m** on inhibition of hβ$_2$M aggregation monitored by ThT fluorescence assay. Different color data points correspond to data from multiple experiments run under identical conditions in the same plate.

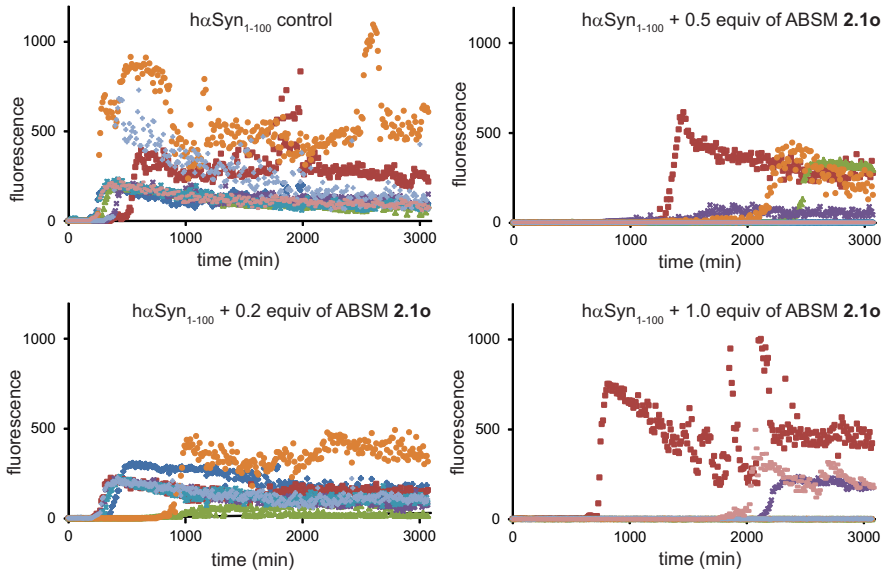

Figure 2.8. Effect of ABSM **2.1o** on inhibition of hαSyn$_{1\text{-}100}$ aggregation monitored by ThT fluorescence assay. Different color data points correspond to data from multiple experiments run under identical conditions in the same plate.

6. Cross-Interaction between Aβ and ABSMs 2.1m and 2.1o. Aβ has been shown to cross-interact with different amyloidogenic proteins containing similar primary sequences.[19] To investigate the cross-interaction of Aβ with ABSMs, we compared interaction of Aβ with ABSM **2.1a** to that with ABSM **2.1m** and to ABSM **2.1o**. ABSMs **2.1m** and **2.1a** have closely homologous sequences in which residues at positions 2, 7, and 8 are identical and residues at positions 3, 4, 5, 9, and 10 are similar, while ABSM **2.1o** and **2.1a** do not (Figure 2.9). These similarities and differences raised the intriguing possibility different cross-interactions of ABSMs **2.1m** and **2.1o** with Aβ.

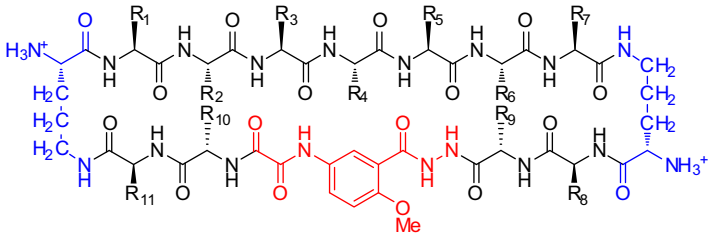

ABSM	R_1	R_2	R_3	R_4	R_5	R_6	R_7	R_8	R_9	R_{10}	R_{11}
2.1a	K	L	V	F	F	A	E	K	L	I	E
2.1m	Y	L	L	Y	Y	T	E	K	V	V	K
2.1o	T	A	V	A	N	K	T	V	F	Y	K

Figure 2.9. Sequence comparison among ABSMs **2.1a**, **2.1m**, and **2.1o**. Identical residues among ABSM **2.1a** and **2.1m** are highlighted in red and similar residues are highlighted in green.

ThT fluorescence assays show that ABSM **2.1m**, like ABSM **2.1a**, inhibits Aβ aggregation, while ABSM **2.1o** has little or no inhibitory effect (Figure 2.10a). Although ABSM **2.1a** and **2.1m** delay Aβ aggregation in a dose-dependent manner (Figures 2.4 and 2.10b), ABSM **2.1a** is more effective at lower doses. ABSM **2.1a** delays $A\beta_{40}$ aggregation by 280% and 430% at 0.2 and 0.5 equivalents respectively (Figures 2.4), while ABSM **2.1m** shows little or no inhibition at 0.2 equivalents and delays $A\beta_{40}$

aggregation by 240% at 0.5 equivalents. ABSM **2.1a** delays $A\beta_{40}$ aggregation by 430% at 1 equivalent, while ABSM **2.1m** delays by 900%, which indicates that ABSM **2.1m** is more effective at higher doses. ThT fluorescence assays also show that ABSM **2.1m** effectively delays $A\beta_{42}$ aggregation, while ABSM **2.1o** causes little or no inhibition (Figure 2.10c). These results suggest that structurally homologous ABSMs can not only interact with their parent amyloid proteins but can also cross interact with different amyloid proteins.

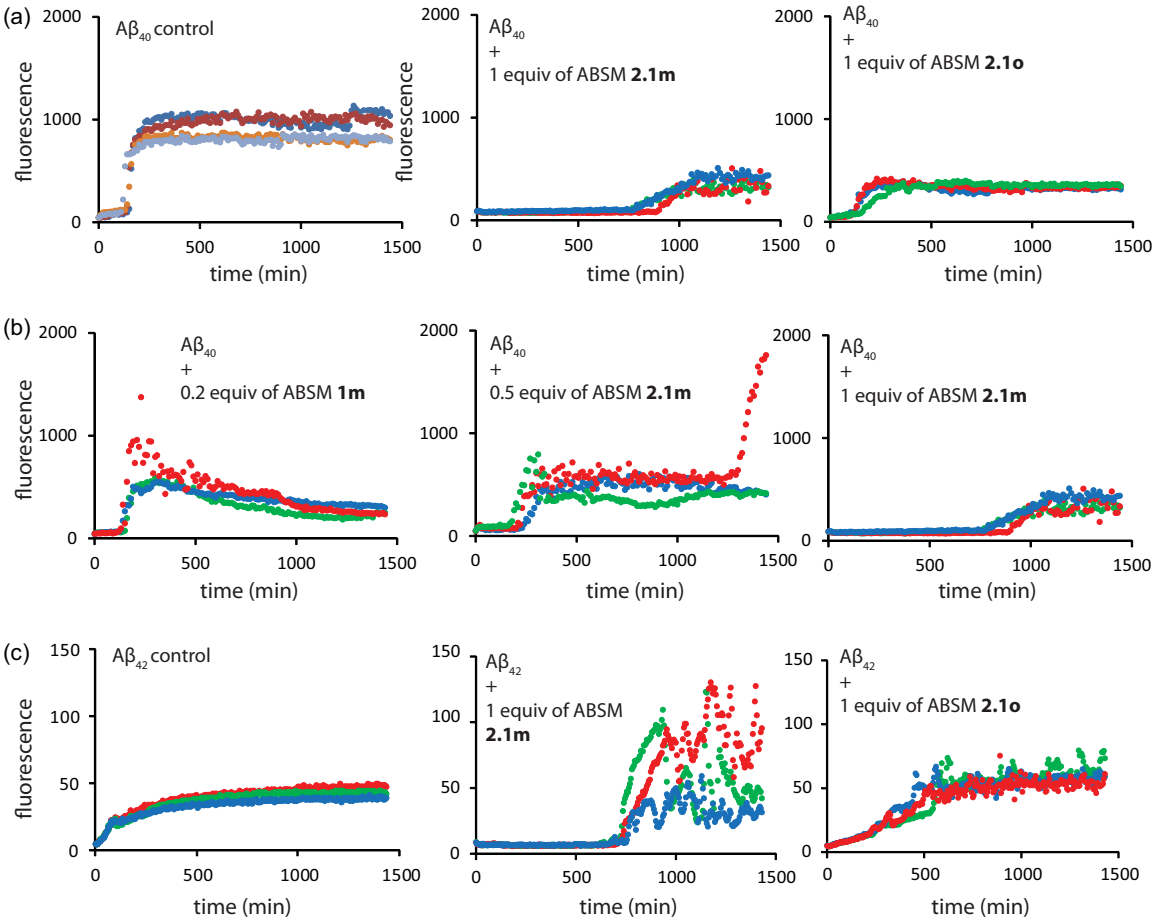

Figure 2.10. (a) Effect of ABSMs **2.1m** and **2.1o** on inhibition of $A\beta_{40}$ aggregation monitored by ThT fluorescence assay. (b) Dose-dependent inhibition of ABSM **2.1m** on Aβ aggregation. (c) Effect of ABSMs **2.1m** and **2.1o** on inhibition of $A\beta_{42}$ aggregation monitored by ThT fluorescence assay. Different color data points correspond to data from multiple experiments run under identical conditions in the same plate.

7. Interaction between Aβ and ABSMs 2.1b, 2.1c, 2.1d, and 2.1f. To investigate the effect of heptapeptide sequences within ABSMs **2.1** derived from $A\beta_{16–23}$ and $A\beta_{29–40}$ on interaction with Aβ, we compared the interaction of $A\beta_{40}$ with ABSMs **2.1b**, **2.1c**, **2.1d**, and **2.1f** to that with ABSM **2.1a**. ThT fluorescence assays show that ABSM **2.1b**, like ABSM **2.1a**, is effective against $A\beta_{40}$ aggregation, while ABSMs **2.1c**, **2.1d**, and **2.1f** has little or no inhibitory effect (Figure 2.11). ABSM **2.1b** delays $A\beta_{40}$ aggregation by 290% at 1 equivalent, while ABSM **2.1a** delays by 430%. While ABSMs containing heptapeptide sequences from the *N*-terminal $A\beta_{16–23}$ inhibit $A\beta_{40}$ aggregation, ABSMs from the *C*-terminal $A\beta_{29–40}$ do not. ABSMs **2.1d** and **2.1f**, instead, accelerate $A\beta_{40}$ aggregation, reducing the duration of the lag phase. This acceleration by ABSM **2.1d** is reminiscent of the seeding effect in $A\beta_{40}$ aggregation.

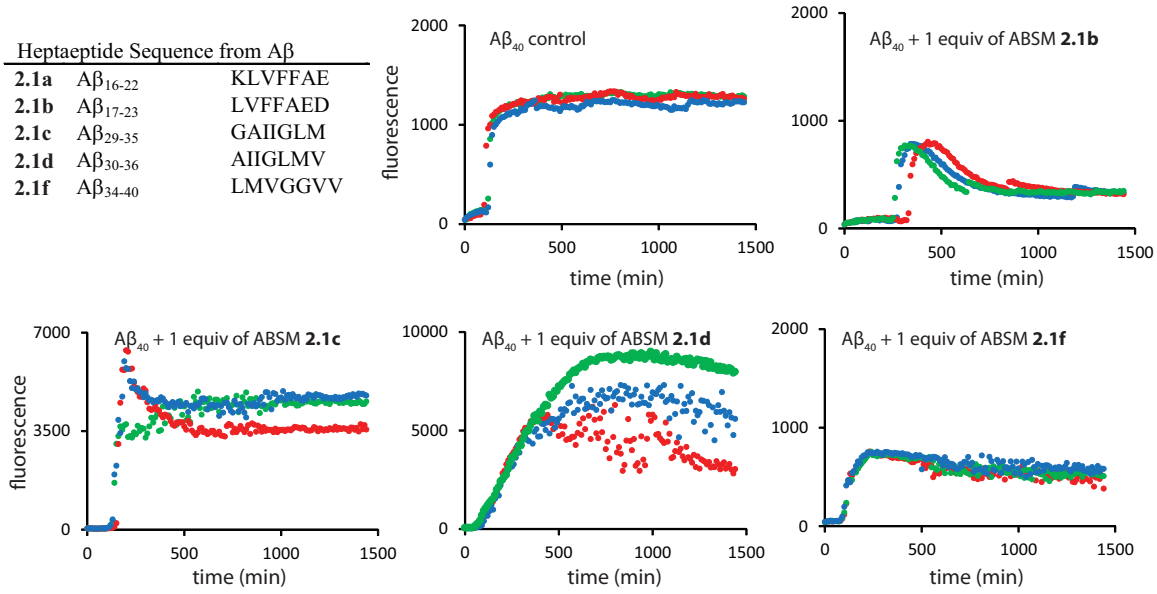

Figure 2.11. Interaction between $A\beta_{40}$ and ABSMs **2.1b**, **2.1c**, **2.1d**, and **2.1f** monitored by ThT fluorescence assay. Different color data points correspond to data from multiple experiments run under identical conditions in the same plate.

The inhibition of $A\beta_{40}$ aggregation by both ABSMs **2.1a** and **2.1b** indicates that the central hydrophobic sequence $A\beta_{17–21}$ is critical to the activity of ABSMs against $A\beta_{40}$ aggregation. This result supports the role of $A\beta_{17-21}$ in Aβ aggregation and suggests that strong interaction of this sequence in these ABSMs with that of the Aβ oligomers delays the lag phase of Aβ aggregation.[12,20]

8. Comparison of the Effect of 42- and 54-Membered Ring Macrocyclic β-Sheets on Aβ Aggregation. We previously introduced 42-membered ring macrocyclic β-sheets **2.4** that contain a pentapeptide in the upper strand. Macrocyclic β-sheets **4** encompass the left and middle portions of ABSMs **2.1** (Figure 2.12). To investigate the effect of the size of macrocyclic β-sheets on amyloid aggregation, we divided the heptapeptide $A\beta_{16-22}$ β-strand of ABSM **2.1a** into three overlapping pentapeptide sequences ($A\beta_{16-20}$, $A\beta_{17-21}$, and $A\beta_{18-22}$). We incorporated these sequences into the smaller macrocycles **2.4a-c** and compared their effect on Aβ aggregation with that of ABSM **2.1a**. We anticipated that ABSM **2.1a** should be more effective against Aβ aggregation because it displays a longer β-strand and provides bigger hydrophobic surface to interact with Aβ.

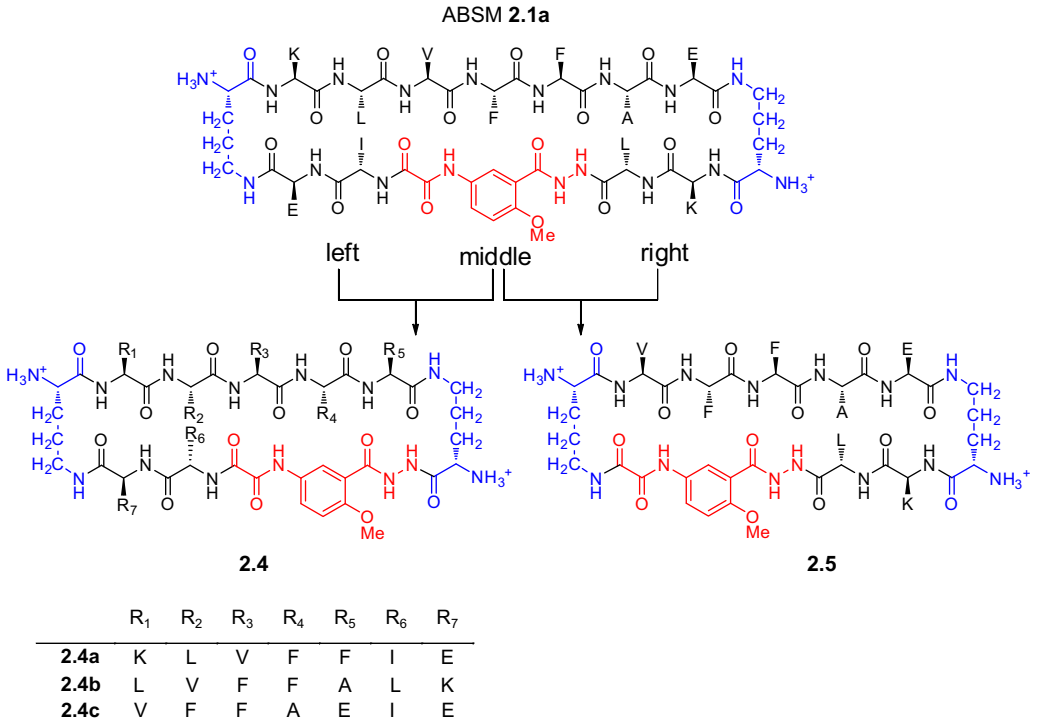

	R_1	R_2	R_3	R_4	R_5	R_6	R_7
2.4a	K	L	V	F	F	I	E
2.4b	L	V	F	F	A	L	K
2.4c	V	F	F	A	E	I	E

Figure 2.12. Structures of 42-membered ring macrocycles **2.4** and **2.5** containing pentapeptide sequences from the amyloidogenic region of Aβ, residues 16-22.

ThT fluorescence assays show that **2.4b** inhibits $A\beta_{40}$ aggregation to a much lesser extent than ABSM **2.1a**, while **2.4a** and **2.4c** have little or no inhibitory effect (Figure 2.13). To further explore the greater activity of ABSM **2.1a**, we designed and synthesized the new 42-membered ring macrocyclic β-sheet **2.5**. Macrocyclic β-sheet **2.5** encompasses the middle and right portions of ABSM **2.1a** (Figure 2.12) and contains a pentapeptide in the upper strand. We incorporated amyloidogenic pentapeptide sequence $A\beta_{18-22}$ into **2.5**. ThT fluorescence assays show that **2.5** inhibits $A\beta_{40}$ aggregation by 250% at 1 equivalent, while **2.4a**, which encompasses the left and middle portions of ABSM **2.1a**, has little or no inhibitory effect. This result indicates that the right portion of ABSM **2.1a** is crucial to its greater activity against Aβ aggregation. A direct comparison of the effects of **2.1a**, **2.4a**, and **2.5** on $A\beta_{40}$ aggregation shows that ABSM **2.1a** is more

effective against Aβ aggregation. This comparison establishes that ABSMs displaying longer β-strands and providing bigger hydrophobic surfaces are an effective design for inhibitors of amyloid aggregation.

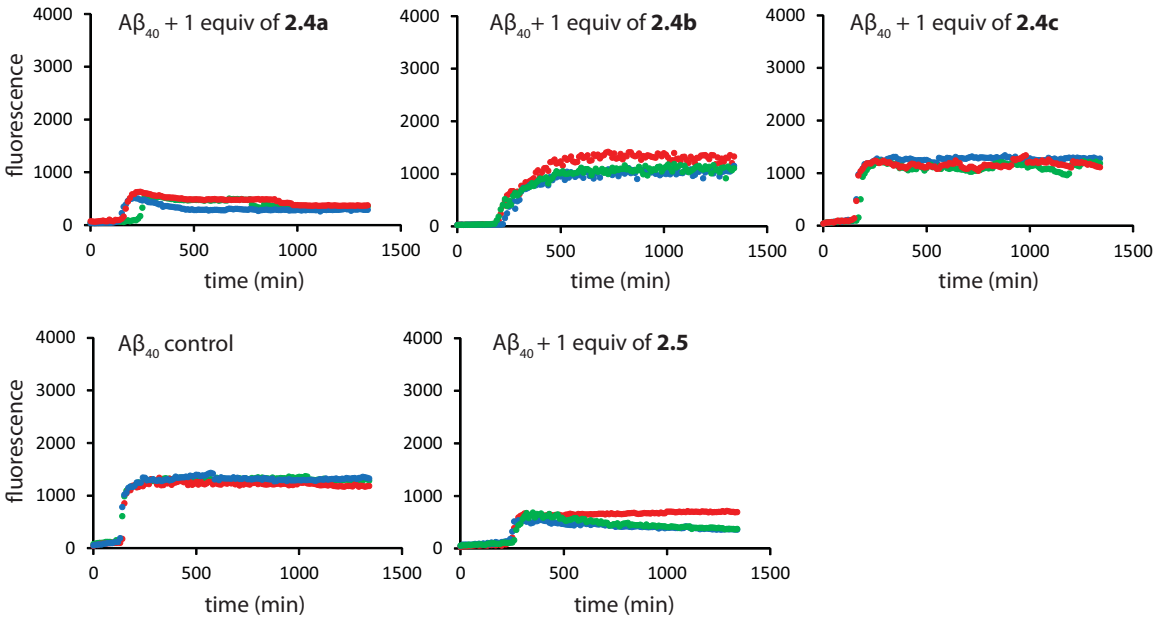

Figure 2.13. Effect of 42-membered ring macrocycles **2.4** and **2.5** containing pentapeptide sequences from the amyloidogenic region of Aβ, residues 16-22, on inhibition of $A\beta_{40}$ aggregation. Different color data points correspond to data from multiple experiments run under identical conditions in the same plate.

9. Self-Association of ABSM 2.1a. To study the self-association of ABSM **2.1a** in water, we measured diffusion coefficients (*D*) of ABSM **2.1a** at different concentrations using DOSY (diffusion-ordered spectroscopy) experiments.[21] ABSM **2.1a** exhibits a *D* value of 19.5 ± 0.2 × 10^{-11} m^2/s at concentrations up to 1.3 mM in D_2O at 298 K. This value is comparable to that which we have seen similarly sized macrocycles in the monomeric state.[22] At higher concentrations, the *D* drops precipitously: 17.8 × 10^{-11} m^2/s at 2.0 mM, 17.1× 10^{-11} m^2/s at 3.3 mM, and 15.7 × 10^{-11} m^2/s at 5.0 mM. Figure 2.14 illustrates these data. These data demonstrate that the self-association of ABSM **2.1a** is cooperative. The self-association does not involve the formation of simple dimers, or even trimers, but rather involves the formation of higher-order oligomers. The formation of these higher-order structures characteristically shows a plateau at low concentrations, followed by the onset of substantial self-association above a higher *critical* concentration, as in the *critical micelle concentration* in micellar self-association.[23] In ABSM **2.1a**, the critical concentration is approximately 1.5 mM in D_2O at 298 K.

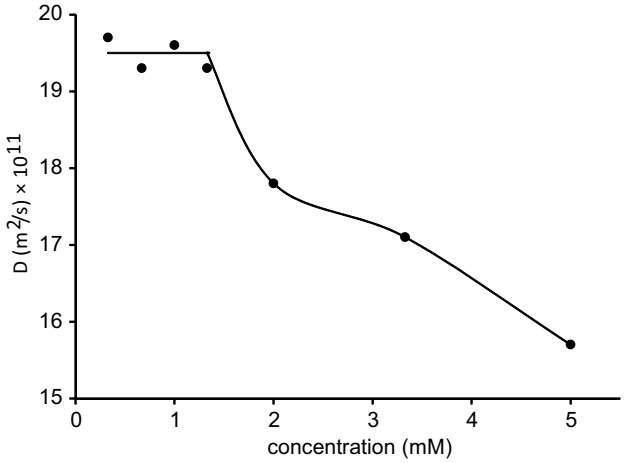

10. Detoxification of Aβ by Amyloid β-Sheet Mimic 2.1a and Lack of Toxicity of Amyloid β-Sheet Mimic 2.1a, 2.1m, and 2.1o. Cell viability (MTT) assays establish that ABSM **2.1a** reduces the toxicity of $A\beta_{40}$ and $A\beta_{42}$ in PC-12 cells (Figure 2.15a) and that ABSMs **2.1a**, **2.1m**, and **2.1o** exhibit little or no toxicity at concentrations up to 50 μM in PC-12, HeLa, and HEK-293 cells (Figure 2.15b). We examined the effect of ABSM **2.1a** on the toxicity of $A\beta_{40}$ and $A\beta_{42}$, because ABSM **2.1a** exhibits the best inhibitory activity among those studied. We first incubated Aβ monomers (5 μM) without ABSM **2.1a** to allow Aβ oligomers and fibrils to form. The resulting Aβ mixtures were directly used in cell viability assays. These assays show that the $A\beta_{40}$ and $A\beta_{42}$ preincubated without ABSM **2.1a** kills 42% and 46% of the PC-12 cells respectively, relative to controls in which the cells are incubated in only PBS buffer solutions (Figure 2.15a).

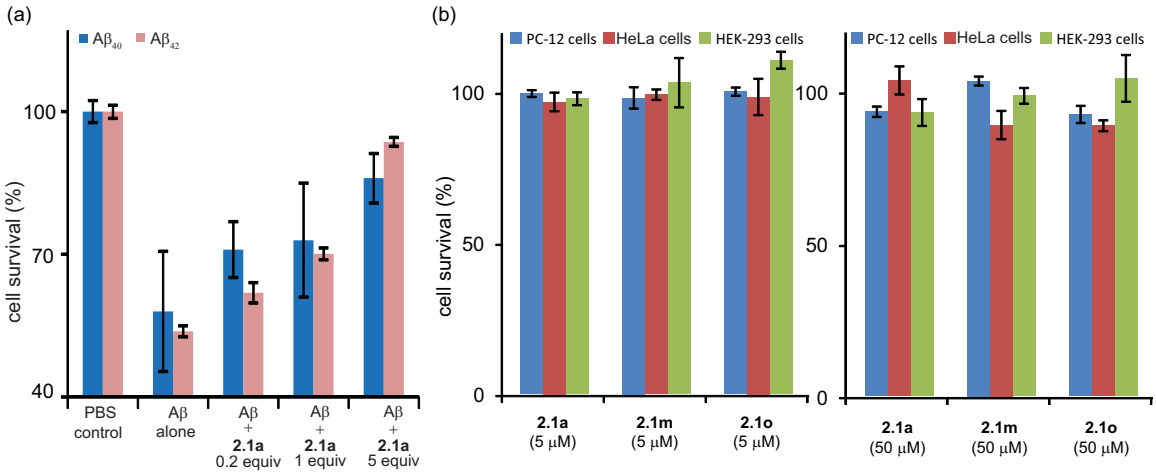

Figure 2.15. (a)Effect of ABSM **2.1a** on $A\beta_{40}$ and $A\beta_{42}$ toxicity toward PC-12 cells. Addition of Aβ decreases cell survival when PC-12 cells are cultured for 24 h with preincubated Aβ. Cell survival increases when cells are cultured for 24 h with a preincubated mixture of ABSM **2.1a** and Aβ in 0.2, 1.0, and 5 molar ratios. Cell survival is given as a percentage relative to controls in which only phosphate-buffered saline (PBS) is added. (b) Toxicity of ABSM **2.1a**, **2.1m**, and **2.1o** towards PC-12, HeLa, and HEK-293 cells. The cell survival of the PBS controls is taken to be 100%. The cell survival of the PBS controls is taken to be 100%. Error bars correspond to standard deviation of four sets of experiments. For experimental details, see the experimental section.

Cell viability assays further establish that preincubation of Aβ with ABSM **2.1a** rescues the cells in a dose-dependent manner. Preincubation of $A\beta_{40}$ and $A\beta_{42}$ with 0.2 equivalents of ABSM **2.1a** reduces the death of PC-12 to 29% and 38% respectively, while preincubation with 1.0 equivalent reduces cell death to 27% and 30% and preincubation with 5 equivalents reduces cell death to 14% and 6%. The rescue of these neuronlike cells by ABSM **2.1a** suggests that ABSMs may reduce the production of toxic amyloid oligomers or bind the oligomers and reduce their toxicity.

Discussion

Amyloid β-sheet mimics **2.1** provide a unique tool with which to elucidate the process of amyloid aggregation. Although many of the details of amyloid aggregation still remain unclear, nucleation-dependent polymerization, in which seeding to form a β-structured nucleus is the rate-determining step, is widely accepted[1, 12]. Based on the nucleation-dependent polymerization, we propose a model for the potent inhibition of Aβ aggregation by ABSM **2.1a**. In this model, ABSM **2.1a** binds early β-structured oligomers and blocks Aβ nucleation (Figure 2.16a). Without ABSM **2.1a**, the unstructured monomer forms β-structured oligomers which, in the rate-determining step, go on to form a β-structured nucleus that ultimately assembles to form cross-β fibrils. The solid line in Figure 2.16a illustrates this pathway. ABSM **2.1a** creates a new aggregation pathway for the early β-structured oligomers. In this pathway, ABSM **2.1a** binds the β-structured oligomers to form Aβ-oligomer-ABSM-**2.1a** complexes and blocks the Aβ oligomer-to-nucleus transition. The dashed line in Figure 2.16a illustrates this pathway.

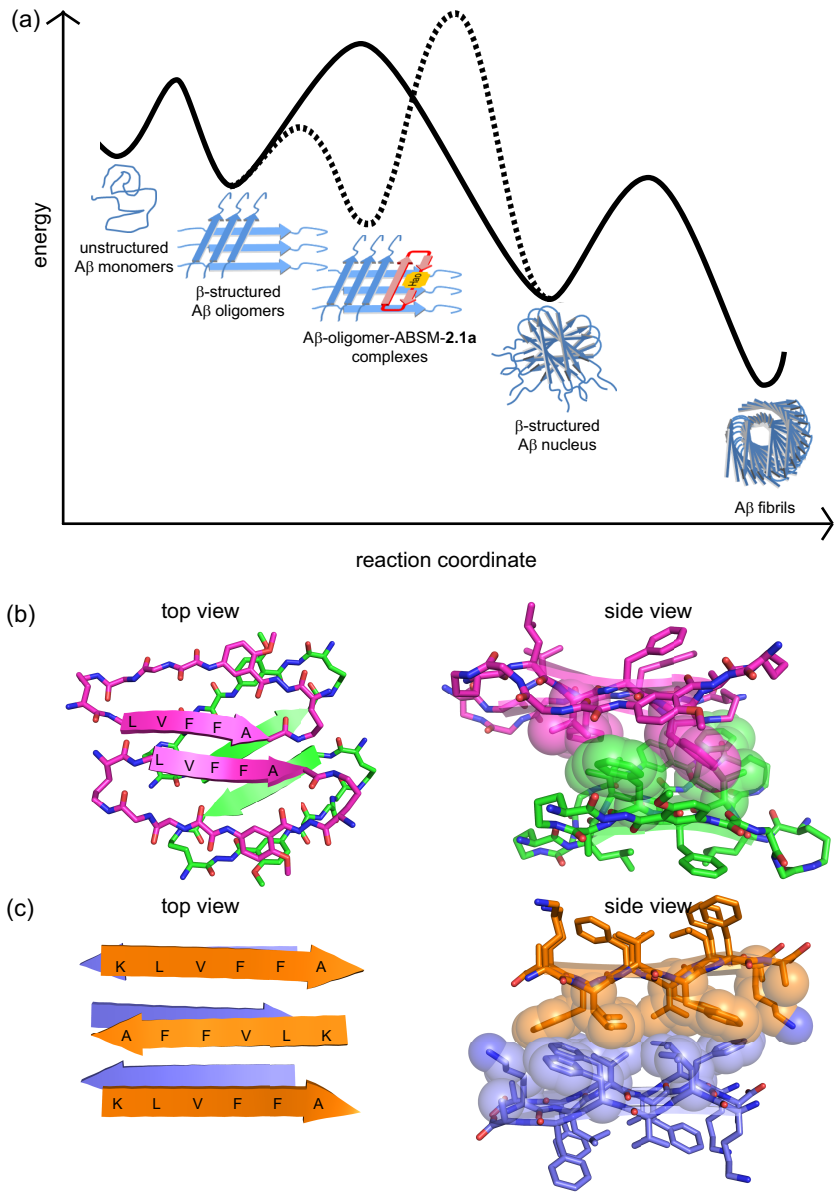

Figure 2.16. (a) Proposed model of inhibition of Aβ aggregation by ABSM **2.1a**. The solid curve corresponds to a pathway in which Aβ aggregates without ABSM **2.1a**. The dashed curve corresponds to an alternative pathway in which ABSM **2.1a** inhibits Aβ aggregation by binding Aβ oligomers. (b) Crystal structure of a macrocyclic peptide containing pentapeptide sequence LVFFA.[7] (PDB ID: 3Q9H) The magenta and green structures correspond to parallel and antiparallel β-sheet dimers formed by the macrocyclic peptide. The side view shows hydrophobic contacts formed between the parallel and antiparallel β-sheet dimers. (c) Crystal structure of the linear peptide KLVFFA.[25] (PDB ID: 3OW9) The orange and purple structures correspond to different layers within the crystal structure. The side view shows hydrophobic contacts between the layers.

It is significant that ABSM **2.1a** substantially delays the aggregation of Aβ at sub-stoichiometric concentrations (as low as 1 μM), e.g. 0.05 equivalents of ABSM **2.1a** per equivalent of Aβ (Figure 2.5), while simple linear peptide fragments derived from Aβ generally show substantial inhibitory effects at stoichiometric or greater concentrations.[24] This observation suggests that ABSM **2.1a** binds a larger oligomer, not the monomer or a smaller oligomer, such as a dimer, trimer, or tetramer. ABSM **2.1a** binds the early β-structured oligomers more strongly than the unstructured monomers bind oligomers, because the recognition β-strand of ABSM **2.1a** is preorganized. This preorganization thus promotes formation of Aβ-oligomer-ABSM-**2.1a** complexes. The complexation may occur through edge-to-edge interactions between the hydrogen-bonding edge of ABSM **2.1a** and exposed hydrogen-bonding groups of the Aβ oligomers and through face-to-face hydrophobic interactions between ABSM **2.1a** and the hydrophobic surfaces of the Aβ oligomers. These types of interactions should take place between the hydrophobic sequence $A\beta_{17–21}$ of ABSM **2.1a** and that of the Aβ oligomers, as observed in the amyloid-related oligomers containing the pentapeptide sequence LVFFA shown in Figure 2.16b and the amyloidlike fibrils from the hexapeptide KLVFFA shown in Figure 2.16c. Similar interactions should also occur in the interactions of other ABSMs with their parent amyloidogenic peptides and proteins. The stabilization of these complexes creates a higher energy barrier to formation of the β-structured nucleus and thus delays or halts fibril formation. Because ABSM **2.1a** cannot sequester all of the equilibrating Aβ oligomers, the Aβ monomers and oligomers eventually succumb to thermodynamics and form Aβ fibrils.

The X-ray crystallographic structure of ABSM **2.1r** may provide insights not only into the stabilization of the dimerization and higher-order supramolecular assembly of ABSMs, but also into the amyloid fibril structures formed by amyloid aggregation. The hydrophobic contacts formed by the Ile, Leu, and Val, at positions 3, 5, and 7 of ABSM **2.1r** (Figure 2.2) are akin to the steric zipper of amyloid-like fibrils formed by fragments $A\beta_{16\text{-}21}$, $A\beta_{30\text{-}35}$, $A\beta_{35\text{-}40}$, and $A\beta_{37\text{-}42}$.[4, 25] Both the layered crystal structure of ABSM **2.1r** and the amyloid-like fibrils are stabilized by hydrophobic contacts. These observations indicate that hydrophobic contact is key in stabilizing amyloid-like fibrils and amyloid fibrils.

The X-ray crystallographic structure of ABSM **2.1r** may also provide insights into the stabilization and structure of amyloid oligomers formed during amyloid aggregation. β-Barrels are emerging as important in the amyloid oligomers that are proving to be the key neurotoxic species in amyloid-related diseases. A toxic small amyloid oligomer formed by KVKVLGDVIEV (K11V)—an amyloidogenic peptide fragment from αB crystallin—forms a β-barrel structure with six β-strands and a filled interior (Figure 2.17a).[26] ABSM **2.1r** forms a β-barrel-like structure with eight β-strands and a filled interior similar to that formed by K11V, in which four units of ABSM **2.1r** pack together through hydrophobic contact and hydrogen bonding to (Figures 2.2d and 2.17b). The β-barrel-like structure of ABSM **2.1r** may illuminate and model the elusive structures of Aβ oligomers that are thought to be the neurotoxic species in Alzheimer's disease. The filled interiors of both β-barrels suggest that tight interresidue contacts with exclusion of water are key in stabilizing the β-barrel-like structures of amyloid oligomers.

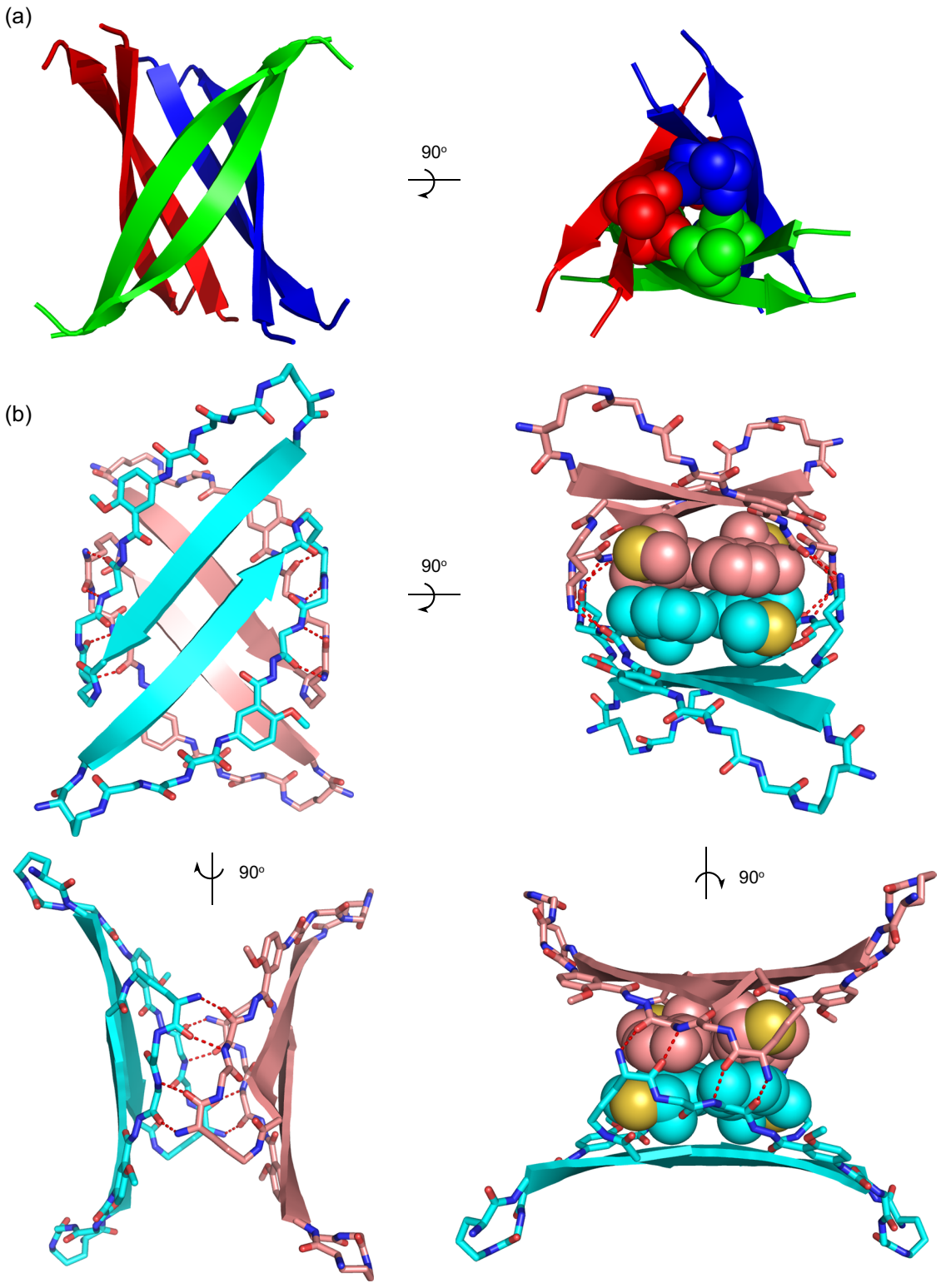

Figure 2.17. (a) The β-barrel formed by peptide fragment KVKVLGDVIEV (K11V) derived from protein αB crystallin (PDB, 3SGO). (b) The β-barrel-like structure formed by ABSM **2.1r** (PDB, 3T4G).

Conclusion

The amyloid β-sheet mimics **2.1** described herein provide a single platform with which to display a variety of amyloidogenic heptapeptide β-strands and provide a rational design for inhibitors to control amyloid aggregation. X-ray crystallographic and ^{1}H NMR studies validate that the design of ABSMs **2.1**, including the cyclicity, Hao template, two $^{\delta}$Orn β-turn mimics, and paired side chains, promotes the formation of β-sheets in which the folding is largely independent of the amino acid sequence. The β-barrel-like structure of ABSM **2.1r** suggests a structural model for the elusive Aβ oligomers and provides insights into other amyloid oligomers.

ABSMs **2.1** can be tailored to inhibit aggregation of different amyloid proteins. The inhibition of Aβ, hβ_2M, and hαSyn$_{1\text{-}100}$ aggregation by ABSMs **2.1** indicates that ABSMs containing one hydrogen-bonding edge and one blocking edge are an effective design for inhibitors of amyloid aggregation. The ability of ABSMs **2.1a**, **2.1m**, and **2.1o** to inhibit amyloid aggregation and to detoxify amyloid aggregates suggests the potential for therapeutic applications in amyloid-related diseases.

References and Notes

1. (a) Chiti, F.; Dobson, C. M., *Annu. Rev. Biochem.* **2006**, *75*, 333–366. (b) Aguzzi, A.; O'Connor, T., *Nat. Rev. Drug. Discov.* **2010**, *9*, 237–248. (c) Bartolini, M.; Andrisano, V., *ChemBioChem* **2010**, *11*, 1018–1035.

2. (a) Greenwald, J.; Riek, R., *Structure* **2010**, *18*, 1244–1260. (b) Tycko, R., Annu. *Rev. Phys. Chem.* **2011**, *62*, 279–299. (c) Eichner, T.; Radford, S. E., *Mol. Cell* **2011**, *43*, 8–18.

3. (a) Lopez de la Paz, M.; Serrano, L., *Proc. Natl. Acad. Sci. USA* **2004**, *101*, 87–92. (b) Goldschmidt, L.; Teng, P. K.; Riek, R.; Eisenberg, D., *Proc. Natl. Acad. Sci. USA* **2010**, *107*, 3487–3492.

4. (a) Nelson, R.; Sawaya, M. R.; Balbirnie, M.; Madsen, A. O.; Riekel, C.; Grothe, R.; Eisenberg, D., *Nature* **2005**, *435*, 773–8. (b) awaya, M. R.; Sambashivan, S.; Nelson, R.; Ivanova, M. I.; Sievers, S. A.; Apostol, M. I.; Thompson, M. J.; Balbirnie, M.; Wiltzius, J. J. W.; McFarlane, H. T.; Madsen, A. O.; Riekel, C.; Eisenberg, D., *Nature* **2007**, *447*, 453–457.

5. (a) Conway, K. A.; Lee, S.-J.; Rochet, J.-C.; Ding, T. T.; Williamson, R. E.; Lansbury, P. T., *Proc. Natl. Acad. Sci. USA* **2000,** *97*, 571–576. (b) Lashuel, H. A., Hartley, D., Petre, B. M., Walz, T.; Lansbury, P. T., *Nature* **2002**, *418*, 291–291.

6. (a) Chimon, S.; Shaibat, M. A.; Jones, C. R.; Calero, D. C.; Aizezi, B.; Ishii, Y., *Nat. Struct. Mol. Biol.* **2007**, *14*, 1157–1164. (b) Bernstein, S. L.; Dupuis, N. F.; Lazo, N. D.; Wyttenbach, T.; Condron, M. M.; Bitan, G.; Teplow, D. B.; Shea, J.-E.; Ruotolo, B. T.; Robinson, C. V.; Bowers, M. T., *Nat Chem* **2009**, *1*, 326–331. (c) Ono, K.; Condron, M. M.; Teplow, D. B., *Proc. Natl. Acad. Sci. USA* **2009**, *106*, 14745–14750.

7. (a) Woods, R. J.; Brower, J. O.; Castellanos, E.; Hashemzadeh, M.; Khakshoor, O.; Russu, W. A.; Nowick, J. S., *J. Am. Chem. Soc.* **2007**, *129*, 2548–2558. (b) Liu, C.; Sawaya, M. R.; Cheng, P.-N.; Zheng, J.; Nowick, J. S.; Eisenberg, D., *J. Am. Chem. Soc.* **2011**, *133*, 6736–6744.

8. Zheng, J.; Liu, C.; Sawaya, M. R.; Vadla, B.; Khan, S.; Woods, R. J.; Eisenberg, D.; Goux, W. J.; Nowick, J. S., *J. Am. Chem. Soc.* **2011**, *133*, 3144–3157.

9. Gellman, S. H., *Curr. Opin. Chem. Biol.* **1998**, *2*, 717–725.

10. Nowick, J. S.; Chung, D. M.; Maitra, K.; Maitra, S.; Stigers, K. D.; Sun, Y., *J. Am. Chem. Soc.* **2000**, *122*, 7654–7661.

11. Nowick, J. S.; Brower, J. O., *J. Am. Chem. Soc.* **2003**, *125*, 876–877.

12. Finder, V. H.; Glockshuber, R., *Neurodegener. Dis.* **2007**, *4*, 13–27.

13. Walsh, P.; Simonetti, K.; Sharpe, S., *Structure* **2009**, *17*, 417–426.

14. Friedhoff, P.; von Bergen, M.; Mandelkow, E.-M.; Davies, P.; Mandelkow, E., *Proc. Natl. Acad. Sci. USA* **1998**, *95*, 15712–15717.

15. Platt, G. W.; Routledge, K. E.; Homans, S. W.; Radford, S. E., *J. Mol. Biol.* **2008**, *378*, 251–263.

16. Vilar, M.; Chou, H.-T.; Lührs, T.; Maji, S. K.; Riek-Loher, D.; Verel, R.; Manning, G.; Stahlberg, H.; Riek, R., *Proc. Natl. Acad. Sci. USA* **2008**, *105*, 8637–18642.

17. Luca, S.; Yau, W.-M.; Leapman, R.; Tycko, R., *Biochemistry* **2007**, *46*, 13505–13522.

18. Cheng, P.-N.; Nowick, J. S., *J. Org. Chem.* **2011**, *76*, 3166–3173.

19. (a) Yan, L.-M.; Velkova, A.; Tatarek-Nossol, M.; Andreetto, E.; Kapurniotu, A., *Angew. Chem., Int. Ed.* **2007**, *46*, 1246–1252. (b) Seeliger, J.; Evers, F.; Jeworrek, C.; Kapoor, S.; Weise, K.; Andreetto, E.; Tolan, M.; Kapurniotu, A.; Winter, R., *Angew.*

Chem., Int. Ed. **2012**, *51*, 679–683. (c) Ma, B; Nussinov, R., *J. Mol. Biol.*, doi:10.1016/j.jmb.2011.11.023.

20. Miller, Y.; Ma, B.; Nussinov, R., *Chem. Rev.* **2010**, *110*, 4820–4838.

21. (a) Yao, S.; Howlett, G. J.; Norton, R. S., *J. Biomol. NMR* **2000**, *16*, 109–119. (b) Cohen, Y.; Avram, L.; Frish, L., *Angew. Chem., Int. Ed.* **2005**, *44*, 520–554.

22. Khakshoor, O.; Demeler, B.; Nowick, J. S., *J. Am. Chem. Soc.* **2007**, *129*, 5558–5569.

23. Nowick, J. S.; Cao, T.; Noronha, G., *J. Am. Chem. Soc.* **1994**, *116*, 3285–3289.

24. (a) Stains, C. I.; Mondal, K.; Ghosh, I., *ChemMedChem* **2007**, *2*, 1674–1692. (b) Sciarretta, K. L.; Gordon, D. J.; Meredith, S. C., *Methods Enzymol.* **2006**, *413*, 273–312.

25. Colletier, J.-P.; Laganowsky, A.; Landau, M.; Zhao, M.; Soriaga, A. B.; Goldschmidt, L.; Flot, D.; Cascio, D.; Sawaya, M. R.; Eisenberg, D., *Proc. Natl. Acad. Sci. USA* **2011**, *108*, 16938–16943.

26. Laganowsky, A.; Liu, C.; Sawaya, M. R.; Whitelegge, J. P.; Park, J.; Zhao, M.; Pensalfini, A.; Soriaga, A. B.; Landau, M.; Teng, P. K.; Cascio, D.; Glabe, C.; Eisenberg, D., *Science* **2012**, *335*, 1228–1231.

Experimental Section for Chapter 2

Contents

Synthesis of ABSMs 2.1. ABSMs **2.1** was easily synthesized by standard Fmoc solid-phase peptide synthesis in which 2-chlorotrityl chloride resin was used as the solid support, followed by solution-phase cyclization, deprotection, and purification. Scheme 2.1 summarizes the synthesis of ABSMs **2.1**. Initially, Boc-Orn(Fmoc)-OH was attached onto 2-chlorotrityl chloride resin and the linear peptide was elongated by standard automated Fmoc solid-phase peptide synthesis, followed by cleavage from the resin under mildly acidic conditions. Then, the linear peptide was cyclized to the corresponding protected cyclic peptide by slow addition to HCTU and DIEA in dilute (ca. 0.5 mM) DMF solution. The cyclization condition used here efficiently avoids problematic epimerization, because the C-terminus of the protected linear peptide comprises an α-amino acid carbamate (Boc-NH-CHR-COOH). The final deprotection with TFA solution followed by RP-HPLC purification yielded ABSMs **2.1** in 20-30% overall yield, based on the loading of Boc-Orn(Fmoc)-OH attached onto the resin.

Representative Synthesis of ABSM 2.1a. Loading of Boc-Orn(Fmoc)-OH to 2-Chlorotrityl Chloride Polystyrene Resin for Solid-Phase Peptide Synthesis.

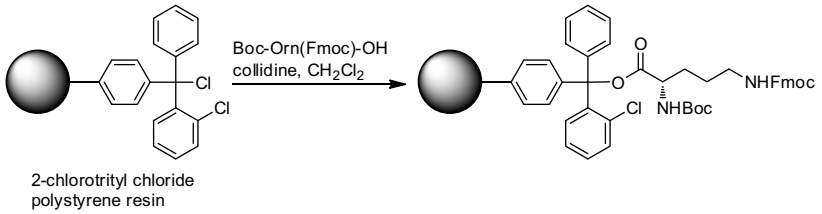

2-Chlorotrityl chloride resin (200 mg, 1.55 mmol/g) was added to a Bio-Rad Poly-Prep chromatography column (10 mL, 0.8 × 4.0 cm). The resin was washed with dry CH_2Cl_2 and suspended in 10 mL of dry CH_2Cl_2 to swell the resin. A solution of Boc-Orn(Fmoc)-OH (0.33 equiv, 46 mg, 0.1 mmol), 2,4,6-collidine (4.6 equiv, 0.16 mL, 175

mg), and 1.6 mL of dry CH_2Cl_2 was added directly to the resin, and the mixture was gently agitated for 4 h. The solution was then drained and the resin was washed with dry CH_2Cl_2 (5 × 7 mL). A mixture of CH_2Cl_2/MeOH/DIEA (17:2:1, 10 mL) was added to the resin, and the mixture was gently agitated for 1 h to cap the unreacted 2-chlorotrityl chloride sites. The capping step was repeated to achieve complete capping. The resin was then washed with dry CH_2Cl_2 followed by DMF. The resin was dried by passing nitrogen through the vessel. The resin loading was determined to be 0.41 mmol/g (80% based on Boc-Orn(Fmoc)-OH) by UV analysis of the Fmoc cleavage product.[1]

Representative Synthesis of Protected Linear Peptides 2.2a.

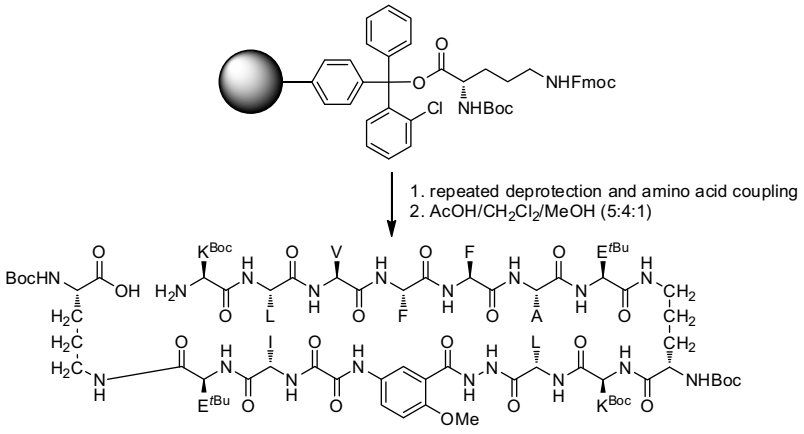

2.2a

The PS-2-chlorotrityl-Orn(Fmoc)-Boc generated from the previous step was washed with DMF (3 × 5 mL) and submitted to cycles of Fmoc solid-phase peptide synthesis on an automated peptide synthesizer using amino acid building blocks: Fmoc-Hao-OH, Fmoc-Orn(Boc)-OH, Fmoc-Lys(Boc)-OH, Fmoc-Glu(*t*Bu)-OH, Fmoc-Phe-OH, Fmoc-Val-OH, Fmoc-Ile-OH, Fmoc-Ala-OH, and Fmoc-Leu-OH. Automated solid-phase peptide synthesis was carried out on a PS3^{TM} Peptide Synthesizer (Protein Technologies, Inc.).[1] Fmoc-Hao-OH was used to introduce the Hao residue during solid-phase peptide

synthesis. Fmoc-Hao-OH was prepared according to published procedures.[2] The protected linear peptide was elongated from the C-terminus to the N-terminus. Each coupling consisted of: (1) Fmoc-deprotection with 20% piperidine in DMF for 3 min; (2) washing with DMF (3 times); (3) coupling of the amino acid (0.5 mmol, 4 equiv) in the presence of HCTU; (4) washing with DMF (6 times). Each amino acid coupling step took 20 min for natural amino acids and 1 h for Hao. Because of the sluggish coupling of Fmoc-Hao-OH into the growing peptide, the Hao coupling reaction was carried out twice without Fmoc deprotection in between. After the last amino acid was coupled onto the growing peptide, the terminal Fmoc group was removed with 20% piperidine in DMF.

The resin with the protected linear peptide was transferred from the reaction vessel of the peptide synthesizer to a Bio-Rad Poly-Prep chromatography column and washed with DMF (3 × 5 mL) followed by CH_2Cl_2 (3 × 5 mL). A mixture of AcOH/CH_2Cl_2/MeOH (5:4:1, 20 mL) was added to the resin, and the suspension was agitated for 1 h. This cleavage solution was collected into a 250-mL round-bottomed flask and the resin was washed with CH_2Cl_2 (3 × 10 mL). The combined solutions were concentrated by rotary evaporation under reduced pressure. Hexanes (ca. 100 mL) were added to the flask and then removed by rotary evaporation to azeotropically remove residual AcOH. The resulting yellowish oil was dissolved CH_2Cl_2 (ca. 5 mL), diluted with hexanes (ca. 100 mL), and concentrated to dryness. The addition of CH_2Cl_2 and hexanes, followed by concentration, was repeated two additional times to remove the residual AcOH. The residue was dried under vacuum to give crude protected linear peptide **2.2a** as a white solid (130 mg, 68% crude yield based on resin loading).

Representative Synthesis of Protected Cyclic Peptides 2.3a.

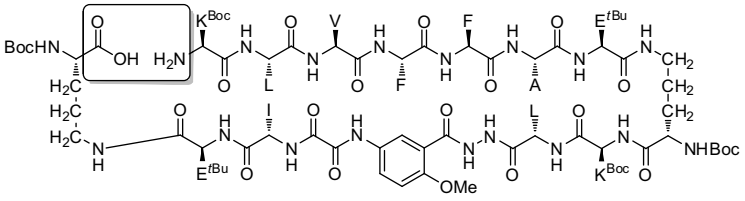

2.2a

HCTU (4 equiv)
DIEA (8 equiv)
DMF

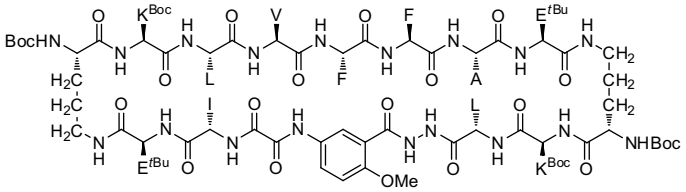

2.3a

Crude protected linear peptide **2.2a** (130 mg, 0.05 mmol) was dissolved in DMF (50 mL). The peptide solution was added in drops via a 250-mL pressure-equalizing addition funnel to a 250-mL round-bottom flask containing a magnetic stirring bar, HCTU (82 mg, 0.20 mmol, 4 equiv), and DIEA (94 μL, 0.40 mmol, 8 equiv) in DMF (50 mL). (The final peptide concentration was 0.5 mM.) The reaction mixture was then stirred under nitrogen for 24 h. DMF was then removed by rotary evaporation under reduced pressure to give crude protected cyclic peptide **2.3a** as a yellowish waxy solid. The crude product was used in final deprotection step without further purification.

Representative Synthesis of ABSM 2.1a.

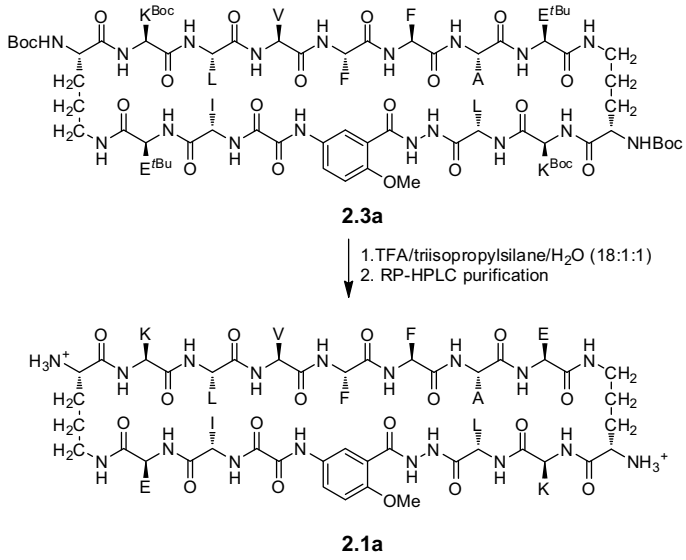

Protected cyclic peptide **2.3a** was dissolved in TFA/triisopropylsilane/H_2O (18:1:1, 20 mL) in a 50-mL round-bottom flask equipped with a nitrogen-inlet adaptor. The solution was magnetically stirred for 2 h. The reaction mixture was then concentrated by rotary evaporation under reduced pressure to give a yellowish oil. The resulting crude peptide **2.1a** was purified by reverse-phase HPLC (gradient elution with 10–50% CH_3CN over 60 min). The pure fractions were lyophilized to give 37 mg of peptide **2.1a** (22% yield, based on resin loading).

HPLC of ABSM 2.1a. Analytical reverse-phase HPLC was performed on an Agilent Zorbax SB-C18 column (50 mm × 4.6 mm) with a gradient of 5–100% CH_3CN in H_2O with 0.1% TFA and a flow of 1.0 mL/min over 20 minutes. Preparative reverse-phase HPLC purification was carried out on a 21.2 x 250 mm Zorbax SB-C18 PrepHT (7-μm particle size) column from Agilent on a Rainin Dynamax system with a flow of 10.0 mL/min. UV detection (214 or 254 nm) was used for analytical and preparative HPLC.

Water and acetonitrile were used as the solvents. Both solvents contained 0.1% biochemical grade TFA.

^{1}H NMR Spectroscopic Studies of ABSMs 2.1. ^{1}H NMR experiments of ABSMs **2.1** were performed in D_2O with the internal standard DSA[3] at 500 MHz at 298K. Solutions of ABSMs **2.1** were prepared gravimetrically by dissolving an appropriate weight of peptides in an appropriate volume of solvent. In calculating molecular weights, all amino groups were assumed to be protonated as the TFA salts. All 2D TOCSY and 2D ROESY spectra were collected with 2048 data points in the f_2 domain and 512 data points in the f_1 domain. Data were processed to a 1024 × 1024 real matrix with a Qsine weighting function and with forward linear prediction in the f_1 domain. The data were processed with the Brüker XwinNMR software.

Diffusion-Ordered Spectroscopy (DOSY) Experiments and Diffusion Constant Measurements of ABSM 2.1a. DOSY experiments comprised a series of 16 pulsed field gradient spin-echo experiments with a 75-ms delay in which the gradient strength was incremented to allow ca. 2%–95% signal attenuation with a linear ramp. Data were processed to give a pseudo-2D spectrum, and the diffusion coefficient was read from the spectrum after careful phasing. Calibration of the gradients was performed on the basis of the diffusion coefficient of residual HOD in D2O (1.9×10^{-9} m^2/s at 298 K).

Crystallization, Data Collection, and Structure Determination. Crystals of ABSM **2.1r** were grown from a 10 mg/mL aqueous stock solution using 35% (v/v) 2-methyl-2,4-pentanediol and pH 6.2 Na/K phosphate buffer at 18 °C using hanging drop vapor diffusion method. X-ray diffraction data were collected at the Advanced Photon Source (APS) and UCLA Crystallization Facility (Table S1). Reflections were integrated and scaled using XDS/XSCALE program packages.[4] Statistical analysis of the reflection intensities showed that the crystals are nearly perfectly twinned with an estimated twin fraction number close to 0.5.[5] Nevertheless, experimental phases were obtained with the apparent space group P4232 by SIRAS method using HKL2MAP.[6,7] The model was built using COOT and was refined using REFMAC in space group P23.[8,9] Coordinates and structure factor amplitudes have been deposited in the Protein Data Bank with accession code 3T4G.

Table S1. Statistics of Refinement

	ABSM **2.1r** (refinement)	ABSM **2.1r** (native)	ABSM **2.1r** (iodide)
Crystal parameters			
Space group	P23	$P4_232$	$P4_232$
Cell dimensions			
a, b, c (Å)	44.4, 44.4, 44.4	44.6, 44.6, 44.6	44.0, 44.0, 44.0
α, β, γ (°)	90, 90, 90	90, 90, 90	90, 90, 90
Molecules in A.U.[a]	2	1	1
Data collection			
X-ray source	In-House[b]	APS (24-ID-C)[c]	APS (24-ID-C)[c]
Wavelength (Å)	1.542	0.9196	1.8443
Resolution (Å)	1.70	1.70	2.04
Reflections observed / unique	29228 / 3384	21581 / 3124	12251 / 1779
Completeness (%)	99.5 (95.9)[d]	99.1 (95.0)	99.6 (98.4)
R_{merge} (%)[e]	3.5 (51.3)	5.2 (31.4)	5.6 (51.6)
$\langle I/\sigma I \rangle$	29.7 (3.1)	19.9 (3.9)	21.4 (3.4)
Refinement			
Resolution (Å)	18.1 – 1.70		
R_{work} (%)[f]	23.6 (24.1)		
R_{free} (%)[g]	27.4 (37.7)		
No. of non-H atoms			
macrocycle	240		
ligand/ion	56		
Overall B-factors	15.7		
R.m.s. deviation			
Bond length (Å)	0.022		
Bond angle (°)	2.729		
PDB accession code	3T4G		

a. A.U. = Asymmetric Unit
b. Data was collected using an FRD rotating anode generator with R-AXIS HTC imaging plate detector.
c. Synchrotron beamline.
d. Values in parentheses correspond to the highest resolution shell.
e. $R_{merge} = \Sigma \mid I - \langle I \rangle \mid / \Sigma I$.
f. $R_{work} = \Sigma \mid F_o - F_c \mid / \Sigma F_o$.
g. $R_{free} = \Sigma \mid F_o - F_c \mid / \Sigma F_o$, calculated using a random set containing 5% reflections that were not included throughout structure refinement.

Expression of $A\beta_{42}$, $h\beta_2M$, and $h\alpha Syn_{1\text{-}100}$. Human wild-type $A\beta_{42}$ were expressed in *E.coli* and purified as described by Finder, Vodopivec, Nitsch, and Glockshuber.[10] The fusion construct was provided as a gift by Prof. Glockshuber and contains a His tag, linkers, soluble polypeptide segment ($NANP_{19}$), and TEV protease recognition site. Briefly, The fusion construct was expressed into inclusion bodies in *E.coli* BL21(DE3). 8 M urea was used to solubilize the inclusion bodies. HisTrap™ HP Columns was used to purify the denatured Aβ fusion proteins, followed by further purification via reversed-phase high-performance liquid chromatography (RP-HPLC). The fusion proteins were lyophilized before TEV protease cleavage. The cleavage reaction was performed at 4 degree in reducing buffer (50 μM Tris-HCL, pH 8.0, 0.5 mM EDTA, and 1 mM DTT) for 30 h with the fusion protein concentration of 50 μM and TEV concentration of 3 μM. $A\beta_{42}$ was purified from the cleavage solution by RP-HPLC. The final product was verified by matrix-assisted laser desorption ionization spectrometry (MALDI-TOF MS).

Wild-type human β_2-microglobulin ($h\beta_2M$) was expressed as inclusion bodies in *E.coli*. The $h\beta_2M$ monomer was refolded as described previously.[11] Briefly, the $h\beta_2M$ inclusion body pellets were washed by 0.1% Triton X-100, 1 M NaCl sequentially and solubilized in 8 M urea with 50 mM Tris-HCl, pH 8.0. Then gradient dialysis was performed for $h\beta_2M$ refolding. The refolded $h\beta_2M$ protein was loaded on Superdex™ 75 column for size exclusion purification. Monomeric $h\beta_2M$ was pooled for $h\beta_2M$ fibrillation inhibition studies.

Truncated human α-synuclein (residues 1-100) was expressed in *E. coli* strain BL21-Gold (DE3) (Agilent Technologies, Santa Clara, CA) at 37 °C through induction with 1 mM isopropyl-β-D-thiogalactopyranoside (IPTG) for 4 h. The cells were

resuspended in a lysis buffer containing 100 mM Tris-HCl (pH 8.0), 100 mM NaCl, and 1 mM ethylenediaminetetraacetic acid (EDTA), and phenylmethylsulfonyl fluoride (PMSF) was also added to make 1 mM concentration. The cell lysate was centrifuged and the supernatant was incubated in 70 °C for 10 minutes. After centrifugation, the supernatant was dialyzed overnight in a buffer containing 10 mM HEPES, pH 7.4 and then loaded to a 5 mL HiTrap SP column (GE Healthcare, Piscataway, NJ) for cation exchange. The column was washed with 10 mM HEPES (pH 7.4) and eluted with a linear gradient of NaCl. The peak fractions were collected, and then concentrated using an Amicon Ultra-15 concentrator (3 kDa MW cutoff; Millipore, Billerica, MA). The concentrated elution was subsequently applied to a Superdex S-75 column (GE Healthcare, Piscataway, NJ). The SEC running buffer contained 20 mM Tris-HCl (pH 8.0). The peak fractions were pooled and concentrated to about 3.5 mg/mL.

ThT Fluorescence Assays.

Effect of ABSM 2.1a on Inhibition of $A\beta_{40}$ Aggregation. ThT fluorescence assays were conducted in 96-well plates (black with flat optic bottom) with shaking in a Gemini XPS fluorescence plate reader (Molecular Devices, 442 nm excitation, 482 nm emission) at 37 °C. Experiments were run in quadruplicate or greater with 20 μM $A\beta_{40}$, 10 mM PBS buffer (pH 7.4), and 20 μM ThT.

Preparation of Buffered ThT Solution (Stock Solution A): A ThT solution was freshly prepared before use. Approximately 4 mg of thioflavin T was dissolved in ca. 20 mL of Nanopure water in a 25 mL Erlenmeyer flask. 10 mL of this solution was filtered through a 0.22 micron filter into a 15-mL plastic centrifuge tube. The concentration of a 1/25 dilution of this solution was determined by UV (ε = 36000 M^{-1} cm^{-1} at 412 nm). An aliquot of this stock solution was combined with H_2O and 5x PBS buffer containing 0.02% NaN_3 (the amount of ThT stock and H_2O are based on the determined concentration of the stock) to obtain 100 μM ThT solution.

Preparation of Peptide Inhibitor Solution (Stock Solution B): A stock solution of ABSM **2.1a** was freshly prepared before use by adding Nanopure water to each tube to obtain 200 μM peptide solutions.

Preparation of $A\beta_{40}$ solution (Stock Solution C): $A\beta_{40}$ (GL Biochem, Shanghai, China) was dissolved in in hexafluoroisopropanol (HFIP) to disrupt preformed aggregates and the HFIP was then evaporated in the hood for 12 h and dried under vacuum for 12 h. The

$A\beta_{40}$ solution was freshly prepared by dissolving $A\beta_{40}$ in 100 mM NaOH in a 1.5 mL Epindorf tube. The mixture was sonicated for 30 seconds. The solution was diluted to 100 μM by addition of Nanopure water. The solution was filtered through 100 kDa Centricon filters that were previously washed 3 times with Nanopure water (10000 rpm for 3 minutes). The $A\beta_{40}$ solution was diluted with Nanopure water to 40 μM.

Preparation of the Wells of the 96-Well Plate. Each well contained 200 μL reaction solution containing 20 μM $A\beta_{40}$, 10 mM PBS buffer (pH 7.4), 20 μM ThT, and various amounts of ABSM **2.1a**. The preparation of each well is summarized in Table S2. The stock solution C was added last to all of the wells, and the plate was immediately inserted into the plate reader. The wells were prepared in quadruplicate or greater. (In the example shown in Figure 2.4, well were prepared in septaplicate.) Representative data were used for further analysis. (In the example shown in Figure 2.4, the five most representative traces are shown and two least representative traces are omitted.) The ThT assay was conducted for 41 h at 37 ºC. Readings were collected every 10 minutes with 5 seconds shaking before first reading and 575 seconds shaking between readings.

Table S2. Preparation of the Wells of the 96-Well Plate.

Wells	Water (μL)	Stock Solution A (μL)	Stock Solution B (μL)	Stock Solution C (μL)
ThT control	160	40	0	0
$A\beta_{40}$ control	60	40	0	100
0.2 equiv of ABSM **2.1a**	56	40	4	100
0.5 equiv of ABSM **2.1a**	50	40	10	100
1.0 equiv of ABSM **2.1a**	40	40	20	100

Effect of ABSM 2.1a on Inhibition of $A\beta_{42}$ Aggregation. ThT fluorescence assays were conducted in 96-well plates (black with flat optic bottom) without shaking in a Varioskan fluorescence plate reader (Thermo Scientific, 444 nm excitation, 484 nm emission) at 37 °C. Experiments were run in quadruplicate or greater with 20 μM $A\beta_{42}$, 10 mM PBS buffer (pH 7.4), and 10 μM ThT.

Preparation of Reaction Solutions and the Wells of the 96-Well Plate. The ThT assay of $A\beta_{42}$ aggregation was performed by preparing reaction solutions containing 20 μM $A\beta_{42}$, 10 μM ThT, and 1, 2, 4, 10, or 20 μM ABSM **2.1a** and then placing 150 μL portions of these solutions into wells in a 96-well plate. For pre-treatment to disaggregate pre-formed $A\beta_{42}$ aggregates: Prior to the assay, lyophilized $A\beta_{42}$ was dissovled in HFIP and evaporated in vaccum, $A\beta_{42}$ was freshly dissoved in 10mM NaOH, followed by sonication. $A\beta_{42}$ was further diluted into PBS at the final concentration of 200uM as a stock. The reaction solution were prepared by combining a 2.0 mM ABSM **2.1a** solution (stock solution A) with a solution of 20 μM $A\beta_{42}$ and 10 μM ThT in PBS (pH 7.4) buffer (stock solution B). Stock solution B was prepared by diluting 1 mM ThT solution and 200 μM $A\beta_{42}$ solution in 10 mM PBS buffer (pH 7.4). Stock solution B was also used as $A\beta_{42}$ control. All solutions used for the assay were spin filtered through a 0.22 micron filter prior to the assay.

Table S3. Preparation of Reaction Solutions of ABSM **2.1a**.

Reaction Solution (900 μL)	Stock Solution A (μL)	Stock Solution B (μL)
0.05 equiv of ABSM **2.1a**	0.45	899.5
0.1 equiv of ABSM **2.1a**	0.9	899.1
0.2 equiv of ABSM **2.1a**	1.8	898.2
0.5 equiv of ABSM **2.1a**	4.5	895.5
1.0 equiv of ABSM **2.1a**	9.0	891

Table S3 summarizes the preparation of the reaction solutions. 150 μL portions of each reaction solution were pipetted into the wells of a 96-well plate. 150 μL portions of 10 μM ThT and 20 μM $A\beta_{42}$ were pipetted into additional wells as controls. The wells were prepared in quadruplicate or greater. Representative data were used for further analysis. The ThT assay was conducted for 24 h at 37 ºC and readings were collected every 10 minutes.

Effect of ABSM 1m on Inhibition of $h\beta_2M$ Aggregation. ThT fluorescence assays were conducted in 96-well plates (black with flat optic bottom) with continuous shaking at 900 rpm in a Varioskan fluorescence plate reader (Thermo Scientific, 444 nm excitation, 484 nm emission) at 37 °C. Experiments were run in quadruplicate or greater with 30 μM $h\beta_2M$, 50 mM phosphate buffer (pH 2), and 10 μM ThT.

Preparation of Reaction Solutions and the Wells of the 96-Well Plate. The ThT assay of $h\beta_2M$ aggregation was performed by preparing reaction solution containing 30 μM $h\beta_2M$, 10 μM ThT, and 6, 15, or 30 μM ABSM **2.1m** and then placing 150 μL portions of these solutions into wells in a 96-well plate. The reaction solution were prepared by combining a 2.0 mM ABSM **2.1m** solution (stock solution A) with a solution of 30 μM $h\beta_2M$ and 10 μM ThT in 50 mM phosphate (pH 2) buffer (stock solution B). Stock solution B was prepared by diluting 1 mM ThT solution and 5 mM $h\beta_2M$ solution in 50 mM phosphate buffer (pH 2). Stock solution B was also used as $h\beta_2M$ control. All solutions used for the assay were spin filtered through a 0.22 micron filter prior to the assay.

Table S4. Preparation of Reaction Solutions of ABSM **2.1m**.

Reaction Solution (1000 μL)	Stock Solution A (μL)	Stock Solution B (μL)
0.2 equiv of ABSM **2.1m**	3	997
0.5 equiv of ABSM **2.1m**	7.5	992.5
1.0 equiv of ABSM **2.1m**	15	985

Table S4 summarizes the preparation of the reaction solutions. 150 μL portions of each reaction solution were pipetted into the wells of a 96-well plate. 150 μL portions of 10 μM ThT and 30 μM hβ_2M were pipetted into additional wells as controls. The wells were prepared in quadruplicate or greater. Representative data were used for further analysis. The ThT assay was conducted for 24 h at 37 ºC and readings were collected every 10 minutes.

Effect of ABSM 2.1o on Inhibition of hαSyn$_{1\text{-}100}$ Aggregation. ThT fluorescence assays were conducted in 96-well plates (black with flat optic bottom) with continuous shaking at 900 rpm in a Varioskan fluorescence plate reader (Thermo Scientific, 444 nm excitation, 484 nm emission) at 37 °C. Experiments were run in quadruplicate or greater with 50 μM hαSyn$_{1\text{-}100}$, 20 mM phosphate buffer (pH 2) with 100 mM NaCl, and 10 μM ThT.

Preparation of Reaction Solutions and the Wells of the 96-Well Plate. The ThT assay of hαSyn$_{1\text{-}100}$ aggregation was performed by preparing reaction solution containing 50 μM hαSyn$_{1\text{-}100}$, 10 μM ThT, and 10, 25, or 50 μM ABSM **1o** and then placing 150 μL portions of these solutions into wells in a 96-well plate. The reaction solutions were prepared by combining a 2.0 mM ABSM **2.1o** solution (stock solution A) with a 1 mM

ThT (stock solution B), a 340 μM hαSyn$_{1-100}$ solution (stock solution C) and the phosphate buffer. hαSyn$_{1-100}$ control was prepared by combining a 340 μM hαSyn$_{1-100}$ solution (stock solution C) with a 1mM ThT (stock solution B) and the phosphate buffer. All solutions used for the assay were spin filtered through a 0.22 micron filter prior to the assay.

Table S5. Preparation of Reaction Solutions with Various Concentrations of ABSM **2.1o**.

Reaction Solution (1200 μL)	Stock Solution A (μL)	Stock Solution B (μL)	Stock Solution C (μL)	Buffer
ThT control	0	12	0	1188
hαSyn$_{1-100}$ control	0	12	177	1011
0.2 equiv of ABSM **2.1o**	6	12	177	1005
0.5 equiv of ABSM **2.1o**	15	12	177	996
1.0 equiv of ABSM **2.1o**	30	12	177	981

Table S5 summarizes the preparation of the reaction solutions and hαSyn$_{1-100}$ control. 150 μL portions of each reaction solution were pipetted into the wells of a 96-well plate. 150 μL portions of 10 μM ThT and 50 μM hαSyn$_{1-100}$ were pipetted into additional wells as controls. The wells were prepared in quadruplicate or greater. Representative data were used for further analysis. The ThT assay was conducted for 51 h at 37 ºC and readings were collected every 10 minutes.

TEM Studies. Samples for TEM studies were taken from the ThT assays above during the delayed lag phase. Samples of $A\beta_{40}$ were prepared by applying aliquots from the wells with 1.0 equivalent of ABSM **2.1a** and without ABSM **2.1a** to TEM grids at 6 h. Samples of $A\beta_{42}$ were prepared by applying aliquots from the wells with 1.0 equivalent of ABSM **2.1a** and without ABSM **2.1a** to TEM grids at 7 h. Samples of $h\beta_2M$ were prepared by applying aliquots from the wells with 1.0 equivalent of ABSM **2.1m** and without ABSM **2.1m** to TEM grids at 2 h. Samples of $h\alpha Syn_{1\text{-}100}$ were prepared by applying aliquots from the wells with 1.0 equivalent of ABSM **2.1o** and without ABSM **2.1o** to TEM grids at 72 h. The samples were pipetted onto formvar and carbon coated electron microscopy grids (Ted Pella, catalog No. 01754-F) and incubated for 3 min. The grids were rinsed with distilled water and stained with 1% (w/v) uranyl acetate solution. Samples were imaged with a Philips CM120 electron microscope at an accelerating voltage of 120 kV. At least three independent experiments were carried out for each sample.

Cell Viability Assays. PC-12 (ATCC, catalog No. CRL-1721), HeLa, and HEK-293 cells were used to evaluate the cytotoxic effect of the ABSMs and Aβ by MTT assays. A CellTiter 96 non-radioactive cell proliferation assay kit (Promega) was used in these MTT assays. HeLa and HEK-293 cells were cultured in DMEM medium with 10% fetal bovine serum, and PC-12 cells in ATCC-formulated RPMI 1640 medium (catalog No. 30-2001) containing 10% heat-inactivated horse serum and 5% fetal bovine serum. All cells were maintained at 37 °C in 5% CO_2.

*Toxicity of ABSM **2.1a**, **2.1m**, and **2.1o** towards PC-12, HeLa, and HEK-293 cells.* PC-12, HeLa, and HEK-293 cells were plated out at 10,000 cells/well in 96-well plates (Costar, catalog No. 3596). The cells were cultured for 20 h at 37 °C in 5% CO_2 before the samples were added. ABSMs **2.1a**, **2.1m**, and **2.1o** were added to each well containing medium. (The total volume is 100 μL and the final concentration is 5 μM or 50 μM.) After cells were incubated with and without ABSMs for 24 h, the dye solution (15 μL, Promega, catalog No. G4000) was added to each well and incubation continued for additional 4 h at 37 °C in 5% CO_2. The solubilization Solution/Stop Mix (100 μL, Promega, catalog No. G4000) was then added to each well. After incubation for 12 h at room temperature, the absorbance was measured at 570 nm. The background absorbance was recorded at 700 nm. Each of the samples was repeated with 4 replicates in three independent experiments. The results were normalized by setting the cell survival of the PBS controls to be 100% and that of the SDS (0.2%) controls to be 0%.

*Detoxification of Amyloid-β by ABSM **2.1a**.* PC-12 cells were plated out at 10,000 cells/well in 96-well plates (Costar, catalog No. 3596). The cells were cultured 20 h at 37 °C in 5% CO_2 prior to addition of the samples. $A\beta_{40}$ and $A\beta_{42}$ monomers (5 μM) with and without ABSM **2.1a** were incubated at 37 °C with and without shaking for 16 h respectively prior to the addition to the cells. The preincubated Aβ solutions with and without ABSM **2.1a** were added to the cells. (The final concentration of the preincubated Aβ solutions is 0.5 μM.) The resulting mixtures were incubated for additional 24 h at 37 °C in 5% CO_2. The absorbance was then measured at 570 nm. The background absorbance was recorded at 700 nm. Each of the samples was repeated with 4 replicates in three independent experiments. The results were normalized by setting the cell survival of the PBS controls to be 100% and that of the SDS (0.2%) controls to be 0%.

References

1. Most standard peptide synthesis procedures followed those in the "Synthesis Notes" section of the **2009**/**2010** Novabiochem catalog.

2. Cheng, P.-N.; Nowick, J. S. *J. Org.Chem.* **2011**, *76*, 3166–3173.

3. Nowick, J. S.; Khakshoor, O.; Hashemzadeh, M.; Brower, J. O. *Org. Lett.* **2003**, *5*, 3511–3513.

4. Kabsch, W. *J. Appl. Crystallogr.* **1993**, *26*, 795–800.

5. *Acta Crystallogr. D Biol. Crystallogr.***1994**, *50*, 760–763.

6. Sheldrick, G. M. *Acta Crystallogr. A* **2008**, *64*, 112–122.

7. Pape, T.; Schneider, T. R. *J. Appl. Crystallogr.* **2004**, *37*, 843–844.

8. Emsley, P.; Cowtan, K. *Acta Crystallogr. D Biol. Crystallogr.* **2004**, *60*, 2126–2132.

9. Vagin, A. A.; Steiner, R. A.; Lebedev, A. A.; Potterton, L.; McNicholas, S.; Long, F.; Murshudov, G. N. *Acta Crystallogr. D Biol. Crystallogr.* **2004**, *60*, 2184–2195.

10. Finder, V. H.; Vodopivec, I.; Nitsch, R. M.; Glockshuber, R. *J. Mol. Biol.* **2010**, *396*, 9–18.

11. Liu, C.; Sawaya, M. R.; Eisenberg, D. *Nat. Struct. Mol. Biol*. **2011**, *18*, 49–55.

Representative Analytical RP-HPLC of ABSM **2.1a**

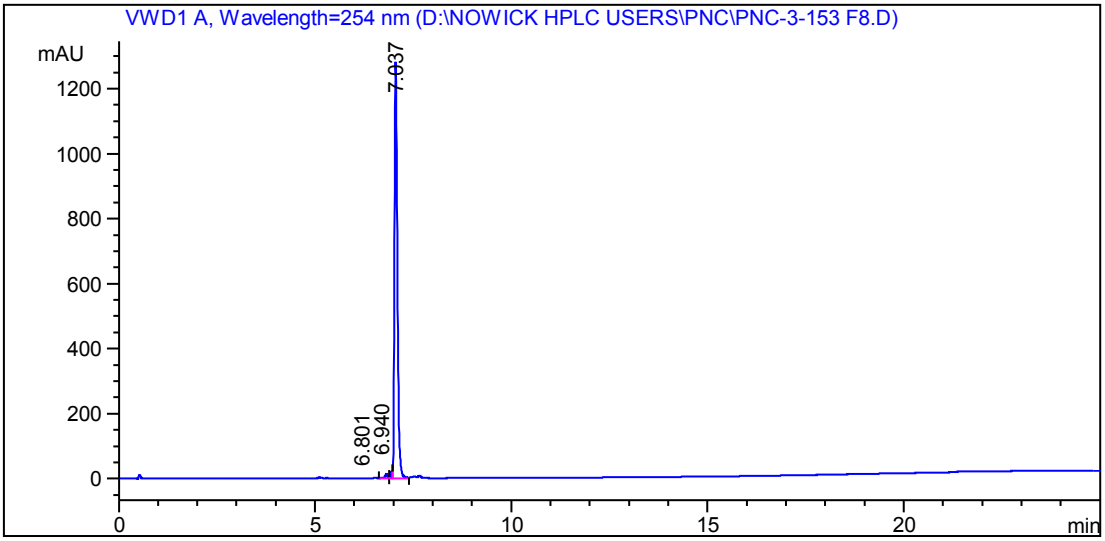

Signal 1: VWD1 A, Wavelength=254 nm

Peak #	RetTime [min]	Type	Width [min]	Area mAU *s	Height [mAU]	Area %
1	6.801	VV	0.0662	59.33563	13.04519	0.8863
2	6.940	VV	0.0447	65.37052	22.11021	0.9765
3	7.037	VV	0.0787	6569.83398	1281.51428	98.1372

Mass spectrum of ABSM **2.1a**

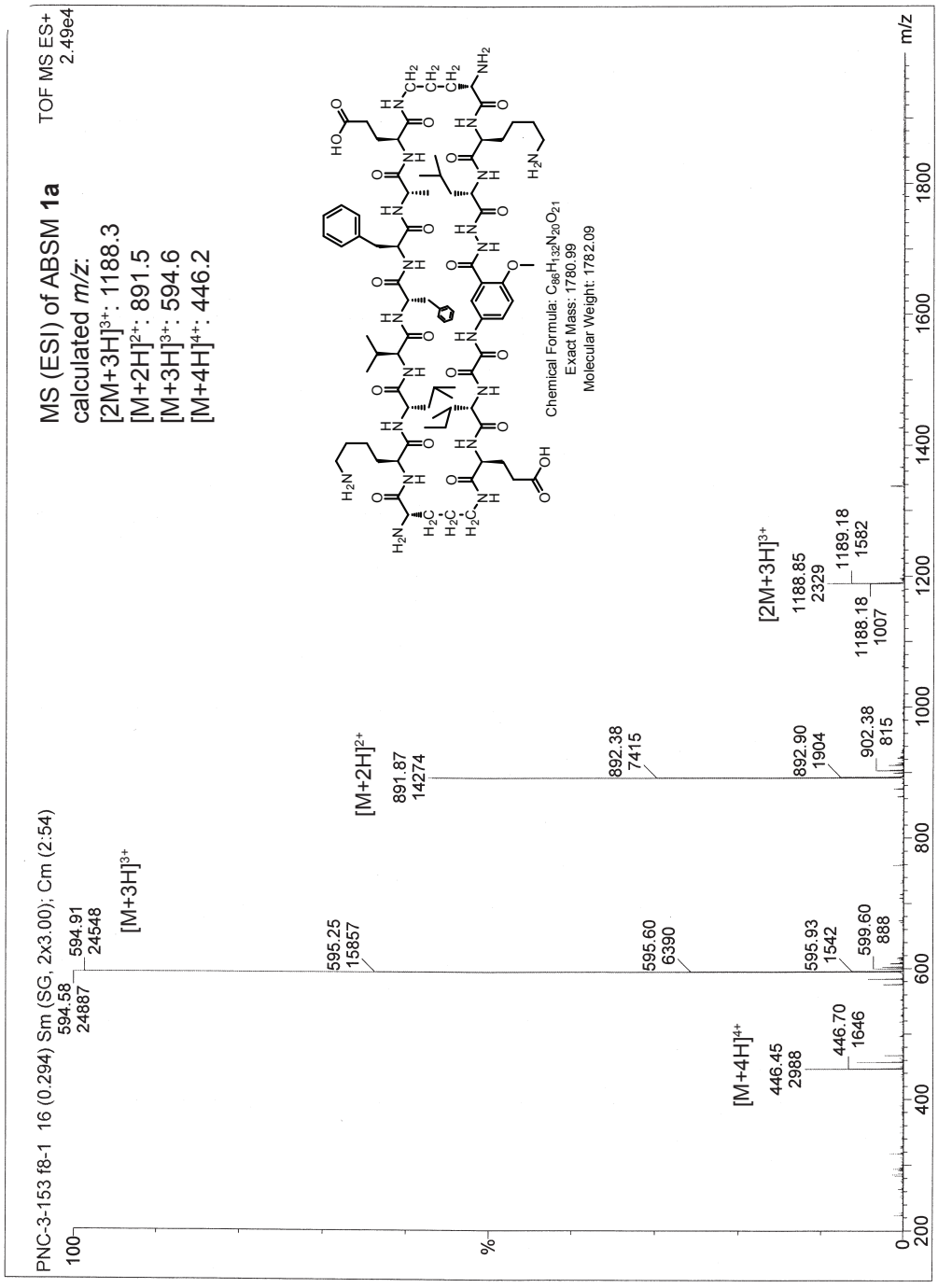

1D ^{1}H NMR spectrum of ABSM **2.1a**, 500 MHz, 2 mM in D_2O, 298K

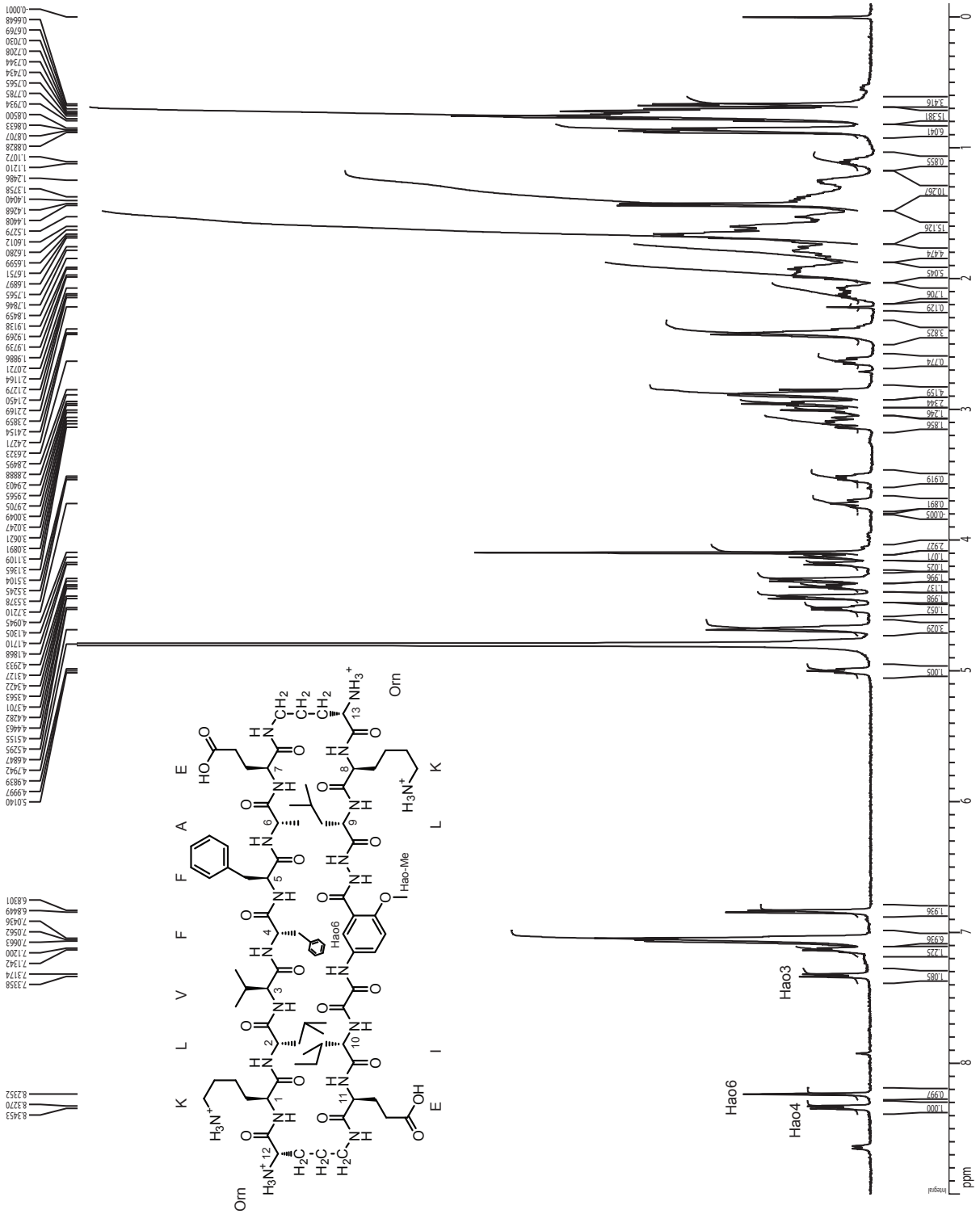

1D ^{1}H NMR spectrum of ABSM **2.1a**, 500 MHz, 2 mM in $_{2}$ D O, 298K

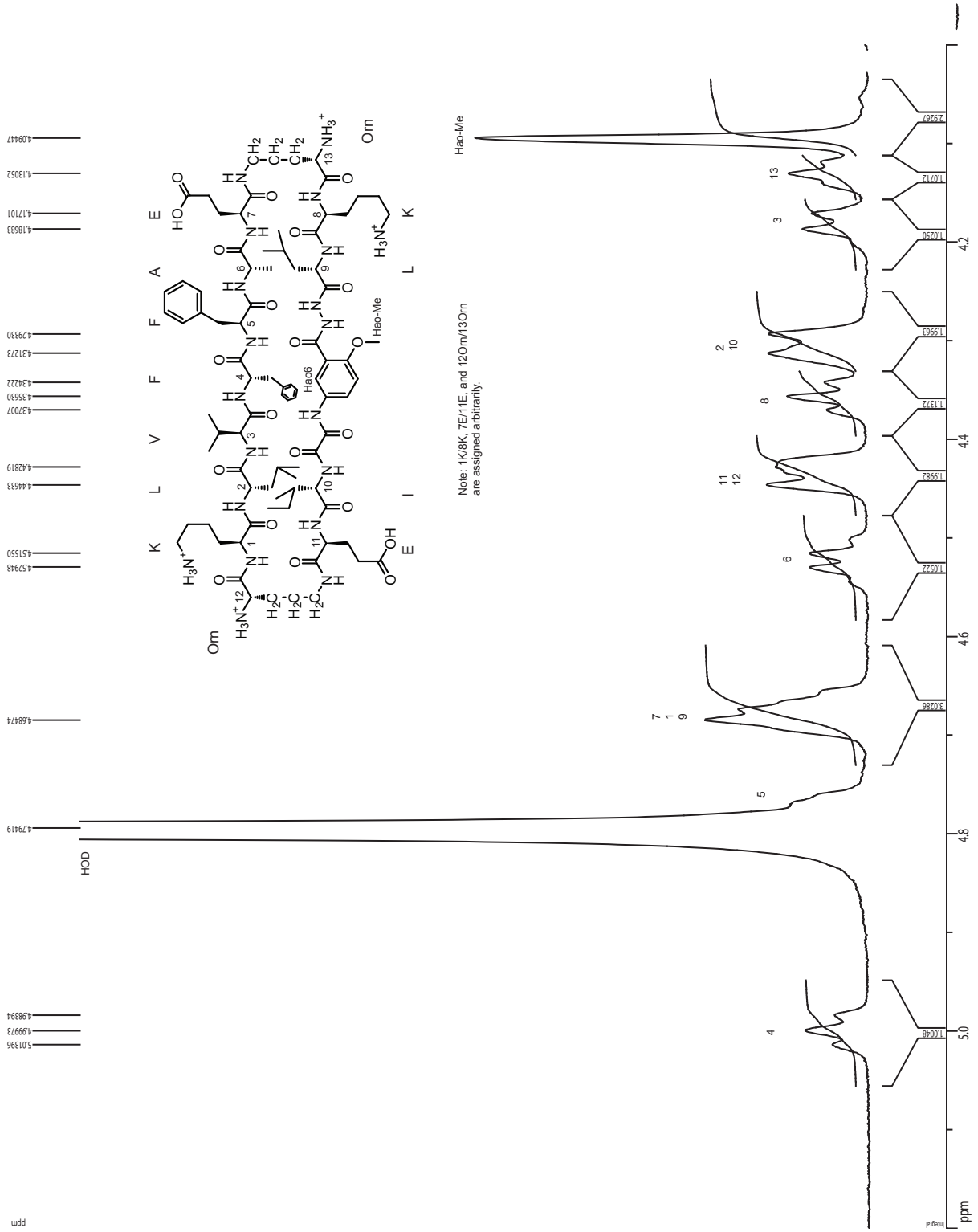

1D ^{1}H NMR spectrum of ABSM **2.1a**, 500 MHz, 2 mM in D_2O, 298K

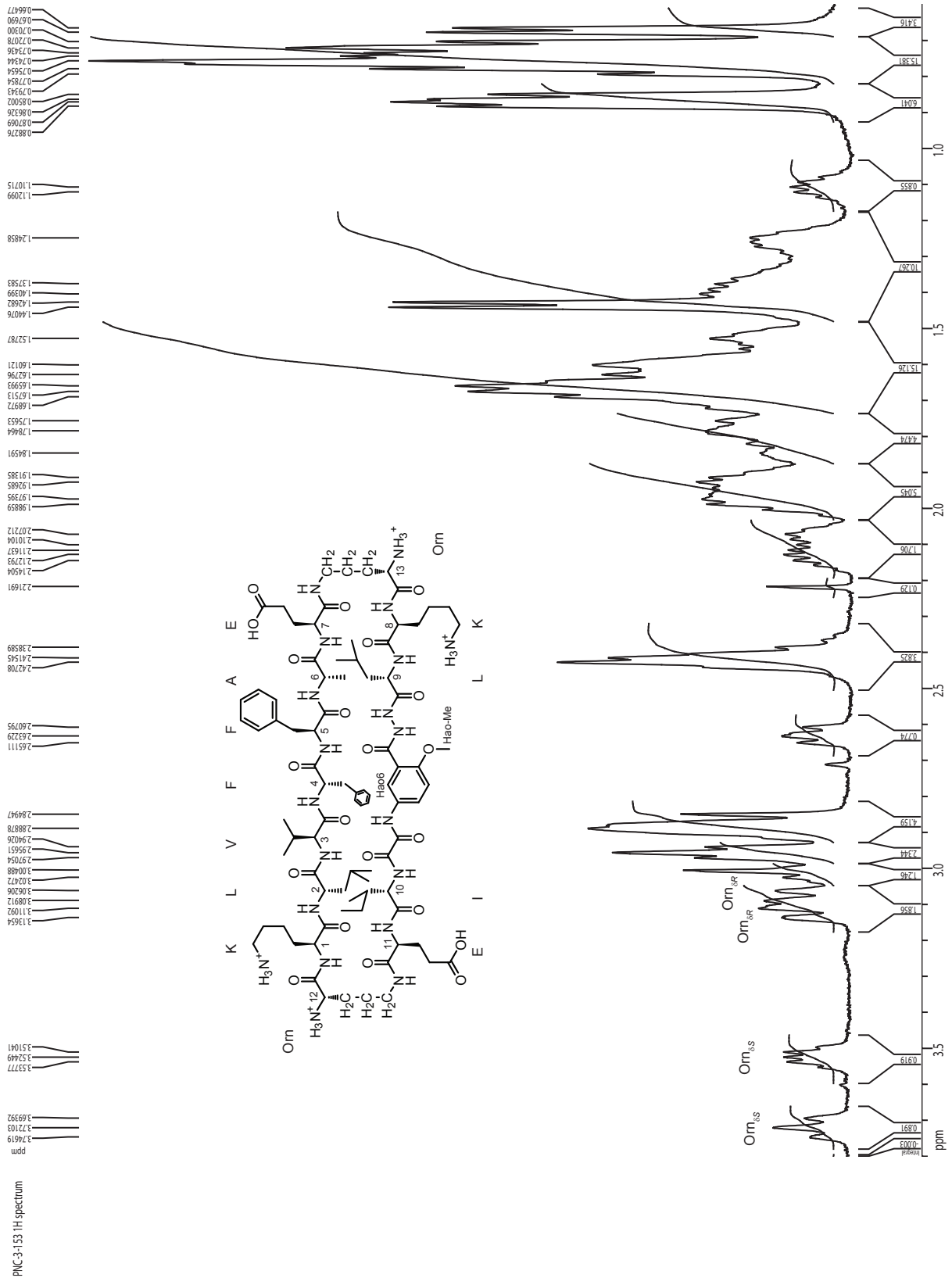

2D TOCSY spectrum of ABSM **2.1a**, 2 mM in D_2O, 298K, 500 MHz
150-ms spin-lock mixing time

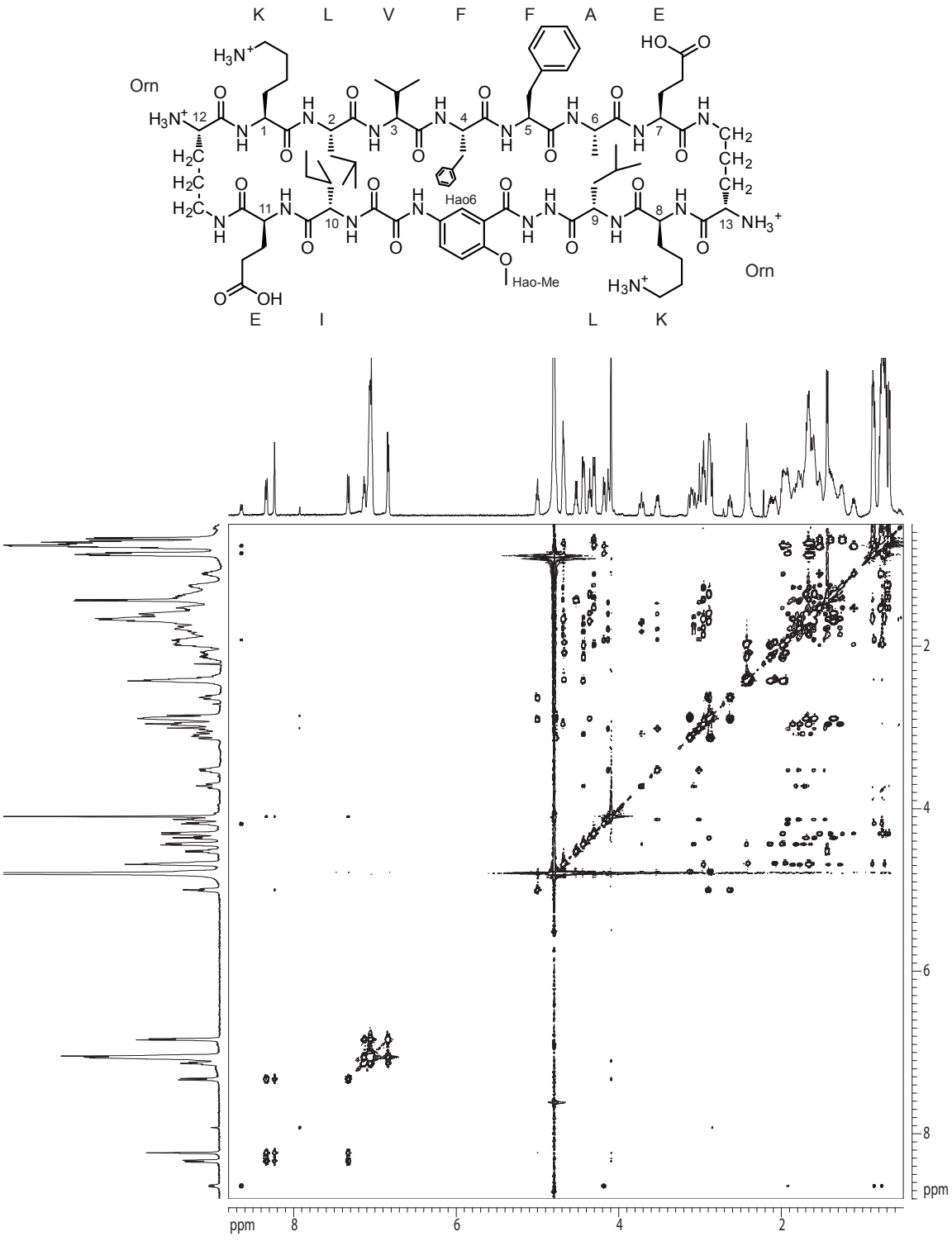

2D TOCSY spectrum of ABSM **2.1a** , 2 mM in D_2O, 298K, 500 MHz
150-ms spin-lock mixing time

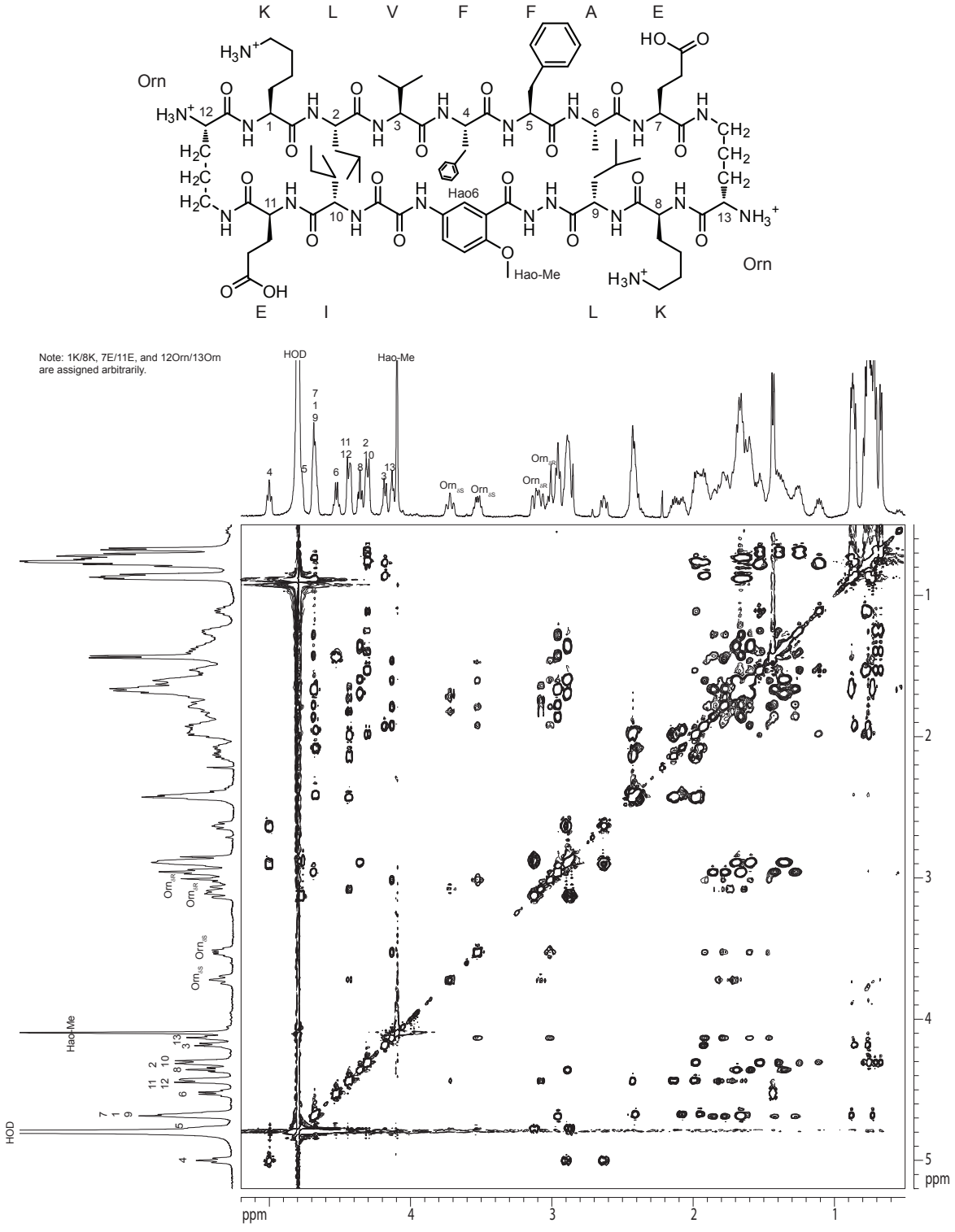

2D TOCSY spectrum of ABSM **2.1a**, 2 mM in D_2O, 298K, 500 MHz
150-ms spin-lock mixing time

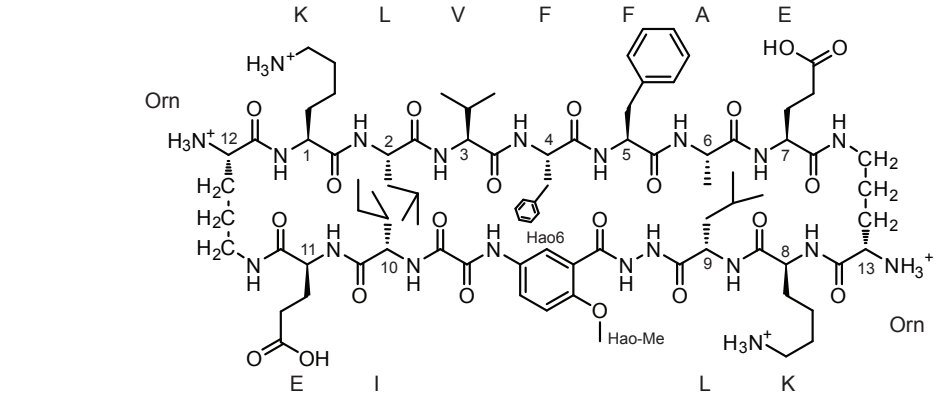

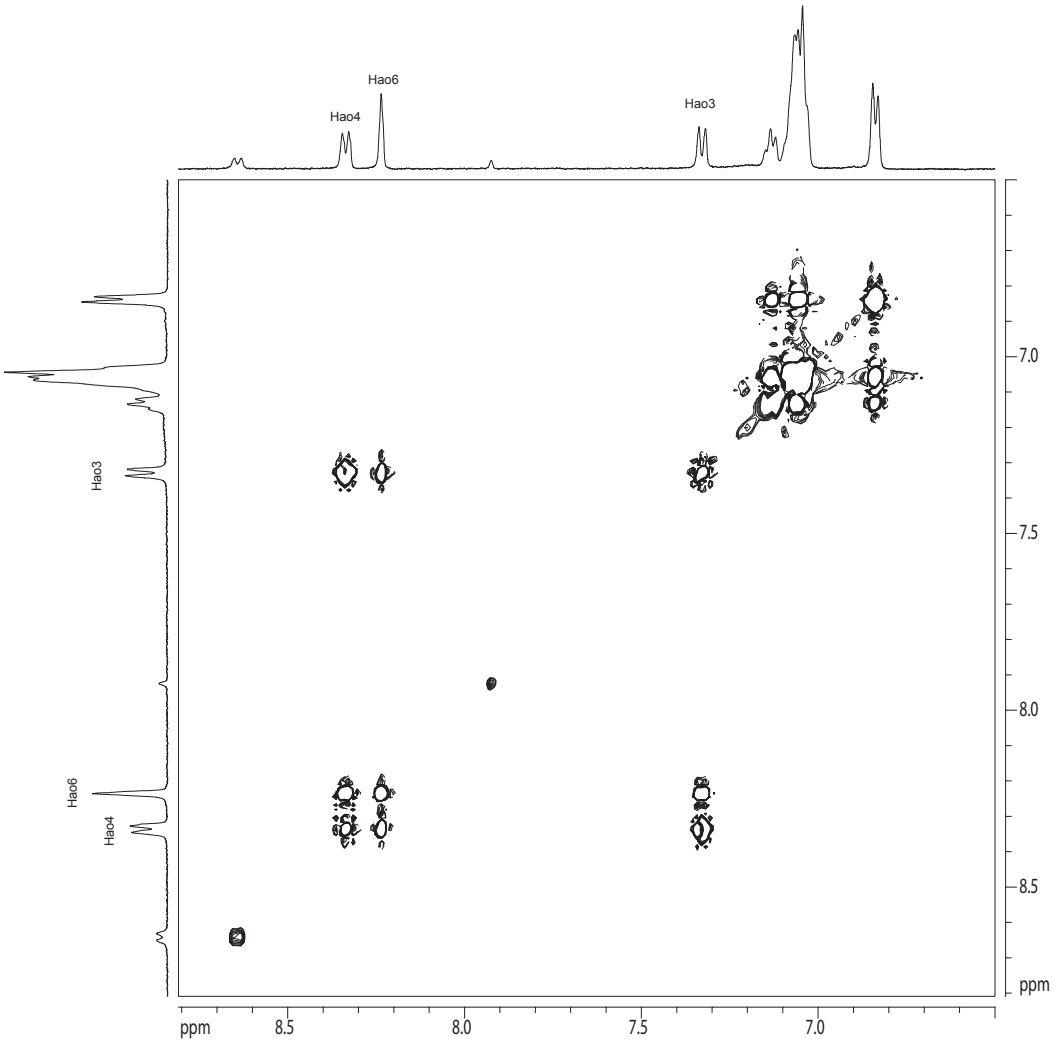

2D ROESY spectrum of ABSM **2.1a**, 2 mM in D_2O, 298K, 500 MHz
300-ms spin-lock mixing time

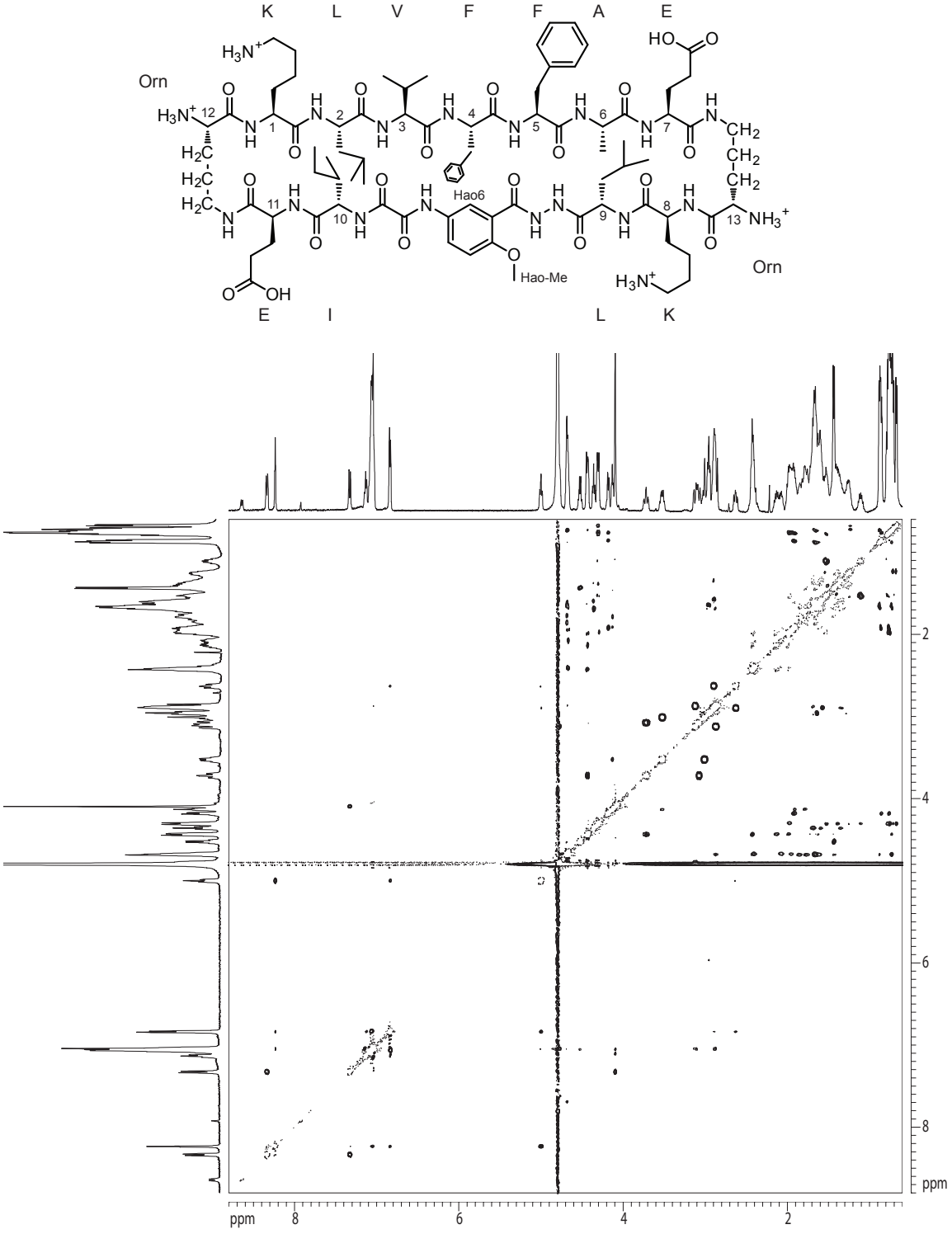

2D ROESY spectrum of ABSM **2.1a** , 2 mM in D_2O, 298K, 500 MHz
300-ms spin-lock mixing time

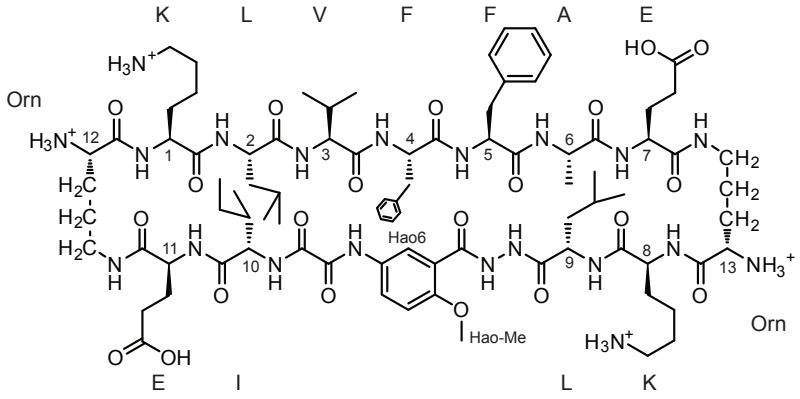

Note: 1K/8K, 7E/11E, and 12Orn/13Orn are assigned arbitrarily.

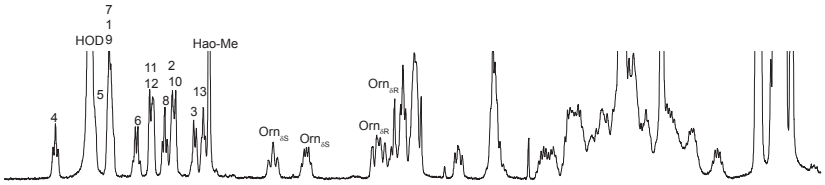

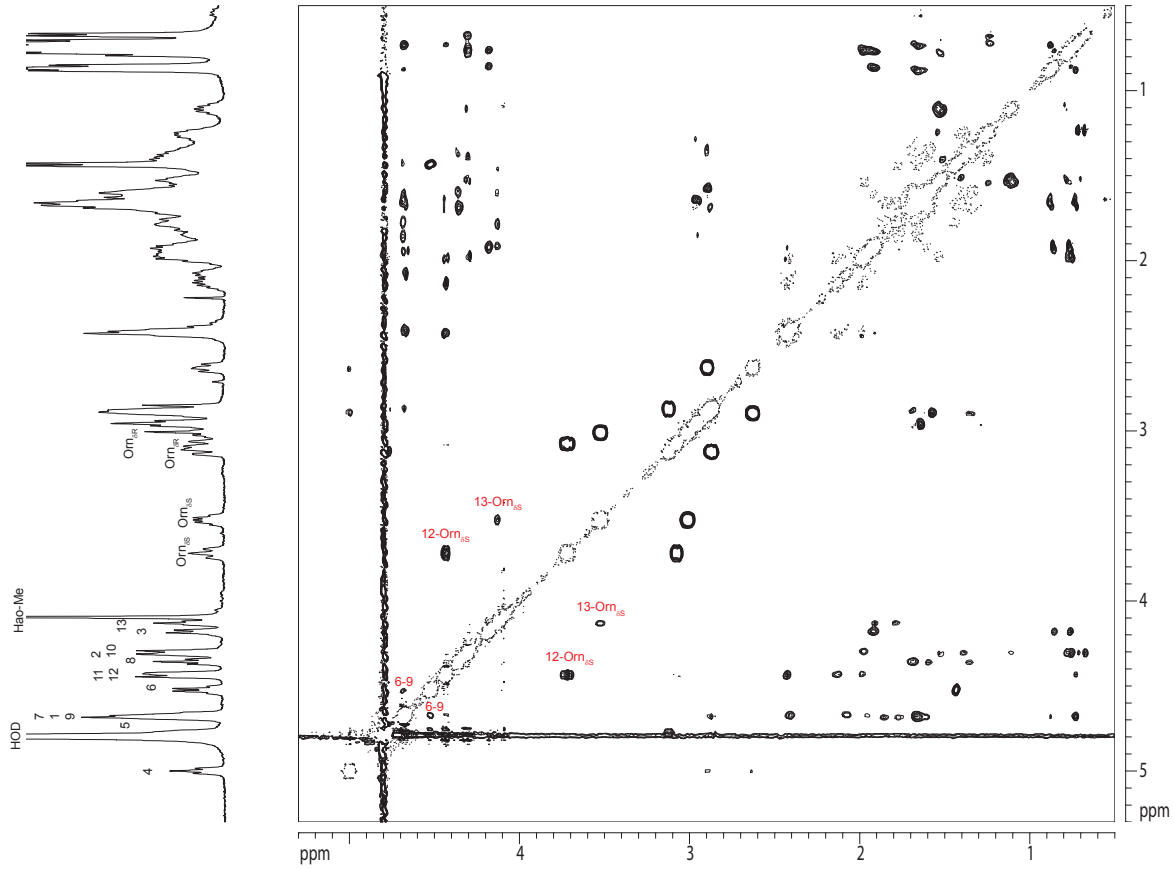

2D ROESY spectrum of ABSM **2.1a**, 2 mM in D_2O, 298K, 500 MHz
300-ms spin-lock mixing time

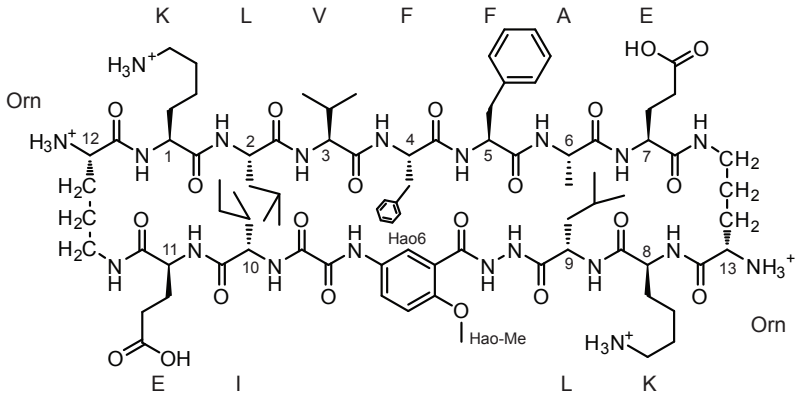

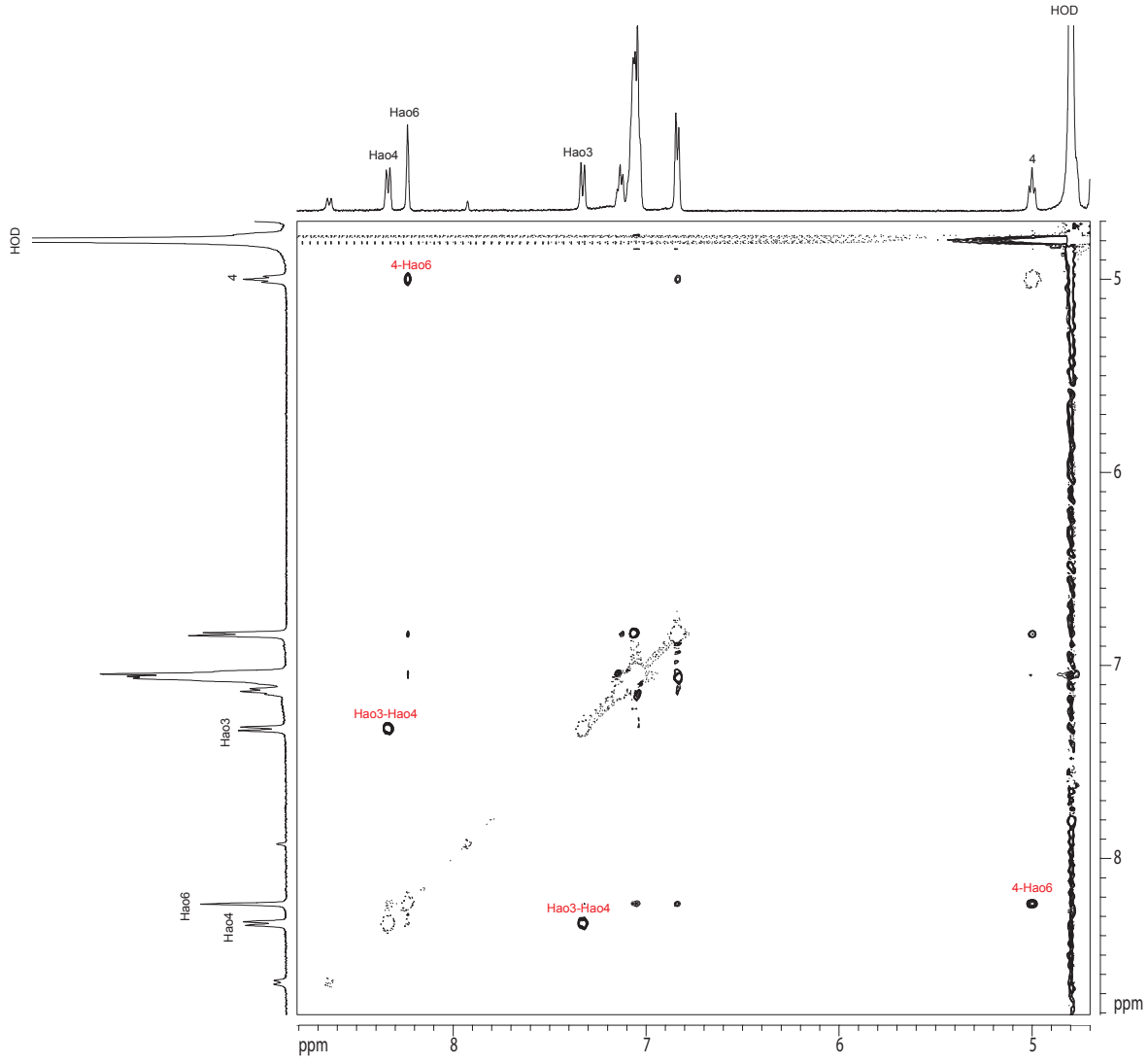

2D ROESY spectrum of ABSM **2.1a**, 2 mM in D_2O, 298K, 500 MHz
300-ms spin-lock mixing time

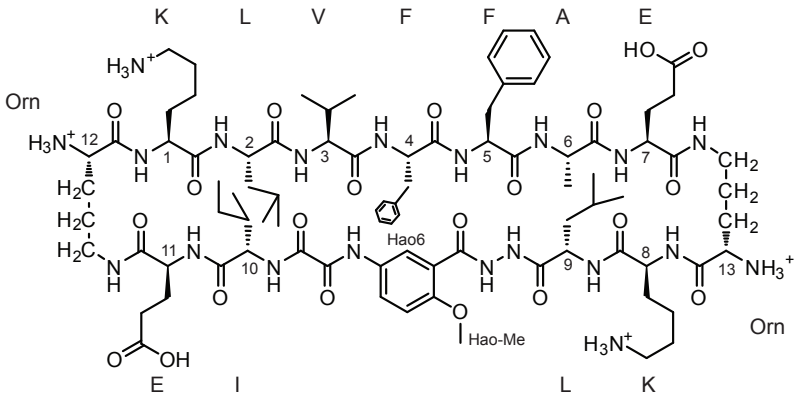

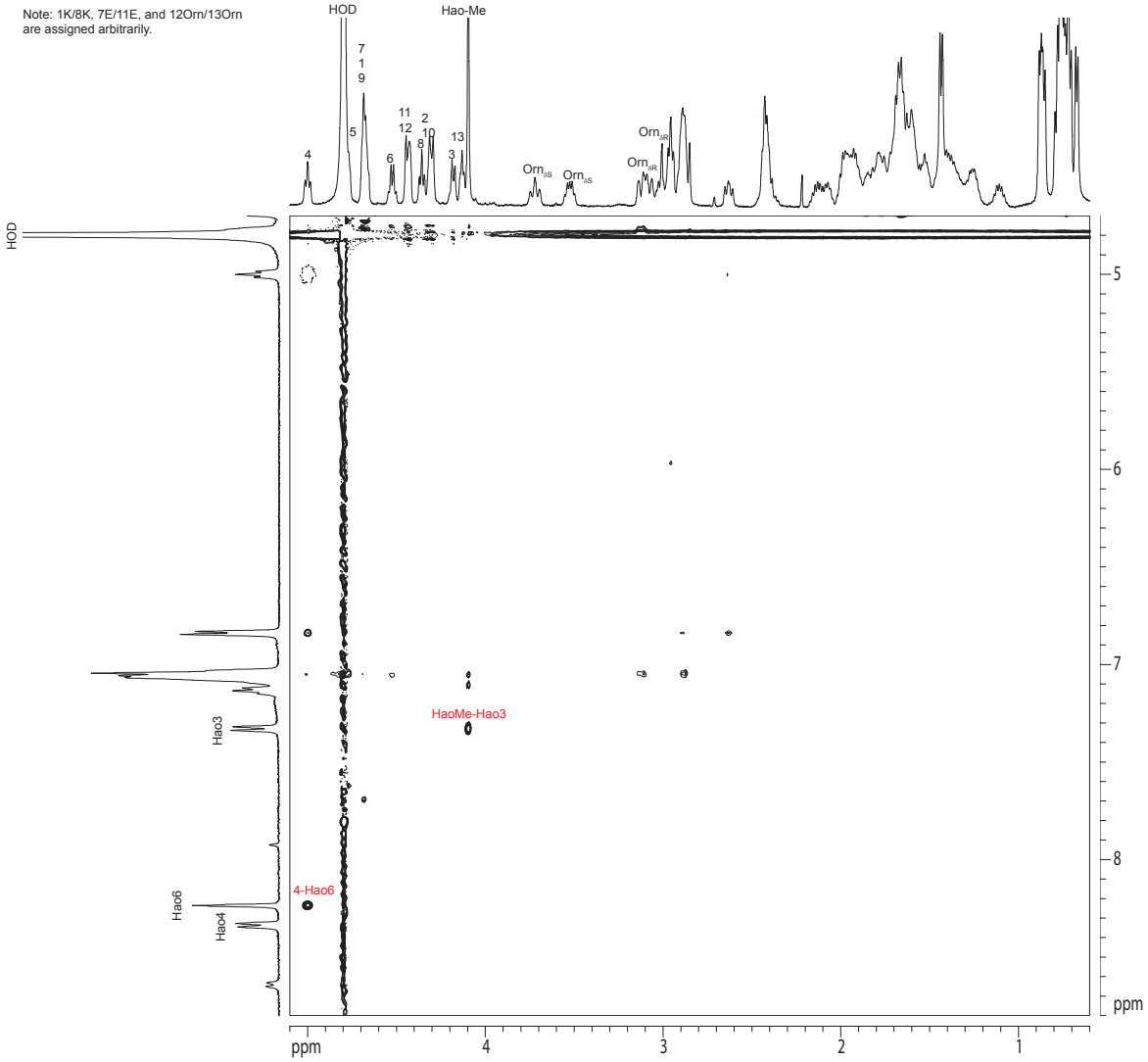

2D ROESY spectrum of ABSM **2.1a**, 2 mM in D_2O, 298K, 500 MHz
300-ms spin-lock mixing time

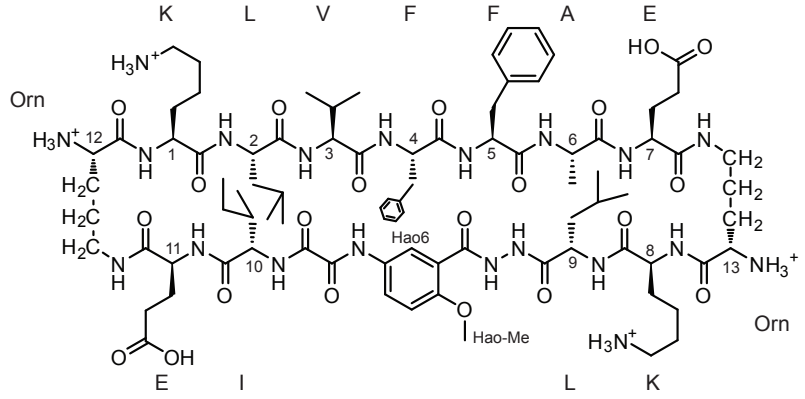

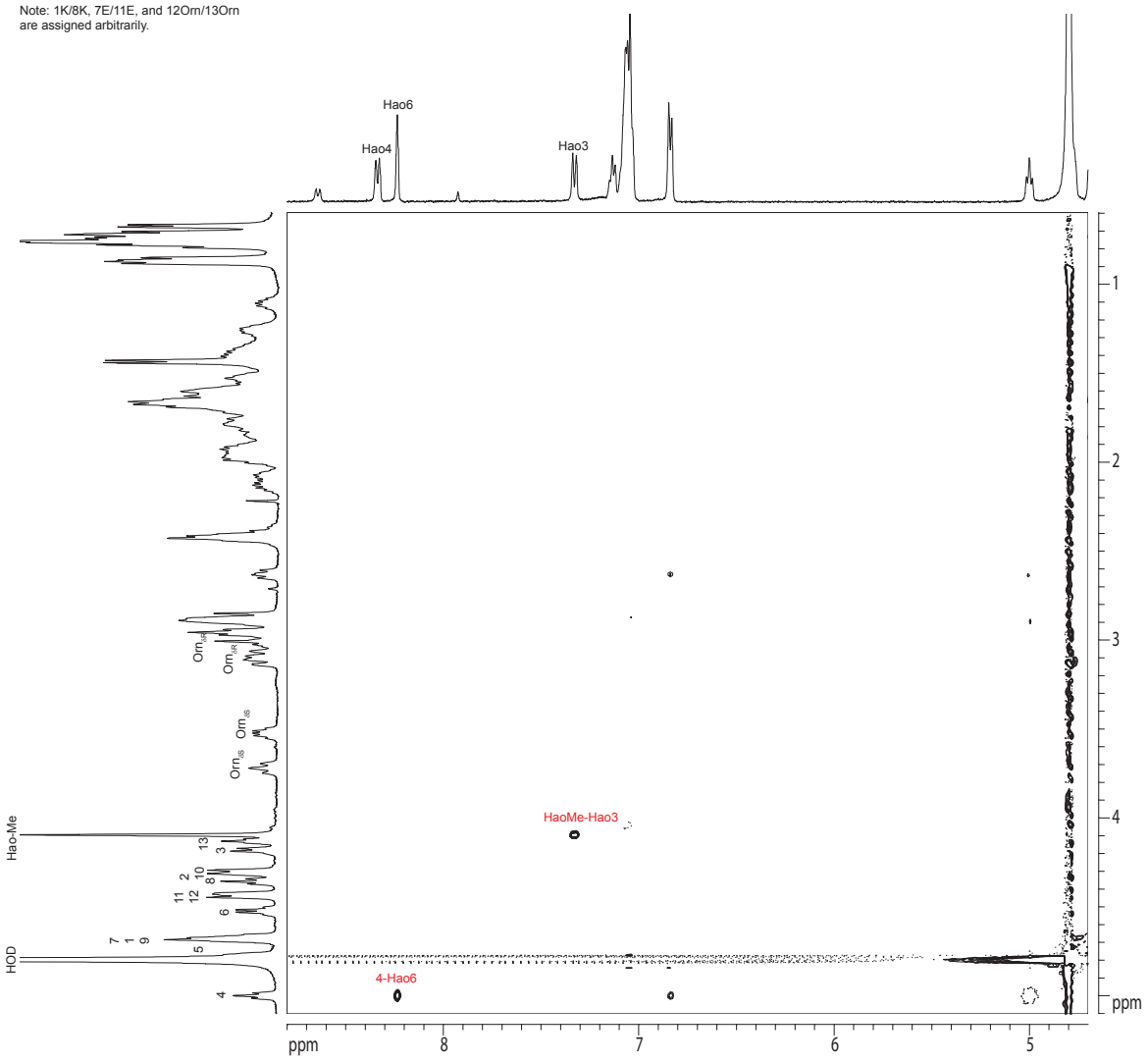

2D DOSY spectrum of ABSM **2.1a**, 5 mM in D_2O, 298K, 600 MHz

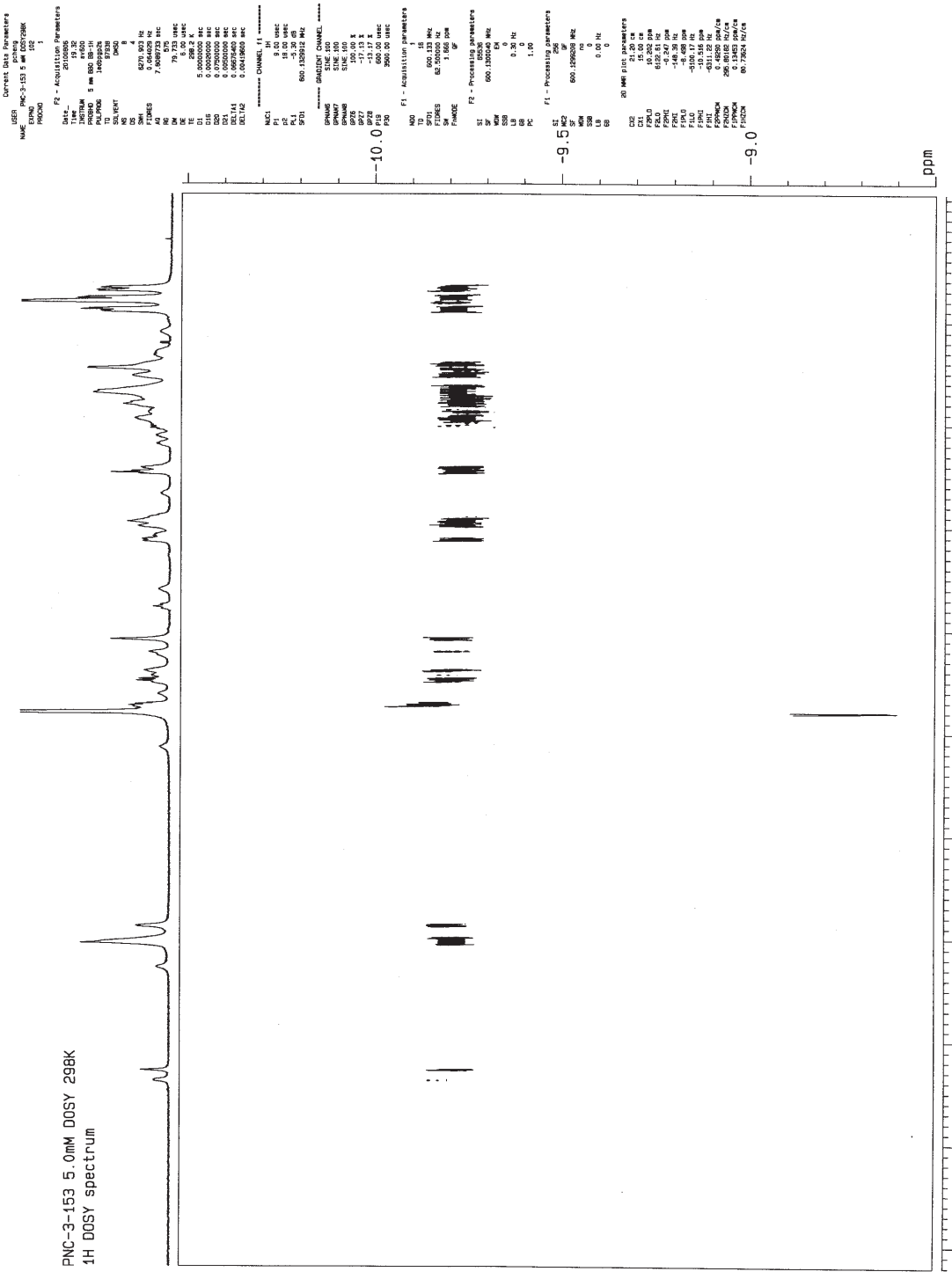

2D DOSY spectrum of ABSM **2.1a**, 3.3 mM in D_2O, 298K, 600 MHz

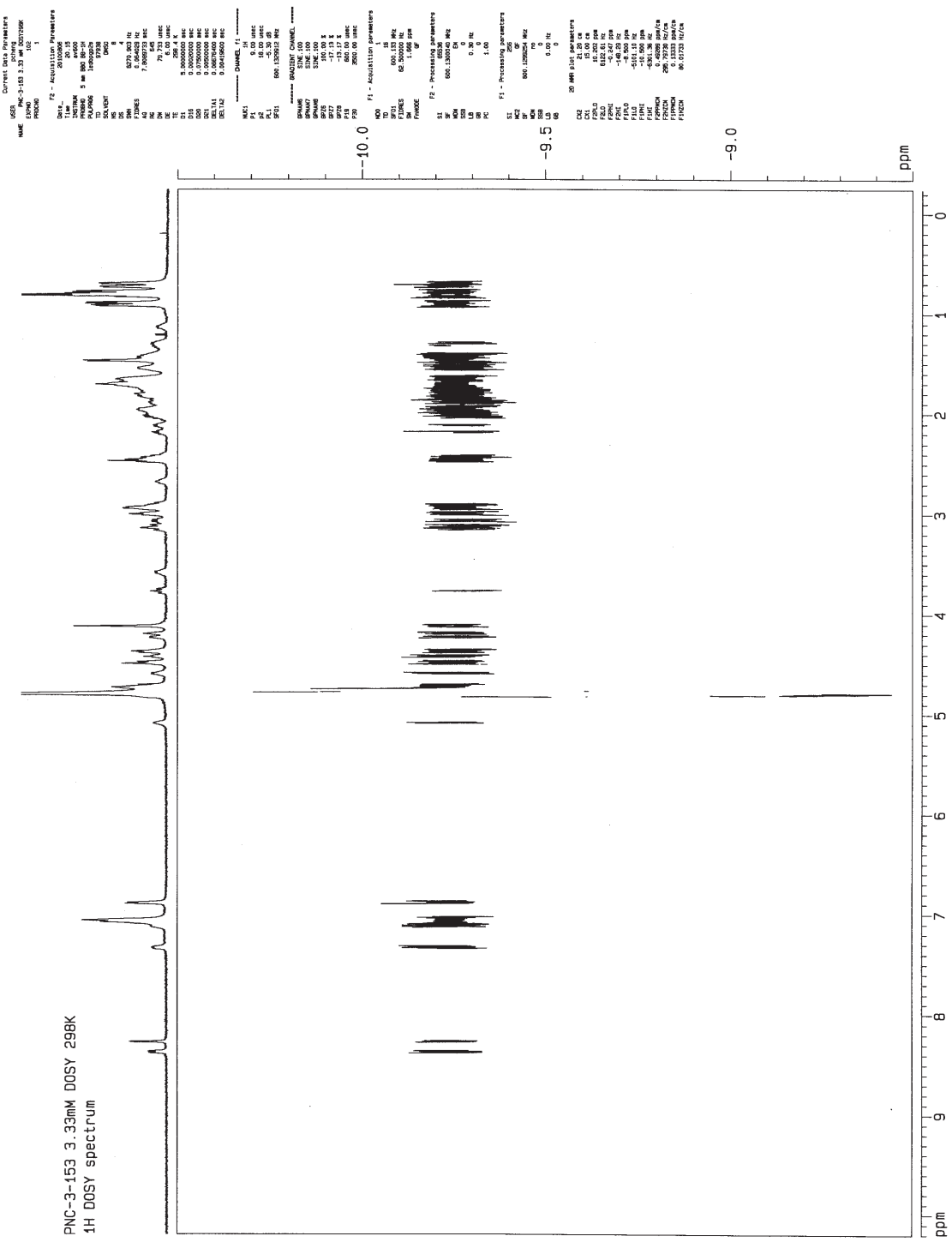

2D DOSY spectrum of ABSM **2.1a**, 2.0 mM in D_2O, 298K, 600 MHz

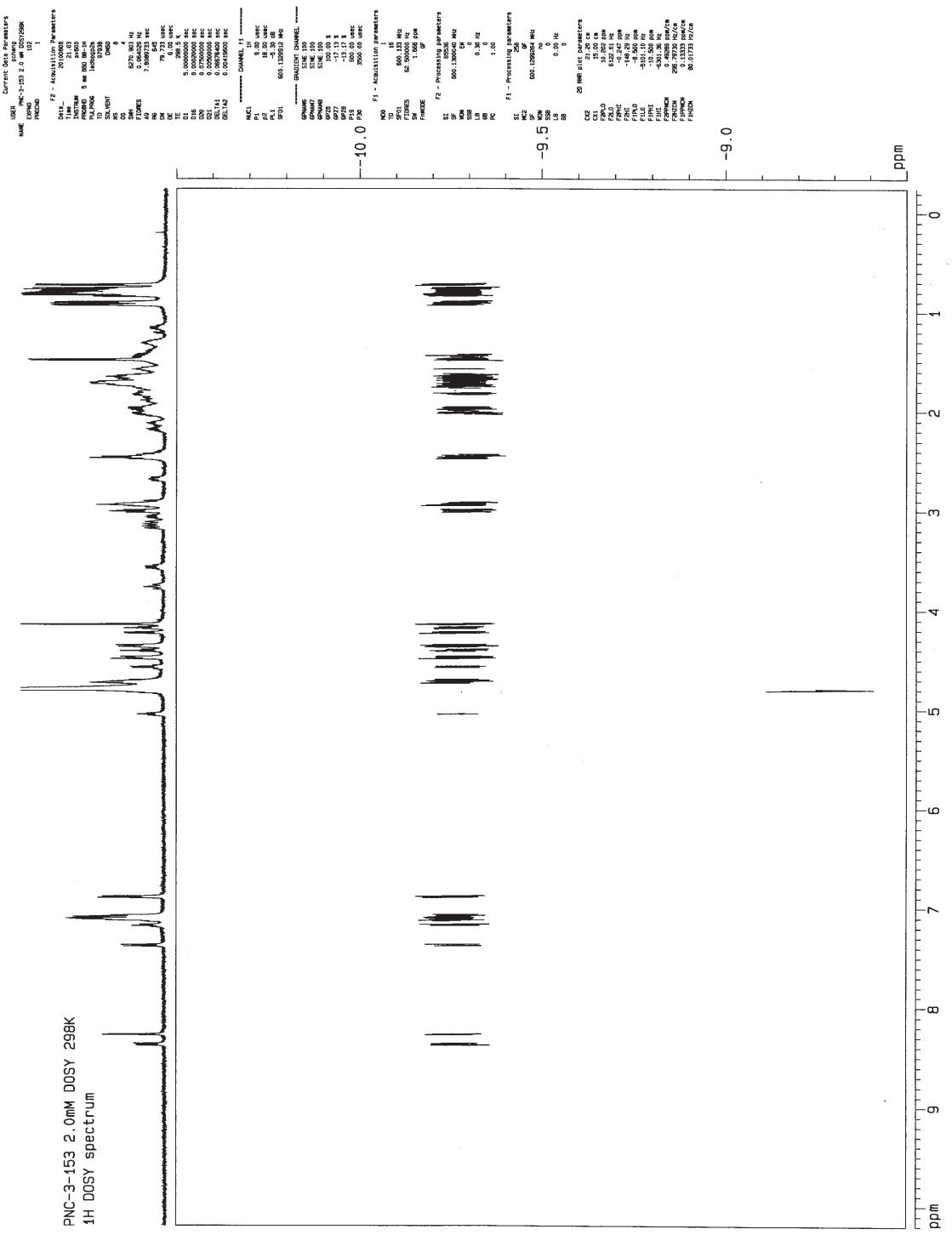

2D DOSY spectrum of ABSM **2.1a**, 1.3 mM in D_2O, 298K, 600 MHz

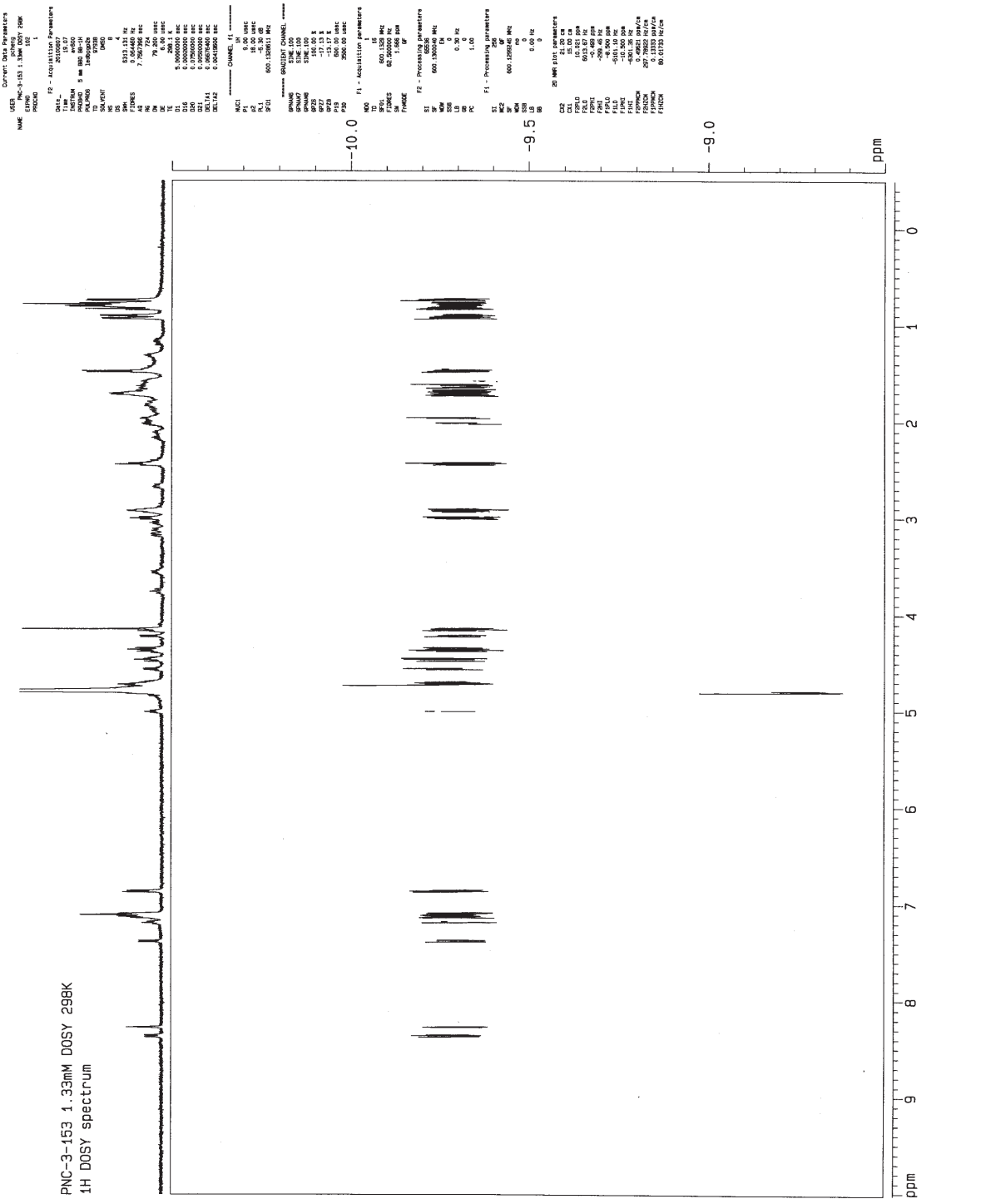

2D DOSY spectrum of ABSM **2.1a**, 1.0 mM in D_2O, 298K, 600 MHz

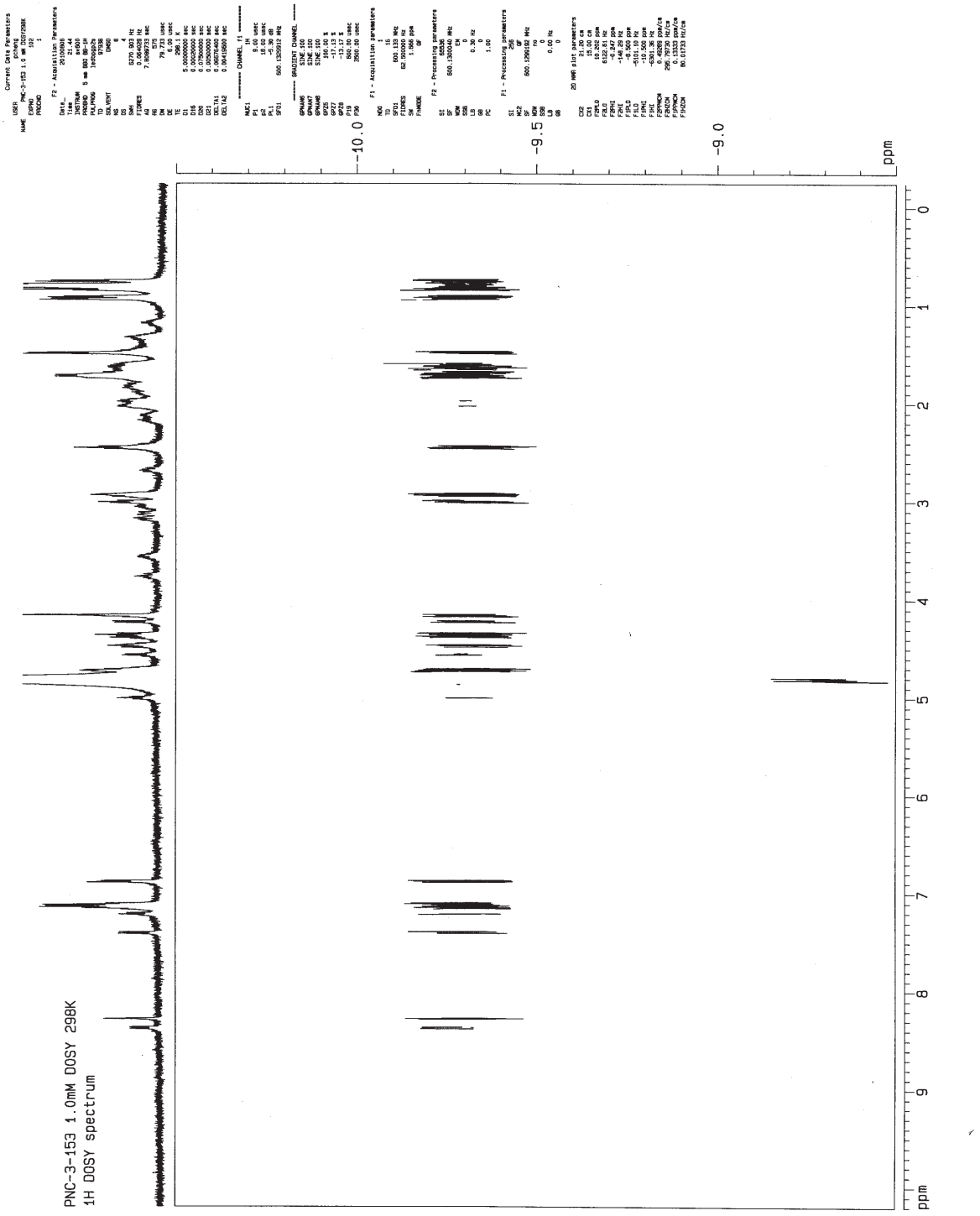

2D DOSY spectrum of ABSM **2.1a**, 0.67 mM in D_2O, 298K, 600 MHz

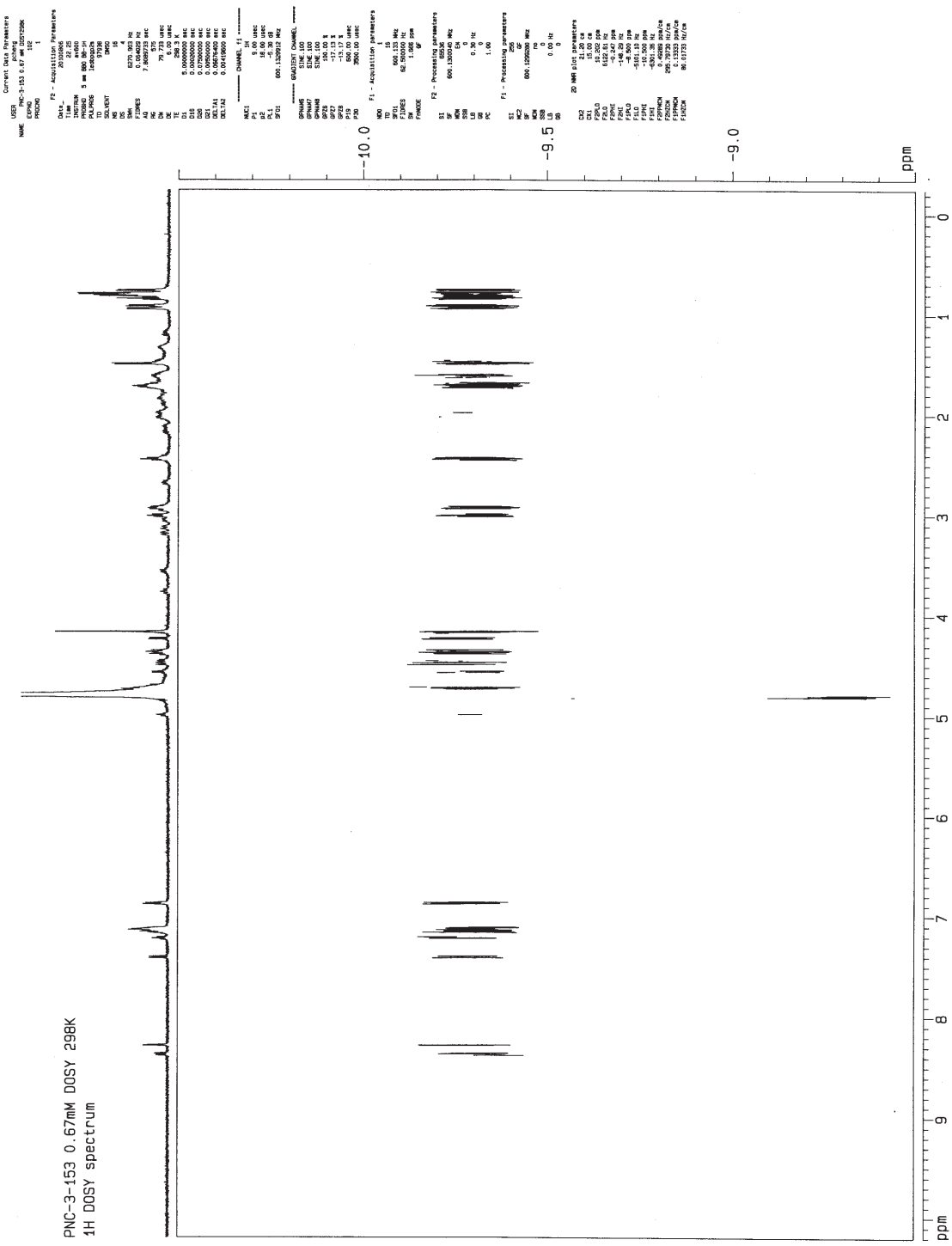

2D DOSY spectrum of ABSM **2.1a**, 0.33 mM in D_2O, 298K, 600 MHz

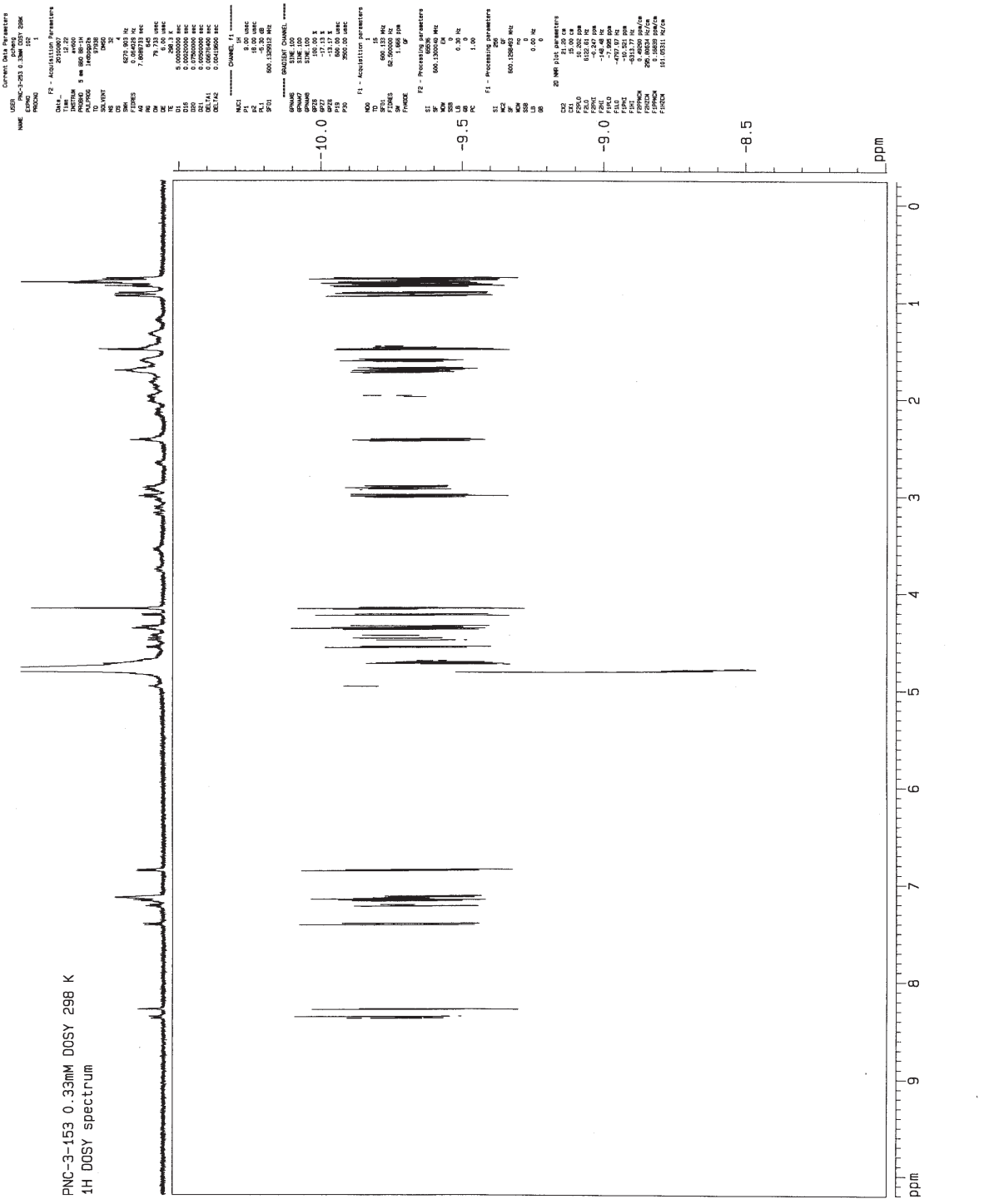

CHAPTER 3

Heterodivalent Linked Macrocyclic β-Sheets with Enhanced Activity against Aβ Aggregation: Two Sites are Better than One

Preamble

Chapter 3 describes the heterodivalent design of the linked macrocyclic β-sheets with enhanced activity against Aβ aggregation. This project started when Dr. R. J. Woods, a former member of the Nowick group, designed and synthesized a divalent linked macrocyclic β-sheet inhibitor (heterodivalent linked macrocyclic β-sheet **3.4e**) against Aβ aggregation based on the published structural models of Aβ fibrils. I continued this project by designing and synthesizing a series of homologous heterodivalent linked macrocyclic β-sheets **3.4a-d**. In doing so, I only learned that heterodivalent β-sheet **3.4a-e** are better inhibitors than their monovalent components (macrocycle **2.4a** and **2.4b**) against Aβ aggregation and that the length of the linker does not substantially affect their activities.

For this reason, I switched the focus from the linkage and the length of linkers of the heterodivalent β-sheet inhibitors to the role of divalency in the inhibitor design. I asked what kind of divalency of the divalent β-sheet inhibitors need, that is, linking two different domains of Aβ or linking two identical ones in the divalent inhibitors. To answer this question, I designed two families of homodivalent linked macrocyclic β-sheets **3.2** and **3.3**. This chapter reports the new understanding about the role of polyvalency in the design of inhibitors against Aβ aggregation that emerged from these studies.

Introduction

Amyloid-β (Aβ) fibrils associated with Alzheimer's disease contain layered β-sheet structures involving β-strands from both the *N*- and *C*-terminal regions of Aβ peptides.[1] NMR-based structural models of Aβ fibrils show that Aβ peptides self-assemble into parallel β-sheets that fold into U-shaped superstructures (Figure 3.1).[2] The two parallel β-sheets of the U-shaped superstructure are layered in an antiparallel fashion. Similar fibril structures also occur in human islet amyloid polypeptide associated with type II diabetes and likely occur more widely in amyloids.[3]

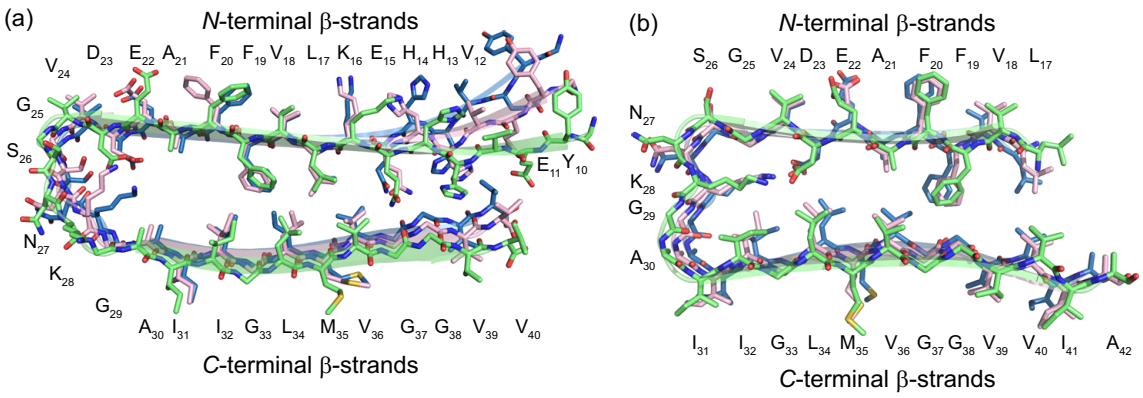

Figure 3.1. NMR-based structural models of Aβ fibrils. (a) Model of $A\beta_{1\text{-}40}$ fibrils. (b) Model of $A\beta_{1\text{-}42}$ fibrils.

Macrocyclic β-sheets containing turn and template units provide useful chemical tools with which to understand and control amyloid aggregation.[4] Our laboratory has introduced 42- and 54-membered ring macrocycles **2.4** and **2.1** that can fold into β-sheet structures and display preorganized β-strands. Macrocycle **2.4** incorporates a pentapeptide β-strand into the upper strand, while macrocycle **2.1** incorporates a heptapeptide β-strand. When these macrocycles display amyloidogenic β-strands, they

are able to inhibit or suppress amyloid aggregation through β-sheet interactions. We have demonstrated that macrocycles **2.4** containing pentapeptide VQIVY can inhibit aggregation of the tau-derived peptide Ac-VQIVYK-NH_2 (AcPHF6) associated with Alzheimer's disease[5] and that macrocycles **2.1** containing amyloidogenic heptapeptide sequences can inhibit aggregation of Aβ, β_2-microglobulin, and α-synuclein and can detoxify Aβ aggregates.[4c,4d] We have also demonstrated that the activity of macrocyclic β-sheets against Aβ aggregation can be dramatically enhanced through expansion from macrocycle **2.4** to macrocycle **2.1**.[4d]

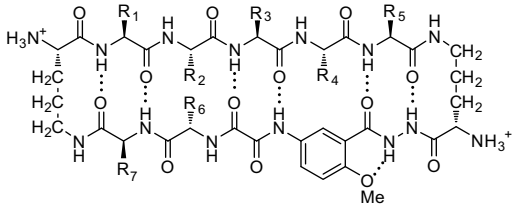

macrocycle **2.4**

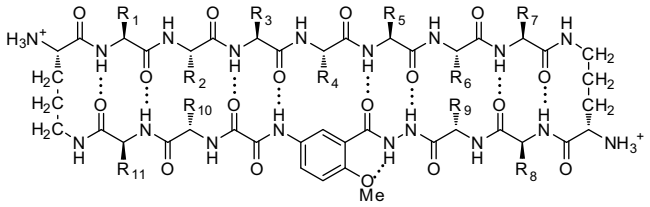

macrocycle **2.1**

Polyvalency is a powerful means for designing ligands that bind more strongly to targets.[6] We have previously shown that macrocycle **2.4** can readily be linked to form divalent macrocyclic β-sheet structures that display two β-sheet domains.[4a] Here, we ask whether this divalency can lead to better inhibitors against Aβ aggregation. To address this question, we designed divalent linked macrocyclic β-sheets by connecting two

macrocycles **2.4** through polyethylene glycol dicarboxylic acid (PEG diacid) linkers **3.1**.[7] We also ask whether targeting two different hydrophobic regions of Aβ with these divalent linked macrocyclic β-sheets would lead better activity than targeting a single hydrophobic region. To address this question, we designed homodivalent linked macrocyclic β-sheets **3.2** and **3.3** and heterodivalent linked macrocyclic β-sheets **3.4**. Homodivalent linked macrocyclic β-sheets **3.2** contain two copies of macrocycle **2.4a** containing $A\beta_{17–21}$ (R_1–R_5 = LVFFA) linked through PEG diacid linkers, while homodivalent linked macrocyclic β-sheets **3.3** contain two copies of macrocycle **2.4b** containing $A\beta_{30–34}$ (R_1–R_5 = AIIGL) linked through PEG diacid linkers. Heterodivalent linked macrocyclic β-sheets **3.4** contain one copy of macrocycle **2.4a** and one copy of macrocycle **2.4b** linked through PEG diacid linkers.

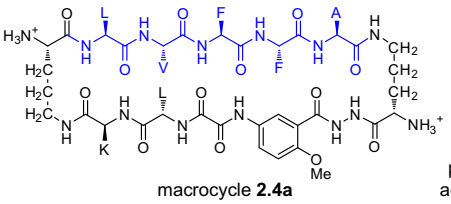

macrocycle **2.4a**

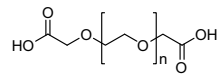

polyethylene glycol dicarboxylic acid linker **3.1a-e**: n = 0, 1, 2, 3, 4

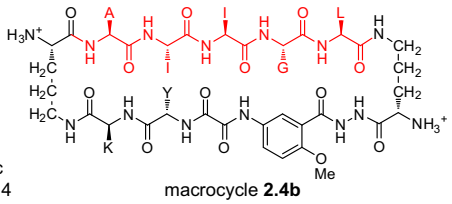

macrocycle **2.4b**

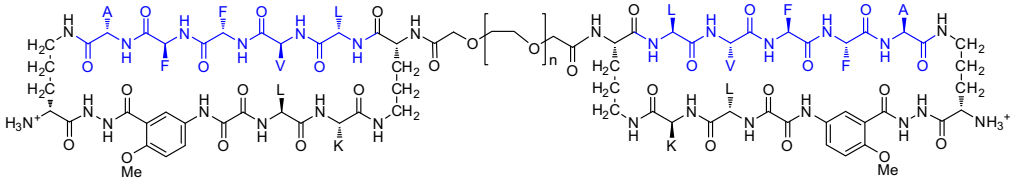

homodivalent linked macrocyclic β-sheet **3.2a**, **3.2e**: n = 0, 4

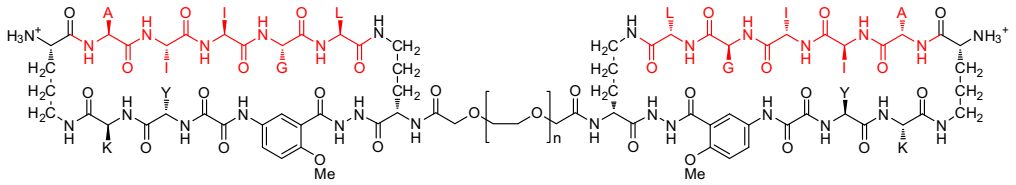

homodivalent linked macrocyclic β-sheet **3.3a**, **3.3e**: n = 0, 4

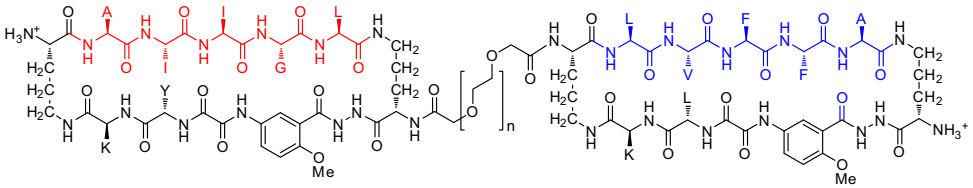

heterodivalent linked macrocyclic β-sheet **3.4a-e**: n = 0, 1, 2, 3, 4

Our studies show that divalent linked macrocyclic β-sheets generally exhibit enhanced activity against Aβ aggregation and that heterodivalent linked macrocyclic β-sheets **3.4** are unexpectedly more active than homodivalent linked macrocyclic β-sheets **3.2** and **3.3**.

Results

1. Syntheses of Divalent Linked Macrocyclic β-Sheets 3.2-3.4. To synthesize divalent linked macrocyclic β-sheets **3.2-3.4**, two macrocycles **3.5** and **3.6**, which each contains a single free amino group in one of the δ-linked ornithine turn units, were

synthesized by according to the published procedures.[4a] To differentiate the two α-amino groups of each macrocycle, Cbz and Boc protecting groups were used to orthogonally protect the two amino groups on the two δ-linked ornithine β-turn turns. Therefore, the Cbz group would be selectively deprotected to free one amino group while the Boc group would remain protected. The liberated amino group would be available for subsequent coupling with PEG diacid linkers **3.1**.

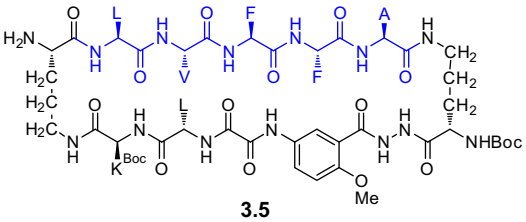

3.5

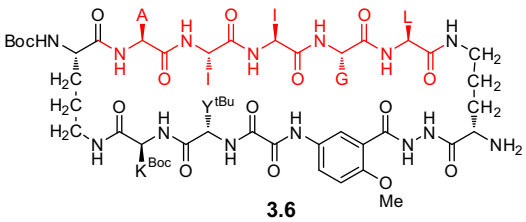

3.6

Macrocycles **3.5** and **3.6** were synthesized by standard Fmoc solid-phase peptide synthesis in which 2-chlorotrityl chloride resin was used as the solid support (Scheme 3.1). First, two different protected ornithine derivatives, Cbz-Orn(Fmoc)-OH and Boc-Orn(Fmoc)-OH, were loaded onto the resin in order to make macrocycles **3.5** and **3.6**, respectively; then the peptides were elongated by using Fmoc chemistry. After the final amino acid was coupled to the growing peptide, the terminal Fmoc group was removed and the linear protected peptide was cleaved from the resin by treatment with a solution of AcOH/MeOH/CH_2Cl_2 (5:1:4). Then, the cyclization was conducted by treatment with HCTU and DIEA in dilute (ca. 0.5 mM) DMF solution. The cyclized peptide was treated with triethylsilane, Pd/C and 10% AcOH in the methanol to remove the Cbz protecting group, followed by reverse-phase HPLC purification to yield macrocycles **3.5** and **3.6**.

Scheme 3.1 Synthesis of Macrocycles **3.5** and **3.6**.

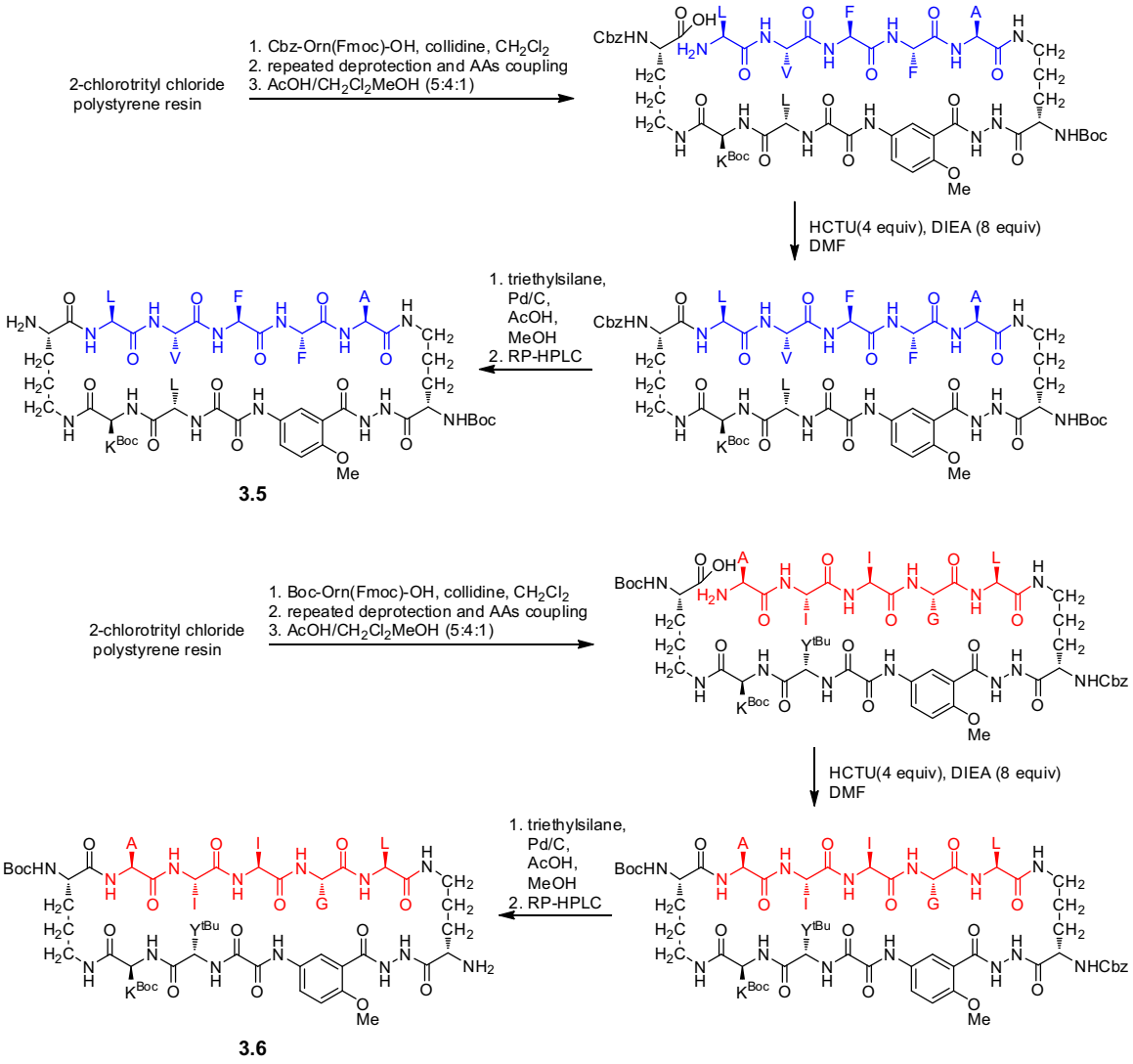

Homodivalent β-sheets **3.2** and **3.3** were synthesized by coupling macrocycles **3.5** or **3.6** with 0.45 molar equivalents of the appropriate PEG diacid linkers **3**, followed by deprotection with TFA solution and reverse-phase HPLC purification. Heterodivalent β-sheets **3.4a-e** were synthesized by first coupling macrocycle **3.6** with a tenfold excess of PEG diacid linkers **3.1a-e** to give monoacids **3.7a-e** (Scheme 3.2). The excess of PEG diacid linkers **3.1a-e** ensured that the major products would only form one amide linkage,

thus leaving one free carboxylic acid group for next coupling. Subsequently, monoacids **3.7a-e** were activated to couple with peptide **3.5** to produce intermediates **3.8**. Without further purification, intermediates **3.8a-e** were deprotected with TFA solution, followed by reverse-phase HPLC purification to yield produce heterodivalent β-sheets **3.4a-e**.

Scheme 3.2 Synthesis of Heterodivalent Macrocyclic β-Sheets **3.4**.

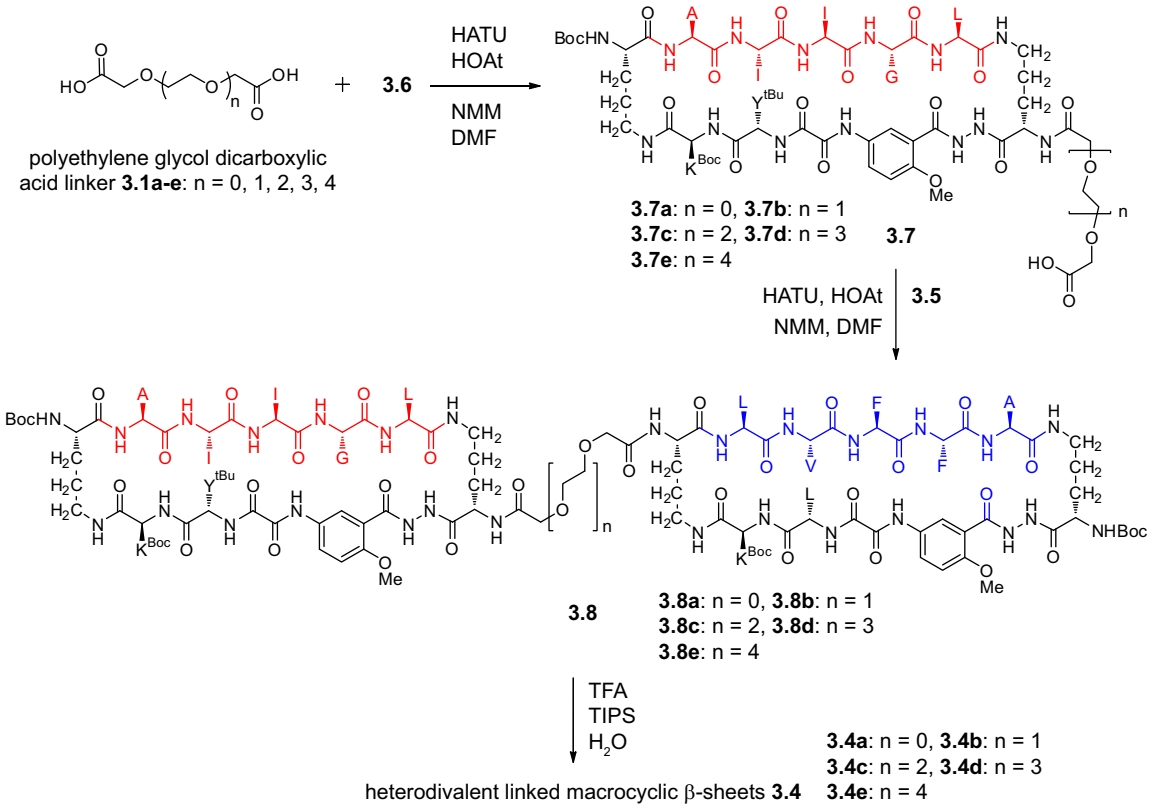

2. Inhibition of Aβ Aggregation by Divalent Linked Macrocyclic β-Sheets.

We used thioflavin T (ThT) fluorescence assays to investigate the effects of divalent β-sheets **3.2-3.4** and monovalent homologues **2.4a** and **2.4b** on $A\beta_{1-40}$ aggregation.[8] The time-course of Aβ aggregation generally demonstrates a sigmoidal curve, containing a lag phase, a growth phase, and an equilibrium phase (Figure 3.2). The duration of the lag phase is widely used as a diagnostic indicator of inhibition of Aβ aggregation. We thus used this lag time to evaluate the activity of **2.4a**, **2.4b**, and **3.2-3.4** against $A\beta_{1-40}$ aggregation.

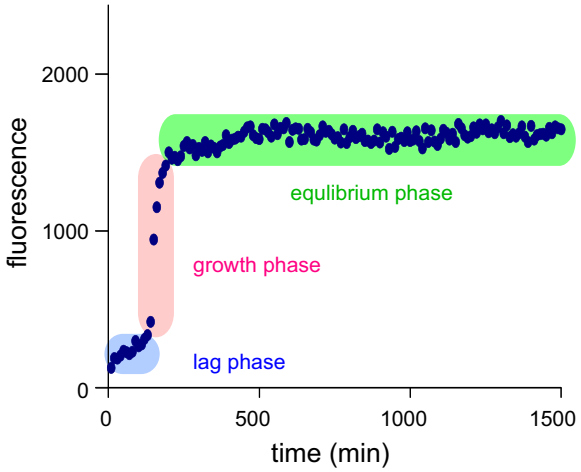

Figure 3.2. Fibrillation kinetics of $A\beta_{1-40}$ monitored by a ThT fluorescence assay. This plot displays three phases of $A\beta_{1-40}$ aggregation: the lag phase, the growth phase, and the equilibrium phase.

ThT fluorescence assays show that macrocycle **2.4a** containing sequence $A\beta_{17-21}$ slightly delays $A\beta_{1-40}$ aggregation, macrocycle **2.4b** containing sequence $A\beta_{30-34}$ accelerates $A\beta_{1-40}$ aggregation, and a mixture of 1 molar equivalent of macrocycle **2.4a** and 1 molar equivalent of macrocycle **2.4b** does not significantly change the lag time (Figure 3.3). Macrocycle **2.4a** delays $A\beta_{1-40}$ aggregation by 30% at 2 equivalents,

increasing the lag time from 107 minutes to 143 minutes, while macrocycle **2.4b** accelerates $A\beta_{1-40}$ aggregation by 50%, reducing the lag time from 107 minutes to 57 minutes. A mixture of 1 equivalent of macrocycle **2.4a** and 1 equivalent of macrocycle **2.4b** exhibits a lag time of 106 minutes, which is within statistical variation of that of $A\beta_{1-40}$ alone. These results are consistent with trends that we have observed in the effects of macrocycles **2** against Aβ aggregation and also support that the central hydrophobic sequence $A\beta_{17-21}$ plays an important role in Aβ aggregation and in the activity of macrocycles **1** and **2** against $A\beta_{1-40}$ aggregation.[4d,9]

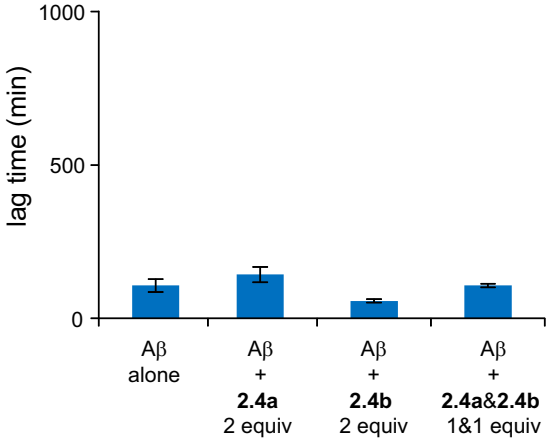

Figure 3.3. Lag time of $A\beta_{1-40}$ aggregation with and without macrocycles **2.4a** and **2.4b**. All ThT assays were carried out on 15 μM $A\beta_{1-40}$ in HEPES buffer at 31°C. (For details, see Figure 3.4.)

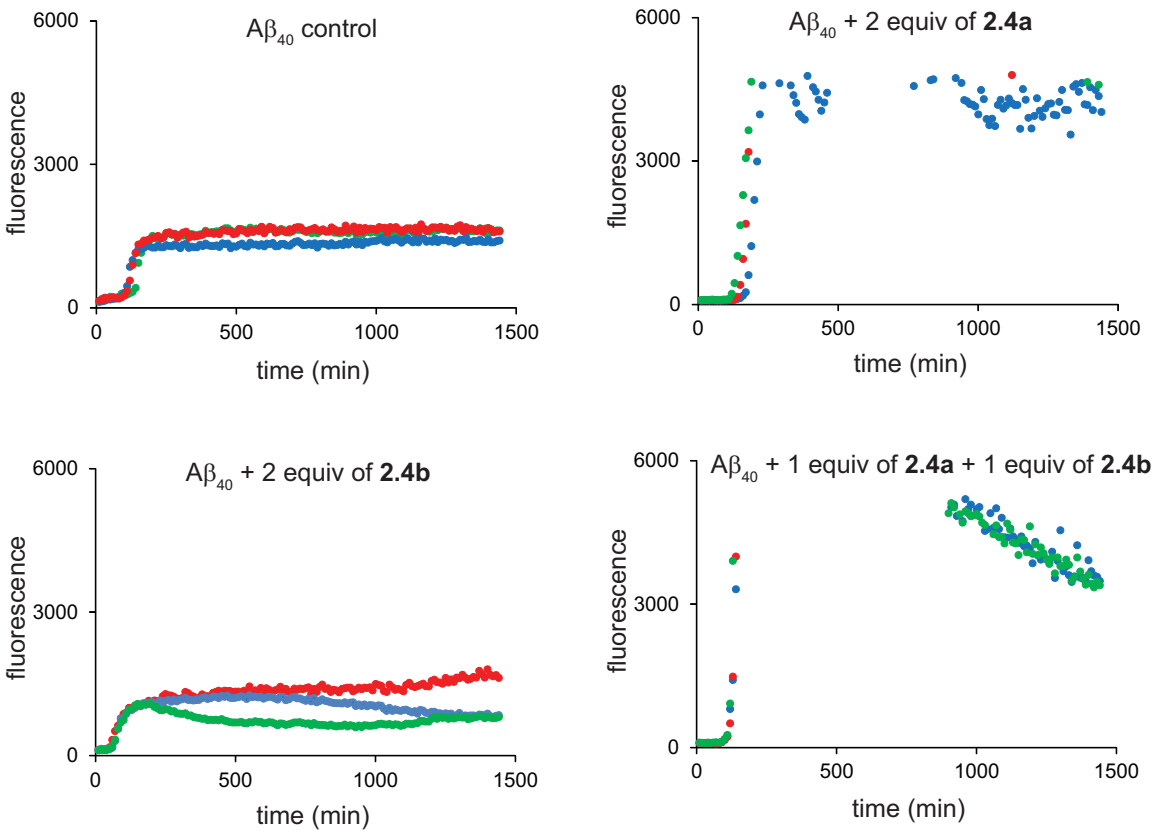

Figure 3.4. Fibrillation kinetics of $A\beta_{1\text{-}40}$ monitored by thioflavin T fluorescence with macrocycles **2.4a** and **2.4b**. These assays were carried out on 15 μM $A\beta_{1\text{-}40}$ peptide in HEPES buffer at 31°C. Data points that exceed the upper limit of fluorescence are omitted for clarity.

ThT fluorescence assays show that heterodivalent β-sheets are not only far more active than their monovalent components but also are dramatically more active against $A\beta_{1-40}$ aggregation than their homodivalent counterparts. Heterodivalent β-sheets **3.4a** and **3.4e** dramatically delay $A\beta_{1-40}$ aggregation by 570% and 660% respectively at 1 equivalent (15 μM), while homodivalent β-sheets **3.2a**, **3.2e**, and **3.3e** slightly delay aggregation by 30–70% and homodivalent and β-sheet **3.3a** accelerates aggregation by 40% (Figures 3.5).

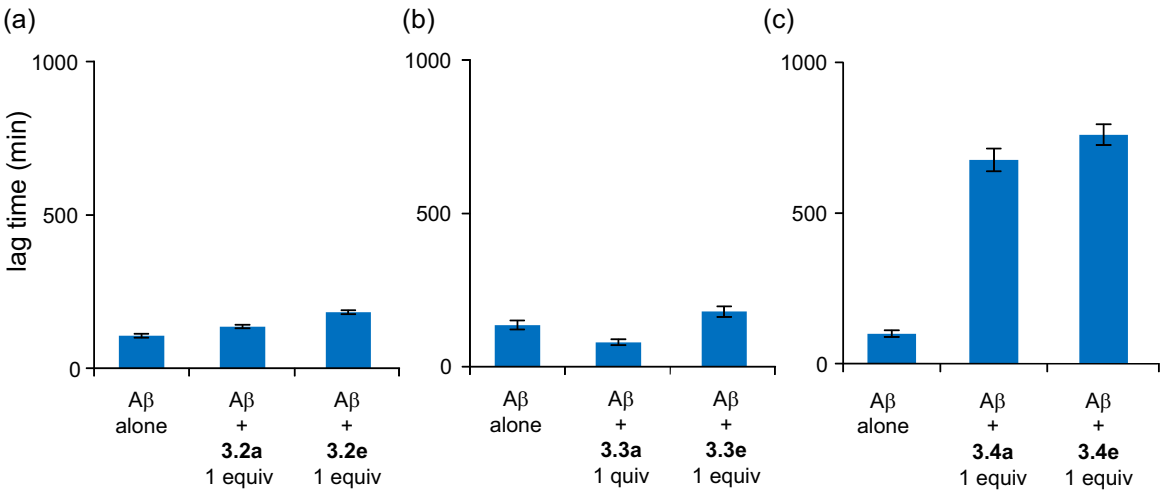

Figure 3.5. (a) Lag time of $A\beta_{1-40}$ aggregation with and without homodivalent β-sheets **3.2a** and **3.2e**. (b) Lag time of $A\beta_{1-40}$ aggregation with and without homodivalent β-sheets **3.3a** and **3.3e**. (c) Lag time of $A\beta_{1-40}$ aggregation with and without heterodivalent β-sheets **3.4a** and **3.4e**. All ThT assays were carried out on 15 μM $A\beta_{1-40}$ in HEPES buffer at 31°C. (For details, see Figure 3.6.)

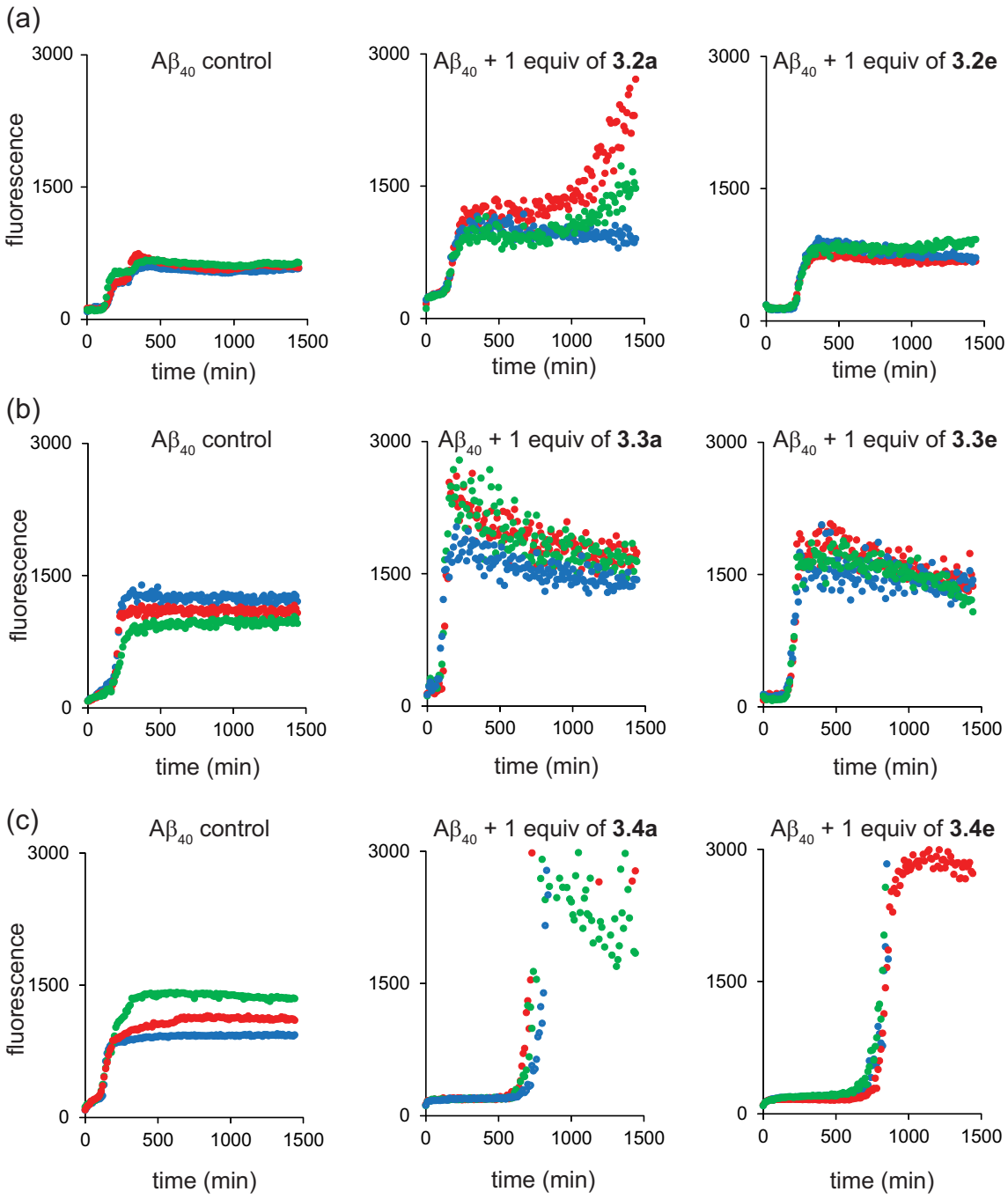

Figure 3.6. Fibrillation kinetics of $A\beta_{1\text{-}40}$ monitored by thioflavin T (ThT) fluorescence with divalent β-sheets **3.2-3.4**. These assays were carried out on 15 μM $A\beta_{1\text{-}40}$ peptide in HEPES buffer at 31°C. Data points that exceed the upper limit of fluorescence are omitted for clarity.

It is interesting that there is no significant difference in lag time between heterodivalent β-sheet **3.4a**, which has a short linker (n = 0), and heterodivalent β-sheet **3.4e**, which has a longer linker (n = 4). To investigate the effect of the linker length, we synthesized additional heterodivalent β-sheets **3.4b-d**, which have linkers of intermediate length (n = 1, 2, and 3). ThT fluorescence assays show that heterodivalent β-sheets **3.4a-e** delay $A\beta_{1-40}$ aggregation by 570–770% at 1 equivalent (Figure 3.7). These results indicate that the size of the PEG-based diacid linkers does not substantially affect the activity of heterodivalent β-sheets **6**. ThT fluorescence assays also show that heterodivalent β-sheets **3.4** inhibit $A\beta_{1-40}$ aggregation at sub-stochiometric concentrations in a dose-dependent manner. Heterodivalent β-sheets **3.4a-e** delay $A\beta_{1-40}$ aggregation at 0.17–1.0 equivalents (2.5–15 μM) by 70–770% (Figure 3.7). Surprisingly, heterodivalent β-sheets **3.4a-e** all nucleate $A\beta_{1-40}$ aggregation at 0.03 equivalents (0.5 μM), accelerating $A\beta_{1-40}$ aggregation by 30–60%. These results indicate that both the activity and the role of the heterodivalent β-sheets in $A\beta_{1-40}$ aggregation depend on their concentrations.

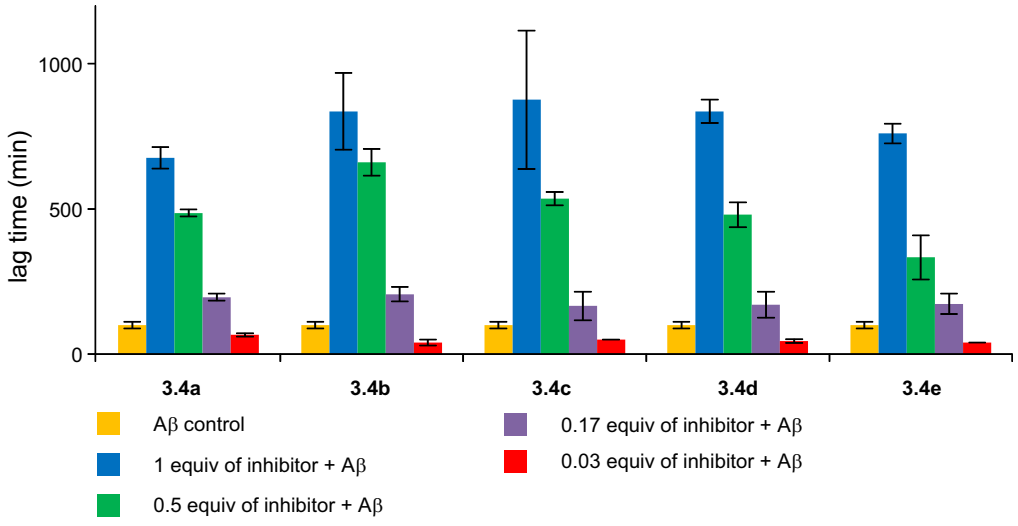

Figure 3.7. Lag time of $A\beta_{1-40}$ aggregation with heterodivalent β-sheets **3.4a-e** at 0.03, 0.17, 0.5, and 1 molar equivalents. All ThT assays were carried out on 15 μM $A\beta_{1-40}$ in HEPES buffer at 31°C. (For details, see Figures 3.8-3.12.)

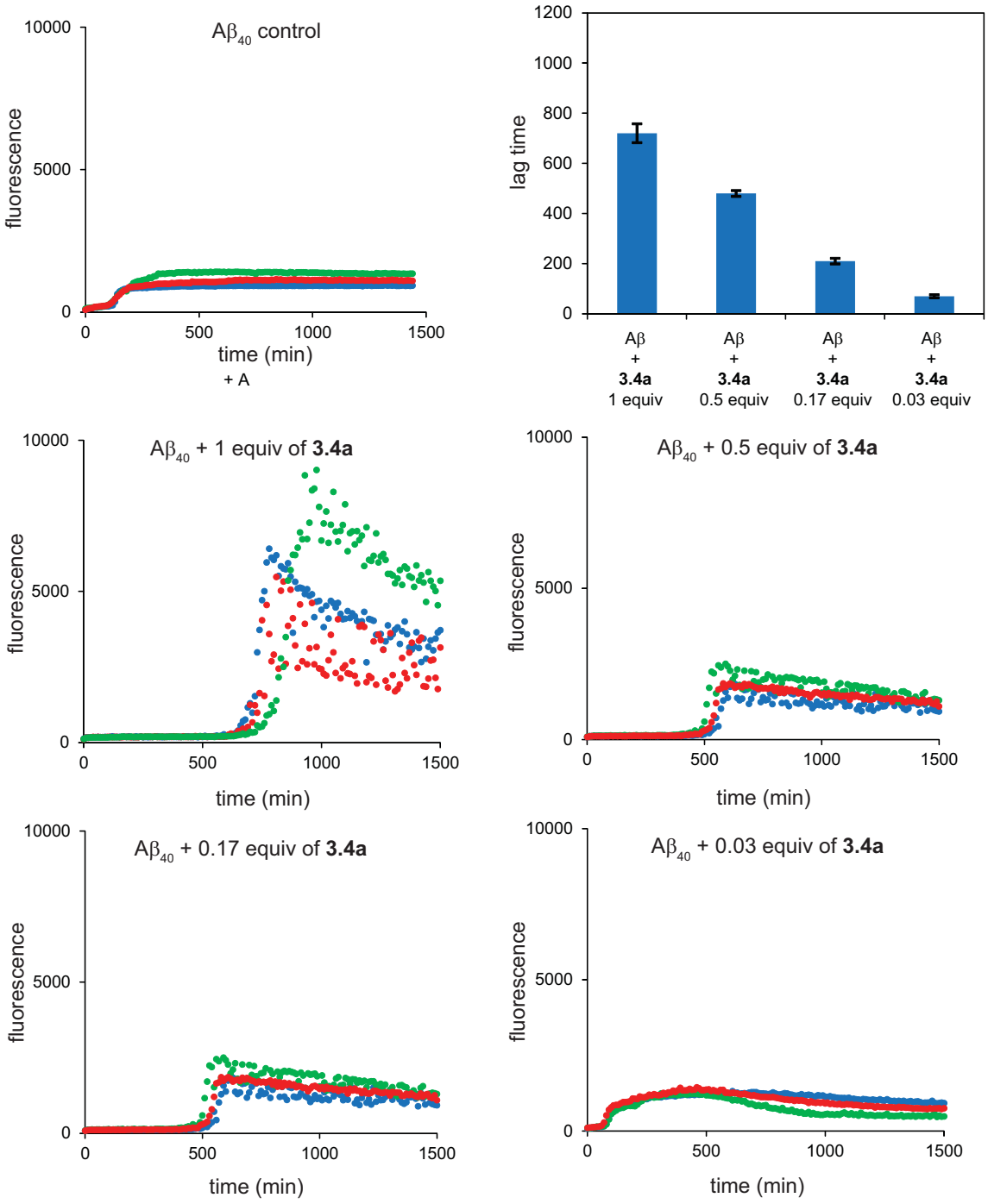

Figure 3.8. Fibrillation kinetics of $A\beta_{1\text{-}40}$ monitored by thioflavin T fluorescence with **3.4a**. These assays were carried out on 15 μM $A\beta_{1\text{-}40}$ peptide in HEPES buffer at 31°C with 0.03, 0.17, 0.5, and 1 equivalent of **3.4a**.

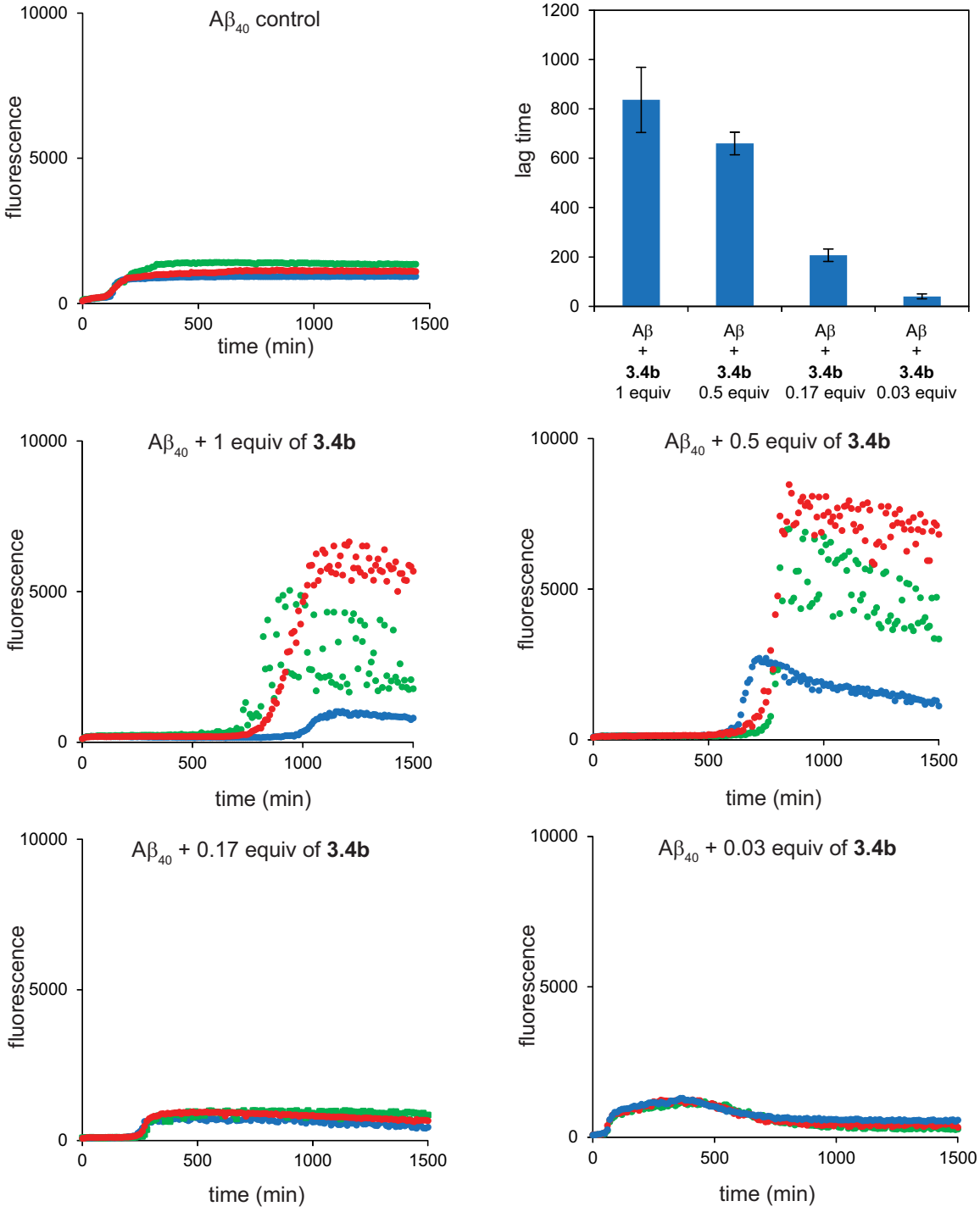

Figure 3.9. Fibrillation kinetics of $A\beta_{1\text{-}40}$ monitored by thioflavin T fluorescence with **3.4b**. These assays were carried out on 15 μM $A\beta_{1\text{-}40}$ peptide in HEPES buffer at 31°C with 0.03, 0.17, 0.5, and 1 equivalent of **3.4b**.

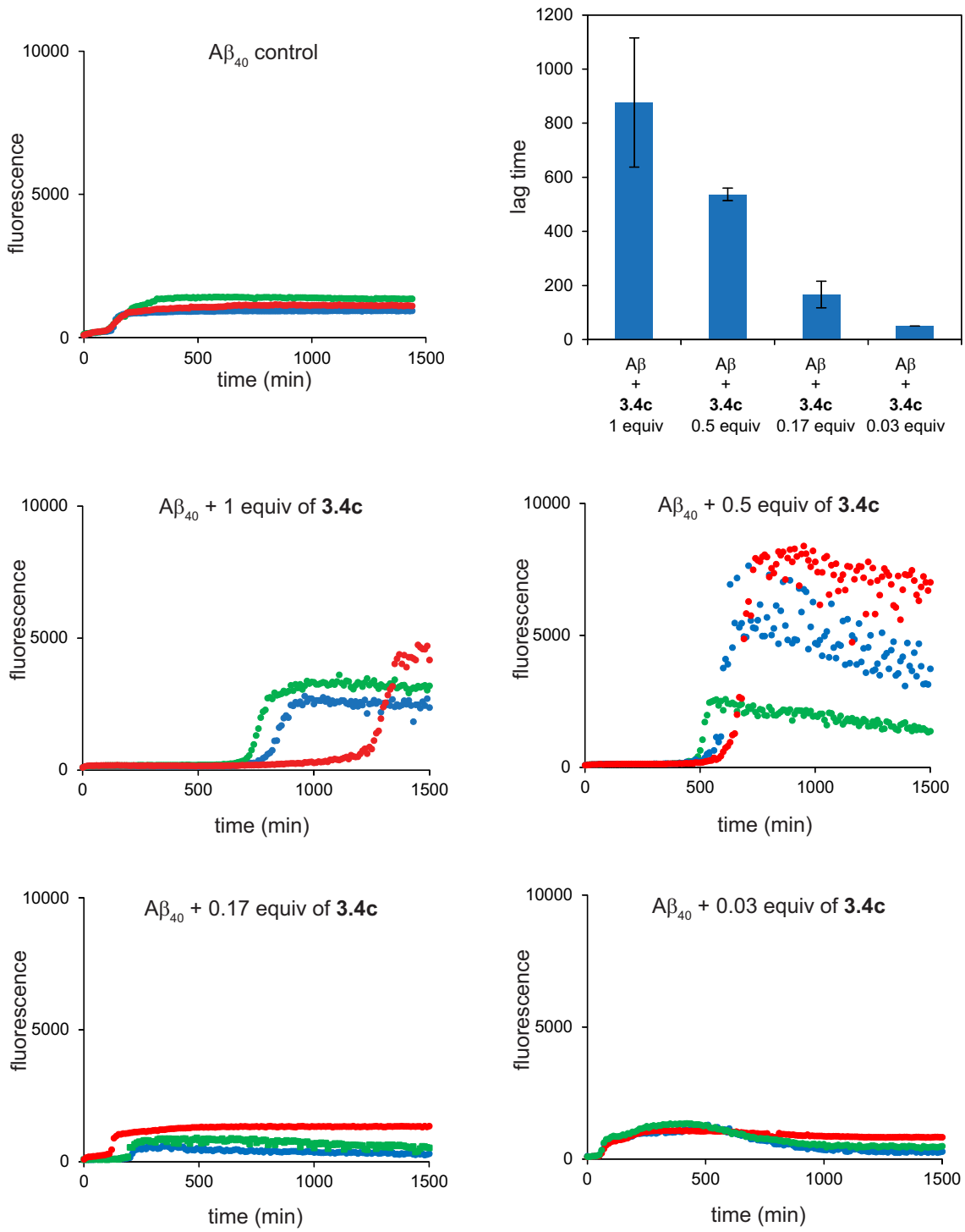

Figure 3.10. Fibrillation kinetics of $A\beta_{1\text{-}40}$ monitored by thioflavin T fluorescence with **3.4c**. These assays were carried out on 15 μM $A\beta_{1\text{-}40}$ peptide in HEPES buffer at 31°C with 0.03, 0.17, 0.5, and 1 equivalent of **3.4c**.

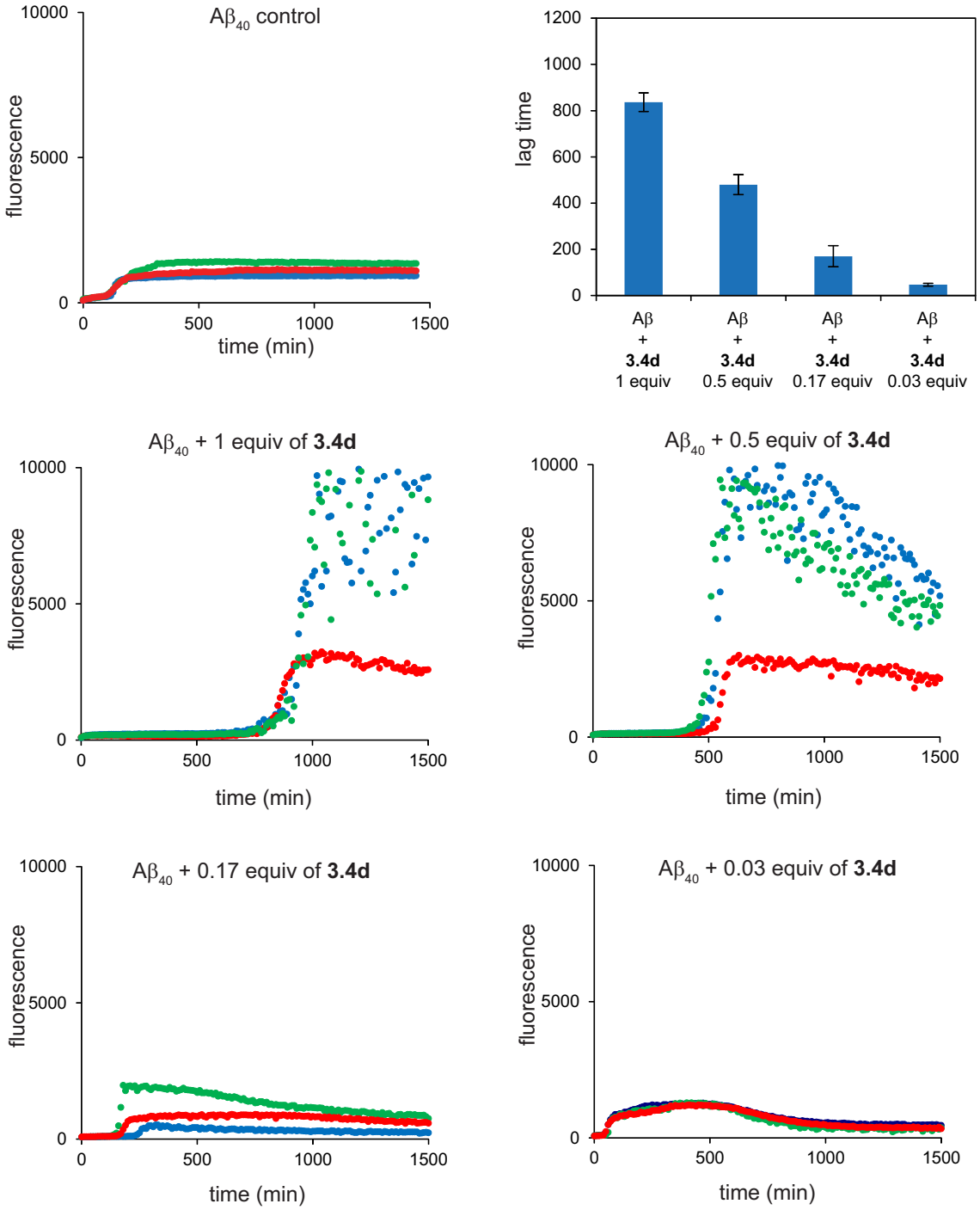

Figure 3.11. Fibrillation kinetics of $A\beta_{1\text{-}40}$ monitored by thioflavin T fluorescence with **3.4d**. These assays were carried out on 15 μM $A\beta_{1\text{-}40}$ peptide in HEPES buffer at 31°C with 0.03, 0.17, 0.5, and 1 equivalent of **3.4d**.

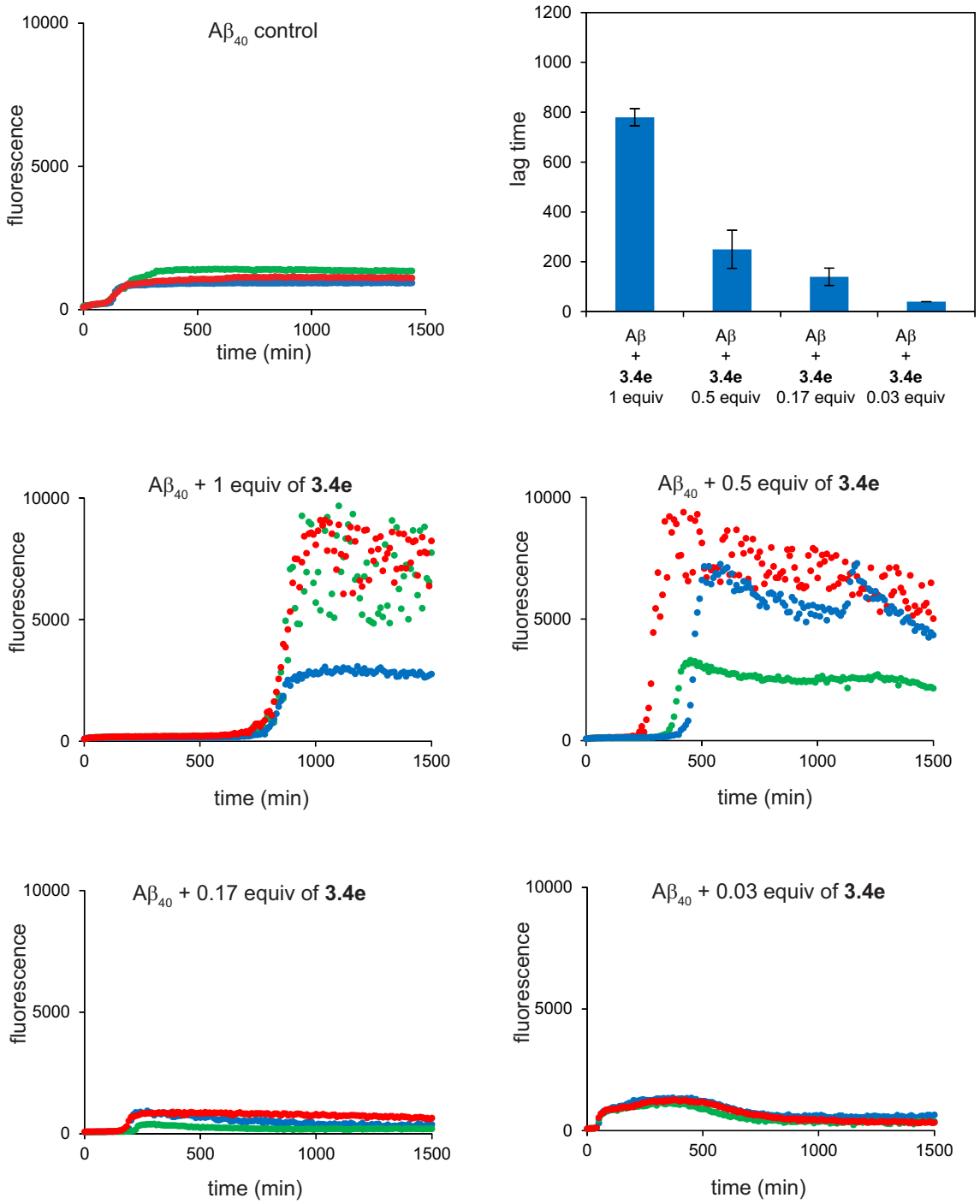

Figure 3.12. Fibrillation kinetics of $A\beta_{1\text{-}40}$ monitored by thioflavin T fluorescence with **3.4e**. These assays were carried out on 15 μM $A\beta_{1\text{-}40}$ peptide in HEPES buffer at 31°C with 0.03, 0.17, 0.5, and 1 equivalent of **3.4e**.

Discussion

It is surprising that the heterodivalent linked β-sheets show enhanced inhibitory activity, given that only one of their components inhibits $A\beta_{1\text{-}40}$ aggregation and the other accelerates aggregation. A model based on both nucleation-dependent polymerization and that which we have previously proposed may explain this enhanced inhibition.[4d,10] In this model, $A\beta_{1\text{-}40}$ aggregates to form early β-structured oligomers, which proceed to form a β-structured nucleus, and finally polymerize to form cross-β fibrils. Inhibitors bind to and stabilize the early β-structured oligomers and thus delay aggregation, while accelerators create a new, lower energy pathway for aggregation. Figure 3.13 provides a reaction free-energy diagram for the native, inhibited, and accelerated $A\beta_{1\text{-}40}$ aggregation with black, blue, and red curves. Better inhibitors bind to the early β-structured oligomers more strongly and thus better delay the formation of the β-structured nucleus.

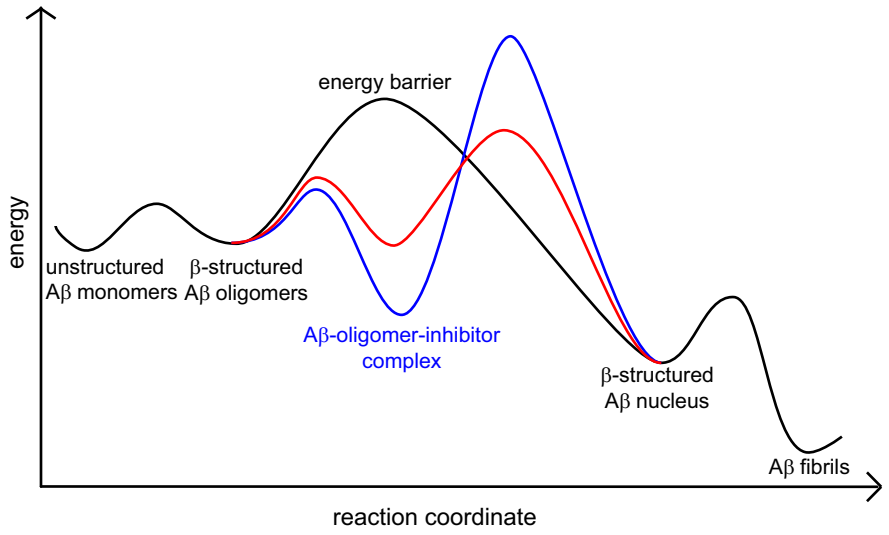

Figure 3.13. Effect of inhibitors and accelerators on the energetics of Aβ aggregation. The black curve corresponds to a pathway in which $A\beta_{1\text{-}40}$ aggregates without inhibitors, while the blue and red curves corresponds to pathways in which $A\beta_{1\text{-}40}$ aggregates with inhibitors and accelerators respectively.

The hydrophobic *N*-terminal $A\beta_{17-21}$ (LVFFA) region forms the core of the β-structured oligomers, in which hydrogen bonding and hydrophobic interactions create a multilayered β-sheet structure (Figure 3.14a). Similar multilayered β-sheet structures are also observed in macrocycle **2.4a** and the amyloid-like fibrils formed by peptide fragment $A\beta_{16-21}$ (KLVFFA).[4b,11] Macrocycle **2.4a** containing the *N*-terminal LFVVA pentapeptide complements and binds to the oligomers though similar types of interactions and thus inhibits aggregation (Figure 3.14b). Macrocycle **2.4b** containing the *C*-terminal AIIGL pentapeptide better complements the *C*-terminal region of $A\beta_{1-40}$ and facilitates the transition of $A\beta_{1-40}$ to the U-shaped superstructure associated with fibrils. In the U-shaped superstructure, the *C*-terminal region also forms β-sheet structure and is packed against the *N*-terminal region. By facilitating the formation of the U-shaped superstructure, macrocycle **2.4b** accelerates aggregation.

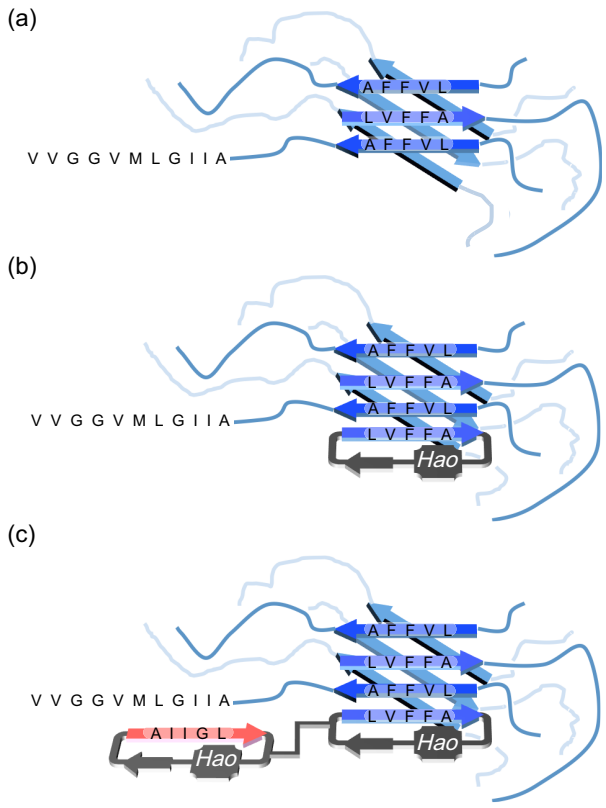

Figure 3.14. Model for enhanced activity of heterodivalent β-sheets **6** against $A\beta_{1\text{-}40}$ aggregation. (a) Aβ oligomer. (b) Aβ-oligomer-**2.4a** complex. (c) Aβ-oligomer-**3.4** complex.

The modest effect of homodivalent linkage in **3.2** and **3.3** suggests that the β-structured oligomers do not present multiple exposed β-sheet edges in sufficient proximity to be bridged by short PEG linkers. Heterodivalent linked macrocyclic β-sheets **3.4** bind to the β-structured oligomers more strongly, because the LFVVA-containing macrocycle can bind to the core of the β-structured oligomers while the AIIGL-containing macrocycle can achieve additional interactions with the *C*-terminal region of $A\beta_{1\text{-}40}$ (Figure 3.14c). While this model explains the dramatically enhanced inhibition by heterodivalent β-sheets **3.4**, it does not explain their acceleration at 0.03 equivalents or the slight inhibition by homodivalent β-sheet **3.3e**. Nevertheless, this working model

provides a framework for the design of even more effective inhibitors that target both the *N*- and *C*-terminal regions of Aβ.

Conclusion

The heterodivalent design of linked macrocyclic β-sheets **3.4** enhances their activity against Aβ aggregation. The enhanced activity suggests that polyvalent inhibitors that can target multiple regions of Aβ are better than ones that only target a single region. The strategy described herein may be able to be applied to design of inhibitors against aggregation of other amyloid proteins and provides new insights into amyloid aggregation.

References and Notes

1. (a) Roychaudhuri, R.; Yang, M.; Hoshi, M. M.; Teplow, D. B., *J. Biol. Chem.* **2009**, *284*, 4749–4753. (b) Jakob-Roetne, R.; Jacobsen, H., *Angew. Chem., Int. Ed.* **2009**, *48*, 3030–3059.

(c) Fändrich, M.; Schmidt, M.; Grigorieff, N., *Trends Biochem. Sci.* **2011**, *36*, 338–345. (d) Tycko, R., *Annu. Rev. Phys. Chem.* **2011**, *62*, 279–99.

2. (a) Lührs, T.; Ritter, C.; Adrian, M.; Riek-Loher, D.; Bohrmann, B.; Döbeli, H.; Schubert, D.; Riek, R., *Proc. Natl. Acad. Sci. U. S. A.* **2005**, *102*, 17342–17347. (b) Petkova, A. T.; Yau, W.-M.; Tycko, R., *Biochemistry* **2006**, *45*, 498–512.

3. (a) Luca, S.; Yau, W.-M.; Leapman, R.; Tycko, R., *Biochemistry* **2007**, *46*, 13505–13522. (b) Hebda, J. A.; Miranker, A. D., *Annu. Rev. Biophys.* **2009**, *38*, 125–152. (c) Wiltzius, J. J. W.; Sievers, S. A.; Sawaya, M. R.; Eisenberg, D., *Protein Sci.* **2009**, *18*, 1521–1530. (d) Middleton, C. T.; Marek, P.; Cao, P.; Chiu, C.-C.; Singh, S.; Woys, A. M.; de Pablo, J. J.; Raleigh, D. P.; Zanni, M. T., *Nature. Chem.* **2012**, *4*, 355–360.

4. (a) Woods, R. J.; Brower, J. O.; Castellanos, E.; Hashemzadeh, M.; Khakshoor, O.; Russu, W. A.; Nowick, J. S., *J. Am. Chem. Soc.* **2007**, *129*, 2548–2558. (b) Liu, C.; Sawaya, M. R.; Cheng, P.-N.; Zheng, J.; Nowick, J. S.; Eisenberg, D., *J. Am. Chem. Soc.* **2011**, *133*, 6736–6744. (c) Zheng, J.; Liu, C.; Sawaya, M. R.; Vadla, B.; Khan, S.; Woods, R. J.; Eisenberg, D.; Goux, W. J.; Nowick, J. S., *J. Am. Chem. Soc.* **2011**, *133*, 3144–3157. (d) Cheng, P.-N.; Liu, L.; Zhao, M.; Eisenberg, D. Nowick, J. S., *Nature. Chem.* **2012**, in press.

5. (a) von Bergen, M.; Friedhoff, P.; Biernat, J.; Heberle, J.; Mandelkow, E. M.; Mandelkow, E. *Proc. Natl. Acad. Sci. U. S. A.* **2000**, *97*, 5129–5134. (b) Inouye, H.; Sharma, D.; Goux, W. J.; Kirschner, D. A. *Biophys. J.* **2006**, *90*, 1774–1789.

6. (a) Mammen, M.; Choi, S.-K.; Whitesides, G. M. *Angew. Chem. Int. Ed.* **1998**, *37*, 2754–2794. (b) Kim, Y.-S.; Lee, J.-H.; Ryu, J. Kim, D.-J. *Curr. Pharm. Des*. **2009**, *15*, 637–658.

7. (a) Zutshi, R.; Shultz, M. D.; Ulysse, L.; Lutgring, R.; Bishop, P.; Schweitzer, B.; Vogel, K.; Franciskovich, J.; Wilson, M.; Chmielewski, J., *Synlett* **1998**, 1040–1044. (b) Wittmann, V.; Takayama, S.; Gong, K. W.; Weitz-Schmidt, G.; Wong, C.-H., *J. Org. Chem.* **1998**, *63*, 5137–5143.

8. LeVine, H. *Methods Enzymol.* **1999**, *309*, 274–284.

9. (a) Tjernberg, L. O.; Näslund, J.; Lindqvist, F.; Johansson, J.; Karlström, A.R.; Thyberg, J.; Terenius, L.; Nordstedt, C. *J. Biol. Chem.* **1996**, *271*, 8545–8548. (b) Sciarretta, K. L.; Gordon, D. J.; Meredith, S. C. Peptide-based inhibitors of amyloid assembly. *Methods Enzymol.* **2006**, *413*, 273–312. (c) Williams, A. D.; Shivaprasad, S.; Wetzel, R., *J. Mol. Biol.* **2006**, *357*, 1283–1294. (d) Estrada, L. D.; Soto, C., *Curr. Top. Med. Chem.* **2007**, *7*, 115–126. (e) Miller, Y.; Ma, B.; Nussinov, R., *Chem. Rev.* **2010**, *110*, 4820–4838.

10. Finder, V. H.; Glockshuber, R., *Neurodegener. Dis.* **2007**, *4*, 13–27.

11. Colletier, J.-P.; Laganowsky, A.; Landau, M.; Zhao, M.; Soriaga, A. B.; Goldschmidt, L.; Flot, D.; Cascio, D.; Sawaya, M. R.; Eisenberg, D., *Proc. Natl. Acad. Sci. U. S. A.* **2011**, *108*, 16938–16943.

Experimental Section for Chapter 3

Content

General Procedures

HPLC grade solvents were purchased from Fisher Scientific. Methylene chloride was further purified by passage through a column of alumina under argon.[1] 2-Chlorotrityl chloride resin, HCTU, and all Fmoc-protected amino acids, except Boc-Orn(Fmoc)-OH and Cbz-Orn(Fmoc)-OH, were purchased from LC Science, AnaSpec, and Novabiochem. Boc-Orn(Fmoc)-OH was purchased from GL Biochem. Biochemical grade trifluoroacetic acid for HPLC was purchased from Acros Organics. Standard grade trifluoroacetic acid for deprotection of peptides was purchased from Oakwood Chemicals. D_2O was purchased from Cambridge Isotopes. Cbz-Orn(Fmoc)-OH, Fmoc-Hao-OH, Fmoc*-Hao-OH and macrocycles **2.4a**, **2.4b**, **3.5**, and **3.6** were synthesized according to published procedures.[2] All other reagents were purchased from Alfa Aesar and the Aldrich Chemical Company. Analytical reverse-phase HPLC was performed on an Agilent Zorbax SB-C18 column (50 mm × 4.6 mm) and Beckman Alltech Alltima C18 "Rocket" column (53 mm x 4.5 mm) with a gradient of 5–100% CH_3CN in H_2O with 0.1% TFA and a flow of 1.0 mL/min over 20 minutes. A 21.2 x 250 mm Zorbax SB-C18 PrepHT (7 μm particle size) column from Agilent on a Rainin Dynamax system was used for preparative HPLC (flow rate 10 mL/min). UV detection (214 or 254 nm) was used for analytical and preparative HPLC. Water and acetonitrile were used as the solvents. Both solvents contained 0.1% biochemical grade TFA.

---

[1] Pangborn, A. B.; Giardello, M. A.; Grubbs, R. H.; Rosen, R. K.; Timmers, F. J. *Organometallics* **1996**, *15*, 1518-1520.

[2] (a) Nowick, J. S.; Chung, D. M.; Maitra, K.; Maitra, S.; Stigers, K. D.; Sun, Y. *J. Am. Chem. Soc.* **2000**, *122*, 7654-7661. (b) Woods, R. J.; Brower, J. O.; Castellanos, E.; Hashemzadeh, M.; Khakshoor, O.; Russu, W. A.; Nowick, J. S., *J. Am. Chem. Soc.* **2007,** *129*, 2548-2558.(c) Cheng, P.-N.; Nowick, J. S., *The J. Org. Chem.***2011**, *76*, 3166-3173.

Synthesis of Homodivalent Linked Macrocyclic β-Sheets 3.2 and 3.3

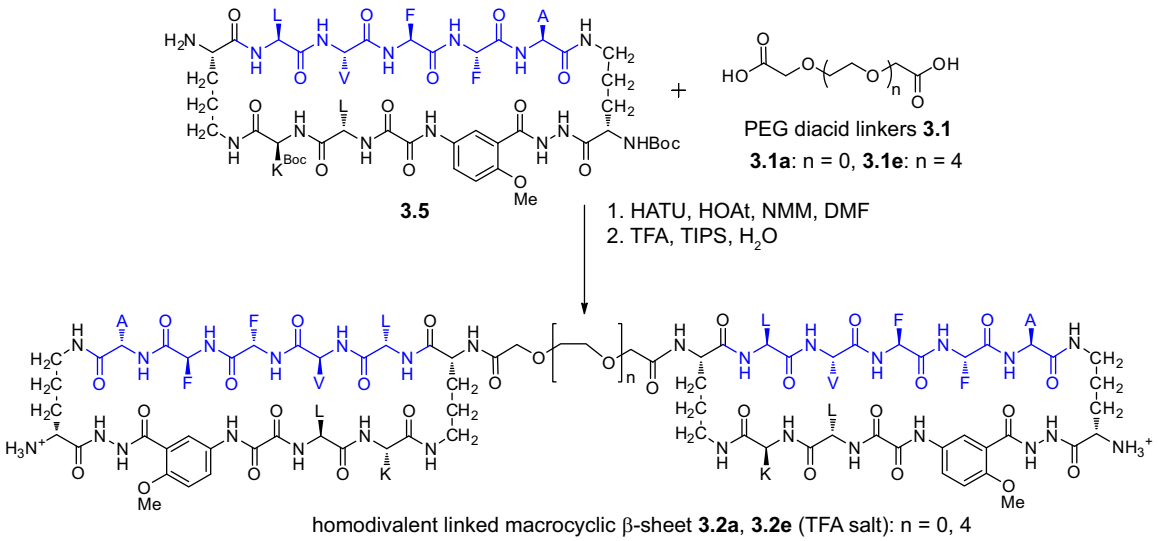

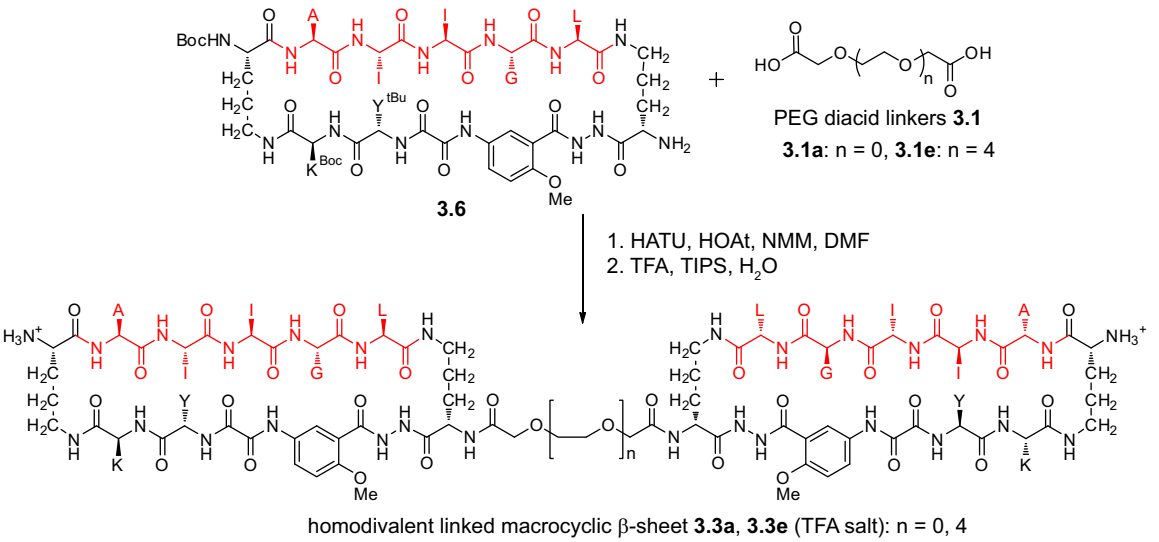

*General procedure for synthesis of homodivalent linked macrocyclic β-sheets **3.2** and **3.3***. PEG-based diacid linkers **3.1** (0.45 equiv) were dissolved in DMF (0.3 mL) in a 1-mL reaction vial charged with a magnetic stirring bar and then treated with HATU (1 equiv), HOAt (1 equiv), and 4-methylmorpholine (NMM, 2 equiv). (The final linker concentration is 40 mM.) After 30 minutes, **3.5** or **3.6** (1 equiv) was added. After 24 hours, the solvent (DMF) was removed by a rotary rotavapor under reduced pressure to

afford a yellowish oil. Crude peptide intermediates were treated with TFA (90% with 5% TIPS and 5% H_2O) without further purification to afford crude peptides **3.2** and **3.3** as yellowish solids. The crude products were purified by reverse-phase HPLC (gradient of 10–50% CH_3CN over 75 min) and lyophilized to produce homodivalent linked macrocyclic β-sheets **3.2** and **3.3**.

*Homodivalent linked macrocyclic β-sheet **3.2a***. Homodivalent β-sheet **3.2a** was synthesized according to the above method. The crude products were purified by reverse-phase HPLC (gradient of 10–50% CH_3CN over 75 min) and lyophilized to produce homodivalent linked macrocyclic β-sheet **3.2a** as a white solid in 52% yield**.** MS (ESI) *m / z* Calcd for $C_{132}H_{194}N_{30}O_{29}$ $[M + 2H]^{2+}$ 1331.8, found 1333.2.

*Homodivalent linked macrocyclic β-sheet **3.2e***. Homodivalent β-sheet **3.2e** was synthesized according to the above method. The crude products were purified by reverse-phase HPLC (gradient of 10–50% CH_3CN over 75 min) and lyophilized to produce homodivalent linked macrocyclic β-sheet **3.2e** as a white solid in 24% yield. MS (ESI) *m / z* Calcd for $C_{140}H_{210}N_{30}O_{33}$ $[M + 2H]^{2+}$ 1419.8, found 1420.5.

*Homodivalent linked macrocyclic β-sheet **3.3a***. Homodivalent β-sheet **3.3a** was synthesized according to the above method. The crude products were purified by reverse-phase HPLC (gradient of 10–50% CH_3CN over 75 min) and lyophilized to produce homodivalent linked macrocyclic β-sheet **3.3a** as a white solid in 51% yield. MS (ESI) *m / z* Calcd for $C_{120}H_{186}N_{30}O_{31}$ $[M + 2H]^{2+}$ 1271.7, found 1272.9.

*Homodivalent linked macrocyclic β-sheet **3.3e**.* Homodivalent β-sheet **3.3e** was synthesized according to the above method. The crude products were purified by reverse-phase HPLC (gradient of 10–50% CH_3CN over 75 min) and lyophilized to produce homodivalent linked macrocyclic β-sheet **3.3e** as a white solid in 62% yield. MS (ESI) *m / z* Calcd for $C_{130}H_{198}N_{30}O_{32}$ $[M + 2H]^{2+}$ 1359.8, found 1360.5.

Synthesis of Heterodivalent Linked Macrocyclic β-Sheets 3.4

Scheme 3.2 Synthesis of Heterodivalent Macrocyclic β-Sheets **3.4**.

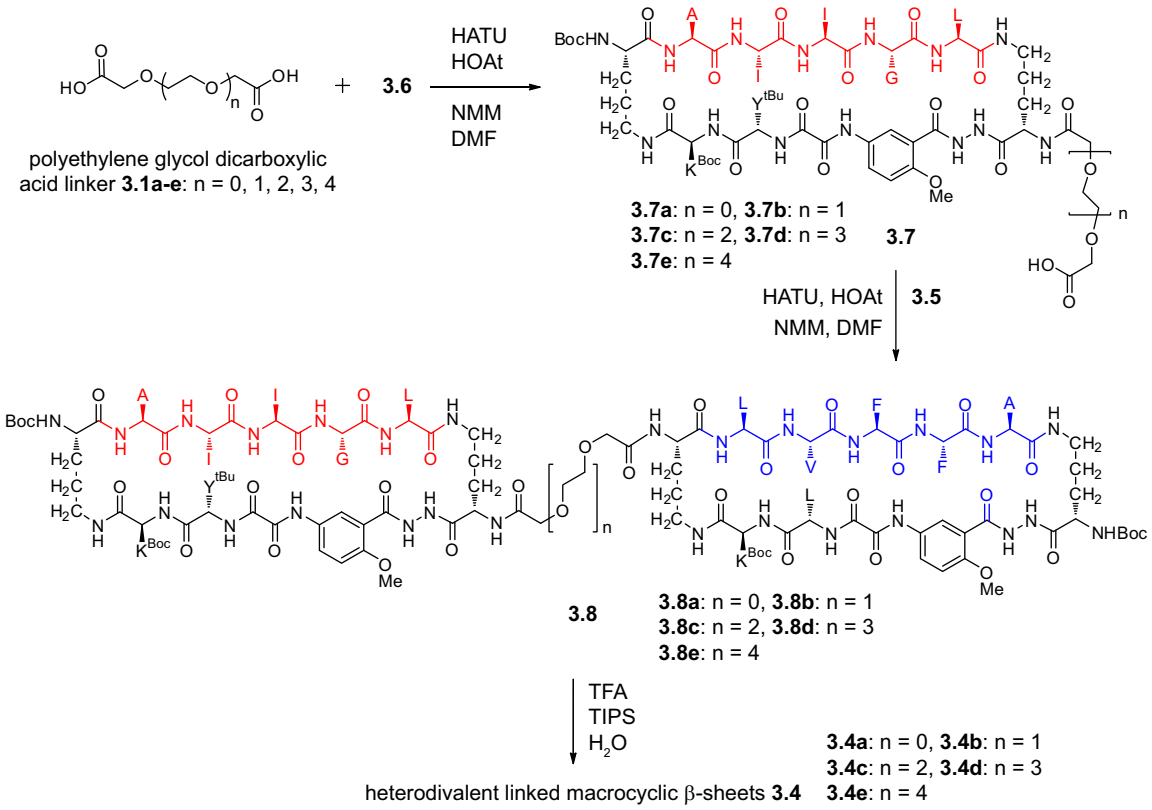

*General procedure for synthesis of intermediates **3.7**.* To prevent peptide **3.6** from reacting with both carboxylic acid groups of PEG-based diacid linkers **3.1**, 10 equivalents of the linkers were used to synthesize intermediates **3.7**. PEG-based diacid linkers **3.1** (10 equiv) were dissolved in a 3-mL reaction vial charged with a magnetic stirring bar and then treated with HATU (20 equiv), HOAt (20 equiv), and 4-methylmorpholine (40 equiv). After 15 minutes, a solution of peptide **3.6** (1 equiv) in DMF was added dropwise over 20 minutes via a syringe to the reaction vial. (The final linker concentration is 100 mM.) After 8 hours, the reaction mixture was transferred to a 250-mL one-necked, round-

bottomed flask charged with H_2O (100 mL) and CH_2Cl_2 (100 mL) and was rigorously stirred to hydrolyze the activated esters. After 15 hours, the organic layer was collected, while the aqueous layer was acidified with AcOH (10 mL) and extracted with CH_2Cl_2 (100 mL) twice. All organic layers were collected together and concentrated to afford a yellowish oil. The oil was dissolved in a small amount of CH_2Cl_2, diluted with excess hexanes, and concentrated to dryness three times to remove residual AcOH. The crude products were purified by reverse-phase HPLC (gradient of 50–90% CH_3CN over 80 min) to afford intermediates **3.7**.

*Intermediate **3.7a***. Intermediate **3.7a** was synthesized according to the above method. The crude products were purified by reverse-phase HPLC (gradient of 50–90% CH_3CN over 80 min) to afford intermediates **3.7a** as a white solid in 43% yield. MS (ESI) *m / z* Calcd for $C_{76}H_{120}N_{15}O_{22}$ $[M + H]^+$ 1594.8, found 1595.2.

*Intermediate **3.7b***. Intermediate **3.7b** was synthesized according to the above method. The crude products were purified by reverse-phase HPLC (gradient of 50–90% CH_3CN over 80 min) to afford intermediates **3.7b** as a white solid in 79% yield. MS (ESI) *m / z* Calcd for $C_{78}H_{124}N_{15}O_{23}$ $[M + H]^+$ 1638.8, found 1638.3.

*Intermediate **3.7c***. Intermediate **3.7c** was synthesized according to the above method. The crude products were purified by reverse-phase HPLC (gradient of 50–90% CH_3CN over 80 min) to afford intermediates **3.7c** as a white solid in 44% yield. MS (ESI) *m / z* Calcd for $C_{80}H_{127}N_{15}NaO_{24}$ $[M + Na]^+$ 1704.9, found 1705.3.

*Intermediate **3.7d**.* Intermediate **3.7d** was synthesized according to the above method. The crude products were purified by reverse-phase HPLC (gradient of 50–90% CH_3CN over 80 min) to afford intermediates **3.7d** as a white solid in 34% yield. MS (ESI) *m / z* Calcd for $C_{82}H_{133}N_{15}O_{25}$ $[M + 2H]^{2+}$ 863.9, found 863.6.

*Intermediate **3.7e**.* Intermediate **3.7e** was synthesized according to the above method. The crude products were purified by reverse-phase HPLC (gradient of 50–90% CH_3CN over 80 min) to afford intermediates **3.7e** as a white solid in 56% yield. MS (ESI) *m / z* Calcd for $C_{84}H_{135}N_{15}Na_2O_{26}$ $[M + 2Na]^{2+}$ 907.9, found 908.3.

*General procedure for synthesis of heterodivalent linked macrocyclic β-sheets **3.4a-e**.* Intermediates **3.7** (1 equiv) were dissolved in DMF (19 mM solution of intermediates **3.7**) in a 3-mL reaction vial and were treated with HATU (1 equiv), HOAt (1 equiv), and 4-methylmorpholine (2 equiv). After 30 minutes, a solution of peptide **3.5** in DMF (38 mM) was added. (The final peptide intermediate concentration was 10 mM.) After 24 hours, the solvent (DMF) was removed by a rotary rotavapor under reduced pressure to afford a yellowish oil. Crude peptide intermediates were treated with TFA (90% with 5% TIPS and 5% H_2O) without further purification to afford crude peptides **3.4a-e** as yellowish solids. The crude products were purified by reverse-phase HPLC (gradient of 10–50% CH_3CN over 75 min) and lyophilized to produce heterodivalent linked macrocyclic β-sheets **3.4a-e**.

*Heterodivalent linked macrocyclic β-sheet **3.4a**.* Heterodivalent β-sheet **3.4a** was synthesized according to the above method. The crude products were purified by reverse-phase HPLC (gradient of 10–50% CH_3CN over 75 min) and lyophilized to produce heterodivalent linked macrocyclic β-sheet **3.4a** as a white solid in 45% yield. MS (ESI) *m / z* Calcd for $C_{126}H_{190}N_{30}O_{30}$ $[M + 2H]^{2+}$ 1301.7, found 1301.7.

*Heterodivalent linked macrocyclic β-sheet **3.4b**.* Heterodivalent β-sheet **3.4b** was synthesized according to the above method. The crude products were purified by reverse-phase HPLC (gradient of 10–50% CH_3CN over 75 min) and lyophilized to produce heterodivalent linked macrocyclic β-sheet **3.4b** as a white solid in 9% yield. MS (ESI) *m / z* Calcd for $C_{128}H_{194}N_{30}O_{31}$ $[M + 2H]^{2+}$ 1323.7, found 1323.7.

*Heterodivalent linked macrocyclic β-sheet **3.4c**.* Heterodivalent β-sheet **3.4c** was synthesized according to the above method. The crude products were purified by reverse-phase HPLC (gradient of 10–50% CH_3CN over 75 min) and lyophilized to produce heterodivalent linked macrocyclic β-sheet **3.4c** as a white solid in 30% yield. MS (ESI) *m / z* Calcd for $C_{130}H_{198}N_{30}O_{32}$ $[M + 2H]^{2+}$ 1345.7, found 1345.3.

*Heterodivalent linked macrocyclic β-sheet **3.4d**.* Heterodivalent β-sheet **3.4d** was synthesized according to the above method. The crude products were purified by reverse-phase HPLC (gradient of 10–50% CH_3CN over 75 min) and lyophilized to produce heterodivalent linked macrocyclic β-sheet **3.4d** as a white solid in 40% yield. MS (ESI) *m / z* Calcd for $C_{132}H_{202}N_{30}O_{33}$ $[M + 2H]^{2+}$ 1367.7, found 1367.7.

*Heterodivalent linked macrocyclic β-sheet **3.4e***. Heterodivalent β-sheet **3.4e** was synthesized according to the above method. The crude products were purified by reverse-phase HPLC (gradient of 10–50% CH_3CN over 75 min) and lyophilized to produce heterodivalent linked macrocyclic β-sheet **3.4e** as a white solid in 45% yield. MS (ESI) *m / z* Calcd for $C_{134}H_{206}N_{30}O_{34}$ $[M + 2H]^{2+}$ 1389.5, found 1389.7.

Thioflavin T Fluorescence Assays of $A\beta_{1\text{-}40}$ Aggregation

ThT fluorescence assays were conducted in 96-well plates (96 Well Optical Bottom Plate, polymer base, NUNC, USA) with shaking in a Gemini XPS fluorescence plate reader (Molecular Devices, 442 nm excitation, 482 nm emission) at 31°C. Experiments were performed in triplicate or greater with 15 μM $A\beta_{1\text{-}40}$, 10 mM HEPES buffer (pH 7.4) and 20 μM ThT.

Preparation of buffered ThT solution: The ThT solution was freshly prepared before use. Approximately 4 mg of Thioflavin T was dissolved in ca. 20 mL of nanopure water in a 25 mL Erlenmeyer flask. 10 mL of this solution was filtered through a 0.2 micron syringe filter into a 15-mL plastic centrifuge tube. The concentration of a 1/25 dilution of this solution was determined by UV (ε = 36000 M^{-1} cm^{-1} at 412 nm). An aliquot of this stock solution was combined with H_2O and 10x HEPES buffer (the amount of ThT stock and H_2O are based on the determined concentration of the stock) to obtain 40 μM ThT in 10 mM HEPES, pH 7.4.

Peptide inhibitor preparation: A stock solution of each peptide inhibitor was freshly prepared before use by adding nanopure water to each tube to obtain 1.5 mM peptide solutions. The stock solution was diluted to 0.15 mM.

Preparation of $A\beta_{1-40}$ solution: The $A\beta_{1-40}$ solution was freshly prepared by dissolving $A\beta_{1-40}$ TFA salt (GL Biochem, Shanghai, China) in 100 mM NaOH in a 1.5 mL Epindorf tube. The mixture was sonicated for 30 seconds. The solution was diluted to 300 μM by addition of nanopure water. The solution was filtered through 100 kDa Centricon filters that were previously washed 3 times with nanopure water (10000 rpm for 3 minutes). The $A\beta_{1-40}$ solution was diluted with nanopure water to 150 μM.

Preparation of the wells of the 96-well plate. (1) A mixing bead (PTFE Teflon Ball Grade 2, 1/8" Diameter, SmallParts, Inc., USA) was added to each well of the 96-well plate. (2) ThT (40 μM, 100 μL) in HEPES buffer was added to each well. (3) Water (100 μL) was added to wells corresponding to ThT background controls. (4) Water (80 μL) was added to wells corresponding to $A\beta_{1-40}$ controls. (5) A total volume (100 μL) of water and inhibitor solutions without $A\beta_{1-40}$ was added to wells corresponding to inhibitor controls. (6) A total volume (80 μL) of water and inhibitor solutions to make different concentrations of interest was added to wells. [Monovalent peptides **2.4a** and **2.4b** are at 30 μM concentration (2 equiv); homodivalent peptides **3.2a**, **3.2e**, **3.3a**, and **3.3e** are at 15 μM (1 equiv); heterodivalent peptides **3.4a-e** are at 0.5 (0.03 equiv), 2.5 (0.17 equiv), 7.5 (0.5 equiv), and 15 μM (1 equiv)concentrations.] (7) 20 μL of 150 μM $A\beta_{1-40}$ solution was added to wells that should contain $A\beta_{1-40.}$ The total reaction volume in each well was

200 μL, with 15 μM $A\beta_{1\text{-}40}$ in a pH 7.4 buffer containing 20 μM ThT, 10 mM HEPES, and 0.02% NaN_3. The 96-well plate was put into the plate reader with excitation and emission at 442 nm and 482 nm respectively. The ThT assay was conducted at 31 ºC (24 hour kinetic experiment, read every 10 minutes, 5 seconds shake before first read, 575 seconds shaking between readings).

3.2a *Mass Spectrum*

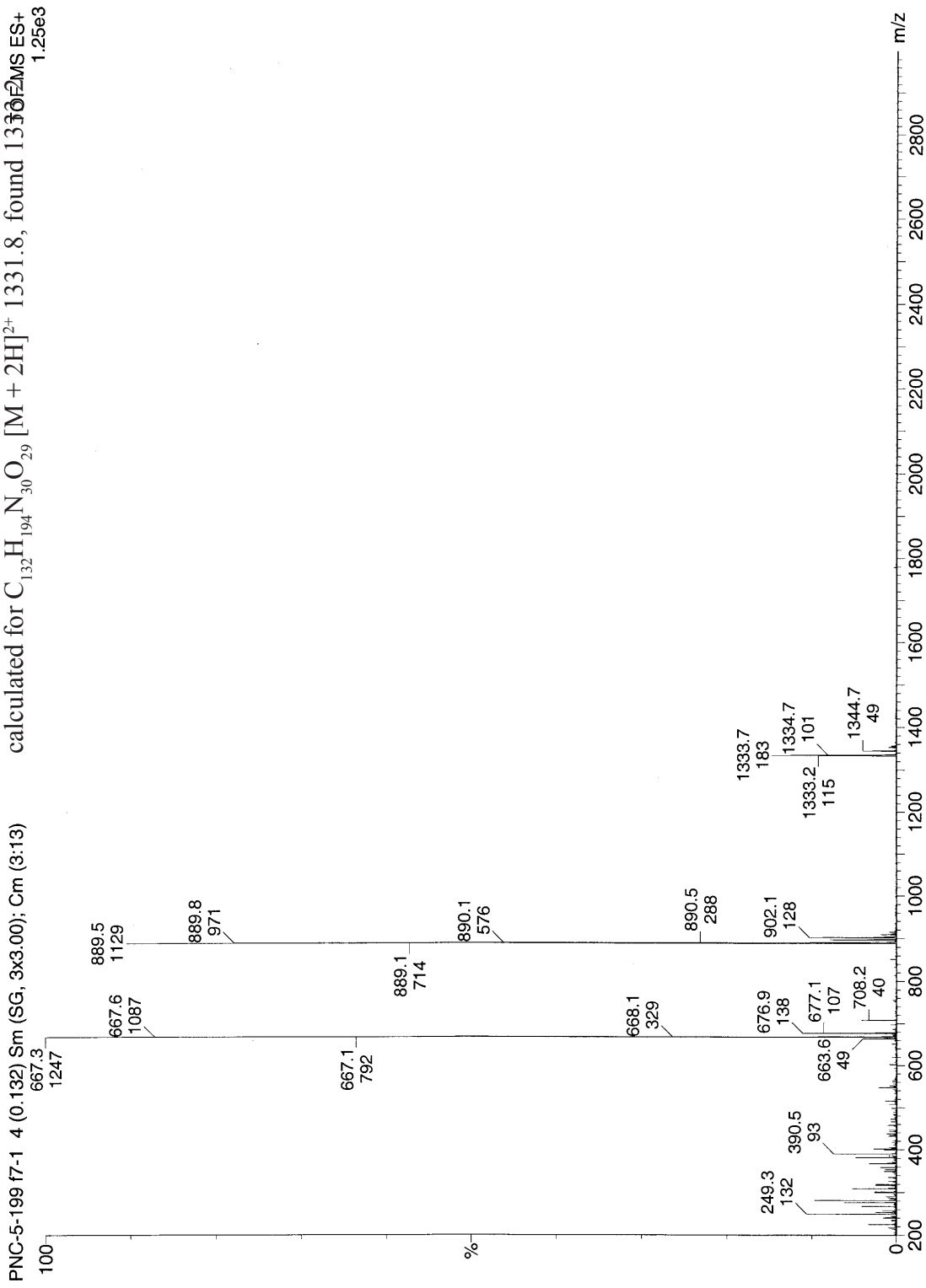

3.2a *HPLC trace*

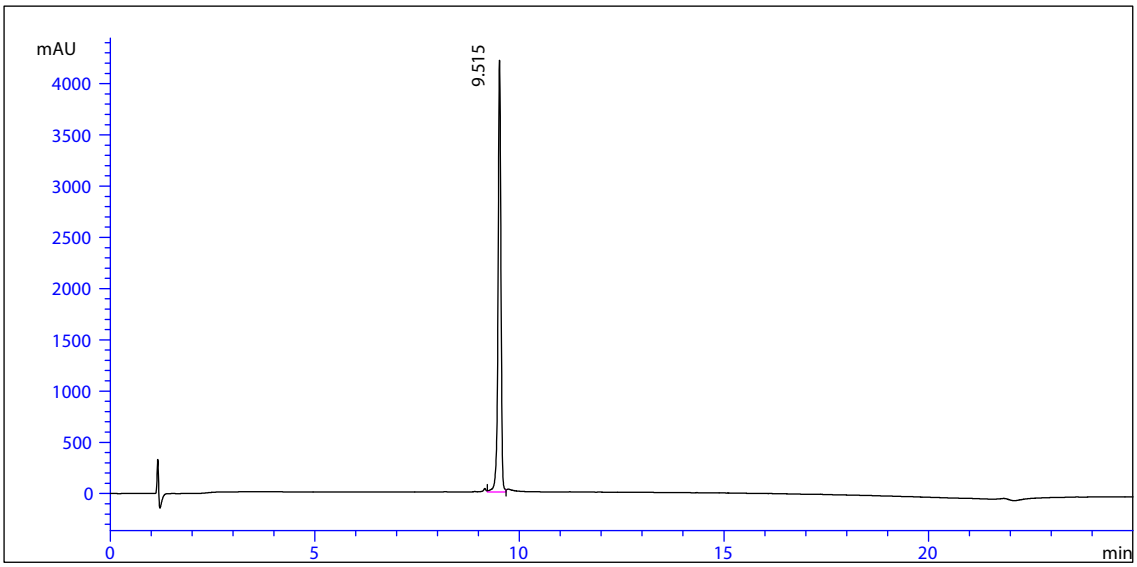

Signal 1: VWD1 A, Wavelength=214 nm

Peak #	RetTime [min]	Type	Width [min]	Area mAU *s	Height [mAU]	A rea %
1	9.515	VV	0.0763	2.07492e4	4220.79980	100 .0000
Totals :				2.07492e4	4220.79980	

***3.3a** Mass Spectroscopy*

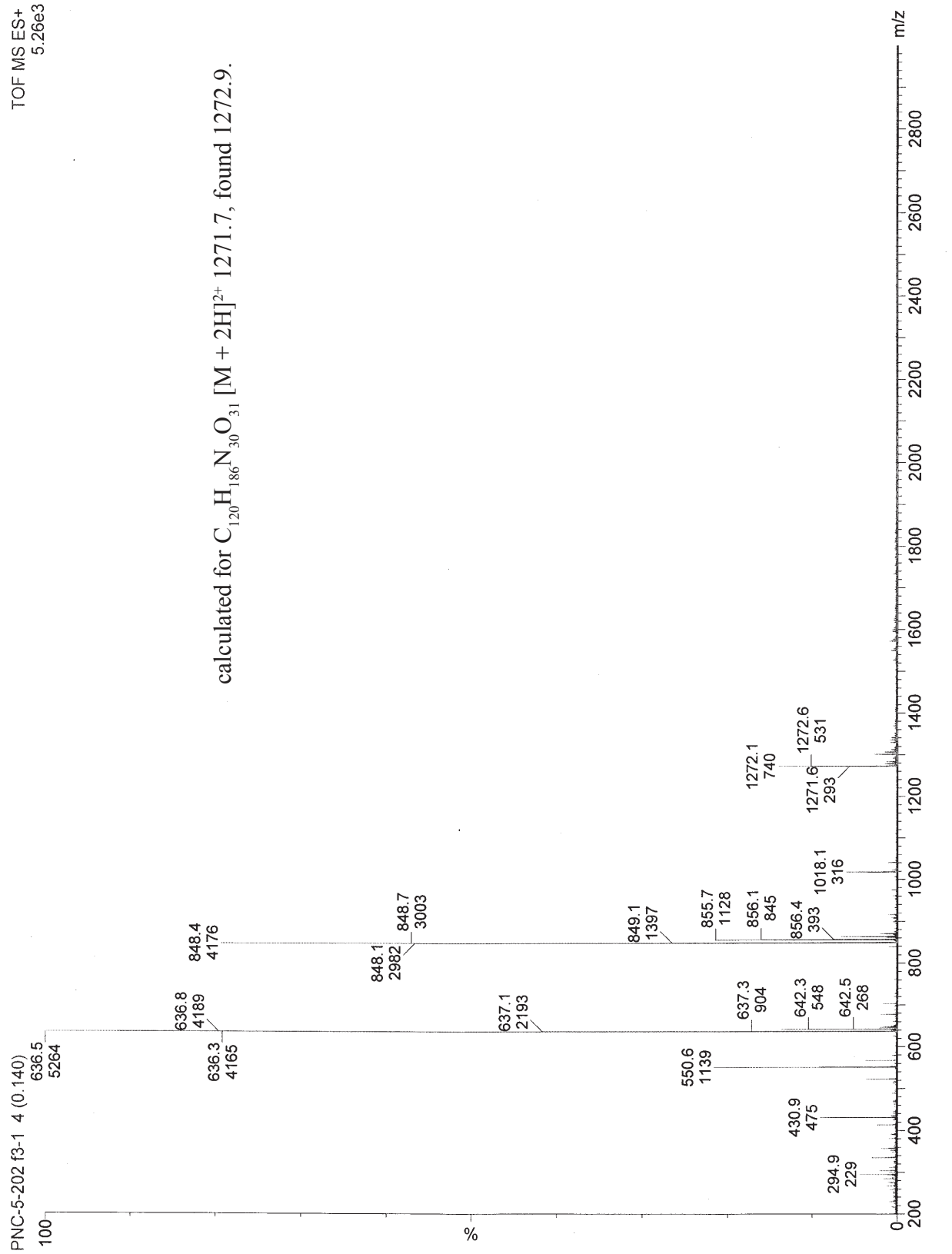

calculated for $C_{120}H_{186}N_{30}O_{31}$ $[M + 2H]^{2+}$ 1271.7, found 1272.9.

3.3a *HPLC trace*

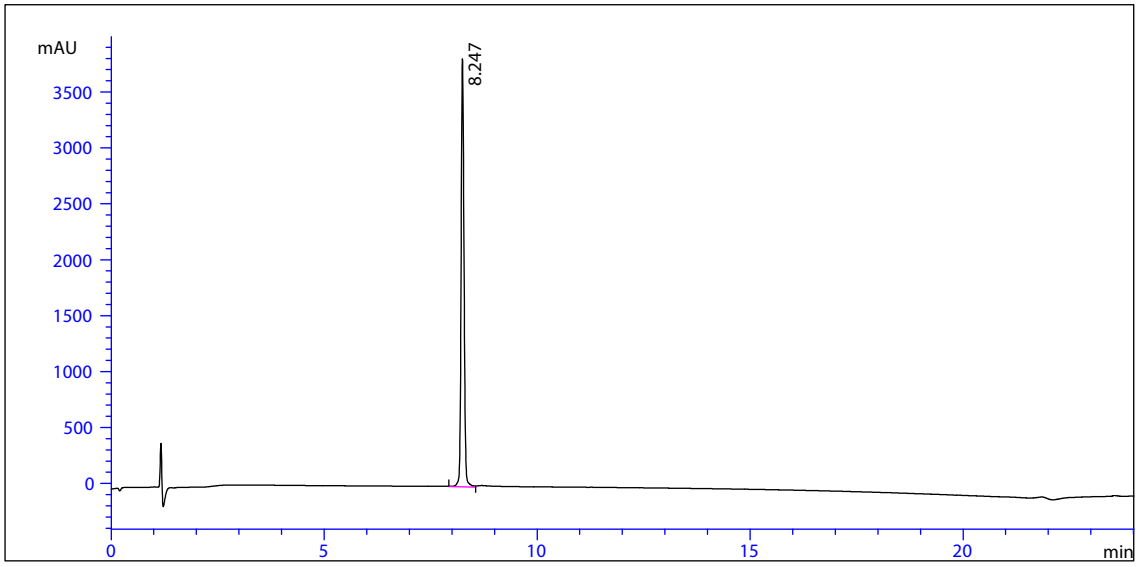

Signal 1: VWD1 A, Wavelength=214 nm

Peak #	RetTime [min]	Type	Width [min]	Area mAU *s	Height [mAU]	Area %
1	8.247	VV	0.0725	1.80608e4	3830.10400	100.0000
Totals :				1.80608e4	3830.10400	

***3.4a** Mass Spectrum*

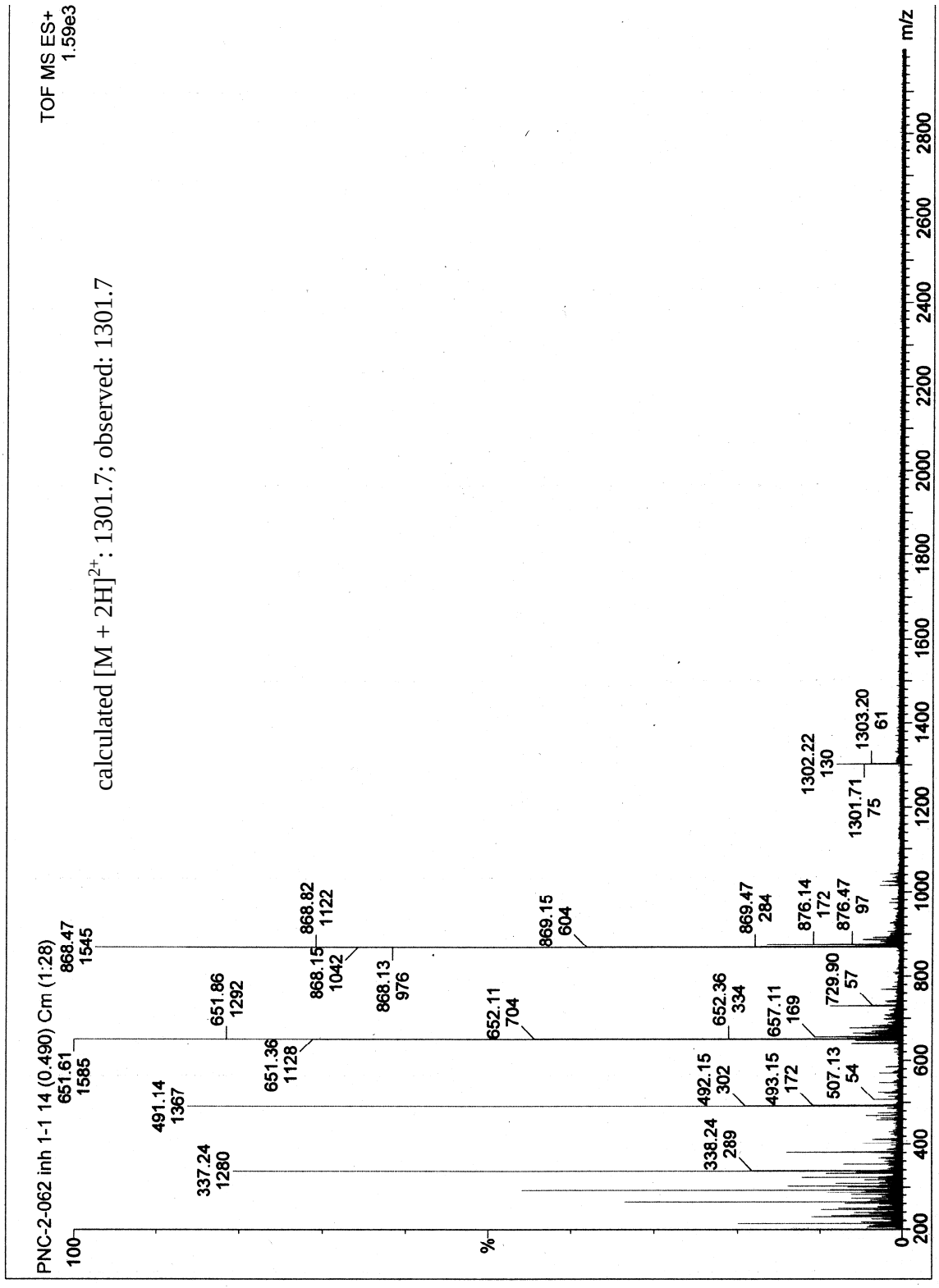

3.4a HPLC Trace

Area % Report

Data File: G:\data\pinnancheng\PNC-1\PNC-1-277
Method: G:\data\Methods\Zorbax 80SB manual\single 5-100 over 20 min 214 nm.met
Acquired: 1/5/2009 2:58:18 PM
Printed: 4/22/2009 9:20:17 PM

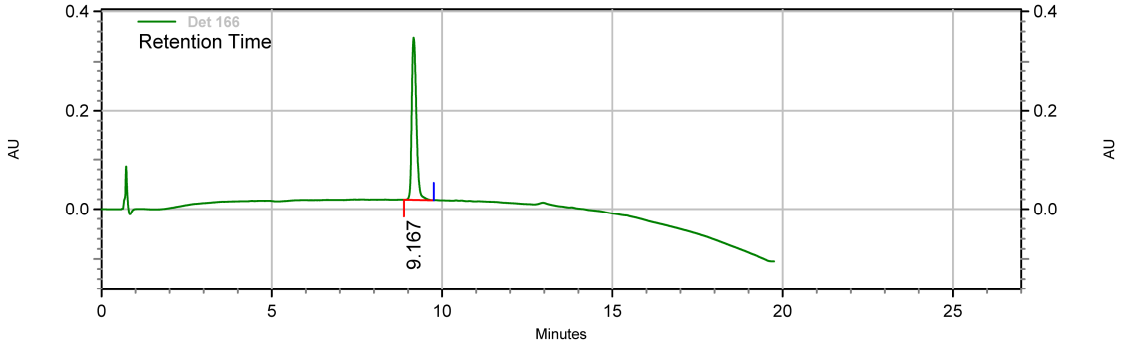

Det 166 Results

Time	Area	Area %	Height	Height %
9.167	3114762	100.00	328668	100.00

Totals				
	3114762	100.00	328668	100.00

3.7a *Mass Spectrum*

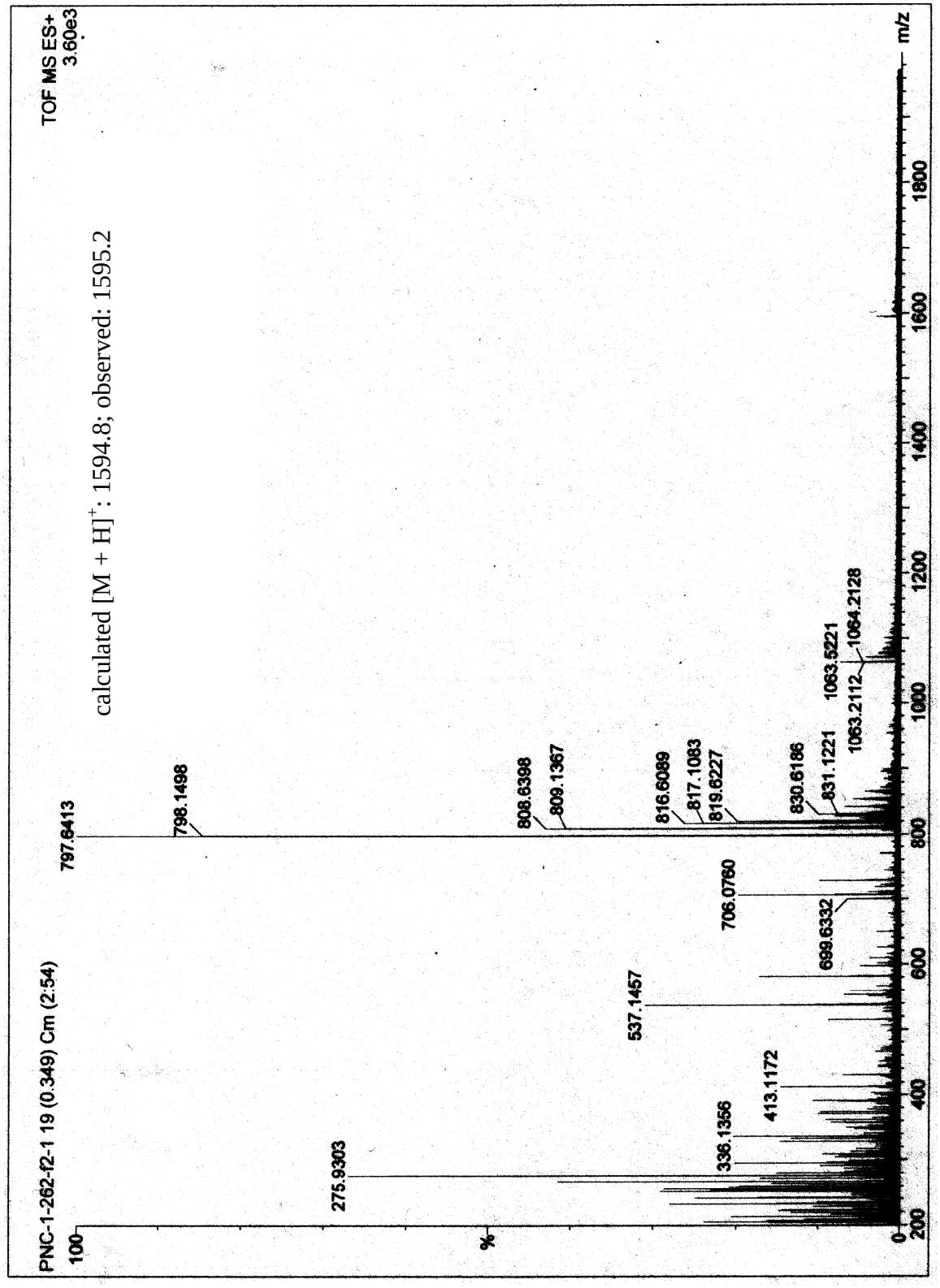

3.7a HPLC Trace

Area % Report

Data File: G:\data\pinnancheng\PNC-1\PNC-1-262
Method: G:\data\Methods\Zorbax 80SB manual\single 5-100 over 20 min 214 nm.met
Acquired: 12/18/2008 3:07:29 PM
Printed: 4/22/2009 9:10:18 PM

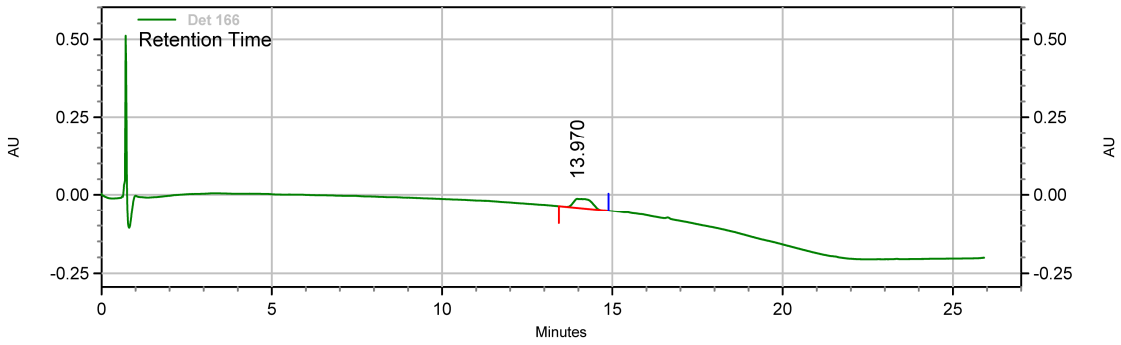

Det 166 Results

Time	Area	Area %	Height	Height %
13.970	1126576	100.00	29285	100.00

Totals	1126576	100.00	29285	100.00

CHAPTER 4

Giant Macrolactams Based on β-Sheet Peptides

Preamble

Chapter 4 describes the design and synthesis of the water-soluble 54-, 78-, and 102-membered ring macrocyclic peptides, which are among the largest synthetic macrolactams. The project of giant macrolactams based on β-sheet peptides started as a side project when I struggled with the project of divalent linked macrocyclic β-sheet inhibitors against Aβ aggregation described in chapter 3. In reading about protein β-sheet structures, I found that chemical model systems of proteins β-sheet are usually smaller than ones in nature. Indeed, chemical models, by definition, are supposed to be simpler and easier to develop, and are able to provide insights into natural systems with complexity.

Our group has previously introduced the 42- and 54-membered ring macrocyclic β-sheet systems (**2.4** and **4.1**). Their structures feature the amino acid Hao, a tripeptide β-strand mimic, and δ-linked ornithine, a β-turn mimic. These two unnatural amino acids help peptides fold into β-sheets and prevent aggregation in water. With these useful tools, I started to seek the possibilities of new chemical models. However, my new chemical model systems did not go smaller and simpler; instead, they went bigger and more complex. I wanted to ask how big water-soluble macrocyclic β-sheets can be based on the design of Hao and δ-linked ornithine. This chapter reports the development of the bigger chemical models of protein β-sheets.

Introduction

Macrocyclization can impart exceptional stability and a variety of biological activities into peptides by enforcing β-sheet structures.[1] Gramicidin S, Θ-defensin, and many cyclotides achieve their antimicrobial activities because of their unusual β-sheet macrolactam structures.[2] Robinson and coworkers have extensively developed macrocyclic peptides that adopt β-sheet structures to present biologically essential epitopes of structured target proteins. These macrocyclic β-sheets have served as antimicrobial peptides, protease inhibitors, p53—HDM2 inhibitors, and Tat protein—transactivation response region RNA inhibitors.[3]

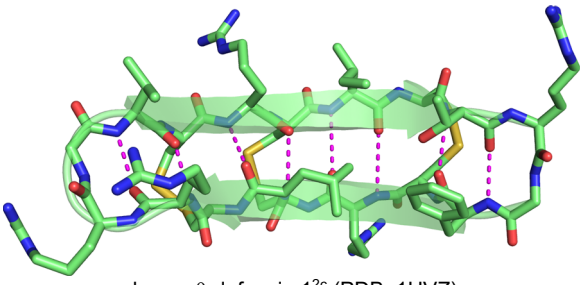

rhesus θ-defensin 1[2c] (PDB, 1HVZ)

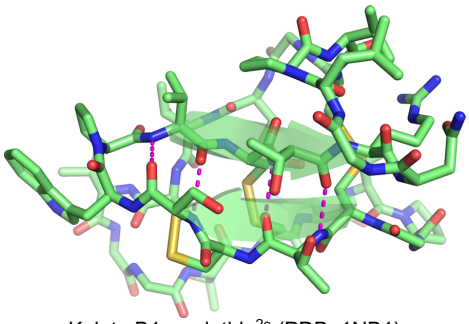

Kalata B1, cyclotide[2e] (PDB, 1NB1)

Macrocyclization provides an efficient strategy to promote and stabilize β-sheet structures by bringing otherwise remote residues into proximity. Nature helps enforce β-sheet structures or other well-defined structures in cyclotides through cyclization by linkage of the *N*- and *C*-termini with a peptide bond.[1,4] Cyclization with side-chain

disulfide bridges also occurs in natural antibacterial peptides, such as tachyplesins and protegrins.[5] Gellman and coworkers have created macrocycles that form stable parallel and antiparallel β-sheets in water through either backbone linkage or side-chain linkage with disulfide bridges.[6] Our research group has introduced macrocyclic β-sheets that are cyclized through δ-linked ornithine.[7]

Synthetic macrocyclic β-sheets can serve as chemical models of protein β-sheets and provide insights into complicated β-sheet interactions in biological systems. The Gellman and Waters groups have demonstrated that macrocyclic β-sheets can act as spectroscopic references for β-sheet structures formed by linear peptides.[6a,8] Our research group has used 42-membered ring macrocyclic β-sheets to inhibit the aggregation of amyloidogenic peptides.[9] We have also shown that 54-membered ring macrocyclic β-sheets can mimic protein quaternary structure through *inter*molecular β-sheet interactions.[7b-f]

Our research group previously introduced the amino acid Hao, a tripeptide β-strand mimic, and δ-linked ornithine ($^{\delta}$Orn), a β-turn mimic.[10] In our macrocyclic β-sheet peptides, Hao not only serves as a template to present one hydrogen-bonding edge for *intra*molecular hydrogen bonding but also minimizes edge-to-edge aggregation through *inter*molecular hydrogen bonding. δ-Linked ornithine serves as a β-turn mimic and helps induce β-hairpin structures. The 42- and 54-membered ring macrocyclic β-sheets **2.4** and **4.1** were constructed from these two key components, and most form well-defined non-aggregating β-sheets in water.

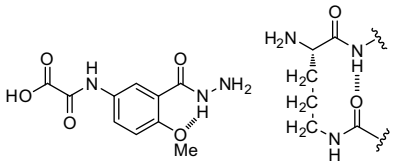

amino acid "Hao" $^{\delta}$Orn β-turn mimic

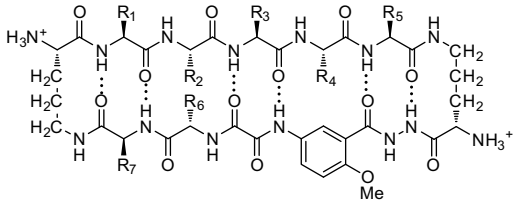

42-membered ring macrocyclic β-sheets **2.4**

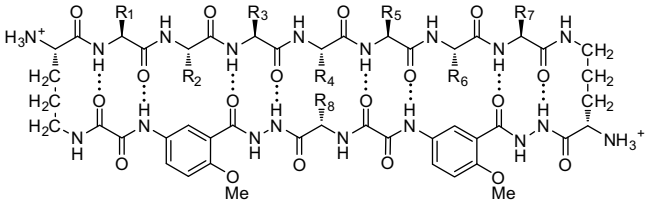

54-membered ring macrocyclic β-sheets **4.1**

In developing these macrocyclic β-sheet peptides, we have become impressed with the reliability of macrocycles in enforcing β-sheet structure and the efficiency of macrocyclization in synthesis. In this chapter, we use natural amino acids, Hao, and δ-linked ornithine to generate water-soluble 54-, 78-, and 102-membered ring macrolactams **4.2a**–**f**, **4.3a** and **4.3b**, **4.4**, and **4.5**. These giant macrocycles were efficiently synthesized by conventional Fmoc-based solid-phase peptide synthesis of the corresponding protected linear peptides, followed by solution-phase cyclization and deprotection. Here, we describe the design, synthesis, and study of these giant macrocycles.

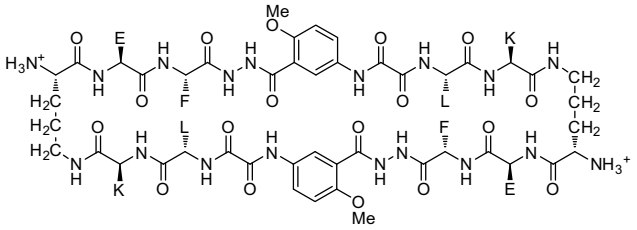

4.2a (TFA salt)

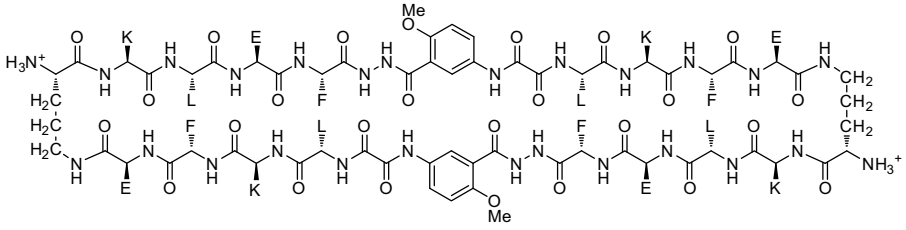

4.3a (TFA salt)

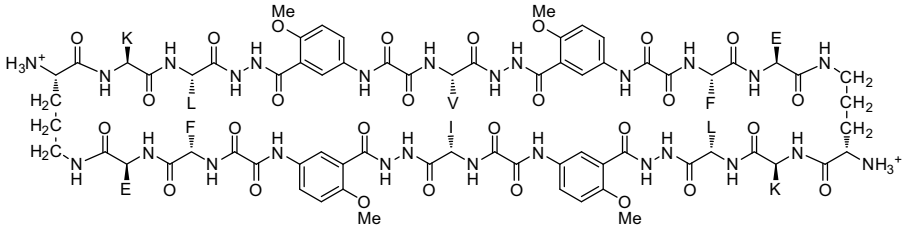

4.4 (TFA salt)

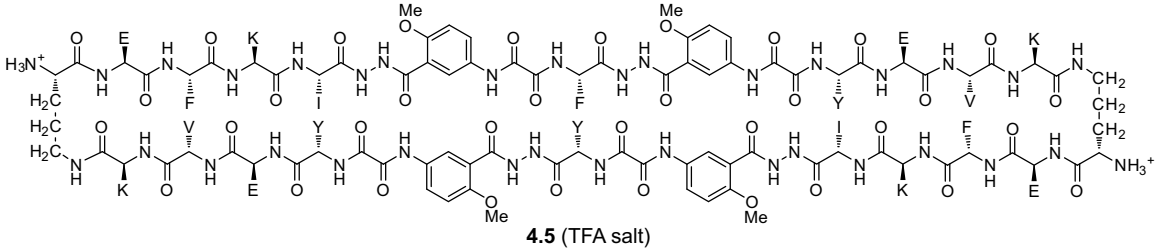

4.5 (TFA salt)

Results and Discussion

1. Synthesis of 54-, 78-, and 102-Membered Ring Macrolactams. Peptide **4.2a** is a 54-membered ring macrolactam containing eight natural amino acids, two Hao units, and two δ-linked ornithines. We chose Lys-Glu pairs for the hydrogen-bonded positions of peptide **4.2a** because of their pairwise statistical and empirical preference for β-sheet formation and to enhance the solubility of peptide **4.2a** in water.[11,12] We chose Phe-Leu pairs for the non-hydrogen-bonded positions, because they statistically favor β-sheet

formation.[12] The Lys-Glu and Phe-Leu pairs provide peptide **4.2a** with two peptide strands Glu-Phe-Hao-Leu-Lys connected by two $^{\delta}$Orn turns. The two Hao units in the middle of each peptide strand were designed to minimize aggregation by blocking *inter*molecular hydrogen bonding among the peptide strands. Although complementary polar and hydrophobic amino acids were selected for initial studies, this design feature was subsequently found to be unnecessary.

Peptide **4.2a** was synthesized by conventional Fmoc-based solid-phase peptide synthesis on 2-chlorotrityl chloride resin, followed by solution-phase cyclization and deprotection. Scheme 1 summarizes this synthesis.[13] The resin was first lightly loaded with Boc-Orn(Fmoc)-OH, using 0.33 equiv of Boc-Orn(Fmoc)-OH per active site on the resin. Unreacted sites on the resin were capped with MeOH. The resin loading was determined to be 0.40 mmol/g by Fmoc cleavage and UV analysis. Protected linear peptide **4.6a** was synthesized by standard automated Fmoc-based solid-phase peptide synthesis, followed by cleavage from the resin with AcOH. A 54% yield of the unpurified protected linear peptide was obtained based on the loading of Boc-Orn(Fmoc)-OH on the resin.

We used Fmoc-Hao-OH—rather than Fmoc*-Hao-OH—to introduce the Hao residue in the syntheses of the protected linear peptides of the 54-, 78-, and 102-membered ring macrolactams.[14] (Jing Zheng, Andrew Lam and other members of the Nowick group developed the procedures for preparing Fmoc-Hao-OH. These procedures are summarized in experimental section.) Fmoc* refers to the 2,7-di-tert-butyl-Fmoc group which is more soluble analogue of the Fmoc group.[10b] Fmoc*-Hao-OH was previously developed by the Nowick group to introduce Hao in Fmoc-based solid-phase

peptide synthesis. Although Fmoc* is more soluble in DMF—and hence easier to work with— its synthesis involves more steps, including the use of toxic phosgene, and costs more.

Scheme 4.1 Synthesis of Peptide **4.2a**

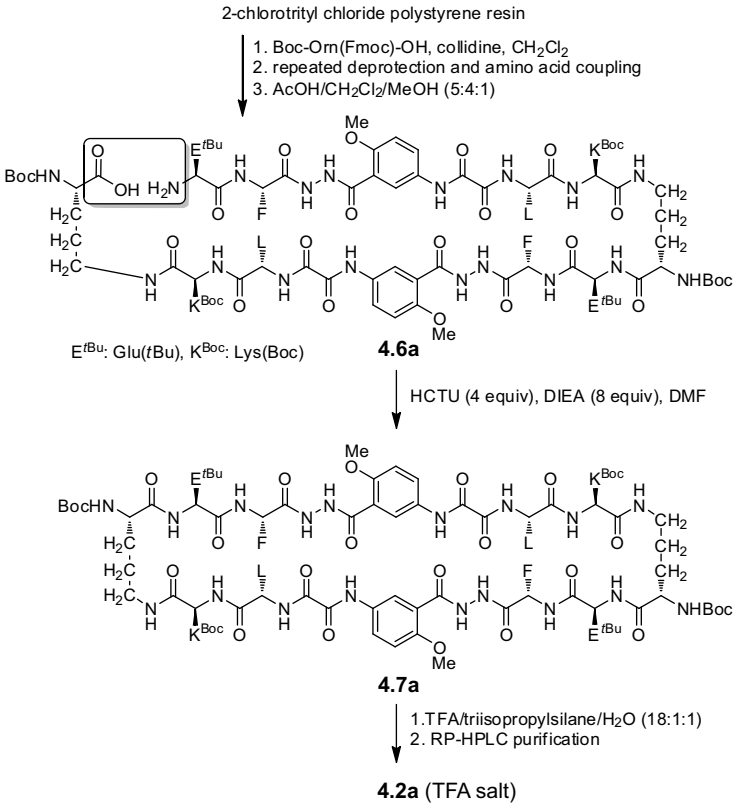

Protected linear peptide **4.6a** was cyclized to the corresponding protected cyclic peptide **4.7a** by using HCTU[15]and *N*,*N*-diisopropylethylamine (DIEA) in DMF.[16] Although we routinely perform macrocyclization at ca. 0.5 mM concentration (e.g., 0.07 mmol peptide in 140 mL of DMF), we have cyclized protected linear peptide **4.6a** at concentrations as high as 10 mM without observing polymerization. These macrocyclization conditions do not result in epimerization because the *C*-terminus of the protected linear peptide comprises an α-amino acid carbamate (Boc-NH-CHR-COOH),

rather than an α-amino acid amide (RCO-NH-CHR-COOH). Final deprotection with trifluoroacetic acid (TFA) followed by reverse-phase HPLC purification produced peptide **4.2a** as the TFA salt in 45% overall yield, based on the loading of Boc-Orn(Fmoc)-OH on the resin. HPLC analysis of protected linear peptide **4.6a** and crude deprotected cyclized peptide **4.2a** shows little degradation in purity on cyclization (Figure 4.1, left).

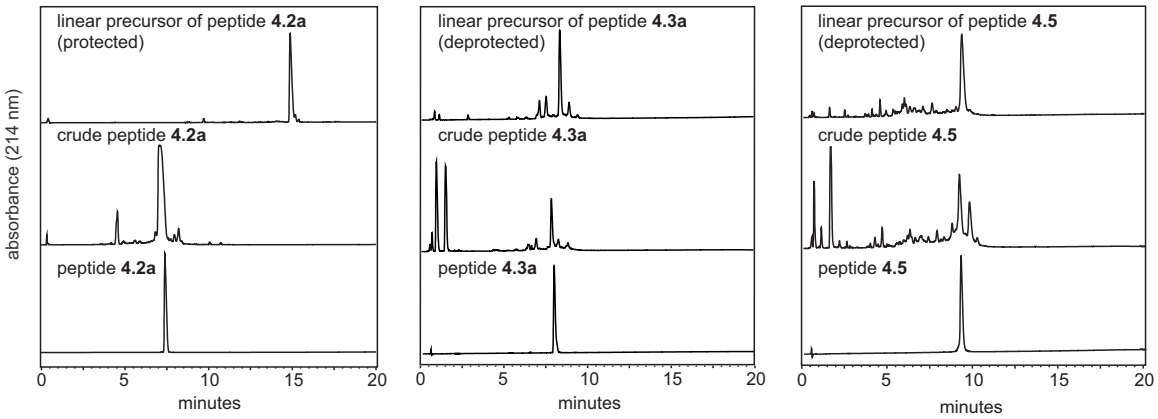

Figure 4.1. Analytical HPLC traces in the syntheses of peptides **4.2a**, **4.3a**, and **4.5**. HPLC data were recorded using an Agilent Zorbax SB-C18 column (50 mm × 4.5 mm) with a gradient of 5–100% CH_3CN in H_2O with 0.1% TFA and a flow of 1.0 mL/min over 20 minutes.

To further investigate whether polymerization would dominate at higher concentrations, e.g. 10.0 mM, during the cyclization step described above, we cyclized peptide **4.6a** at 0.5 and 10.0 mM in parallel. HPLC analysis of cyclic peptide **4.7a** shows comparable purities of the crude products from cyclization at 0.5 and 10 mM concentrations (Figure 4.2). These HPLC traces indicate that macrocyclization causes no or little polymerization. If polymers or oligomers were to form under these conditions, the HPLC traces from cyclization at 10 mM would show substantially greater impurity than that at 0.5 mM.

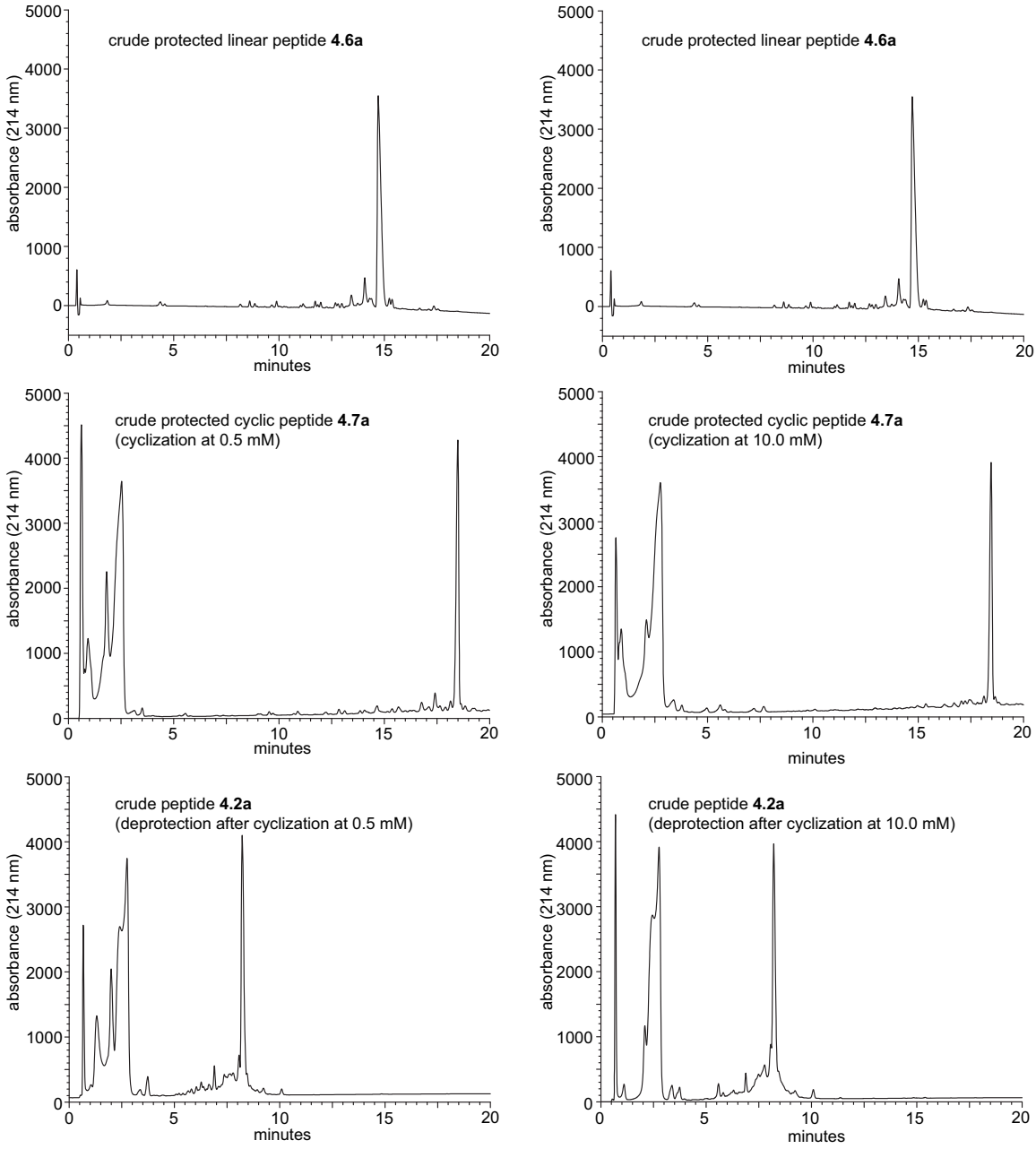

Figure 4.2. Analytical HPLC traces in the syntheses of peptide **4.2a** through cyclization at 0.5 mM (left) and 10 mM (right) concentrations. HPLC analysis of cyclic peptide **4.7a** shows comparable purities of the crude products from cyclization at 0.5 mM (left) and 10 mM (right) concentrations, indicating that macrocyclization causes no or little polymerization. After deprotection, both synthesis conditions show the comparable crude purities of peptide **4.2a**. HPLC data were recorded using an Agilent Zorbax SB-C18 column (50 mm × 4.5 mm) with a gradient of 5–100% CH_3CN in H_2O with 0.1% TFA and a flow of 1.0 mL/min over 20 minutes.

To determine whether we could generate larger macrocyclic peptides, we designed 78- and 102-membered ring macrocyclic homologues of **4.2a**. Peptides **4.3a** and **4.4** are both 78-membered ring macrolactams: peptide **4.3a** contains two Hao units while peptide **5** contains four Hao units. We designed peptide **4.3a** by directly extending both ends of the upper and lower peptide strands of peptide **4.2a** to give Lys-Leu-Glu-Phe-Hao-Leu-Lys-Phe-Glu. This peptide strand comprises Hao in the middle, flanked by two tetrapeptides. We designed peptide **4.4** using the upper peptide strand Lys-Leu-Hao-Val-Hao-Phe-Glu and the lower peptide strand Lys-Leu-Hao-Ile-Hao-Phe-Glu. The four Hao units should provide peptide **4.4** with better protection from edge-to-edge aggregation through *inter*molecular hydrogen bonding. We chose Val and Ile for the middle positions of the upper and lower β-strands, because these residues favor β-sheet formation. The synthesis of peptides **4.3a** and **4.4** followed the procedures described above. Cyclization of the corresponding protected linear peptides **4.9a** and **4.10**, followed by deprotection with TFA and reverse-phase HPLC purification, produced peptides **4.3a** and **4.4** as the TFA salts in 32% and 23% overall yield, respectively. As in the synthesis of the smaller homologue, HPLC analysis of the linear precursor of peptide **4.3a** and its cyclization product, crude peptide **4.3a**, shows little degradation in purity on cyclization (Figure 4.1, middle).

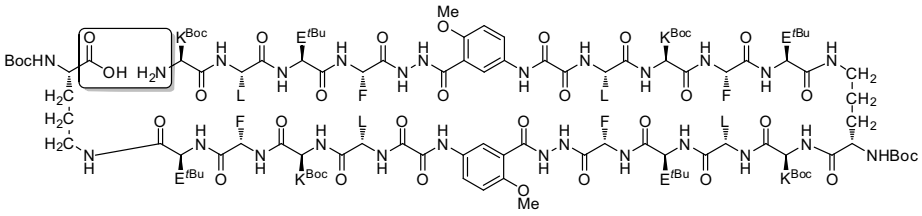

4.8a

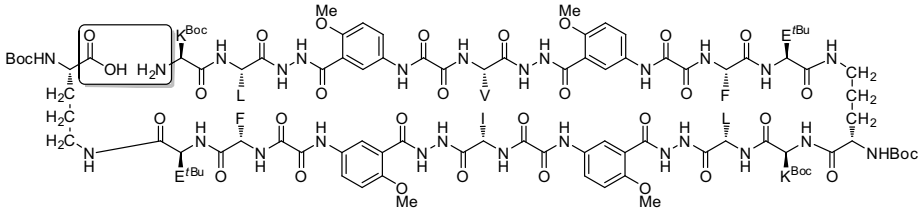

4.9

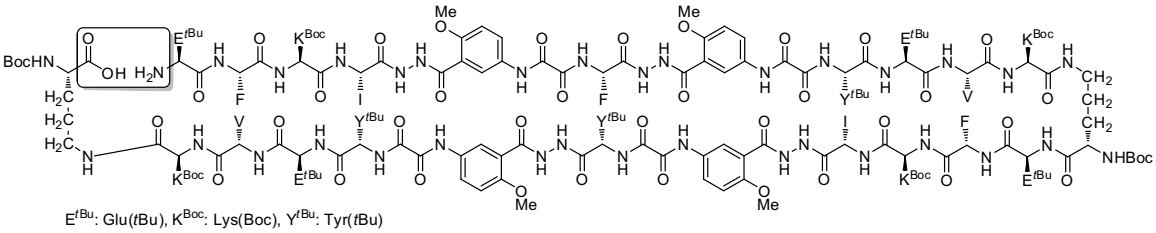

E^{tBu}: Glu(*t*Bu), K^{Boc}: Lys(Boc), Y^{tBu}: Tyr(*t*Bu)

4.10

Peptide **4.5** is a 102-membered ring macrolactam, an expanded homologue of peptide **4.4**. We designed peptide **4.5** using a core structure similar to that of peptide **4.4**, with the upper peptide strand Glu-Phe-Lys-Ile-Hao-Phe-Hao-Tyr-Glu-Val-Lys and the lower peptide strand Glu-Phe-Lys-Ile-Hao-Tyr-Hao-Tyr-Glu-Val-Lys. We synthesized peptide **4.5** using the procedures described above. Cyclization of the corresponding protected linear peptide **4.10**, followed by deprotection with TFA and reverse-phase HPLC purification, produced peptide **4.5** as the TFA salt in 13% overall yield. Unlike the syntheses of the smaller macrocycles, HPLC analysis of the linear precursor of peptide **4.5** and its cyclization product, crude peptide **4.5**, shows moderate degradation in purity on cyclization (Figure 4.1, right).

In all of these syntheses, the protected linear peptides are easily prepared by standard automated Fmoc-based solid-phase peptide synthesis. Macrocyclization of

protected linear peptides **4.6a**, **4.8a**, **4.9**, and **4.10** is surprisingly easy to achieve. The macrocyclization does not appear to cause polymerization and does not require highly dilute conditions in which large volumes of solvent, slow addition, or syringe pumps are used. After deprotection with TFA, peptides **4.2a**, **4.3a**, **4.4**, and **4.5** are easy to purify by reverse-phase HPLC. The yields of these peptides drop from 45% to 13% when the macrocycles increase from a 54-membered ring to a 102-membered ring. The lower yield of peptide **4.5** may result from the formation of more impurities in the synthesis of the corresponding linear peptide and the further formation of impurities upon macrocyclization. The diminished yields and increasing impurities suggest that the syntheses of macrolactams above 102-membered rings may encounter more difficulties.

2. Design, Synthesis, and Study of a Cyclic Control. To test whether the efficient cyclization of these macrocyclic peptides requires the formation of a preorganized β-sheet structure to template cyclization, we designed and synthesized peptide **4.11**, which cannot form a preorganized β-sheet structure. Peptide **4.11** is a homologue of peptide **4.2a** in which two amino acids have been deleted from the "bottom" strand. The deletion makes the "bottom" strand shorter than the "top" strand and thus prevents the formation of a hydrogen-bonded β-sheet structure. Linear precursor **4.12** cyclized cleanly when subjected to the cyclization conditions used for the other macrocycles. Peptide **4.11** was isolated in 36% yield after macrocyclization, deprotection, and HPLC purification. The successful synthesis of peptide **4.11** suggests that macrocyclization of these linear peptides is able to proceed without preorganization through β-sheet formation. Although this experiment demonstrates that preorganization is

not required for macrocyclization, it does not preclude that preorganization may facilitate macrocyclization.

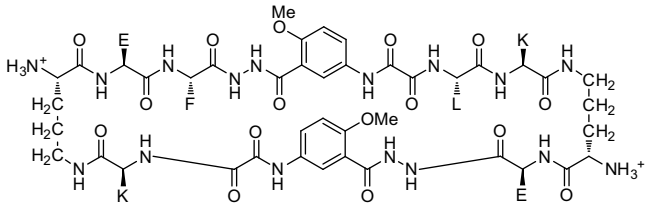

4.11 (TFA salt)

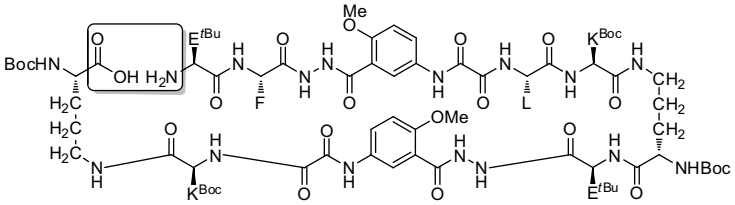

E^{tBoc}: Glu(*t*Bu), K^{Boc}: Lys(Boc)

4.12 (TFA salt)

3. ^{1}H NMR Structural Studies of 54-, 78-, and 102-Membered Ring Macrolactams.

1D, 2D TOCSY, and 2D ROESY ^{1}H NMR studies of the 54-, 78-, and 102-membered ring macrolactams establish the folding of peptides **4.2a**, **4.3a**, and **4.4**.[17] *Inter*strand NOEs are a hallmark of well-defined β-sheet structures. Most notably, antiparallel β-sheets exhibit a pattern of strong NOEs between the α-protons in non-hydrogen-bonded positions. δ-Linked ornithine forms a well-defined β-turnlike structure with characteristic NOEs and magnetic anisotropy.[10e] In a well-folded $^{\delta}$Orn turn structure, the *pro-S* δ-proton ($H_{\delta S}$) shows a strong NOE with the α-proton and the two diastereotopic δ-protons exhibit ca. 0.6 ppm magnetic anisotropy ($\Delta\delta^{\delta}$Orn) in water. Additional indicators of β-sheet folding, such as downfield shifting of the α-protons,

appear to be less applicable to these macrolactams, possibly because of magnetic anisotropy of the Hao amino acid.

The ^{1}H NMR spectrum of peptide **4.2a** at 2.0 mM in D_2O shows sharp, disperse resonances, indicating peptide **4.2a** to be non-aggregating in water. The ROESY spectrum of peptide **4.2a** exhibits a strong *inter*strand NOE associated with the twofold symmetrical contact between the α-protons of Leu and Phe and between the α- and *pro-S* δ-protons of the $^{\delta}$Orn turns (Figure 4.3a).[18] These NOEs suggest peptide **4.2a** to adopt a well-folded β-sheet structure in aqueous solution. The 600 MHz ROESY spectrum of peptide **4.2a** in H_2O/D_2O (9:1) shows additional *inter*strand NH–NH and H_{α}–NH NOEs, further supporting the complete folding of peptide **4.2a** in water. Figure 4.3b summarizes these key H_{α}– H_{α}, NH–NH, and H_{α}–NH NOEs.[19] Peptide **4.2a** exhibits a $\Delta\delta^{\delta}$Orn value of 0.59 ppm, suggesting it to contain well-folded $^{\delta}$Orn turns and thus to adopt a well-defined β-sheet structure. Collectively, both the strong *inter*strand NOEs and the large $\Delta\delta^{\delta}$Orn value of peptide **4.2a** demonstrate that peptide **4.2a** adopts a β-sheet structure in aqueous solution.

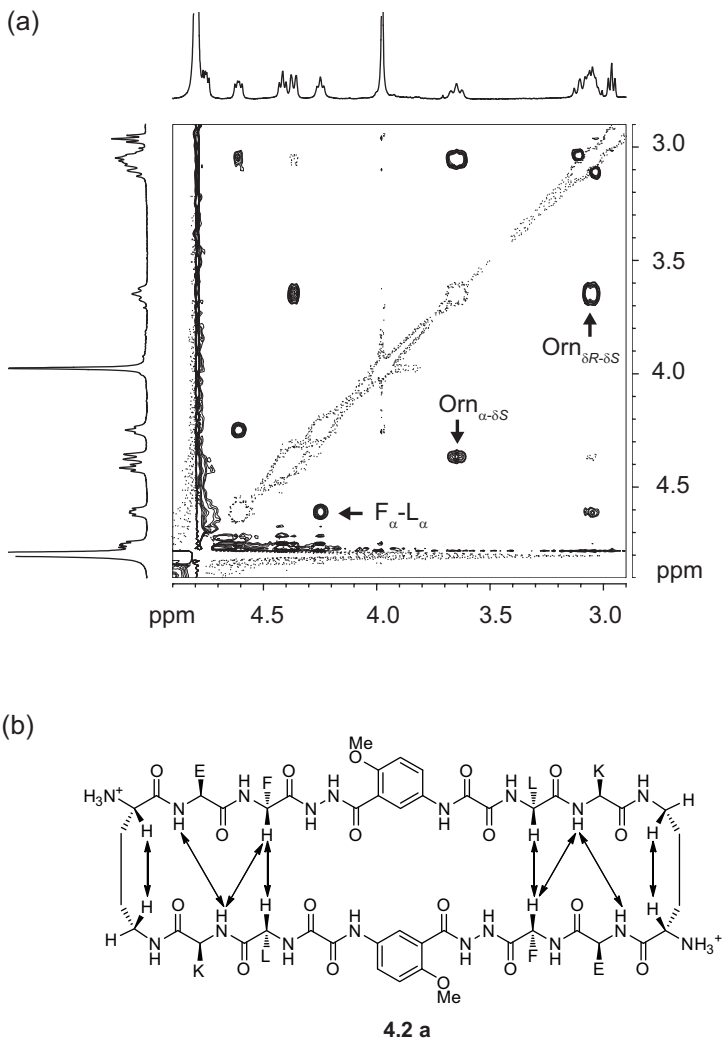

Figure 4.3. (a) Selected expansion of the ROESY spectrum of peptide **4.2a** (2.0 mM in D_2O at 500 MHz and 298 K with a 300-ms spin lock time). (b) Key *inter*strand H_α–H_α, NH–NH, and H_α–NH NOEs of peptide **4.2a** observed in H_2O/D_2O (9:1) at 2.0 mM and 298 K.

Upon increasing the concentration of peptide **4.2a** to 10 mM, its ^{1}H NMR spectrum broadens slightly, suggesting that self-association occurs at higher concentrations. To investigate the degree of self-association of peptide **4.2a**, we measured its diffusion coefficients at different concentrations using DOSY (diffusion-ordered spectroscopy) experiments.[20] Self-association diminishes the diffusion coefficient. Dimerization, for example, results in a smaller diffusion coefficient, about 0.7–0.8 that of

the monomer. Peptide **4.2a** exhibits decreasing diffusion coefficients upon increasing concentrations up to 10.0 mM in D_2O at 298 K: 17.3×10^{-11} m^2/s at 0.3 mM, 16.9×10^{-11} m^2/s at 1.0 mM, 15.8×10^{-11} m^2/s at 2.0 mM, 15.1×10^{-11} m^2/s at 3.3 mM, 14.7×10^{-11} m^2/s at 5.0 mM, and 14.1×10^{-11} m^2/s at 10.0 mM. These changes in diffusion coefficients suggest that peptide **4.2a** is largely monomeric at submillimolar and low millimolar concentrations, but self-associates at higher concentrations.

The 600 MHz ^1H NMR spectrum of peptide **4.3a** shows sharp resonances in D_2O at 1.0 mM and 298 K. The spectrum is severely broadened at concentrations above 5.0 mM, indicating self-association at higher concentrations. At 1.0 mM, peptide **4.3a** exhibits a diffusion coefficient of 14.4×10^{-11} m^2/s in D_2O at 298 K, consistent with its larger size than peptide **4.2a** and little self-association. Peptide **4.3a** exhibits a $\Delta\delta^{\delta}$Orn value of 0.56 ppm and a strong NOE between the α- and *pro-S* δ-protons of the $^{\delta}$Orn turns, indicating the $^{\delta}$Orn turns of peptide **4.3a** are in well-folded β-turnlike structures. Although the ROESY spectrum of peptide **4.3a** exhibits a strong NOE between the α-protons of Leu and Phe, the α-proton resonances of the two types of Leu residues overlap, preventing unambiguous elucidation of key contacts between the Leu and Phe α-protons (Figure 4.4).

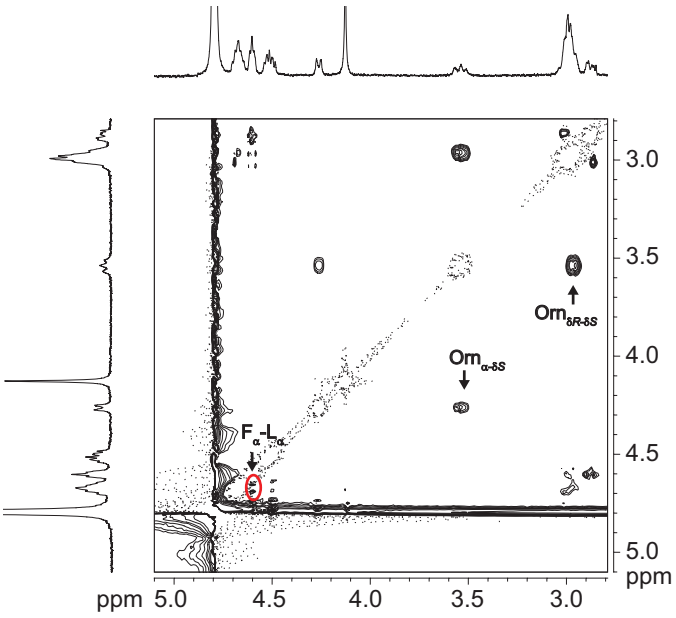

Figure 4.4. Selected expansion of the ROESY spectrum of peptide **4.3a** (1.0 mM in D_2O at 500 MHz and 298 K with a 300-ms spin lock time). The ambiguous NOEs between the Leu and Phe α-protons are circled in red.

To address this ambiguity, we synthesized peptide **4.3b**, a close homologue of peptide **4.3a** in which the Leu-Phe pairs at positions 2–15 and 10–7 were replaced with Val-Tyr pairs. The ROESY spectrum of peptide **4.3b** in D_2O at 288 K shows strong *inter*strand NOEs between the Val and Tyr α-protons and between the Leu and Phe α-protons (Figure 4.5). These *inter*strand NOEs unambiguously demonstrate the β-sheet structure of peptide **4.3b**. Peptide **4.3b** exhibits a strong NOE between the α- and *pro-S* δ-protons of the $^{\delta}$Orn turns and a $\Delta\delta^{\delta}$Orn value of 0.52 ppm, suggesting near complete folding of the $^{\delta}$Orn turns. The *inter*strand NOEs and well-defined β-turn structures substantiate that peptide **4.3b** adopts a well-folded β-sheet in aqueous solution.

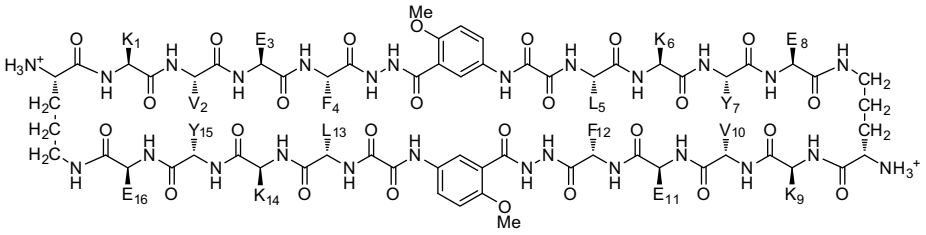

4.3b (TFA salt)

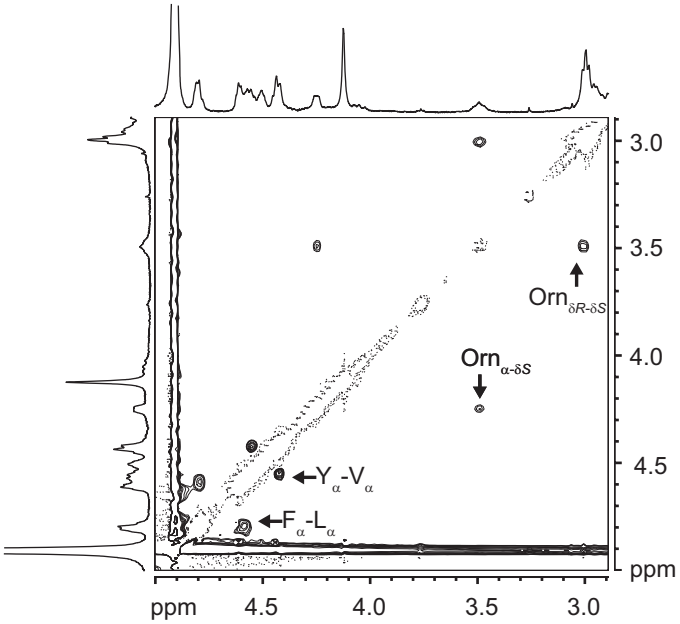

Figure 4.5. Selected expansion of the ROESY spectrum of peptide **4.3b** (1.0 mM in D_2O at 500 MHz and 288 K with a 200-ms spin lock time).

Peptide **4.4** shows severe broadening of the ^{1}H NMR spectrum in D_2O at submillimolar concentrations, suggesting severe self-association and precluding ^{1}H NMR structural studies. For this reason, we studied peptide **4.4** in methanol (CD_3OD) rather than in water. Although the ^{1}H NMR spectrum of peptide **4.4** in CD_3OD shows slight broadening, the resonances of peptide **4.4** can be assigned. The ROESY spectrum in CD_3OD exhibits strong NOEs, indicating peptide **4.4** to adopt a β-sheet structure in methanol (Figure 4.6). Peptide **4.4** shows a $\Delta\delta^{\delta}$Orn value of 0.70 ppm in methanol, suggesting it to contain well-folded $^{\delta}$Orn turns and thus to adopt a well-folded β-sheet

structure. The greater $\Delta\delta^{\delta}$Orn value of peptide **4.4** in methanol may result from a more structured conformation through stronger hydrogen bonding in a solvent less competitive than water.[21]

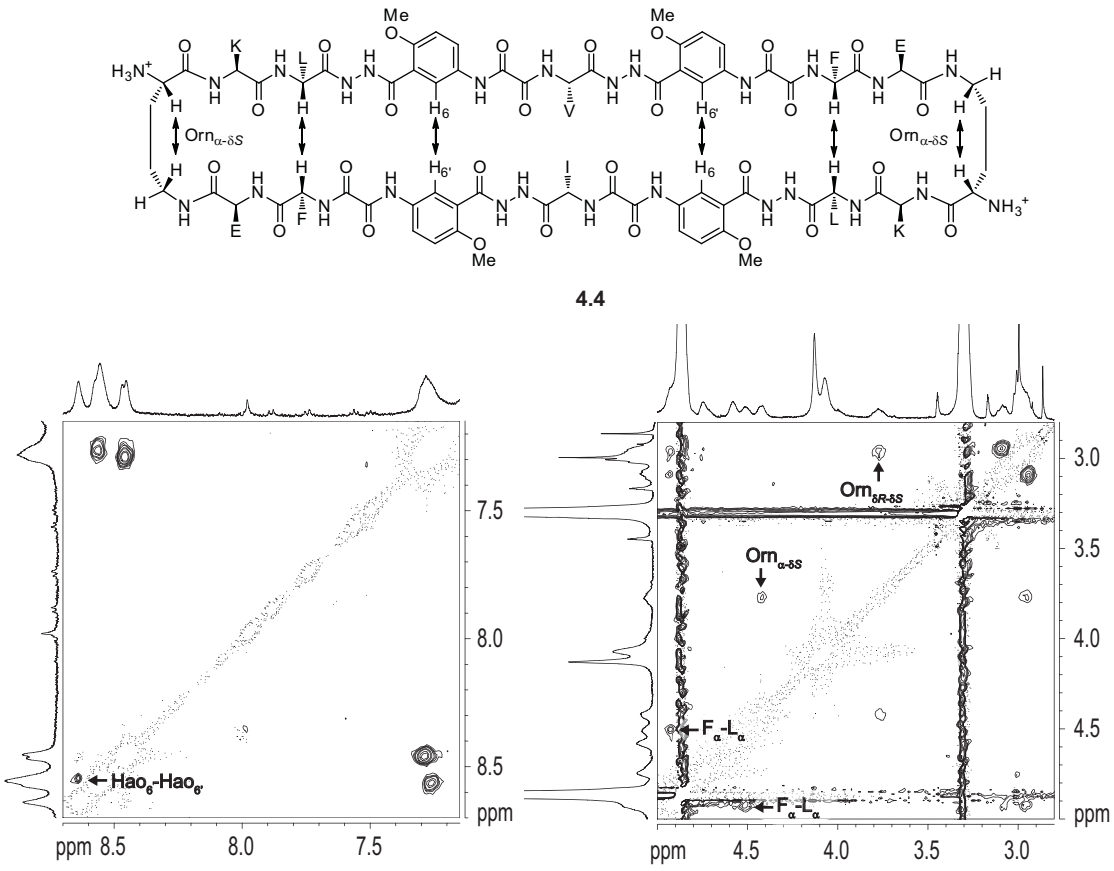

Figure 4.6. Key NOEs of peptide **4.4** observed in CD_3OD and selected expansion of the ROESY spectrum of peptide **4.4** (1.0 mM in D_2O at 500 MHz and 298 K with a 300-ms spin lock time).

Peptide **4.5** exhibits severely broadened ^{1}H NMR resonances both in water and in methanol, precluding further ^{1}H NMR structural investigation in these solvents. The severe broadening of the ^{1}H NMR spectra of peptides **4.4** and **4.5** leads to an interesting question: whether macrolactams containing more Hao units have greater propensity to self-associate in water. Both peptides **4.4** and **4.5** contain four Hao units, while peptides

4.2 and **4.3** only contain two. Although the Hao units help block aggregation through *inter*molecular edge-to-edge hydrogen bonding, they also impart more hydrophobic aromatic surfaces. The greater hydrophobic surface area may lead to more self-association through face-to-face hydrophobic interactions.

4. Effect of the Sequence on Folding of 54-Membered Ring Macrocyclic β-Sheets 4.2. To examine the effect of side-chain interactions in non-hydrogen-bonded positions on folding, we designed and synthesized peptides **4.2b**–**e** in which the Phe-Leu side-chain pairs were respectively replaced with Leu-Leu, Phe-Phe, Tyr-Trp, and Phe-Tyr (Table 4.1). Peptides **4.2b**–**e** show $\Delta\delta^{\delta}$Orn values of 0.26, 0.18, 0.58, and 0.35 ppm, respectively (Figure 4.7). The $\Delta\delta^{\delta}$Orn values suggest that peptide **4.2d** forms a well-folded β-sheet in aqueous solution, while peptides **4.2b**, **4.2c**, and **4.2e** form partially folded β-sheets. These studies demonstrate that the side-chain pairs in the non-hydrogen-bonded positions play a role in the folding of peptides **3** and that Phe-Leu and Tyr-Trp pairs lead to better folding.

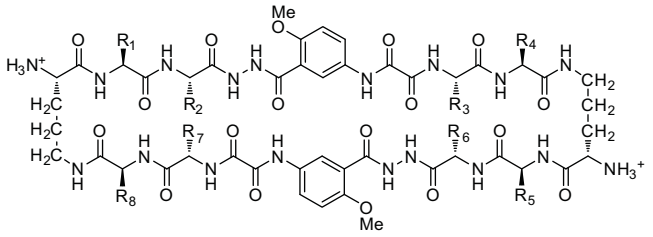

4.2 (TFA salt)

Table 4.1. Amino Acids at Positions R_1-R_8 of Peptides **4.2**

peptide	R_1	R_2	R_3	R_4	R_5	R_6	R_7	R_8
4.2a	Glu	Phe	Leu	Lys	Glu	Phe	Leu	Lys
4.2b	Glu	Leu	Leu	Lys	Glu	Leu	Leu	Lys
4.2c	Glu	Phe	Phe	Lys	Glu	Phe	Phe	Lys
4.2d	Glu	Tyr	Trp	Lys	Glu	Tyr	Trp	Lys
4.2e	Glu	Phe	Tyr	Lys	Glu	Phe	Tyr	Lys
4.2f	Val	Phe	Leu	Lys	Val	Phe	Leu	Lys

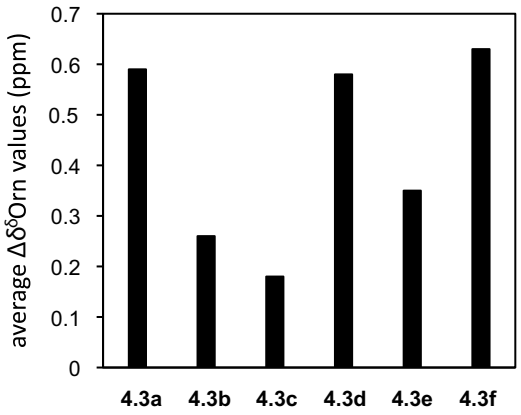

Figure 4.7. $\Delta\delta^{\delta}$Orn values of peptides **4.2** in D_2O at 298 K.

To investigate whether the Lys-Glu pairs in the hydrogen-bonded positions are necessary to achieve the complete folding of peptides **4.2**, we designed and synthesized peptide **4.2f**, a close analogue of peptide **4.2a** in which the two Glu residues are replaced with two Val residues. Peptide **4.2f** exhibits a $\Delta\delta^{\delta}$Orn value of 0.63 ppm in D_2O, suggesting it to be completely folded in aqueous solution. The complete folding of

peptide **4.3f** indicates that salt bridges between Lys and Glu are not necessary to stabilize the folded β-sheet structures. Consistent with this observation, the uncorrected pH of peptides **4.2** and **4.3** in D_2O ranges from 1.9 to 2.8, and acidifying peptides **4.2a** and **4.3b** with 10 mM DCl has little effect upon their $\Delta\delta^{\delta}$Orn values.

5. Design, Synthesis, and Study of Acyclic Controls. To verify that macrocyclization promotes β-sheet formation, we designed peptides **4.13** and **4.14** as acyclic controls. Peptide **4.13** is a homologue of the "upper" peptide strand of peptide **4.2a**, while peptide **4.14** is a homologue of both the "upper" and "lower" peptide strands linked by a single $^{\delta}$Orn β-turn mimic. ^{1}H NMR studies of peptide **4.13** in D_2O do not show an NOE between the Leu and Phe α-protons, suggesting that peptide **4.13** does not dimerize to form β-sheetlike structures in aqueous solution. Consistent with a monomeric structure, peptide **4.13** exhibits a diffusion coefficient of 25.7×10^{-11} m^2/s in D_2O at 2.2 mM and 298 K. Peptide **4.14** also does not show NOEs between the Leu and Phe α-protons and only exhibits a $\Delta\delta^{\delta}$Orn value of 0.24 ppm in D_2O at 1.9 mM and 298 K, suggesting the absence of significant β-sheetlike structure and only minimal folding in aqueous solution. The diffusion coefficient of peptide **4.14** under these conditions is 19.0×10^{-11} m^2/s, which is comparable to those measured for peptides **4.2** and appropriately less than that of peptide **4.13**. The absence of significant β-sheetlike dimerization of peptide **4.13** and folding of peptide **4.14** confirms that macrocyclization is necessary for creating β-sheet structure in peptide **4.2a**.

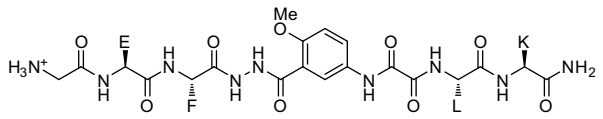

4.13 (TFA salt)

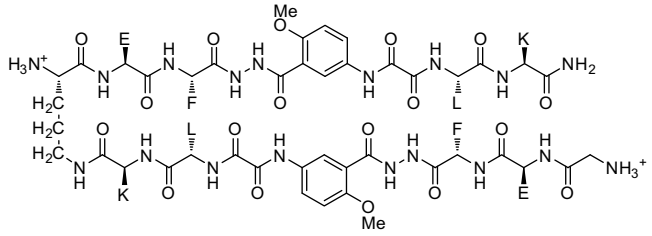

4.14 (TFA salt)

Conclusion

These studies demonstrate that macrocyclization to synthesize giant macrolactams is surprisingly efficient. Macrocyclization does not require extremely dilute conditions to avoid polymerization in cyclizing the corresponding protected linear peptides. Although the present studies are focused on β-sheet structures, the efficient cyclization does not appear to require preorganization through β-sheet formation.

The water-soluble 54-, 78-, and 102-membered ring macrocyclic peptides prepared in these studies are among the largest synthetic macrolactams. These giant macrolactams are easy to synthesize and purify. Macrocyclization requires a few hundreds of milliliters of DMF to produce tens of milligrams of macrocyclic peptides as fluffy white solids after purification and lyophilization. This synthesis provides sufficient quantity of samples for characterization and further studies. Macrocyclization is an effective means to promote and stabilize β-sheet structures, and ^{1}H NMR structural studies show that macrolactams **4.2** and **4.3** adopt β-sheet structures in aqueous solution.

We envision giant macrolactams to be a fruitful area for further research. With incorporation of biologically relevant amino acid sequences, macrocyclization may

impart peptide-based macrolactams with unique three-dimensional structures and potential biological activities such as those of cyclotides. Moreover, large peptide-based macrolactam structures may be suitable for supramolecular chemistry and nanotechnology. It is not clear whether there is an upper limit to the size of the macrolactam structures that can be prepared, and the synthesis of even larger macrolactams may be envisioned.

References and Notes

1. (a) Cascales, L.; Craik, D. J. *Org. Biomol. Chem.* **2010**, *8*, 5035–5047. (b) Jagadish, K.; Camarero, J. A. *Pept. Sci.* **2010**, *94*, 611–616. (c) Gerlach, S. L.; Rathinakumar, R.; Chakravarty, G.; Göransson, U.; Wimley, W. C.; Darwin, S. P.; Mondal, D. *Pept. Sci.* **2010**, *94*, 617–625. (d) Mylne, J. S.; Wang, C. K.; van der Weerden, N. L.; Craik, D. J. *Pept. Sci.* **2010**, *94*, 635–646. (e) Colgrave, M. L.; Korsinczky, M. J. L.; Clark, R. J.; Foley, F.; Craik, D. J. *Pept. Sci.* **2010**, *94*, 665–672.

2. (a) Kondejewski, L. H.; Farmer, S. W.; Wishart, D. S.; Kay, C. M.; Hancock, R. E. W.; Hodges, R. S. *J. Biol. Chem.* **1996**, *271*, 25261–25268. (b) Gibbs, A. C.; Kondejewski, L. H.; Gronwald, W.; Nip, A. M.; Hodges, R. S.; Sykes, B. D.; Wishart, D. S. *Nat. Struct. Biol.* **1998**, *5*, 284−288. (c) Trabi, M.; Schirra, H. J.; Craik, D. J. *Biochemistry* **2001**, 40, 4211–4221. (d) Gibbs, A. C.; Bjorndahl, T. C.; Hodges, R. S.; Wishart, D. S. *J. Am. Chem. Soc.* **2002**, *124*, 1203–1213. (e) Rosengren K. J.; Daly, N. L.; Plan, M. R.; Waine, C.; Craik, D. J. *J. Biol. Chem.* **2003**, *278*, 8606–8616. (f) Gallo, S. A.; Wang, W.; Rawat, S. S.; Jung, G.; Waring, A. J.; Cole, A. M.; Lu, H.; Yan, X.; Daly, N. L.; Craik, D. J.;

Jiang, S.; Lehrer, R. I.; Blumenthal, R. *J. Biol. Chem.* **2006**, *281*, 18787–18792. (g) Tran, D.; Tran, P.; Roberts, K.; Osapay, G.; Schaal, J.; Ouellette, A.; Selsted, M. E. *Antimicrob. Agents Chemother.* **2008**, *52*, 944–953.

3. (a) Späth, J.; Stuart, F.; Jiang, L.; Robinson, J. A. *Helv. Chim. Acta.* **1998**, *81*, 1726–1738. (b) Athanassiou, Z.; Patora, K.; Dias, R. L. A.; Moehle, K.; Robinson, J. A.; Varani, G. *Biochemistry* **2006**, *46*, 741–751. (c) Fasan, R.; Dias, R. L. A.; Moehle, K.; Zerbe, O.; Obrecht, D.; Mittl, P. R. E.; Grütter, M. G.; Robinson, J. A. *ChemBioChem* **2006**, *7*, 515–526. (d) Robinson, J. A. *Acc. Chem. Res.* **2008**, *41*, 1278–1288. (e) Robinson, J. A., et al. *Science* **2010**, *327*, 1010–1013.

4. Conlan, B. F.; Gillon, A. D.; Craik, D. J.; Anderson, M. A. *Pept. Sci.* **2010**, *94*, 573–583.

5. (a) Tam, J. P.; Lu, Y.-A.; Yang, J.-L. *Biochem. Biophys. Res. Commun.* **2000**, *267*, 783–790. (b) Tam, J. P.; Lu, Y.-A.; Yang, J.-L. *J. Biol. Chem.* **2002**, *277*, 50450–50456. (c) Gottler, L. M.; de la Salud Bea, R.; Shelburne, C. E.; Ramamoorthy, A.; Marsh, E. N. G. *Biochemistry* **2008**, *47*, 9243–9250.

6. (a) Syud, F. A.; Espinosa, J. F.; Gellman, S. H. *J. Am. Chem. Soc.* **1999**, *121*, 11577–11578. (b) Stanger, H. E.; Syud, F. A.; Espinosa, J. F.; Giriat, I.; Muir, T.; Gellman, S. H. *Proc. Natl. Acad. Sci.* **2001**, *98*, 12015–12020.(c) Espinosa, J. F.; Syud, F. A.; Gellman, S. H. *Protein Sci.* **2002**, *11*, 1492–1505. (d) Freire, F.; Gellman, S. H. *J. Am. Chem. Soc.* **2009**, *131*, 7970–7972.

7. (a) Woods, R. J.; Brower, J. O.; Castellanos, E.; Hashemzadeh, M.; Khakshoor, O.; Russu, W. A.; Nowick, J. S. *J. Am. Chem. Soc.* **2007**, *129*, 2548–2558. (b) Khakshoor, O.; Demeler, B.; Nowick, J. S. *J. Am. Chem. Soc.* **2007**, *129*, 5558–5569. (c) Khakshoor,

O.; Nowick, J. S. *Curr. Opin. Chem. Biol.* **2008**, *12*, 722–729. (d) Nowick, J. S. *Acc. Chem. Res.* **2008**, *41*, 1319–1330. (e) Khakshoor, O.; Nowick, J. S. *Org. Lett.* **2009**, *11*, 3000–3003. (f) Khakshoor, O.; Lin, A. J.; Korman, T. P.; Sawaya, M. R.; Tsai, S.-C.; Eisenberg, D.; Nowick, J. S. *J. Am. Chem. Soc.* **2010**, *132*, 11622–11628.

8. Tatko, C. D.; Waters, M. L. *J. Am. Chem. Soc.* **2002**, *124*, 9372–9373.

9. Zheng, J; Liu, C.; Sawaya, M. R.; Vadla, B.; Khan, S.; Woods, R. J.; Eisenberg, D.; Goux, W. J.; Nowick, J. S. Submitted to *J. Am. Chem. Soc.*

10. (a) Nowick, J. S.; Tsai, J. H.; Bui, Q.-C. D.; Maitra, S. *J. Am. Chem. Soc.* **1999**, *121*, 8409–8410. (b) Nowick, J. S.; Chung, D. M.; Maitra, K.; Maitra, S.; Stigers, K. D.; Sun, Y. *J. Am. Chem. Soc.* **2000**, *122*, 7654–7661. (c) Nowick, J. S.; Lam, K. S.; Khasanova, T. V.; Kemnitzer, W. E.; Maitra, S.; Mee, H. T.; Liu, R. *J. Am. Chem. Soc.* **2002**, *124*, 4972–4973. (d) Nowick, J. S.; Chung, D. M. *Angew. Chem., Int. Ed.* **2003**, *42*, 1765–1768. (e) Nowick, J. S.; Brower, J. O. *J. Am. Chem. Soc.* **2003**, *125*, 876–877. (f) Chung, D. M.; Nowick, J. S. *J. Am. Chem. Soc.* **2004**, *126*, 3062–3063. (g) Chung, D. M.; Dou, Y.; Baldi, P.; Nowick, J. S. *J. Am. Chem. Soc.* **2005**, *127*, 9998–9999. (h) Nowick, J. S. *Org. Biomol. Chem.* **2006**, *4*, 3869–3885.

11. (a) Smith, C. K.; Regan, L. *Science* **1995**, *270*, 980–982. (b) Smith, C. K.; Regan, L. *Acc. Chem. Res.* **1997**, *30*, 153–161.

12. Wouters, M. A.; Curmi P. M. G. *Proteins: Struct, Funct., Genet.* **1995**, 22, 119–131.

13. Most standard peptide synthesis procedures followed those in the "Synthesis Notes" section of the 2009/2010 Novabiochem catalog.

14. Fmoc*-Hao-OH has been described previously in reference 10b. Fmoc* refers to the 2,7-di-*tert*-butyl-Fmoc group. This more soluble analogue of the Fmoc group is described

in Stigers, K. D.; Koutroulis, M. R.; Chung, D. M.; Nowick, J. S. *J. Org. Chem.* **2000**, *65*, 3858–3860. For details of the preparation of Fmoc-Hao-OH, see the experimental section.

15. (a) Montalbetti, C. A. G. N.; Falque, V. *Tetrahedron* **2005**, *61*, 10827–10852. (b) Hood, C. A.; Fuentes, G.; Patel, H.; Page, K.; Menakuru, M.; Park, J. H. *J. Pept. Sci.* **2008**, *14*, 97–101. (c) Valeur, E.; Bradley, M. *Chem. Soc. Rev.* **2009**, *38*, 606–631.

16. In the cyclization step, most macrocyclic peptides were synthesized using HCTU/DIEA/DMF. Cyclization using HCTU/DIEA/DMF produces yellowish impurities that remain after deprotection with TFA. When these colored impurities proved difficult to remove by HPLC purification, cyclization was alternatively performed with HBTU/HOBt/*N*-methylmorpholine/DMF.[15]

17. ^{1}H NMR studies were performed in D_2O with DSA as an internal standard. DSA is described in Nowick, J. S.; Khakshoor, O.; Hashemzadeh, M.; Brower, J. O. *Org. Lett.* **2003,** *5*, 3511–3513. Resonances were assigned by 1D, 2D TOCSY, and 2D ROESY ^{1}H NMR studies. ^{1}H NMR studies of peptide **4.2a** were also performed in H_2O/D_2O (9:1) with water suppression to observe amide resonances and allow sequence-specific assignment of the resonances.

18. NOEs between the two Hao units cannot be observed due to symmetry.

19. The hydrazide N–H resonances are broadened by chemical exchange with H_2O, and the NOEs involving these protons can not be observed under conditions of the ROESY experiments.

20. (a) Yao, S.; Howlett, G. J.; Norton, R. S. *J. Biomol. NMR* **2000**, *16*, 109–119. (b) Cohen, Y.; Avram, L.; Frish, L. *Angew. Chem., Int. Ed.* **2005**, *44*, 520–554.

21. Previous studies have shown that a well-folded $^{\delta}$Orn turn exhibits a $\Delta\delta^{\delta}$Orn value of 1.3 ppm in a chloroform solution. For details, see reference 10c.

Experimental Section for Chapter 4

Content

General Procedures

Methylene chloride and tetrahydrofuran (THF) were further purified by passage through a column of alumina under argon.[1] Automated solid-phase peptide synthesis was carried out on a PS3^{TM} Peptide Synthesizer (Protein Technologies, Inc.).[2] Either Fmoc*-Hao-OH or Fmoc-Hao-OH was used to introduce the Hao residue during solid-phase peptide synthesis. Fmoc*-Hao-OH was prepared according to published procedures.[3] The preparation of Fmoc-Hao-OH is described on page S6. Analytical reverse-phase HPLC was performed on an Agilent Zorbax SB-C18 column (50 mm × 4.6 mm) with a gradient of 5–100% CH_3CN in H_2O with 0.1% TFA and a flow of 1.0 mL/min over 20 minutes. Preparative reverse-phase HPLC purification was carried out on a 21.2 x 250 mm Zorbax SB-C18 PrepHT (7-μm particle size) column from Agilent on a Rainin Dynamax system with a flow of 10.0 mL/min. UV detection (214 or 254 nm) was used for analytical and preparative HPLC. Water and acetonitrile were used as the solvents. Both solvents contained 0.1% biochemical grade TFA.

---

[1] Pangborn, A. B.; Giardello, M. A.; Grubbs, R. H.; Rosen, R. K.; Timmers, F. J. *Organometallics* **1996**, *15*, 1518–1520.

[2] Most standard peptide synthesis procedures followed those in the "Synthesis Notes" section of the 2009/2010 Novabiochem catalog.

[3] Nowick, J. S.; Chung, D. M.; Maitra, K.; Maitra, S.; Stigers, K. D.; Sun, Y. *J. Am. Chem. Soc.* **2000**, *122*, 7654–7661.

^{1}H NMR experiments of peptides **3**–**6** were performed in D_2O with an internal standard DSA[4] at 500 MHz and at 600 MHz. Solutions of peptides **3**–**6** were prepared gravimetrically by dissolving an appropriate weight of peptides in an appropriate volume of solvent. In calculating molecular weights, all amino groups were assumed to be protonated as the TFA salts. The ^{1}H NMR resonances of peptide **3a** were assigned by 2D TOCSY and 2D ROESY. In order to observe amide resonances for further resonance assignments, the ^{1}H NMR studies of peptide **3a** were also performed in H_2O/D_2O mixtures (9:1) with water suppression at 600 MHz. All 2D TOCSY and 2D ROESY spectra were collected with 2048 data points in the f_2 domain and 512 data points in the f_1 domain. Data were processed to a 1024 × 1024 real matrix with a Qsine weighting function and with forward linear prediction in the f_1 domain. The data were processed with the Brüker XwinNMR software.

Synthesis of Fmoc-Hao-OH

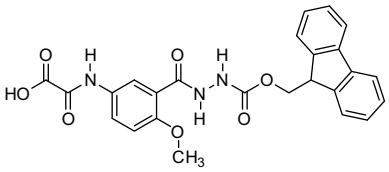

The amino acid Fmoc-Hao-OH (5-HO_2CCONH-2-MeO-C_6H_3-CONHNHFmoc) was prepared using procedures reported for the preparation of Fmoc*-Hao-OH, Fmoc*-Hao$^{K(Boc)}$-OH, and Fmoc*-Hao$^{D(tBu)}$-OH as described in references 3 and 5.[3,5] Fmoc-

[4] Nowick, J. S.; Khakshoor, O.; Hashemzadeh, M.; Brower, J. O. *Org. Lett.* **2003**, *5*, 3511–3513.

[5] Khasanova, T. V.; Khakshoor, O.; Nowick, J. S., *Org. Lett.* **2008**, *10*, 5293–5296.

$NHNH_2$ was coupled with 2-methoxy-5-nitro-benzoic acid using EDC and HOAt as described in reference 5. The product (5-NO_2-2-MeO-C_6H_3-CONHNHFmoc) was isolated from the mixture by precipitation with water. The nitro group was reduced to the amino group by hydrogenation with H_2 and Pd/C in THF-CH_3OH (4:1) as described in references 3 and 5. The resulting amine (5-NH_2-2-MeO-C_6H_3-CONHNHFmoc) was coupled with ethyl oxalyl chloride and pyridine as described in references 3 and 5, with exception that THF was used as the solvent instead of CH_2Cl_2. The ester product (5-EtO_2CCONH-2-MeO-C_6H_3-CONHNHFmoc) was isolated by filtration (to remove precipitated byproducts) followed by concentration of the filtrate and trituration of the residue with acetonitrile. The ester was hydrolyzed to Fmoc-Hao-OH as described in references 3 and 5.

Loading of Boc-Orn(Fmoc) to 2-Chlorotrityl Chloride Polystyrene Resin for Solid-Phase Peptide Synthesis.

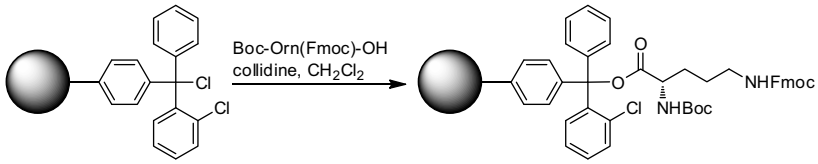

2-Chlorotrityl chloride resin (300 mg, 1.55 mmol/g) was added to a Bio-Rad Poly-Prep chromatography column (10 mL, 0.8 × 4.0 cm). The resin was washed with dry CH_2Cl_2 and suspended in 10 mL of dry CH_2Cl_2 to swell the resin. A solution of Boc-Orn(Fmoc)-OH (0.33 equiv, 70 mg, 0.15 mmol), 2,4,6-collidine (12 equiv, 0.24 mL, 220 mg) and 2.4 mL of dry CH_2Cl_2 was added directly to the resin, and the mixture was gently agitated for 4 hours. The solution was then drained and the resin was washed with

dry CH_2Cl_2 (5 times). A mixture of CH_2Cl_2/MeOH/DIEA (17:2:1, 10 mL) was added to the resin, and the mixture was gently agitated for 1 hour to cap the unreacted 2-chlorotrityl chloride sites. The capping step was repeated to achieve complete capping. The resin was then washed with dry CH_2Cl_2 followed by DMF. The resin was dried by passing nitrogen through the vessel. The resin loading was determined to be 0.40 mmol/g (78% based on Boc-Orn(Fmoc)-OH) by UV analysis of the Fmoc cleavage product.[2] Loadings of 60% to 80% were typically observed in various repetitions of this procedure.

Synthesis of Protected Linear Peptides 4.6, 4.8, 4.9, 4.10, and 4.12. Representative Synthesis of Protected Linear Peptide 4.6a.

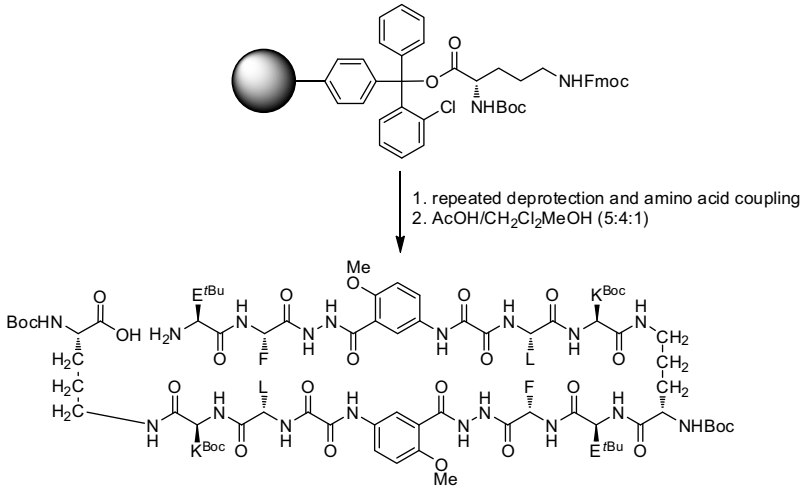

4.6a

The PS-2-chlorotrityl-Orn(Fmoc)-Boc generated from the previous step was washed with DMF (3 × 5 mL) and submitted to cycles of Fmoc solid-phase peptide synthesis on an automated peptide synthesizer using amino acid building blocks: Fmoc*-Hao-OH, Fmoc-Lys(Boc)-OH, Fmoc-Glu(*t*Bu)-OH, Fmoc-Phe-OH, and Fmoc-Leu-OH. The linear peptide was elongated from the C-terminus to the N-terminus. Each coupling consisted of: (1) Fmoc-deprotection with 20% piperidine in DMF for 3 min; (2) washing

with DMF (3 times); (3) coupling of the amino acid (0.5 mmol, 4 equiv) in the presence of HCTU; (4) washing with DMF (6 times). Each amino acid coupling step took 20 min for natural amino acids and 1 h for Hao. Because of the sluggish coupling of Fmoc*–Hao–OH into the growing peptide, the Hao coupling reaction was carried out twice without Fmoc* deprotection in between. After the last amino acid was coupled onto the growing peptide, the terminal Fmoc group was removed with 20% piperidine in DMF.

The resin with the linear peptide was transferred from the reaction vessel of the peptide synthesizer to a Bio-Rad Poly-Prep chromatography column and washed with DMF (3 × 5 mL) followed by CH_2Cl_2 (3 × 5 mL). A mixture of AcOH/CH_2Cl_2/MeOH (5:4:1, 20 mL) was added to the resin, and the suspension was agitated for 1 h. This cleavage solution was collected into a 250-mL round-bottomed flask and the resin was washed with CH_2Cl_2 (3 × 10 mL). The combined solutions were concentrated by rotary evaporation under reduced pressure. Hexanes (ca. 100 mL) were added to the flask and then removed by rotary evaporation to azeotropically remove residual AcOH. The resulting yellowish oil was dissolved CH_2Cl_2 (ca. 5 mL), diluted with hexanes (ca. 100 mL), and concentrated to dryness. The addition of CH_2Cl_2 and hexanes, followed by concentration, was repeated two additional times to remove the residual AcOH. The residue was dried under vacuum to give crude protected linear peptide **4.6a** as a white solid (153 mg, 54% crude yield based on resin loading).

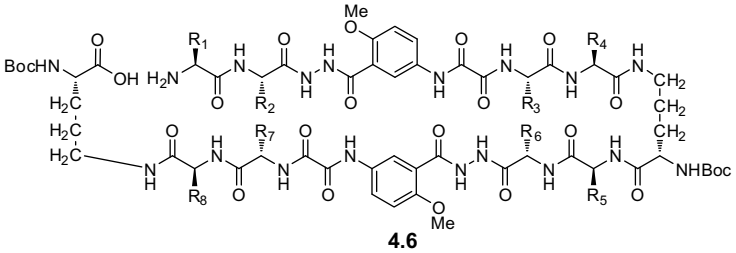

4.6

peptide	R_1	R_2	R_3	R_4	R_5	R_6	R_7	R_8
4.6a	Glu^{tBu}	Phe	Leu	Lys^{Boc}	Glu^{tBu}	Phe	Leu	Lys^{Boc}
4.6b	Glu^{tBu}	Leu	Leu	Lys^{Boc}	Glu^{tBu}	Leu	Leu	Lys^{Boc}
4.6c	Glu^{tBu}	Phe	Phe	Lys^{Boc}	Glu^{tBu}	Phe	Phe	Lys^{Boc}
4.6d	Glu^{tBu}	Tyr^{tBu}	Trp	Lys^{Boc}	Glu^{tBu}	Tyr^{tBu}	Trp	Lys^{Boc}
4.6e	Glu^{tBu}	Phe	Tyr^{tBu}	Lys^{Boc}	Glu^{tBu}	Phe	Tyr^{tBu}	Lys^{Boc}
4.6f	Val	Phe	Leu	Lys^{Boc}	Val	Phe	Leu	Lys^{Boc}

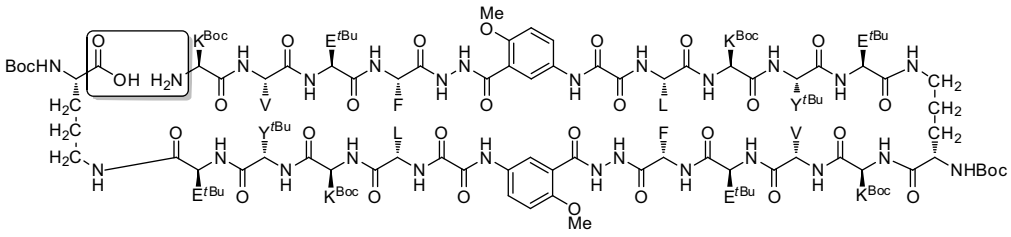

4.8b

Synthesis of Protected Cyclic Peptides 4.7, 4.15, 4.16, and 4.17. Representative Synthesis of Protected Cyclic Peptide 4.7a.

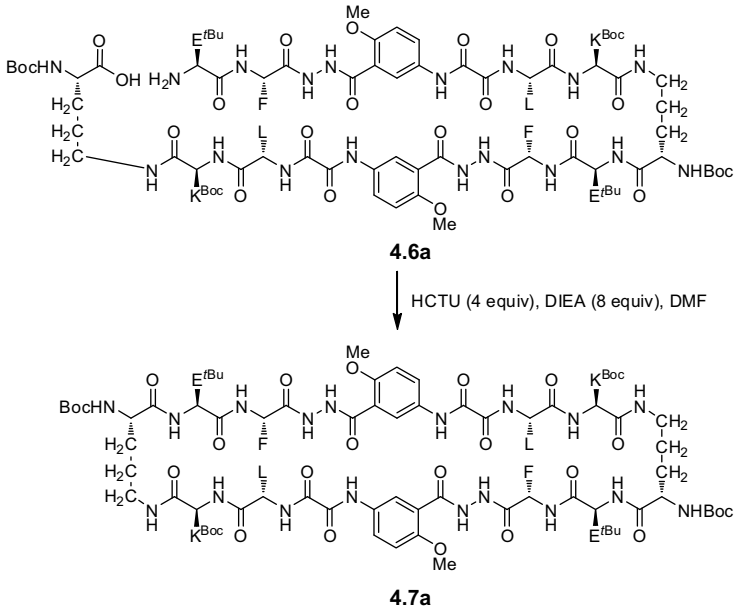

4.6a

4.7a

Crude protected linear peptide **4.6a** (153 mg, 0.068 mmol) was dissolved in DMF (70 mL). The peptide solution was added in drops via a 250-mL pressure-equalizing addition funnel to a 250-mL round-bottom flask containing a magnetic stirring bar, HCTU (111 mg, 0.27 mmol, 4 equiv), and DIEA (94 μL, 0.54 mmol, 8 equiv) in DMF (70 mL). (The final peptide concentration was 0.5 mM.) The reaction mixture was then stirred under nitrogen for 24 h. DMF was then removed by rotary evaporation under reduced pressure to give crude protected cyclic peptide **4.7a** as a yellowish waxy solid. The crude product was used in final deprotection step without further purification.

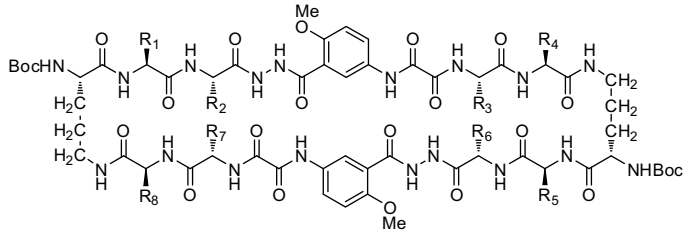

4.7

peptide	R_1	R_2	R_3	R_4	R_5	R_6	R_7	R_8
4.7a	Glu^{tBu}	Phe	Leu	Lys^{Boc}	Glu^{tBu}	Phe	Leu	Lys^{Boc}
4.7b	Glu^{tBu}	Leu	Leu	Lys^{Boc}	Glu^{tBu}	Leu	Leu	Lys^{Boc}
4.7c	Glu^{tBu}	Phe	Phe	Lys^{Boc}	Glu^{tBu}	Phe	Phe	Lys^{Boc}
4.7d	Glu^{tBu}	Tyr^{tBu}	Trp^{Boc}	Lys^{Boc}	Glu^{tBu}	Tyr^{tBu}	Trp^{Boc}	Lys^{Boc}
4.7e	Glu^{tBu}	Phe	Tyr	Lys^{Boc}	Glu^{tBu}	Phe	Tyr	Lys^{Boc}
4.7f	Val	Phe	Leu	Lys^{Boc}	Val	Phe	Leu	Lys^{Boc}

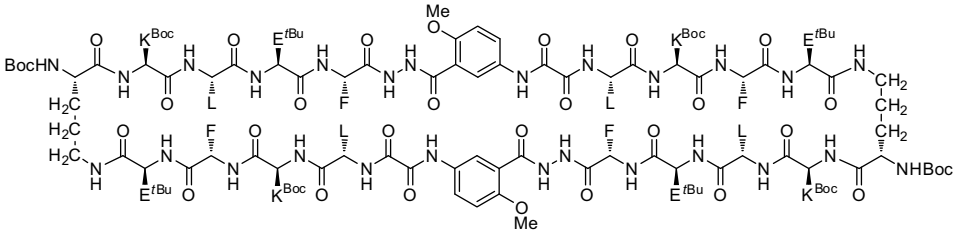

4.15a

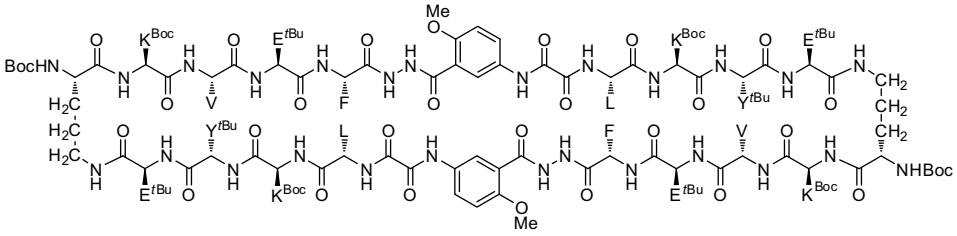

4.15b

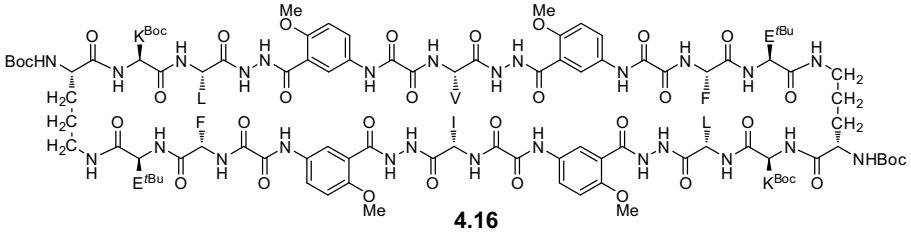

4.16

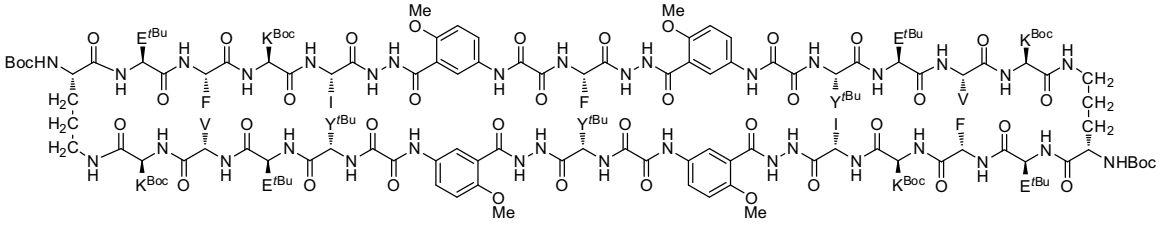

4.17

Synthesis of Peptides 4.2, 4.3, 4.4, 4.5, and 4.11. Representative Synthesis of Peptide 4.2a.

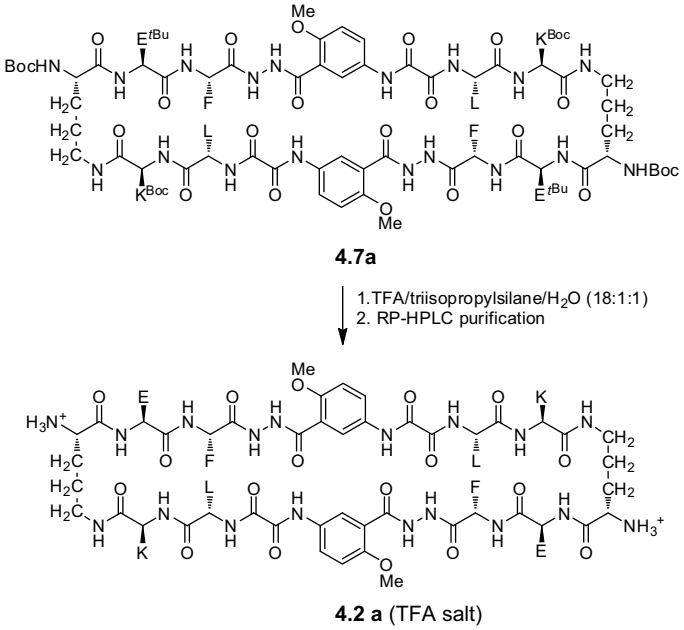

Protected cyclic peptide **4.7a** was dissolved in TFA/triisopropylsilane/H_2O (18:1:1, 20 mL) in a 50-mL round-bottom flask equipped with a nitrogen-inlet adaptor. The solution was magnetically stirred for 2 h. The reaction mixture was then concentrated by rotary evaporation under reduced pressure to give a yellowish oil. The resulting crude peptide **4.2a** was purified by reverse-phase HPLC (gradient elution with 20–50% CH_3CN over 60 min). The pure fractions were lyophilized to give 110 mg of peptide **4.2a** (45% yield, based on resin loading).

Synthesis of Peptides 4.13 and 4.14.

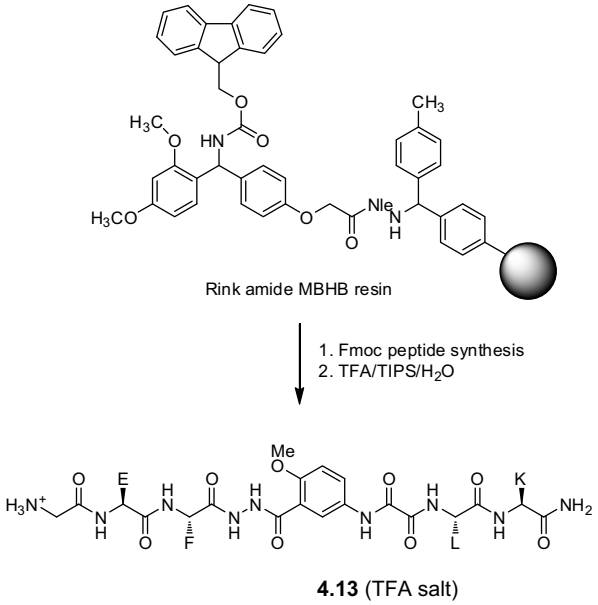

4.13 (TFA salt)

Peptides **4.13** and **4.14** were prepared by the solid-phase peptide synthesis procedures described above, except that the Rink amide MBHB resin was used as the solid support and peptides **4.13** and **4.14** were cleaved from resin by using TFA/triisopropylsilane/H_2O (18:1:1).

Yields of Peptides 4.2, 4.3, 4.4, 4.5, 4.11, 4.13, and 4.14.

peptide	yield	peptide	yield	peptide	yield
4.2a	45 %	**4.3a**	32%	**4.14**	43%
4.2b	22%	**4.3b**	24%		
4.2c	35%	**4.4**	23%		
4.2d	39%	**4.5**	13%		
4.2e	25%	**4.11**	36%		
4.2f	22%	**4.13**	67%		

Diffusion-Ordered Spectroscopy (DOSY) Experiments and Diffusion Constant Measurements of Peptides 4.2, 4.3, 4.4, 4.5, 4.11, 4.13, and 4.14.

DOSY experiments comprised a series of 16 pulsed field gradient spin-echo experiments with a 75-ms delay in which the gradient strength was incremented to allow ca. 2%–95% signal attenuation with a linear ramp.[6] Data were processed to give a pseudo-2D spectrum, and the diffusion coefficient was read from the spectrum after careful phasing. Calibration of the gradients was performed on the basis of the diffusion coefficient of residual HOD in D_2O (1.9×10^{-9} m^2/s at 298 K).[7]

Diffusion Coefficients (*D*) in D_2O at 298K.

peptide	*D* (10^{-11} m^2/s)	conc. (mM)
4.2a	17.3	0.3
	16.9	1.0
	15.8	2.0
	15.1	3.3
	14.7	5.0
	14.1	10.0
4.2b	19.0	2.0
4.2c	15.1	2.0
4.2d	14.5	1.0
4.2e	14.8	2.0
4.2f	17.0	1.0
4.3a	14.4	1.0
4.11	20.4	2.0
4.13	25.7	2.2
4.14	19.0	1.9

[6] Wu, D.; Chen, A.; Johnson Jr., C.S. *J. Magn. Reson.* **1995**, *A115*, 260–264.

[7] Longsworth, L. G. *J. Phys. Chem*. **1960**, *64*, 1914–1917.

Analytical RP-HPLC of peptide **4.2a**

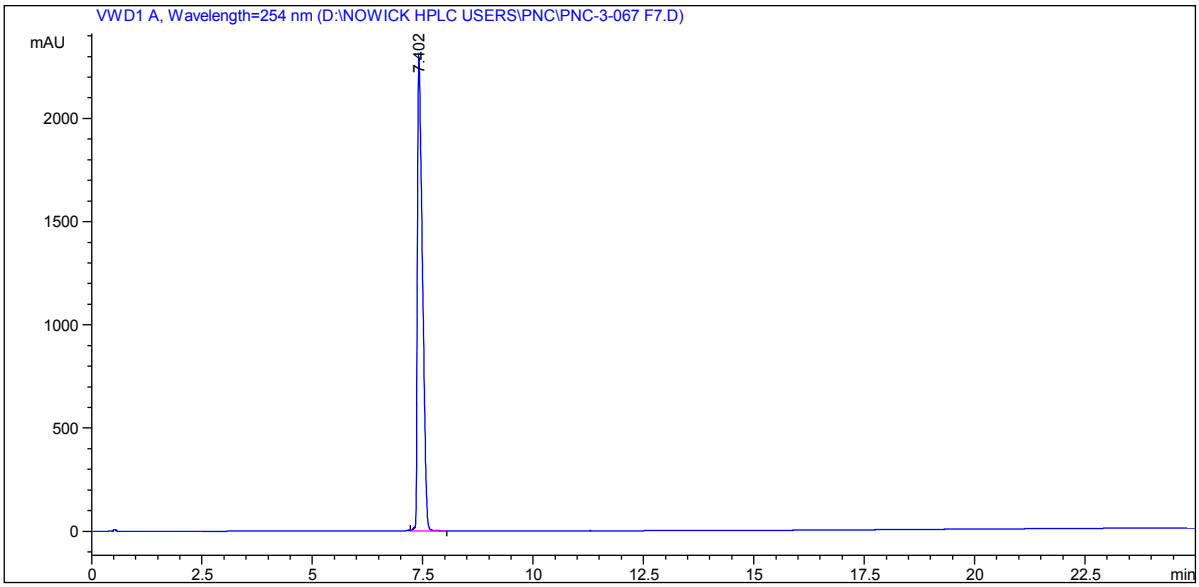

Signal 1: VWD1 A, Wavelength=254 nm

Peak #	RetTime [min]	Type	Width [min]	Area mAU *s	Height [mAU]	Area %
1	7.402	VB	0.1251	1.83205e4	2297.25977	100.0000
Totals :				1.83205e4	2297.25977	

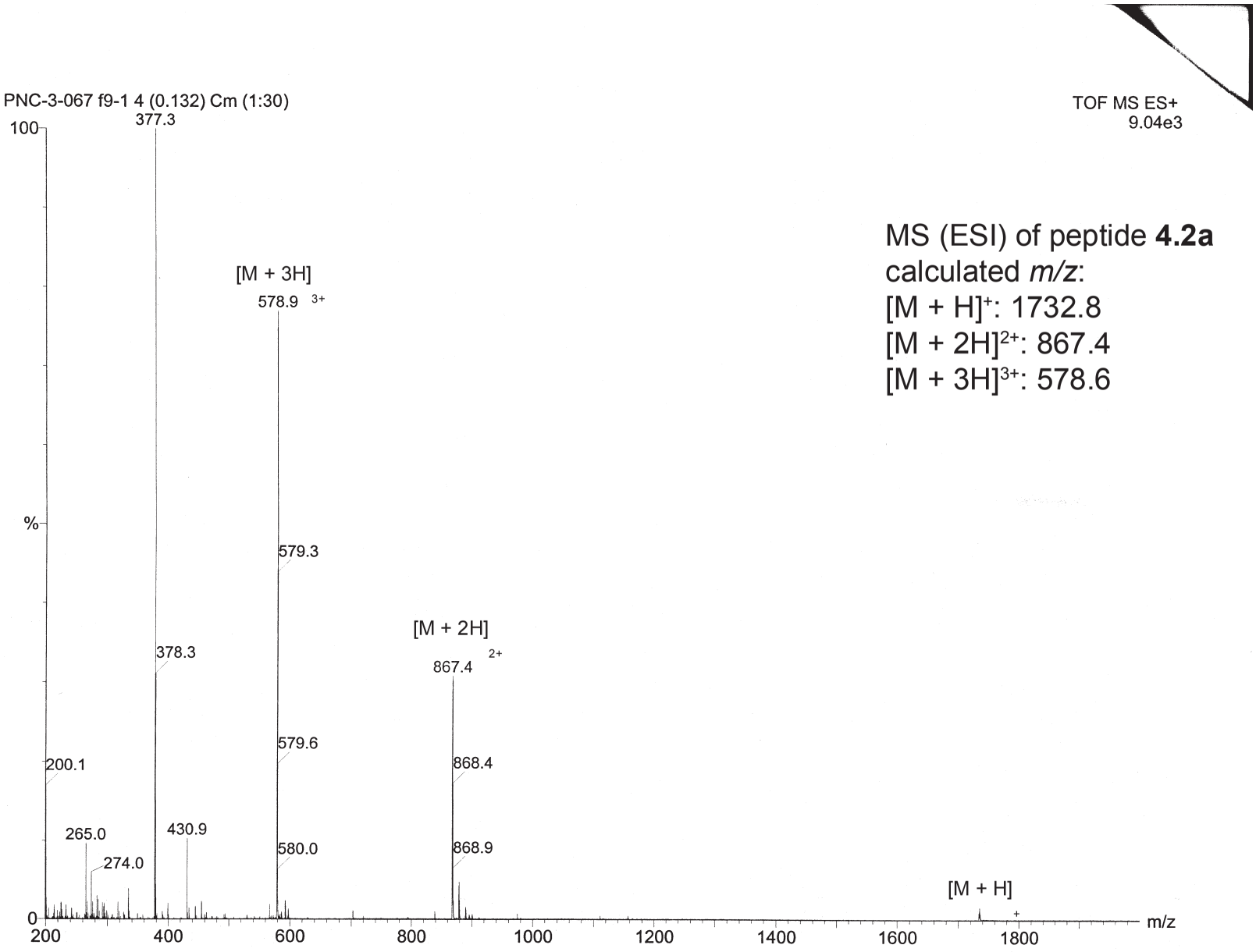

MS (ESI) of peptide **4.2a**
calculated *m/z*:
$[M + H]^{+}$: 1732.8
$[M + 2H]^{2+}$: 867.4
$[M + 3H]^{3+}$: 578.6

1D ^{1}H NMR spectrum of peptide **4.2a**, 2 mM in D_2O, 298K, 500 MHz

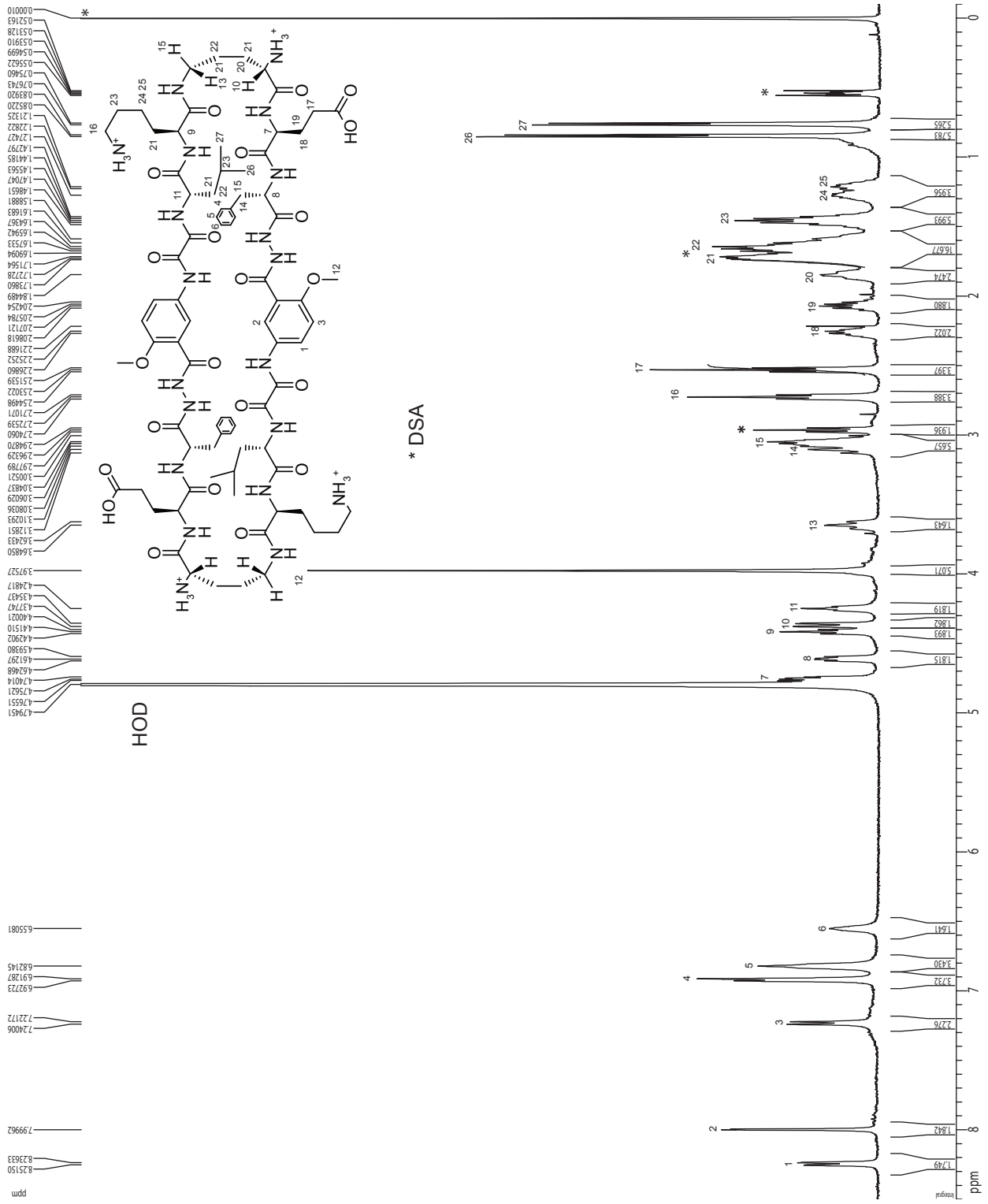

2D TOCSY spectrum of peptide **4.2a**, 2 mM in D_2O, 298K, 500 MHz
150-ms spin-lock mixing time

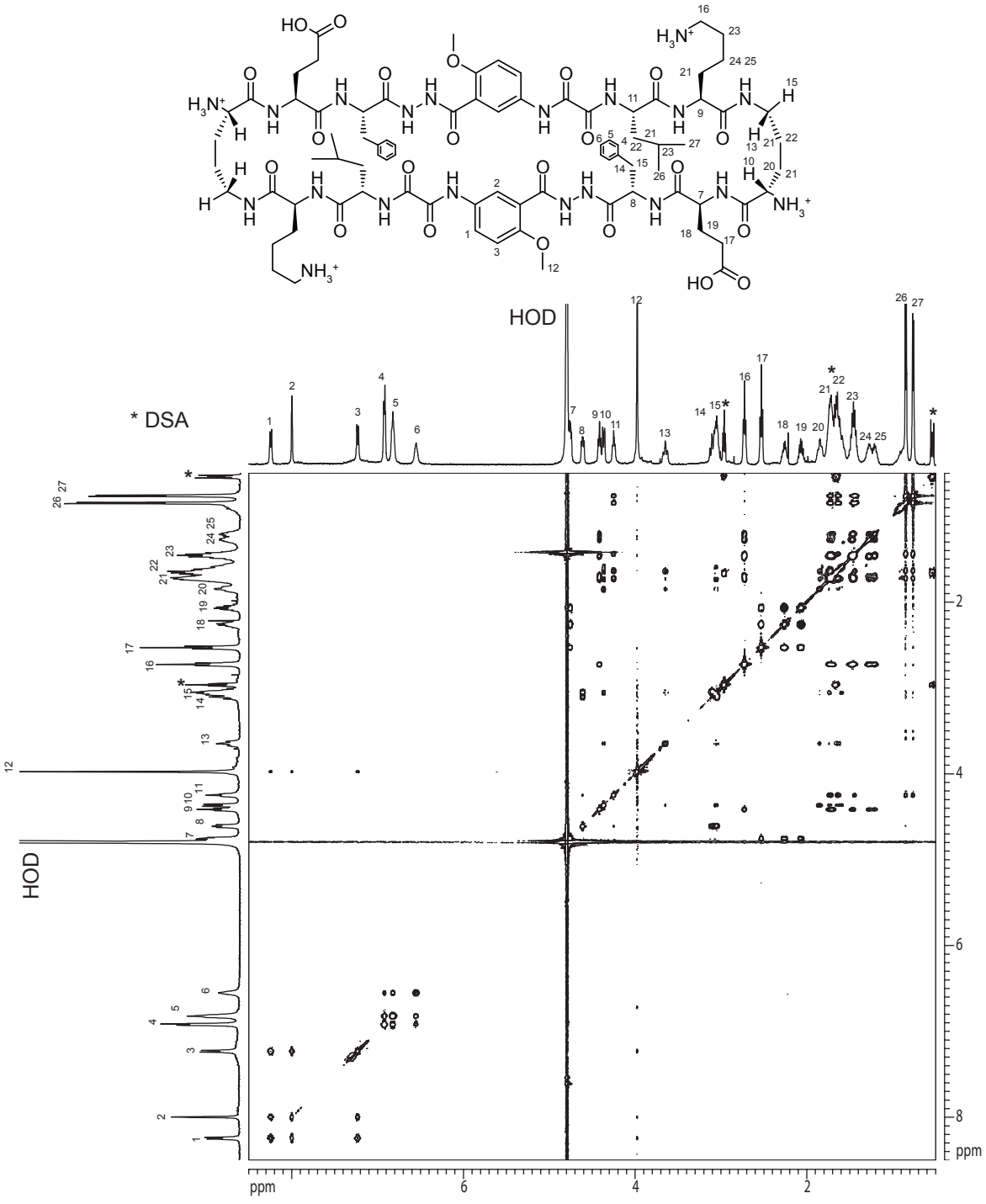

2D ROESY spectrum of peptide **4.2a**, 2 mM in D_2O, 298K, 500 MHz, 300-ms spin-lock mixing time

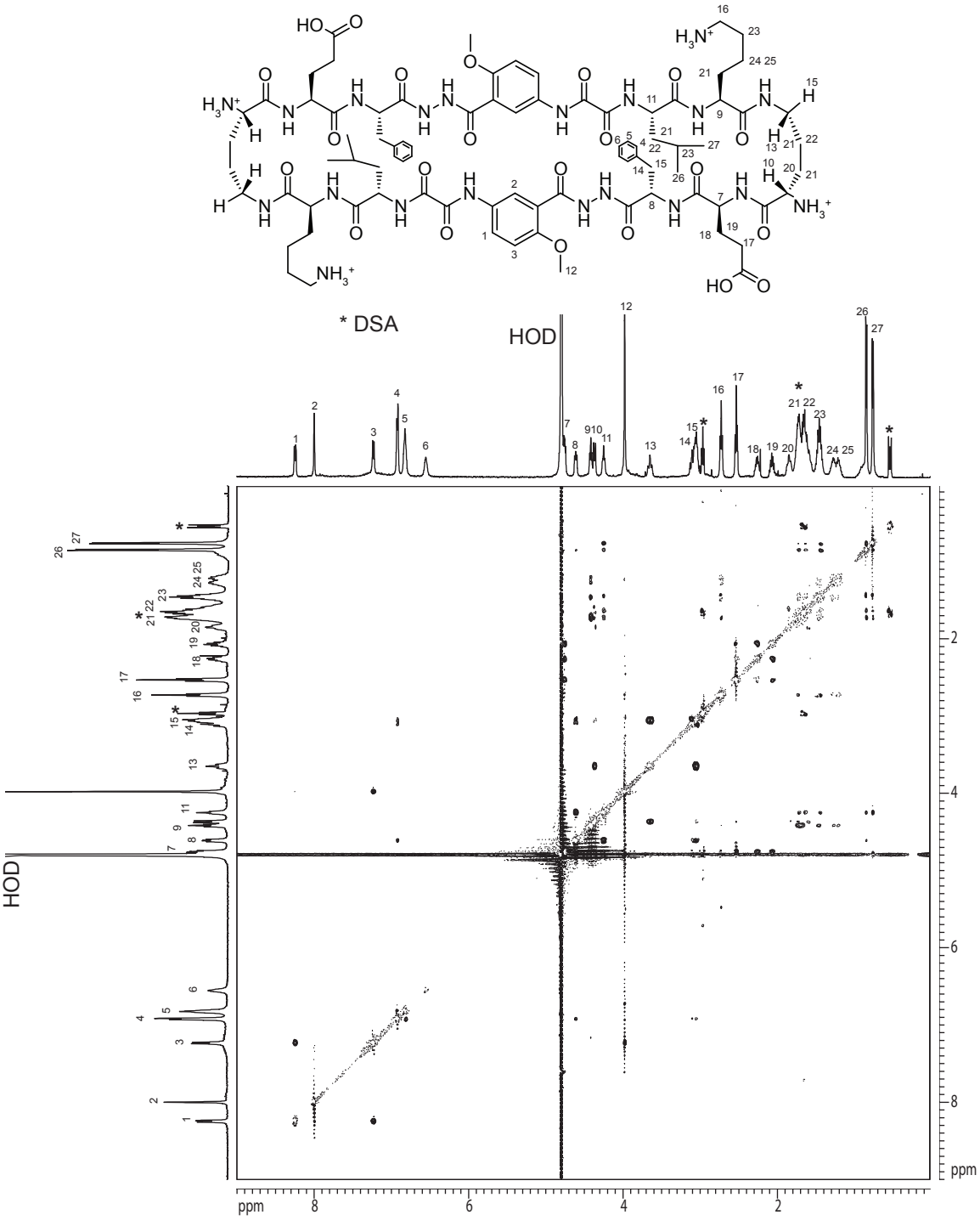

1D ^{1}H NMR spectrum of peptide **4.2a** with water suppression, 2 mM in 9:1 H_2O/D_2O, 298K, 600 MHz

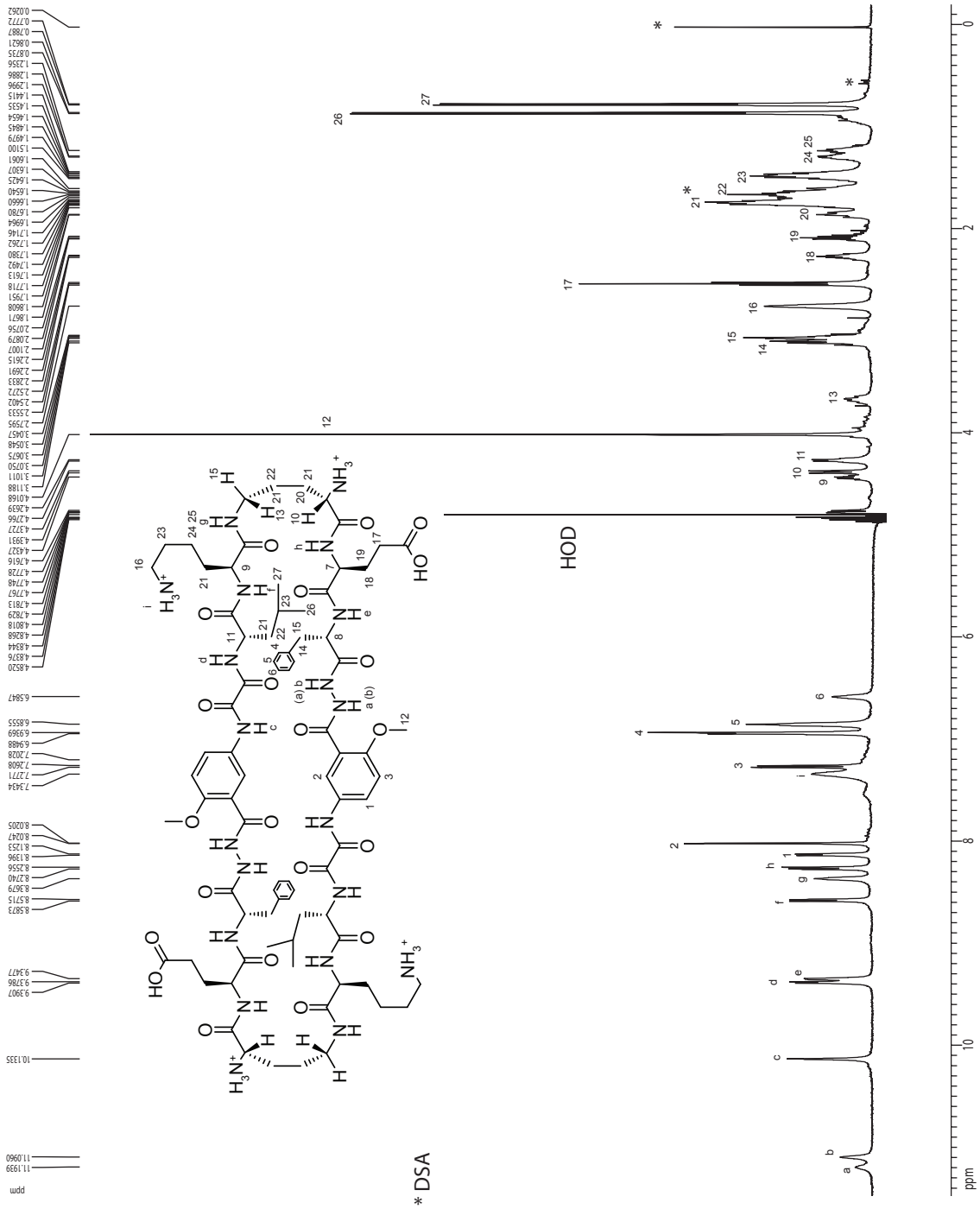

2D TOCSY spectrum of peptide **4.2a** with water suppression,
2 mM in 9:1 H_2O/D_2O, 298K, 600 MHz, 200-ms spin-lock mixing time

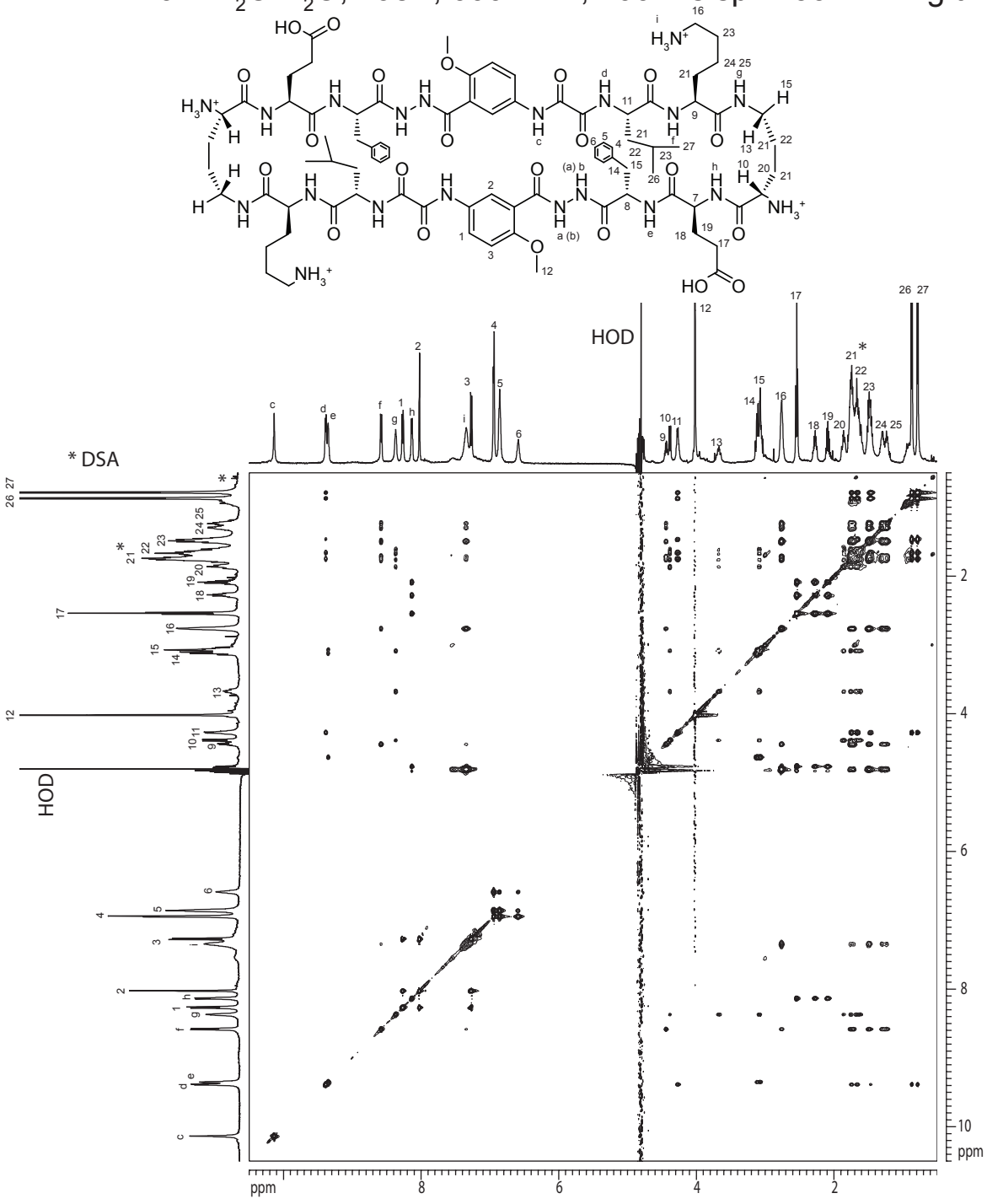

2D ROESY spectrum of peptide **4.2a** with water suppression,
2 mM in 9:1 H_2O/D_2O, 298K, 600 MHz, 200-ms spin-lock mixing time